University of Strathclyde

Department of Pure and Applied Chemistry

The development of copper complexes as medical imaging agents

Lynsey Dunbar

Thesis submitted to the Department of Pure and Applied Chemistry, University of Strathclyde, in fulfilment of the requirements for degree of Doctor of Philosophy

2015

Signed: Date:

<u>Acknowledgements</u>

Abstract

Studies building on existing research into the development of in vivo oxidant sensors which could be used as magnetic resonance (MR) imaging agents for the early detection of oxidative stress have been carried out. A series of N_2S_2 copper macrocyclic systems have been synthesised building on previous studies. The compounds have been modified at various positions to further enhance the suitability of these species as magnetic resonance imaging agents. The modifications include the introduction of oxo and sulfur based pendant arms at the nitrogen donor atoms, the introduction electron withdrawing and electron donating groups at various positions on the ring and the use of softer donor atoms to produce an S_4 and S_3N system. The stability and suitability of the complexes were challenged using a number of techniques including spectrophotometric titrations, cyclic voltammetry and T_1 relation NMR.

The stability of the copper centre of the macrocycles was challenged with a biologically relevant sequestration agent (bovine serum albumin). It was found that 5 coordinate copper macrocycles are the most stable. The electrochemical reversibility of the complexes was tested using cyclic voltammetry to identify which compounds were capable of redox reversibility. A sulfur based pendant arm complex (compound **52**) showed promise. Studies using ascorbate and hypochlorite demonstrate that this compound will survive chemical reduction and re-oxidation returning an acceptable percentage reversibility.

To assess the potential of all of the complexes for use as imaging agents, the effect of the complexes on the T_1 relaxation time was tested over a range of concentrations. This was compared with a Gd-DTPA control and original parent complex (compound **2**). The modifications made very little difference to the T_1 relaxation times. Although the relaxivity is low the studies indicates that the modified complexes may have some viability for use and warrant further investigation.

Contents

Glossary

cis-5,6,7,8,9,10,16,17-octahydrodibenzo [1,4,8,11]dithiadiazacyclotetradecine
copper tetrafluoroborate
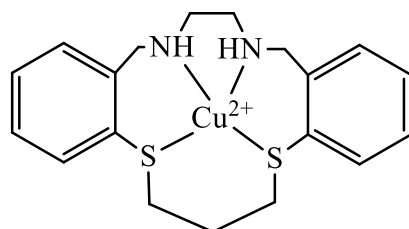
Compound **1**

cis-7,8,14,15,16,17,18,19-octahyro-dibenzo[1,5,9,12]dithiadiazacyclopentadecine
copper tetrafluorborate
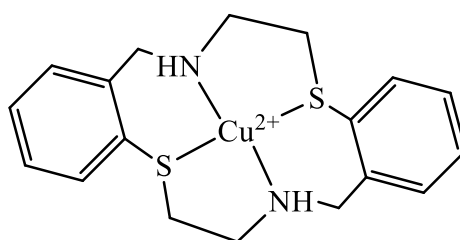
Compound **2**

trans- 6,7,8,9,15,16,17,18-octahydrodibenzo[1,8,4,11]dithiadiazacyclotetradecine
copper tetrafluoroborate
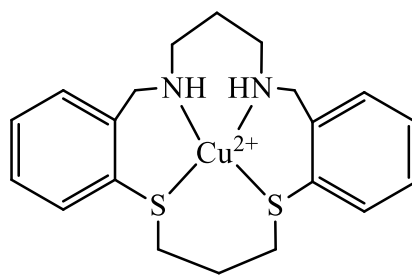
Compound **3**

cis- 5,6,7,8,9,10,11,17,18,19-decahydrodibenzo[1,5,9,13]dithiadiazacyclohexadecine copper tetrafluoroborate

Compound **4**
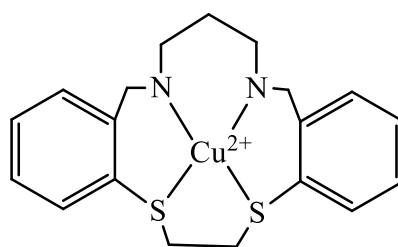
cis- 6,7,8,9,10,11,17,18-octahydro-dibenzo[1,4,8,12]dithiadiazacyclopentadecine copper tetrafluoroborate
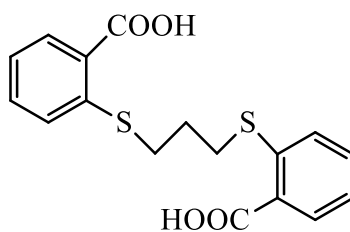
Compound **5**

2,2'-(propane-1,3diylbis(sulfanediyl))dibenzoic acid

Compound **6**
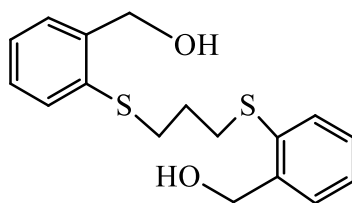
(propane-1,3-diylbis(sulfanediyl))bis(2,1-phenylene)dimethanol

Compound **7**
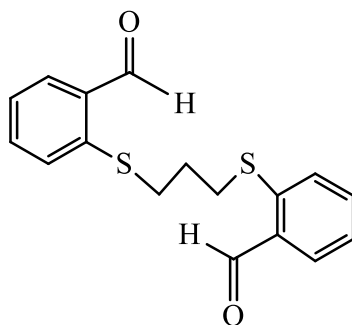
2,2'-(propane-1,3-diylbis(sulfanediyl))dibenzaldehyde

Compound **8**
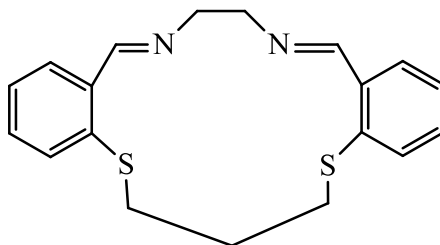
(14E,18E)-7,8,16,17tetrahydro-6H-dibenzo[1,5,9,12]dithiadiazacyclopentadecine

Compound **9**
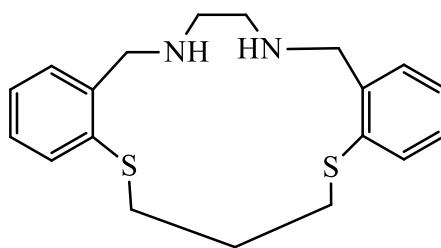
7,8,14,15,16,17,18,19-octahydro-6H-dibenzo[1,5,9,12]dithiadiazacyclopentadecine

Compound **10**
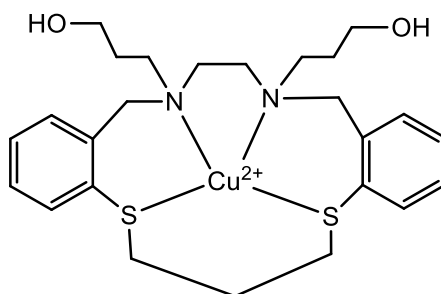
3,3'-(7,8,16,17-tetrahydro-6H-dibenzo[1,5,9,12]dithiadiazacyclopentadecine-
15,18(14H,19H)-diyl)bis(propan-1-ol) copper tetrafluoroborate

Compound **11**
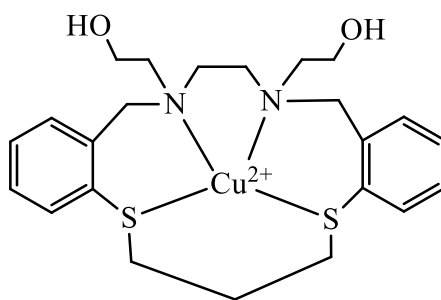
2,2'-(7,8,16,17-tetrahydro-6H-dibenzo[1,5,9,12]dithiadiazacyclopentadecine-
15,18(14H,19H)-diyl)diethanol copper tetrafluroborate

Compound **12**

2,2'-(7,8,16,17-tetrahydro-6H-dibenzo[1,5,9,12]dithiadiazacyclopentadecine-
15,18(14H,19H)-diyl)diacetic acid copper tetrafluoroborate

Compound **13**

2,2'-(7,8,16,17-tetrahydro-6H-dibenzo[1,5,9,12]dithiadiazacyclopentadecine-15,18(14H,19H)-diyl)diethanol

Compound **14**

3,3'-(7,8,16,17-tetrahydro-6H-dibenzo[1,5,9,12]dithiadiazacyclopentadecine-15,18(14H,19H)-diyl)bis(propan-1-ol)

Compound **15**
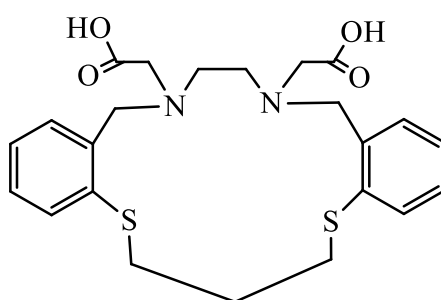
2,2'-(7,8,16,17-tetrahydro-6H-dibenzo[1,5,9,12]dithiadiazacyclopentadecine-15,18(14H,19H)-diyl)diacetic acid

Compound **16**
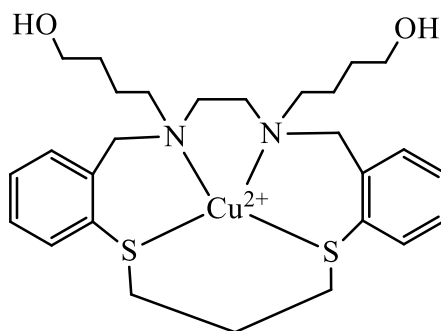
4,4'-(7,8,16,17-tetrahydro-6H-dibenzo[1,5,9,12]dithiadiazacyclopentadecine-15,18(14H,19H)-diyl)bis(butan-1-ol) copper tetrafluoroborate

Compound **17**
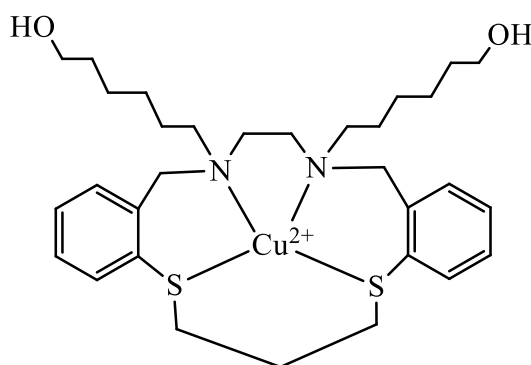
6,6'-(7,8,16,17-tetrahydro-6H-dibenzo[1,5,9,12]dithiadiazacyclopentadecine-15,18(14H,19H)-diyl)bis(hexan-1-ol) copper tetrafluoroborate

Compound **18**
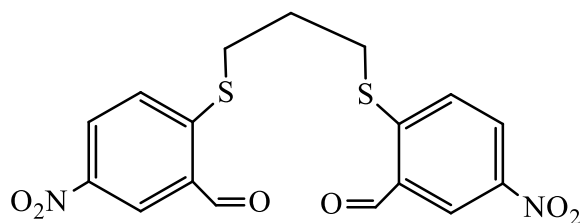
6,6'-(propane-1,3-diylbis(sulfanediyl))bis(3-nitrobenzaldehyde)

Compound **19**
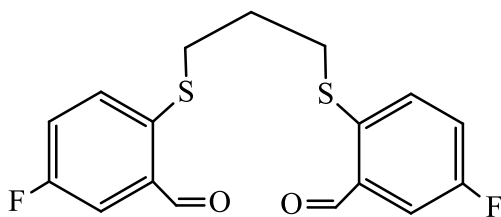
6,6'-(propane-1,3-diylbis(sulfanediyl))bis(3-fluorobenzaldehyde)

Compound **20**
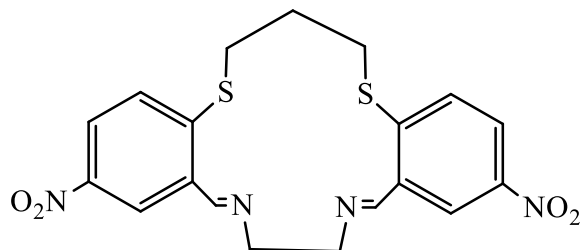
(14E,18E)-2,12-dinitro-7,8,16,17-tetrahydro-6H-
dibenzo[1,5,9,12]dithiadiazacyclopentadecine

Compound **21**
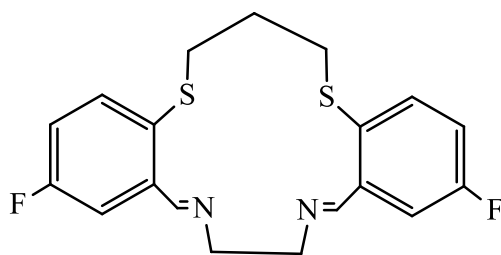
(14*E*,18*E*)-2,12-difluoro-7,8,16,17-tetrahydro-6*H*-
dibenzo[*f*,*n*][1,5,9,12]dithiadiazacyclopentadecine

Compound **22**
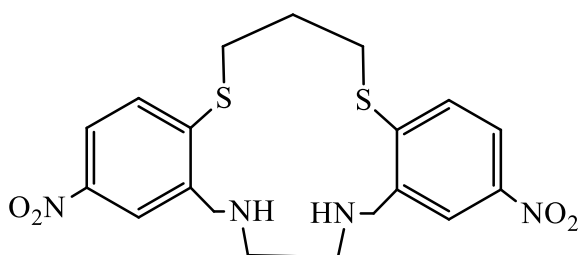
2,12-dinitro-7,8,14,15,16,17,18,19-octahydro-6H-
dibenzo[1,5,9,12]dithiadiazacyclopentadecine

Compound **23**
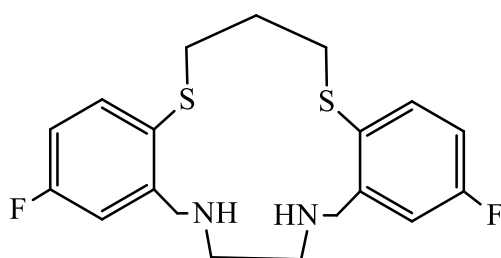
2,12-difluoro-7,8,14,15,16,17,18,19-octahydro-6*H*-
dibenzo[*f*,*n*][1,5,9,12]dithiadiazacyclopentadecine

Compound **24**
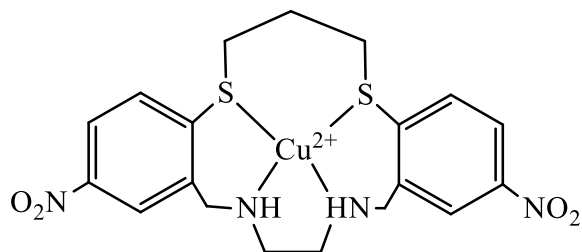
2,12-dinitro-7,8,14,15,16,17,18,19-octahydro-6H-
dibenzo[1,5,9,12]dithiadiazacyclopentadecine copper tetrafluoroborate

Compound **25**
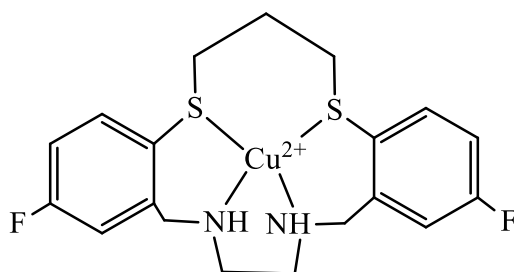
2,12-difluoro-7,8,14,15,16,17,18,19-octahydro-6H-
dibenzo[*f,n*][1,5,9,12]dithiadiazacyclopentadecine copper tetrafluoroborate

Compound **26**
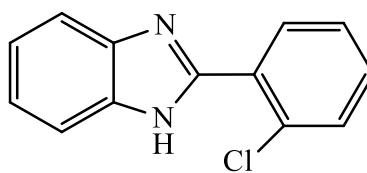
2-(2-chlorophenyl)-1*H*-benzo[*d*]imidazole

Compound **27**
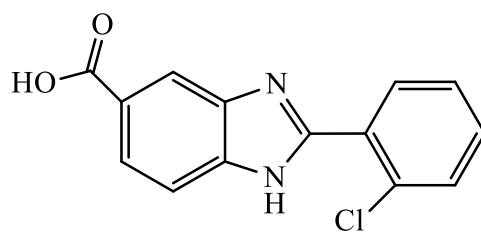
2-(2-chlorophenyl)-1*H*-benzo[*d*]imidazole-5-carboxylic acid

Compound **28**
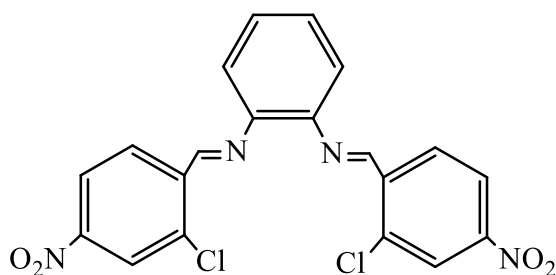
(N^{1}E,N^{2}E)-N^1,N^2-bis(2-chloro-4-nitrobenzylidene)benzene-1,2-diamine

Compound **29**
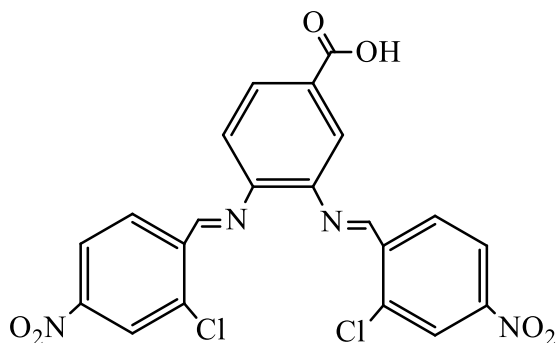
3,4-bis((E)-(2-chloro-4-nitrobenzylidene)amino)benzoic acid

Compound **30**
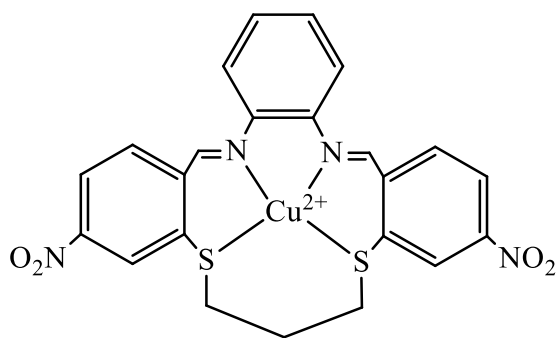
(5E,20E)-9,17-dinitro-13,14-dihydro-12H-tribenzo[1,5,9,12]dithiadiazacyclopentadecine copper tetrafluoroborate

Compound **31**
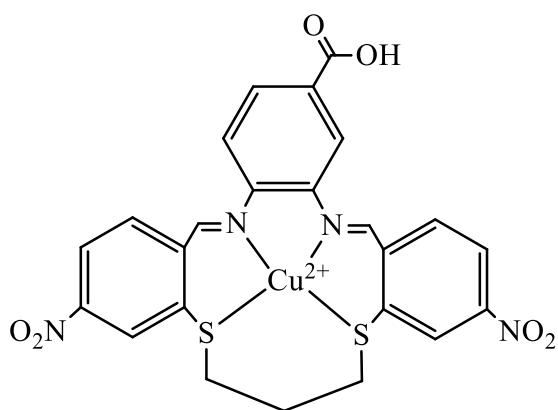
(5E,20E)-9,17-dinitro-13,14-dihydro-12H-tribenzo[1,5,9,12]dithiadiazacyclopentadecine-2-carboxylic acid copper tetrafluoroborate

Compound **32**
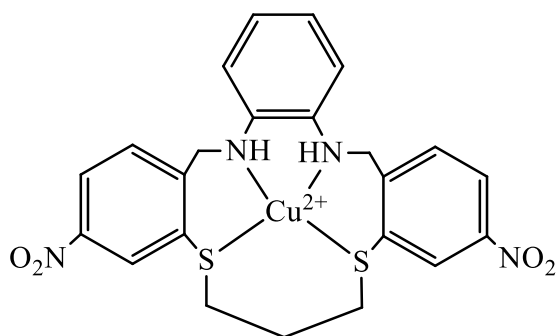
9.17-dinitro-6,12,13,14,20,21-hexahydro-5H-
tribenzo[1,5,9,12]dithiadiazacyclopentadecine copper tetrafluoroborate

Compound **33**
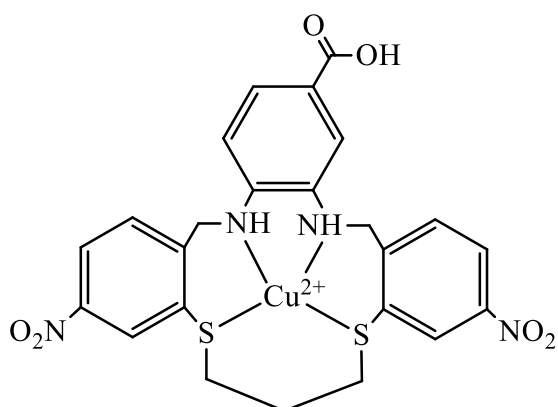
9,17-dinitro-6,12,13,14,20,21-hexahydro-5H-
tribenzo[1,5,9,12]dithiadiazacyclopentadecine-2-carboxylic acid copper
tetrafluoroborate

Compound **34**
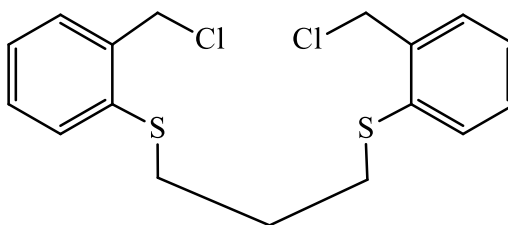
1,3-bis((2-(chloromethyl)phenyl)thio)propane

Compound **35**
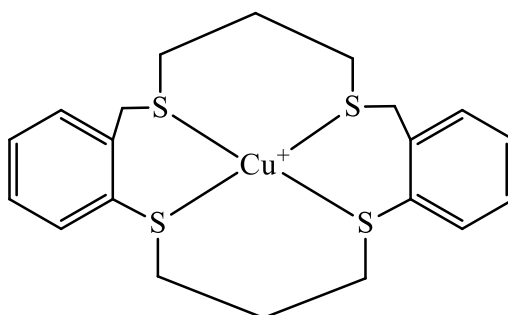
5,7,811,17,18,19-octahydrodibenzo[b.k][1,5,9,13]tetrathiacyclohexadecine copper tetrafluoroborate

Compound **36**
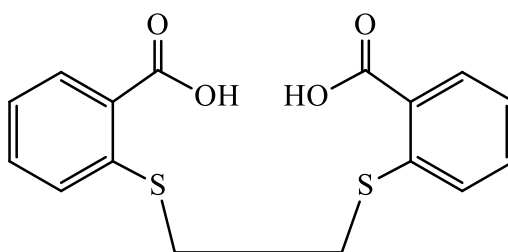
2,2'-(ethane-1,2-diylbis(sulfanediyl))dibenzoic acid

Compound **37**
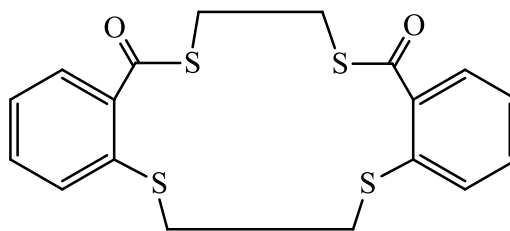
7,8,16,17-tetrahydrodibenzo[*e*,*m*][1,4,8,11]tetrathiacyclotetradecine-5,10-dione

Compound **38**
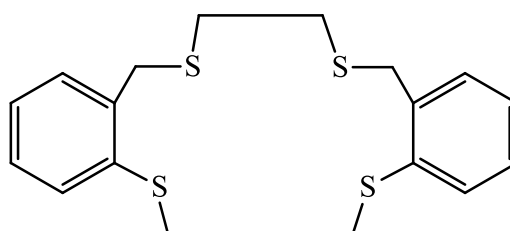
5,7,8,10,16,17-hexahydrodibenzo[*e*,*m*][1,4,8,11]tetrathiacyclotetradecine

Compound **39**
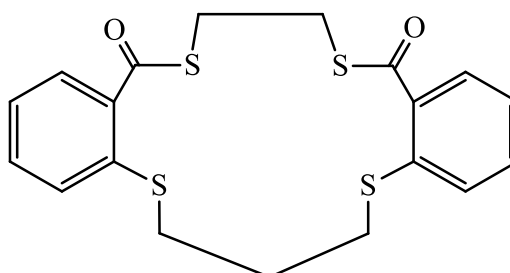
7,8,16,17-tetrahydro-6*H*-dibenzo[*f*,*m*][1,4,8,12]tetrathiacyclopentadecine-14,19-dione

Compound **40**
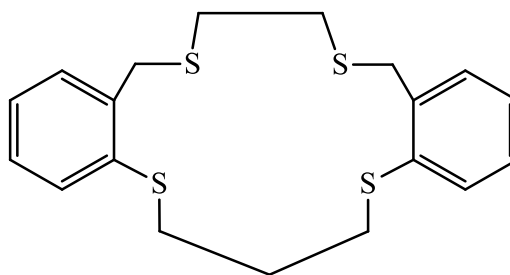
7,8,14,16,17,19-hexahydro-6*H*-dibenzo[*f*,*m*][1,4,8,12]tetrathiacyclopentadecine

Compound **41**
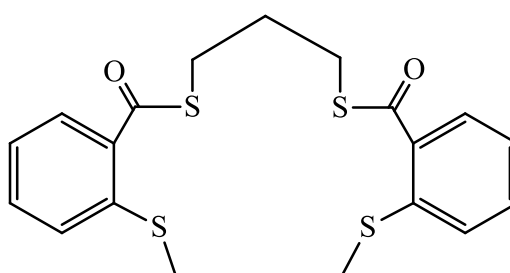
8,9,17,18-tetrahydro-5*H*-dibenzo[*e*,*n*][1,4,8,12]tetrathiacyclopentadecine-5,11(7*H*)-dione

Compound **42**
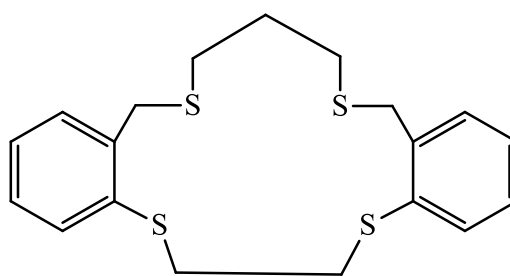
7,8,9,11,17,18-hexahydro-5*H*-dibenzo[*e*,*n*][1,4,8,12]tetrathiacyclopentadecine

Compound **43**
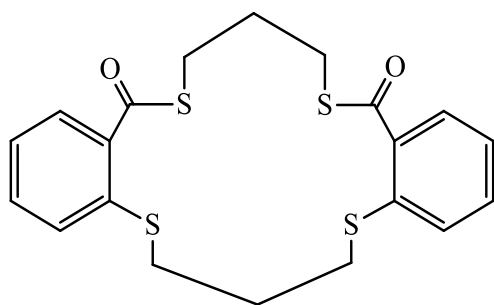
8,9,18,19-tetrahydrodibenzo[*b*,*k*][1,5,9,13]tetrathiacyclohexadecine-5,11(7*H*,17*H*)-dione

Compound **44**
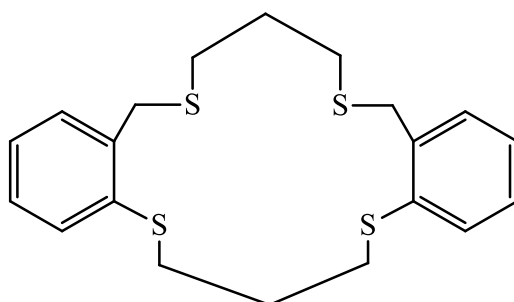
5,7,8,9,11,17,18,19-octahydrodibenzo[*b*,*k*][1,5,9,13]tetrathiacyclohexadecine

Compound **45**
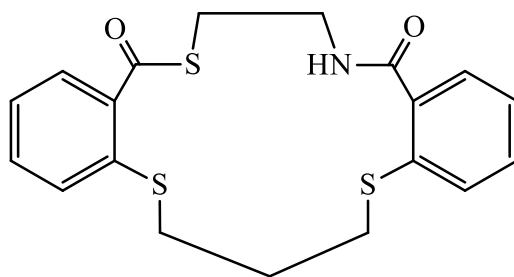
7,8,17,18-tetrahydrodibenzo[*f*,*m*][1,8,12,4]trithiaazacyclopentadecine-14,19(6*H*,16*H*)-dione

Compound **46**
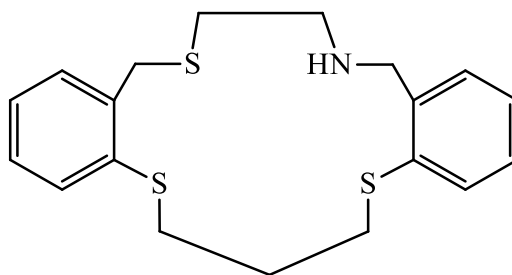
6,7,8,14,16,17,18,19-octahydrodibenzo[*f*,*m*][1,8,12,4]trithiaazacyclopentadecine

Compound **47**
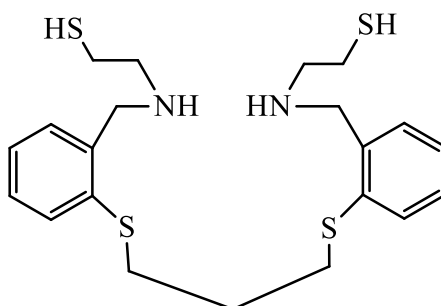
2,2'-(((((propane-1,3-diylbis(sulfanediyl))bis(2,1-phenylene))bis(methylene))bis(azanediyl))diethanethiol

Compound **48**
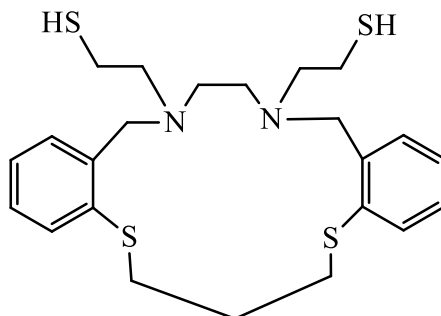
2,2'-(7,8,16,17-tetrahydro-6*H*-dibenzo[*f*,*n*][1,5,9,12]dithiadiazacyclopentadecine-15,18(14*H*,19*H*)-diyl)diethanethiol
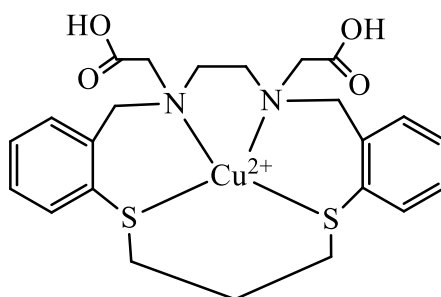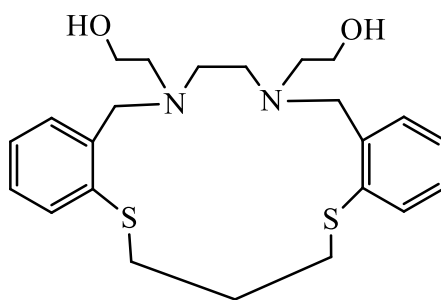
Compound **49**
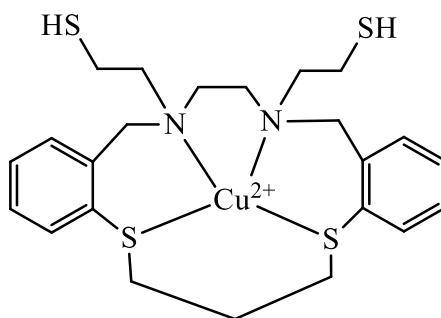
2,2'-(7,8,16,17-tetrahydro-6H-dibenzo[*f*,*n*][1,5,9,12]dithiadiazacyclopentadecine-15,18(14H,19H)-diyl)diethanethiol copper tetrafluroborate
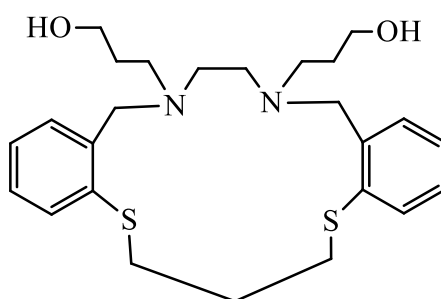
Compound **50**
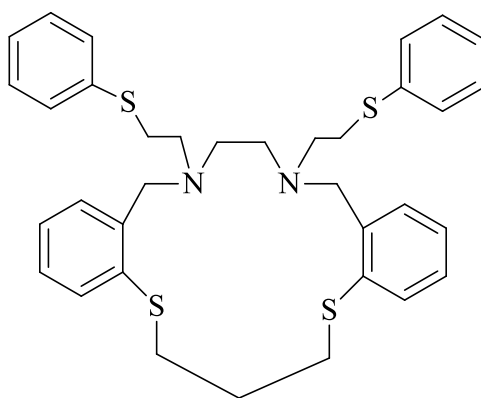
15,18-bis(2-(phenylthio)ethyl)-7,8,14,15,16,17,18,19-octahydro-6*H*-dibenzo[*f*,*n*][1,5,9,12]dithiadiazacyclopentadecine

Compound **51**
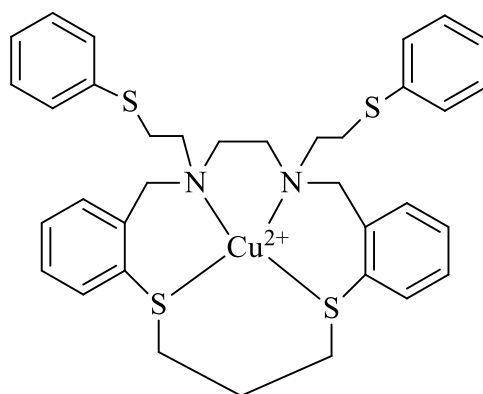
15,18-bis(2-(phenylthio)ethyl)-7,8,14,15,16,17,18,19-octahydro-6H-
dibenzo[f,n][1,5,9,12]dithiadiazacyclopentadecine copper tetrafluoroborate

Compound **52**

Chapter 1

Introduction

1.1 Inflammatory disease

Inflammatory diseases, where the cause is acute or chronic stimulation of the immune system resulting from exogenous damage, autoimmune response or infection are of major clinical importance. The diagnosis of these conditions is difficult until the pathology is well advanced. This limits the possibility of prevention and makes treatment more complicated and less successful.[1] It would therefore be greatly beneficial if it were possible to diagnose these conditions while they are in their early stages. To achieve this, preferably a simple and non-invasive method of detecting and measuring the extent of an inflammatory process within the body must be identified.

When the human body becomes injured or infected, a number of physiological changes occur in the infected area. There is local vasodilatation, increased permeability of the capillaries, and infiltration of the damaged tissue by white blood cells. These changes constitute the inflammatory response, which appears to be geared to bringing plasma proteins and cells to the point of injury.[2,3]

Extensive inflammation results in the injured tissue becoming infiltrated by polymorphonuclear leukocytes, particularly neutrophils. The neutrophils produce reactive oxygen species (ROS) which are microbiocidal and when an excess in production occurs the host tissue can be damaged. One ROS is the superoxide radical anion, which is generated by the respiratory burst, and then converted to hydrogen peroxide. The effect of this is to shift the redox balance of the surrounding tissues to a more oxidising state, this is referred to as oxidative stress. Thus, if it were possible to analyse the oxidant flux it could be possible to assess the disease and its severity through its oxidative pathology. Metal complexes could be of immense value in this assessment. Many metal complexes are initially found in a reduced and diamagnetic state but can be oxidised to a paramagnetic form through, in this case, *in-vivo* oxidation. Under these conditions it should be possible to employ the complex as a contrast agent and image oxidative stress using magnetic resonance imaging (MRI). This can be done because the T_1 relaxation of water will be altered by paramagnetic complexes only at the site of inflammation, thus allowing the extent and severity of the inflammation to be measured directly from the MRI contrast.[3]

1.2 Magnetic Resonance Imaging (MRI)

MRI has become an important technique in the medical world. An MRI scanner, consists of a large magnet, radiofrequency (RF) coils, gradient coils and a computer system. The magnet is needed to produce a uniform and static external magnetic field, which will align the nuclei of atoms in the volume of the patient lying inside the magnet. It is usually only the atoms with an odd number of protons and neutrons that align themselves in the direction of the magnetic field. This is because they produce their own magnetic field and act like tiny bar magnets. The effect of these small nuclear magnets is not normally seen in tissue, as the magnetic fields are in random orientation and tend to cancel each other out. The nuclei of atoms with an even number of protons and neutrons (e.g. ^{12}C) do not produce a magnetic field.[4]

NO FIELD   MAGNETIC
                                                              FIELD
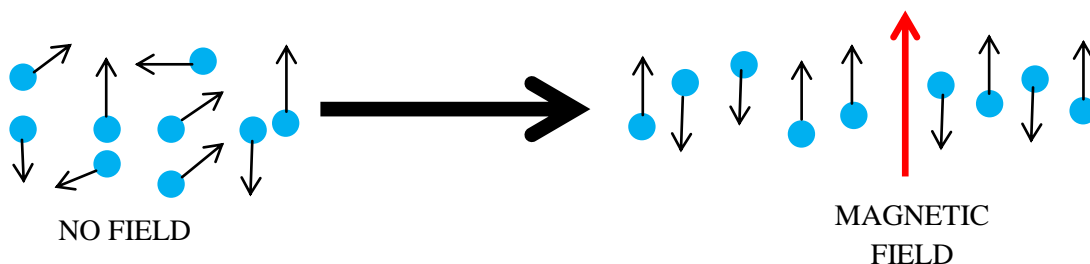
Figure 1.1: A diagram demonstrating nuclei alignment with the applied MRI magnetic field.

The radiofrequency (RF) coils are shaped into curved panels which surround the patient during scanning. They act as a generator for RF excitation and as a receiver to detect the return signal. The RF signal which is generated is pulsed, and forms a magnetic field at 90º to the main magnetic field. This tilts the nuclei which are in alignment with the external magnetic field, and because they are spinning, the nuclei act like gyroscopes. They rotate around the direction of the main magnetic field while they slowly return to their original orientation. This action is called precession. By rotating in this manner the bar magnets cause a current to flow in a detection coil, which acts like an aerial attached to a radiofrequency receiver.[4]

Precession circle

External
magnetic
field (B_0)
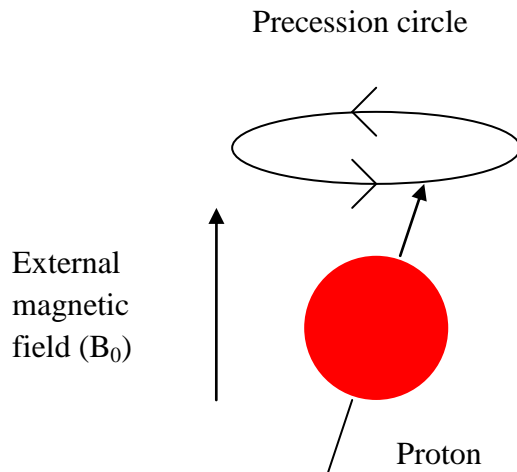
Proton

Figure 1.2: A sketch of the effect of a magnetic field on a proton.[5]

The signal is very small and easily obscured by other RF noise from the environment, patient and coil. To construct an image it is necessary to know where the signal originates from with respect to the point of origin in the magnetic field. This is achieved by using gradient coils, which produce an additional magnetic field which varies across the image being scanned. The frequency of the detected signals depends upon the strength of the magnetic field, and as this is now varied, depending on the signal frequency received it is possible to relate it to the area it has originated from.

The image is formed by a specialised computer programme. The image relates to the relaxation time, which is the time taken for the signal to disappear. There are two different types of relaxation, T_1 (longitudinal) and T_2 (transverse). They form the basis for contrast differences on the images.[4]

1.3 Relaxation times

The effect of an RF pulse is to transfer energy from the transmitting coils to the protons. This excess energy results in a non-Boltzmann distribution of the populations of the parallel and anti-parallel energy states. In the vector model, the M_z component has been reduced from its equilibrium value of M_0, and the M_x and/or M_y components have a non-zero value. Each of the magnetisation components M_z, M_x, and M_y are characterised by differential equations, known as the Bloch equations:

$$dM_x/dt = \gamma \, M_y \, (B_0 - \omega/\gamma) - M_x/T_2 \qquad \text{(Equation 1.1)}$$

$$dM_y/dt = \gamma \, M_z \, B_1 - \gamma \, M_x \, (B_0 - \omega/\gamma) - M_y/T_2 \qquad \text{(Equation 1.2)}$$

$$dM_z/dt = -\gamma \, M_y B_1 - M_z - M_0/T_1 \qquad \text{(Equation 1.3)}$$

Where the nuclear magnetization $\mathbf{M} = (M_x, M_y \text{ and } M_z)$. γ = the gyromagnetic ratio. The z component of the magnetic field $\mathbf{B}$ is composed of two terms: B_0, is constant in time and B_1 is time dependant and helps with the spatial decoding of the NMR signal. ω = the angular frequency and T_2 = the transverse relaxation.

The return of M_z to its equilibrium value of M_0 is governed by the longitudinal (T_1) relaxation time. Immediately after an RF pulse of arbitrary tip angle α, the M_z component is given by $M_0 \cos \alpha$. The value of M_z at a time t after the RF pulse is given by:

$$M_z \, (t) = M_0 \cos \alpha + (M_0 - M_0 \cos \alpha) \, (1 - e^{-t/T1}) \qquad \text{(Equation 1.4)}$$

For example, after a 90° pulse the value M_z is given by

$$M_z \, (t) = M_0 \, (1 - e^{-t/T1}) \qquad \text{(Equation 1.5)}$$

The physical basis for T_1 relaxation involves the protons losing their energy to the surrounding lattice, hence why the longitudinal relaxation is often also referred to as spin-lattice relaxation. Different tissues have different values for T_1, and this difference forms the

basis for initial tissue contrast in the MR image. The values of T_1 also depends upon magnetic field strength.[5]

Once the magnetisation is tipped, the M_x and M_y components of magnetisation relax back to their thermal equilibrium values of zero with a time constant (T_2), commonly known as the transverse relaxation time:

$$dM_x/dt = - M_x/T_2 M_x, \qquad \text{(Equation 1.6)}$$

$$dM_y/dt = M_y/T_2 \qquad \text{(Equation 1.7)}$$

If an RF pulse of arbitrary tip angle α is applied along the x axis, then immediately after the pulse there is no M_x component of magnetization, and the M_y component is given by $M_0 \sin \alpha$. The value of M_y at time t after the RF pulse is given by

$$M_y(t) = M_0 \sin \alpha \, e^{-t/T2} \qquad \text{(Equation 1.8)}$$

The physical basis of the decay of the T_2 magnetisation is different from that of longitudinal relaxation. T_2 relaxation involves the loss of "phase coherence" of the magnetisation of the protons precessing in the transverse plane. Even in a perfectly homogenous magnetic field, the magnetic moments of different protons precess at slightly different frequencies due to variations in their interactions with neighbouring nuclei. As a result, the net magnetisation decreases as a function of time.

Similar to T_1, different tissues in the body have an influence on the values of T_2. These differences can also be used to differentiate between soft tissues in clinical images. Once again, the values depend on the strength of the magnetic field. In fact, the loss in phase coherence of the transverse magnetization arises from two different mechanisms. The first is "pure" T_2 decay outlined above. The second arises from spatial variations in the strength of the magnetic field within the body. There are two major sources for these variations. The first is the intrinsic magnet design, that is, it is impossible to design a magnet which produces a perfectly uniform magnetic field over the entire patient. The second source is local variations in the magnetic field due to the different magnetic susceptibilities of different tissues: this

effect is particularly pronounced at air/tissue and bone/tissue boundaries. Together, these factors produce a loss of phase coherence, which is characterized by a relaxation time T^+_2. The overall relaxation time that governs the decay of transverse magnetization is a combination of signal loss due to T_2 and T^+_2 effects, and is designated by T^*_2, the value of which is given by:

$$1/T^*_2 = 1/T^+_2 + 1/T_2 \qquad \text{(Equation 1.9)}$$

In the field of high resolution NMR spectroscopy for chemical analysis, the value of T^+_2 is very small (because the sample is small and spatially homogenous) and so the value of T^*_2 is well approximated by T_2.[6]

1.4 Contrast agents

In many clinical diagnoses, there is sufficient contrast to noise ratio (CNR) on the appropriately T_1-, T_2- or proton density- weighted image in order to distinguish pathological from healthy tissue. However, in certain situations, the CNR can be low. In this case, MRI contrast agents can be used to increase the CNR between healthy and diseased tissue. There are two basic classes of MRI contrast agent: paramagnetic agents and superparamagnetic agents, also called ferromagnetic agents. Paramagnetic agents primarily shorten the T_1 of the tissue in which they accumulate. Rapid T_1 – weighted sequences are used in order to minimize the total imaging time, with tissue in which the agent accumulates appearing brighter on the image. Superparamagnetic agents accumulate primarily in healthy rather than pathological tissue, and shorten the T_2 and T^*_2 values of the tissue. Therefore, a tumour for example, can be detected as an area of high signal intensity using a T_2- or T^*_2- weighted sequence. As will become apparent we are more concerned with the use of paramagnetic agents for the use of detecting inflammatory disease.[6] Paramagnetic contrast agents are based on metal ions that have a large number of unpaired electrons, these substances are affected by a magnetic field.

1.4.1 Use of Lanthanides in MRI

Lanthanide chemistry is dominated by the +3 oxidation state, which is generated by an atom losing one 5d and two 6s electrons.[7] Lanthanide (III) ions are paramagnetic due to their unpaired 4f electrons.[7,8] They have a wide variety of coordination numbers, mostly 6-12, but complexes with coordination numbers of 2, 3 and 4 are also known.[7] Lanthanides have been used in the past as anti-emetics and as treatments for tuberculosis[9]. Other uses are as antibacterials and as anti-cancer agents.[10] However their predominant use now is in the field of MRI, where they are used as contrast agents. Although MRI on its own can give an anatomical image, this can be greatly enhanced by the use of contrast agents. There has been some work published on the use of dysprosium (III) and europium (II) as potential imaging agents.[11,12] However, the metal cation currently found in four out of six clinically approved contrast agents is gadolinium (III). It is highly paramagnetic, with 7 unpaired electrons, the dominant isotopes are quadrupolar and its complexes display fast exchange kinetics (Table 1.1).[8]

Nucleus	No unpaired electrons	Nuclear Spin	Isotope	% abundance	Rate of ligand exchange (s^{-1})
Gadolinium	7	3/2	^{155}Gd	14.7	10^9
		3/2	^{157}Gd	15.7	
Vanadium	3	7/2	^{51}V	99.8	10^3
Manganese	5	5/2	^{55}Mn	100	5×10^7
Copper	1	3/2	^{63}Cu	69.1	10^9
		3/2	^{65}Cu	30.9	

Table 1.1: Comparison of some of the 1st row transition metals and gadolinium.

Most free metals are toxic at clinical concentrations and as such the presence of chelating ligands are necessary. Due to the fact that the magnetic moment of an electron is approximately 660 times larger than that of a proton, the unpaired electrons result in the metal ion having a very large magnetic moment hence the reason that paramagnetic ions assist relaxation. The MRI signal is not detected directly from the contrast agent, but through

its effect on the relaxation times of neighbouring water molecules.[13] The interaction between the unpaired electrons of the metal ion and the water molecules cause the proton T_1 and T_2 relaxation times of the water to be shortened, the effect being quantified by the relaxivity of the agent:

$$1/T_{1,C} = 1/T_{1,0} + \alpha_1 C \qquad \text{(Equation 1.10)}$$

Where:

$T_{1,C}$ = T_1 of water containing a concentration C of the contrast agent

$T_{1,0}$ = the corresponding value without contrast agent

α_1 = the T_1 relaxivity of the contrast agent

There are two mechanisms which result in enhanced relaxation efficiency. These are termed "inner sphere" and "outer sphere" relaxation. As an example of how they operate, gadolinium 1,4,7,10-tetraazacyclododecane-1,4,7,10-tetraacetic acid (Gd-DOTA)⁻ is shown below. It is currently one of the most commonly used paramagnetic imaging agents, there is one ligand binding site that is vacant and is the site of water (O9) exchange.
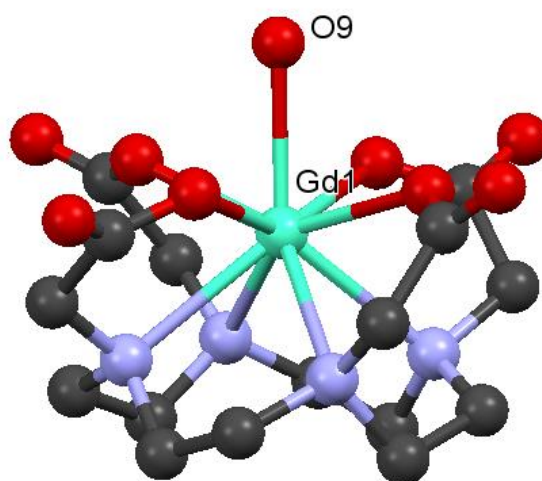
Figure 1.3: Molecular structure of Gd(DOTA)⁻ (Dotarem®)[14] with water bound to structure. The structure has been redrawn from the deposited crystallographic data (ccdc 612534). The proton positions were absent from the file provided.

A water molecule can temporarily bind at the vacant position on gadolinium and will be relaxed very efficiently due to its proximity to the unpaired electrons on the metal ion. This process is called inner-sphere relaxation. On the time scale of the imaging sequence, up to 7 water molecules are bound, relaxed and released (table 1.1). Water molecules that diffuse close to the agent, but are not bound, undergo a process called outer sphere relaxation, which is not as efficient as inner-sphere relaxation, but still results in shortened relaxation times.[13]

The T_1 relaxation rate (R_1^{obs}) can be easily measured *in- vivo*. This is typically made up of 3 parameters; a diamagnetic contribution (R_1^{o}), a paramagnetic contribution relative to inner sphere water exchange with bulk solvent (R_{1p}^{is}) and a paramagnetic contribution relative to water molecules diffusing into the outer sphere (R_{1p}^{os}; Equation 1.11) A fourth contribution from non-bonded water in the second sphere typically hydrogen bonded to the chelating ligand can sometimes also be present.[15]

$$R_1^{obs} = R_1^{o} + R_{1p}^{is} + R_{1p}^{os} \qquad \text{(Equation 1.11)}$$

Gadolinium based contrast agents are now being designed which measure chemical characteristics of the body such as tissue pH and the partial pressure of oxygen ($p[O_2]$). To act as pH reporters the MRI contrast agents have to provide responsiveness to pH that does not require prior knowledge of the actual concentration of the contrast agent. Gianolio *et al.*[16] are developing a new ratiometric method based on inclusion of the Gd-DO3Asa complex (Figure 1.4) in liposomes. The amphiphilic metal complex, containing a sulfonamide moiety whose protonation changes the coordination properties of the metal chelate, experiences a different intraliposomial distribution depending on the pH conditions. The ratiometric method consists of measuring the pH dependence of the ratio between the longitudinal paramagnetic contribution to the water proton relaxation rates (R_1p) at two different magnetic fields, thus removing the concentration dependence of the MR signal.[16,17]
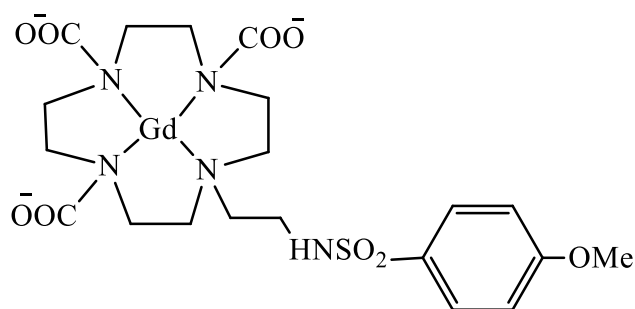
Figure 1.4: Structural formula of Gd-DO3Asa. [16]

pH sensitive liposomes have also been reported by Lokling *et al.*[18] pH-sensitive liposomes consist of systems containing a paramagnetic metal complex in the inner aqueous cavity, whereas their membrane is designed to give low permeability to water molecules at neutral pH. These liposomes are essentially MRI-silent at neutral pH, with a marked increase of the water proton relaxation rates at acidic pH, where protonation of a substituent of the lipidic components leads to a change in the lipid organization.

Hypoxia occurs in various diseases, including cancer, ischaemia and chronic and acute vascular diseases. In cancer, this is due to extensive tumour growth and inadequate tumour vascular structure resulting in an insufficient oxygen and nutrient supply from blood vessels in solid tumours, which often contain hypoxic regions in which oxygen concentration is very low.[19] Therefore, imaging agents for hypoxia would be a useful diagnostic tool. For hypoxia sensors, the enhancement of the MRI signal intensity should be induced via bio-reduction of the contrast agent under hypoxic conditions.[20] Similar to the pH sensitive agents previously discussed with a sulphonamide moiety, the hypoxia sensing gadolinium based contrast agent bears a nitrobenzenesulfonamide moiety. The nitrobenzenesulfonamide moiety shows low R_1 relaxivity under physiological conditions due to intramolecular chelation of the nitrogen anion of the sulfonamide moiety to the Gd (III) centre. Further, under hypoxic conditions, the nitro group is expected to be reduced to an amino group, and so the complex should show high R_1 relaxivity, because the sulfonamide nitrogen is protonated and can no longer coordinate to the Gd (III) centre.

Gadolinium based contrast agents are also being developed for the sensing of zinc and copper.[21,22] Kasala *et al.* are currently investigating the possibility of using gadolinium

contrast agents for the detection of genetic disorders such as Wilson's and Menkes diseases (Figure 1.5) which arise from mutations in copper handling proteins, and disruption in copper homeostasis which is associated with a number of neurodegenerative pathologies such as Parkinson's and Alzheimer's disease.[22] So interest has also turned to the development of a gadolinium based contrast agent which is capable of copper binding.[23]
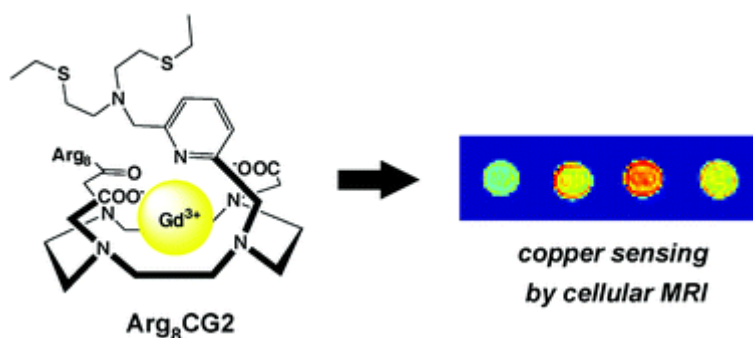
Figure 1.5: *In cellulo* relaxivity measurements and T_1-weighted phantom images using a Menkes disease model cell line demonstrate the utility of Arg$_8$CG2 to report on biological perturbations of exchangeable copper pools.[23]

Auld is investigating the used of gadolinium contrast agents for the detection of zinc. Zinc exists exclusively as the divalent ion (Zn^{2+}) in biology with most Zn^{2+} bound to proteins that play an important role in controlling gene transcription and metalloenzyme function.[24] Similarly to contrast agents for the detection of copper, the macrocycles designed for zinc detection are complex again making their clinical use unlikely.

There is ongoing research into the possibility of using $Gd(IO_3)_3.2H_2O$ nanomaterials (nanoparticles, nanorods, nanosheets etc.) as an MRI-CT (computed tomography) dual contrast agent.[25] As previously discussed MRI is an invaluable diagnostic tool for many diseases, however Gd-based contrast agents only provides soft tissue images i.e only structural information and no chemical information. CT is very useful for the imaging of hard body parts (e.g bones, hardened diseases) and also for the imaging of moving organs as it generally takes less than 10 minutes to record an image.   However CT is somewhat harmful as it uses high energy X-ray radiation. Lee *et al.*[25] are studying the possibility of an MRI-CT that combines the strength of both techniques. Triiodobenzene is a commercially available CT contrast agent (e.g Optiray and Ultravist) As previously discussed Gd based contrast

agents are the most commonly used contrast agent so it is hoped that the combination of both are complimentary to each other.

1.4.2 The CEST effect

Another advance has been in the development of chemical exchange saturation transfer (CEST) agents.[26] As the name suggests CEST involves chemical exchange of a nucleus from one site to a chemically different site. It exploits the ability of NMR to resolve different signals arising from protons on different molecules. By selectively saturating a particular proton signal (associated with a particular molecule or CEST agent) that is in exchange with the surrounding water molecules, the MRI signal from the surrounding bulk water molecules is also attenuated. Images obtained with and without an RF pulse reveal the location of the CEST agent (Figure 1.6). The chemical exchange must be in the intermediate region where exchange is fast enough to efficiently saturate the bulk water signal but slow enough that there is a chemical shift difference between the exchangeable proton and the water proton resonances.

The magnitude of the CEST effect therefore depends on both the exchange rate and the number of exchangeable protons:

$$M_s/M_0 \approx 1/1+k_1T_1 \qquad\qquad \text{(Equation 1.12)}$$

$$k_1 = n[\text{agent}]k_{CE} \qquad\qquad \text{(Equation 1.13)}$$

Where: k_{CE} = the single site exchange rate, n = the number of exchangeable
protons/molecules and T_1 the spin-lattice relaxation time in the presence of the saturating
pulse.

In concept, CEST has 3 main advantages over traditional molecular imaging techniques. The image is controlled by radio-frequency (RF) pulses and can be turned on and off at will. Furthermore the endogenous molecules of interest, in some cases, can be directly detected therefore eliminating the need for the contrast agent to be delivered to and specifically react with the molecule of interest (Figure 1.7). A variant of the CEST technique, known as

PARACEST, may be much more sensitive than traditional molecular imaging techniques and should be able to detect nanomolar concentrations.[27]
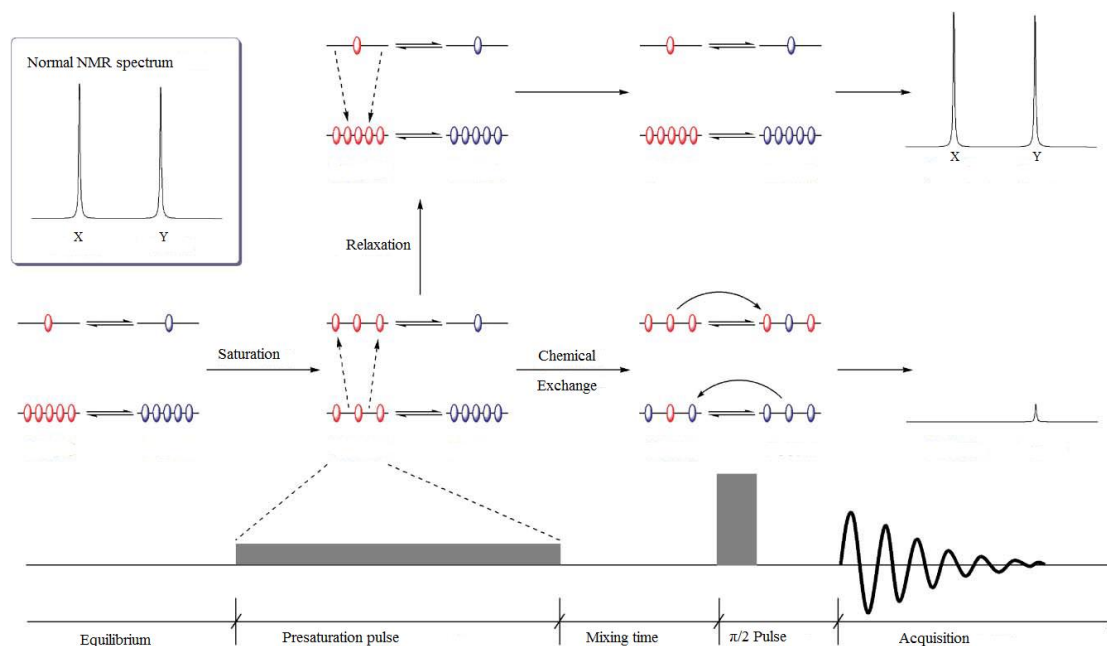
Figure 1.6: Adaptation of schematic representing chemical exchange saturation (CEST) effect on NMR spectra vs. no CEST. [26]

PARACEST typically relies on water exchange between the bulk water and the water bound to paramagnetic lanthanide complexes. Saturation of the lanthanide ion bound water resonance leads to attenuation of the bulk water signal via water exchange. The large paramagnetic shift of the bound water molecules allows them to tolerate much faster exchange rates with the bulk water while still remaining in the intermediate exchange regime, therefore providing much more efficient saturation of the bulk water signal and much greater CEST sensitivity. The advantages of this are that a pre-administration image is not required and co-agents can be used together. A europium (III) DOTA-tetraamide PARACEST agent has been recently developed for the detection of singlet oxygen which plays a significant role in many biochemical processes. Sensitivity has increased even further with the use of LIPOCEST agents. Mobile water protons are encapsulated in a nano-sized liposome with a CEST agent. The potential for water exchange is much greater as $10^6 - 10^9$ molecules can be localized near the complex.[26]
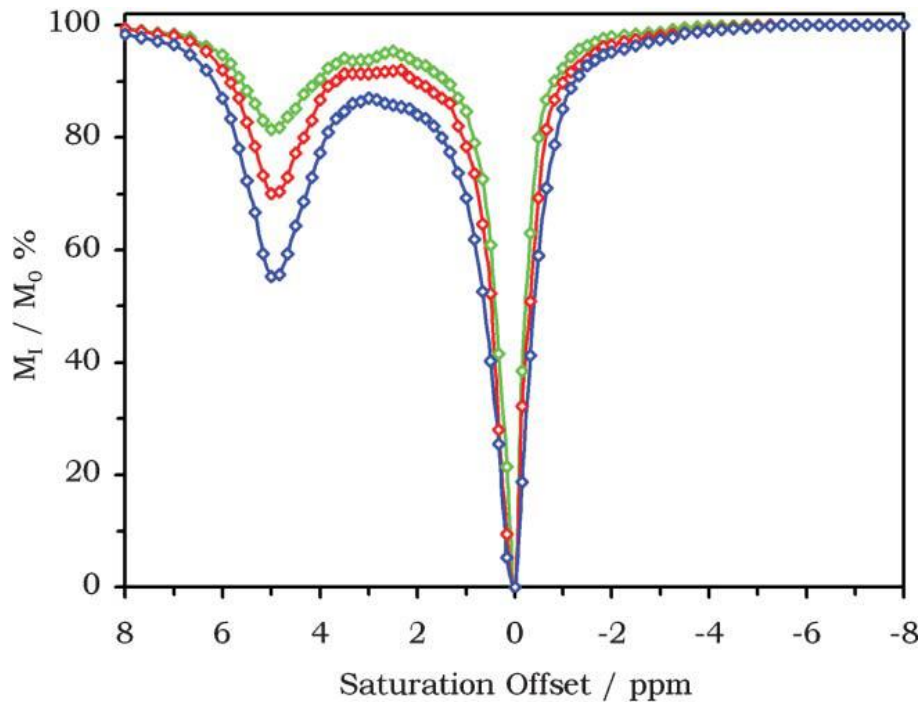
Figure 1.7: CEST spectra demonstrating where the CEST effect reduces the intensity of the bulk water signal and appears as a second negative peak. 125 mM (blue), 62.5 mM (red), 31.25 mM (green), solutions of barbituric acid recorded and 300 MHz, pH 7.0 and 37°C.[26]

Possible uses for these agents have been suggested.[27] An emerging area of MRI contrast agents are responsive agents. Contrast agents that respond to changes in the concentration of biologically important species are of particular interest as these agents would render MRI a true molecular imaging technique in addition to anatomical imaging. In addition to changes in pH, the rate of proton exchange is also affected by the temperature. The rate of exchange accelerates with increasing temperature according to the Arrhenius equation (Equation 1.14). This changes the shape and decreases the magnitude of the peaks in the CEST spectrum in a linear fashion as temperature is increased.

$$k = Ae^{\frac{-Ea}{RT}}$$ (Equation 1.14)

1.4.3 Non-lanthanide based contrast agents

Gd-DTPA (diethylenetriaminepentaacetic acid) is known to have a good relaxivity and high water solubility.[28] However, recent studies have revealed that Gd(III) based contrast agents could trigger the epidemiology of nephrogenic systemic fibrosis in patients.[29] The use of alternative metals as contrast agents is currently being investigated. Mn(II) based compounds are front runners as a possible alternative agent as they have 5 unpaired electrons and a relatively fast rate of water exchange (5 x $10^7 s^{-1}$).[30] Huang *et al*. have investigated the use of manganese by synthesising a Mn-DTPA modified complex with the natural compound chitosan (CS) to improve the solubility, relaxivity and safety of Mn(II) based contrast agents.[31] Although the solubility, relaxivity and safety of these complexes are increased in comparison to previous Mn(II) based contrast agents the altered ligand is very complex and thus difficult to synthesise.

Among the various parameters that characterize a biological environment, the partial pressure of oxygen (p[O_2]) appears to be relevant in a number of pathological conditions including strokes and tumours.[16] The availability of contrast agents whose relaxivity is dependent upon p[O_2)]would be useful to obtain a better separation of arterial and venous blood as well as to develop novel applications of functional MRI. The simplest design of p[O_2]-responsive contrast agents is based on a complex whose metal ion can switch between two redox states characterized by different relaxation properties. Mn(II)/Mn(III) contrast agents in a porphyrin ligand system are being studied for this use.[32] As a model for this application Aime *et al*.[33] have considered Mn(II) and Mn(III) complexes with 5,10,15,20-tetrakis-(p-sulfonatophenyl) porphinate (tpps), whose relaxometric properties have been widely investigated (Figure 1.8).[33,34] Moreover, this system shows a high affinity to tumour cells and, because of this property, it has been considered as a potential candidate for photodynamic therapy of cancer.[35]
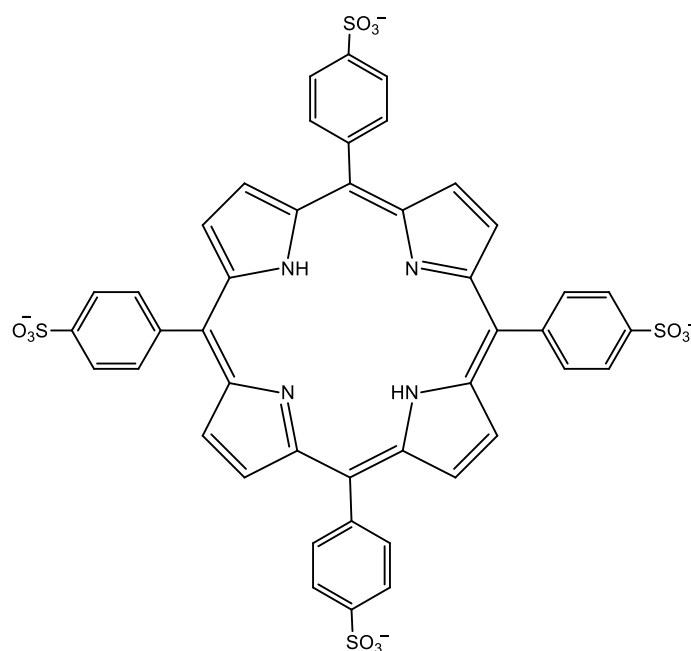
Figure 1.8: Structure of 5,10,15,20-tetrakis-(p-sulfonatophenyl) porphinate.[34]

The possibility of using iron has been discussed as a transition metal with potential to be used as a contrast agent for MRI.[36] Despite Fe(II) and Fe(III) both having unpaired electrons, the difference of one electron is enough to induce a 30-fold smaller molar relaxivity for Fe (II).[37] Superparamagnetic iron oxide (SPIO) nanoparticles have allowed MRI to make great advances in studying gene delivery, cell tracking, drug delivery, tumour diagnosis, and many other applications (Figure 1.9).[37,38] Another way to obtain excellent MR contrast effects is to utilize hollow oxide nanoparticles. Hollow nanoparticles are drawing great attention because of their wide range of applications including catalysis, nanoelectronics, photonics, drug delivery systems, nanoreactors, lubrication, and chemical storage.[39,40] Nontoxic cleaved iron oxide nanoparticles (CIONPs) from hydrophobic FeO nanoparticles (HIONPs) are made in three steps: surface coating with PEG-phospholipid, oxidation under water, and removal of the FeO phase with acidic buffer (Figure 1.9). With their complex surface structure, the CIONPs demonstrated better R_2 relaxivities than HIONPs. The CIONPs have potential for use as delivery vehicles for drugs or active ingredient because of their cleaved spheres. [41,42,43]
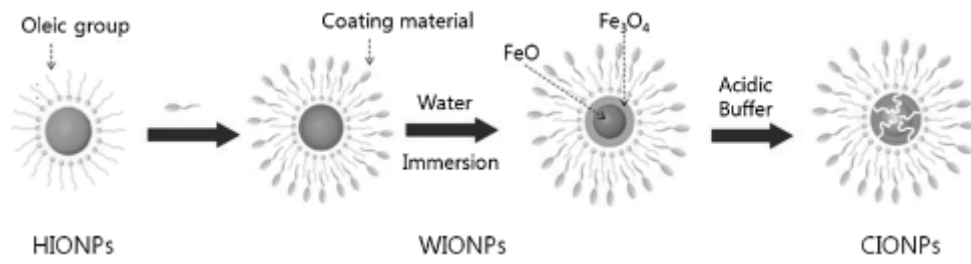
Figure 1.9: Schematic of the method used to prepare the iron oxide nanoparticle contrast agents.[41]

1.5 Redox sensitive contrast agents – the requirements

In order to develop a contrast agent capable of sensing oxidative stress, there are a number of properties which must first be considered:

Redox sensitivity: A redox active metal must be used that has at least two available oxidation states, so that it can locate and quantify oxidants *in vivo.*

Redox potential: The complex should have a redox potential value that matches those found for biologically relevant oxidants (~1.2 V vs. Normal Hydrogen Electrode (NHE)).[44]

Geometry and magnetism: The complex should be introduced into the body in its reduced form and, once oxidised, should become paramagnetic to effect the change in the MRI. Hence this ligand should be able to accommodate different geometries and be able to adjust to a change in metal character (hard & soft) when required.

Aqueous solubility: The complex must be soluble in aqueous media in both its oxidised and reduced forms and be stable at physiological pH.

Chemical stability: The metal centre must be effectively restrained by the ligand system to avoid harming the patient via metal poisoning.

Previous studies have attempted to optimise these factors in such a way that the potential of redox active contrast agents can be demonstrated.[45,46]

1.5.1 Choice of Metal

As previously discussed, gadolinium based contrast agents are the best and most commonly used contrast agents. However, they would not be suitable for the detection of inflammatory disease as gadolinium itself is not redox active.

Previous work at Strathclyde University has identified copper as a potentially suitable metal.[46] It has two common oxidation states. The observation that the lower oxidation state is diamagnetic and the higher oxidation state paramagnetic is of significance. This makes it ideal for the purpose outline above. Unfortunately copper (II) only has 1 unpaired electron. However, its rate of ligand exchange (Table 1.2) is comparable to Gadolinium (1×10^9 s^{-1}) and its dominant isotopes are quadropolar (I=3/2).
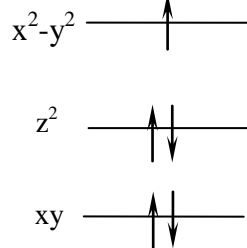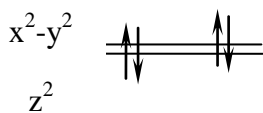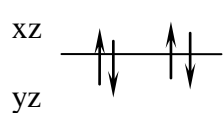
Property	Copper Complex	
Oxidation State	+1	+2
Magnetism	Diamagnetic	Paramagnetic
d-electron configuration	10	9
Geometry	Tetrahedral Cu(I)	Distorted Square Planar Cu(II)
Orbital Splitting		

Table 1.2: Properties of copper (I) and copper (II) complexes.

Copper complexes can exist in two oxidation states. When in the lower oxidation state, d^{10}-Cu(I) has no unpaired electrons (diamagnetic) and generally adopts a tetrahedral geometry. Conversely, when in the higher oxidation state, d^9- Cu (II) features an unpaired electron (paramagnetic) and has a distorted planar geometry. These properties suggest that there is potential to develop a copper contrast agent that when administered in the diamagnetic form, will oxidise when it reaches the area of oxidative stress and enhance MRI accordingly.

1.5.2 Ligand Design

Previous work has indicated that the copper should be complexed to a macrocyclic ligand. A macrocycle is a cyclic molecule constructed of three or more donor atoms in a ring of at least nine atoms.[45,46] It is generally found that complexes with multidentate ligands are more stable than complexes containing the same number of equivalent monodentate ligands, and that macrocycles are, in turn, more thermodynamically and kinetically stable than their related acyclic counterparts. This theory is known as the macrocyclic effect. A macrocycle core also provides a structure to which additional functionality may be incorporated.[47]

Initial studies concentrated on developing an open chain tetradentate Schiff base ligand (Figure 1.10). These studies on donor types identified the N_2S_2 donor set to be the most appropriate (appendix 1). Although these open chain complexes showed promise with regard to redox activity, the presence of the imine meant that they were hydrolytically unstable. The open chain was converted into a ring by connecting the sulfurs with a second alkyl chain.[45] This series of compounds were used to study ring size. These studies demonstrated that ring size between 14 and 18 atoms formed the most stable metal complexes. Although the complexes displayed enhanced stability via the macrocyclic effect, the ligands remained unstable to hydrolysis. Consequently, the imine was reduced to give the current macrocyclic motif (Figure 1.10). [48]
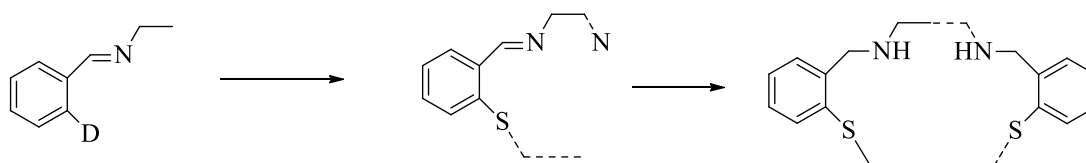
Figure 1.10: Progression in ligand design. Open Schiff base ligands, macrocyclic Schiff base ligands, reduced Schiff base macrocycles. D = O, N ,S.

1.6 Previous Work

In this study the macrocyclic complexes prepared previously will be tested as possible contrast agents. For the reasons briefly discussed above our attention was focussed on a series of cyclic amine-thioether copper complexes. A number of these complexes have been characterised in earlier studies (Figure 1.11).[49,50]
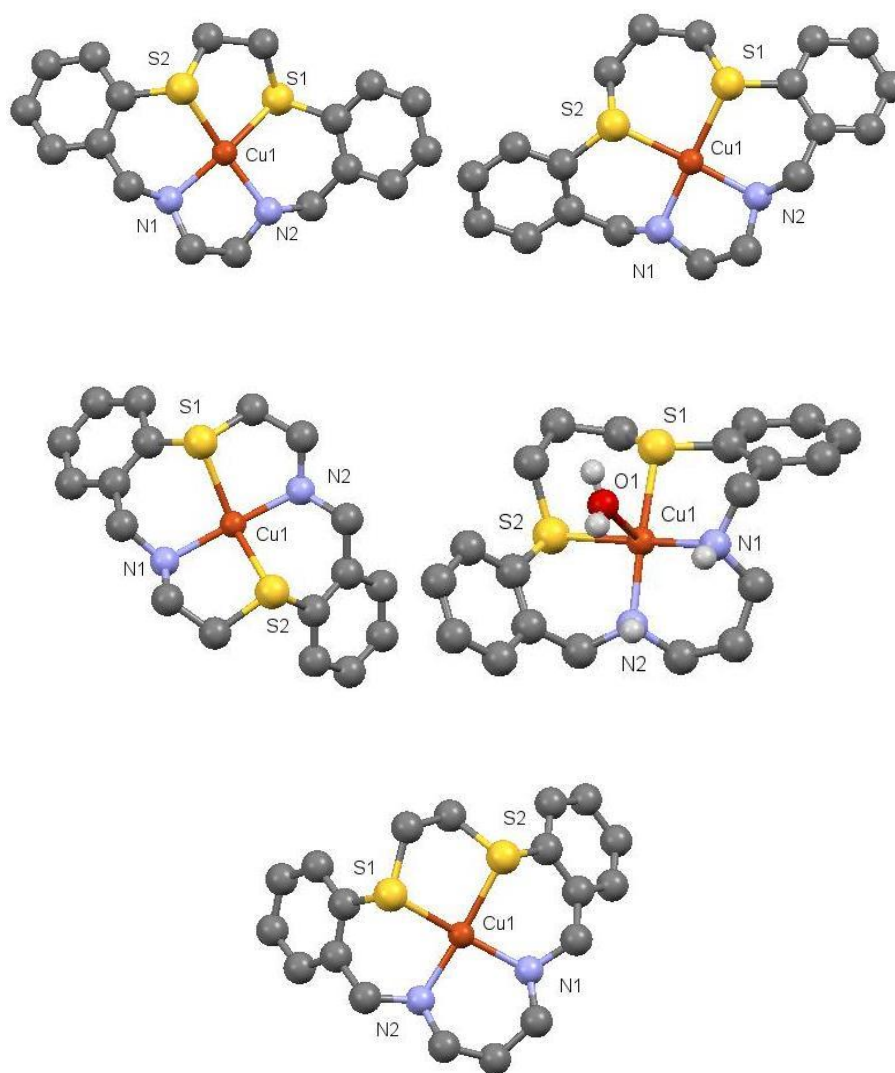
Figure 1.11: The X-ray crystal stuctures of Cu(II) complexes **1** (top left), **2** (top right), **3** (middle left), **4** (H_2O) (middle right) and **5** (bottom).[49,50] (Refer to glossary for full structures and names).The coordinated water on **4** demonstrates the potential mechanism for relaxation. For clarity only the hydrogen atoms on the amine and water functionalities are shown.

The properties and behaviour of the copper macrocycles are important for the evolution of a copper based contrast agent. As such a series of stability tests were carried out on the above cyclic amine-thioether copper (II) complexes.[48,49] The current compounds were all isolated in their copper (II) form and as such the study of their redox behaviour was conducted in reverse. The complexes were firstly challenged with biologically relevant reducing agents e.g. ascorbic acid (Vitamin C), glutathione and α-tocopherol (Vitamin E). Figure 1.12 shows the reaction profile of the family of copper (II) macrocycles when challenged with ascorbic acid.
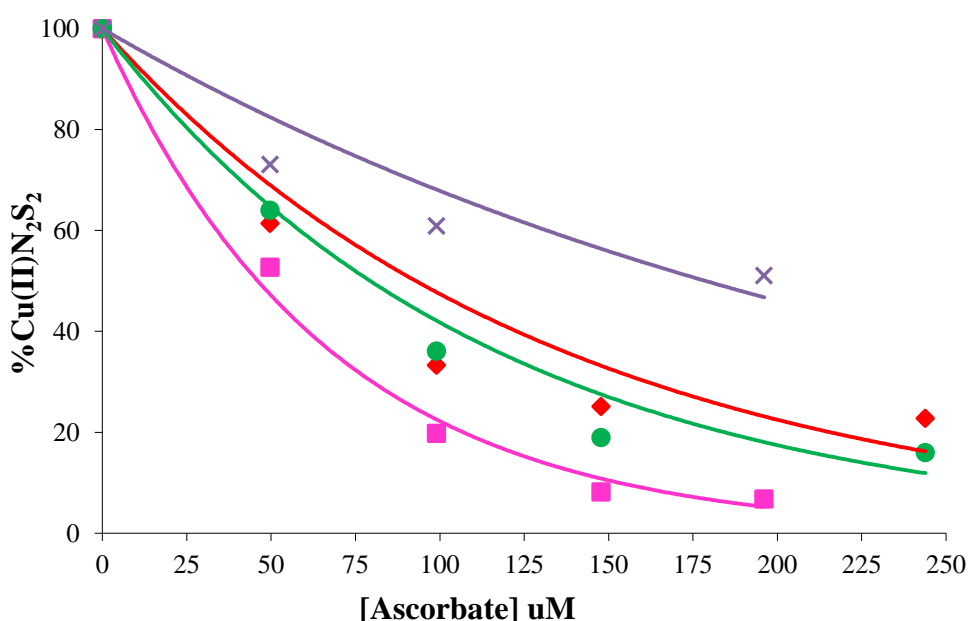
Figure 1.12: The ascorbate reduction of $[CuH_4N_2S_2]^{2+}$ under physiological conditions (Tris buffer at pH 7.4, 0.1 M NaCl).[51] ♦, **1**; ■, **2**; x, **3**; •, **4**.

The results indicated that despite the similarity in the coordination sphere of the copper there was wide variation in the performance of the complexes. From the above graph it is clear that **2** is most effectively reduced by ascorbic acid. Similar results were obtained using glutathione. The studies using vitamin E were conducted in DMSO to mimic the hydrophobic regions of the body. This species is also a good reducing agent. The complex which performed best in this study was **2**.

23

The compounds were then reduced with ascorbate and re-oxidised with sodium hypochlorite. Sodium hypochlorite is the most powerful biologically relevant oxidising agent and it is produced by neutrophils during inflammatory response.[3]

From the results in Figure 1.13 it can be seen that all of the complexes are re-oxidised when reacted with sodium hypochlorite but no complex is oxidised back to 100% copper (II). The highest percentage of reoxidation was only 60%. An excess of sodium hypochlorite was added and the oxidation was not improved. After 800 μM the complexes started to show signs of degradation, suggesting the demetallation of the complexes.
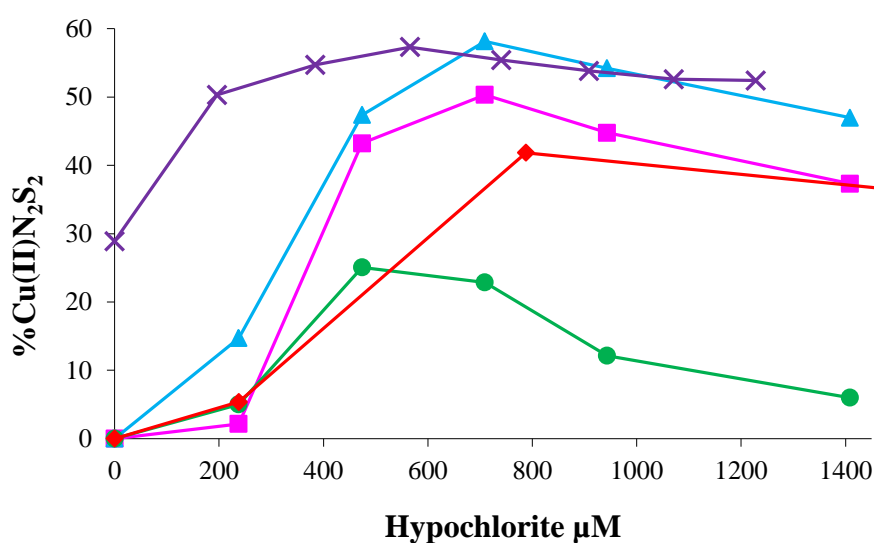
Figure 1.13: The oxidation of copper (I) macrocyclic complexes.[51] ♦, **1**; x, **2** ; • **3** ; ■, **4** ; ▲, **5**.

Overall oxidation of the compounds from copper (I) to copper (II) is poor. It is neither stoichiometric nor is the mass balance good. Mass spectrometry suggested that the ligand was being oxidised and that this led to demetallation of the complex.

The stability of the complexes to sequestration agents such as ethylenediaminetetraacetic acid (EDTA) and bovine serum albumin (BSA) was tested to evaluate the propensity for the metal to migrate from the ligand to complex biological species. If the copper is easily removed the complex will no longer function as a contrast agent. The complex is also likely to be toxic. When challenged with BSA all of the compounds showed evidence that the copper was

migrating from the macrocycle to the protein (Figure 1.14). None of the complexes are stable in the presence of BSA and this suggests that none of these complexes are currently stable enough to be used as contrast reagents within the body. A similar graph was obtained when the complexes were tested with EDTA.[51]
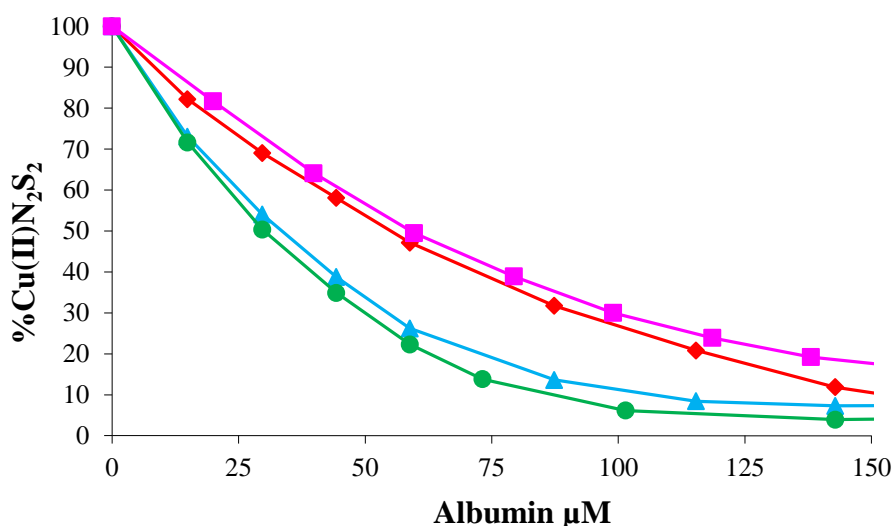
Figure 1.14: The treatment of the copper(II) macrocyclic complexes with BSA[51] ♦, **1**; ■, **2** ; •, **4** ; ▲, **5**.

The electrochemical behaviour of the family of N_2S_2 macrocycles was studied (Table 3) and the potentials were found to vary between 0.77 and 0.96 V vs. Normal Hydrogen Electrode (NHE). This is too low a potential for the complex to be reduced to copper (I) it is believed that an optimum potential would be between 1.20 and 1.50V vs. NHE.

Compound	Ring size	Potential vs. NHE Water (V)	MeCN (V)
1	14	0.79	0.97
2	15	0.77	0.85
3	14	n/a	0.81
4	16	0.82	0.85
5	15	0.96	0.65

Table 1.3: Electrochemical data for the copper macrocycles obtained previously. The *cis/trans* $Cu[(H_4N_{xx}S_{yy})]^{n+}{}_{.n}BF_4$ complexes were analysed in acetonitrile (0.1 M $^tBu_4NBF_4$: Potentials recorded vs. Ferrocene at 100 mV/s)[49] and water (0.1 NaCl: Potentials recorded vs. $[Fe(CN)_6]^{3-}$ at 100 mV/s)$^{-1}$. The *trans*-amine macrocycles were not sufficiently soluble in water for analysis, and were only analysed in acetonitrile. Data adapted from Trotter *et al.* 2010.[49] The values for the complexes are expressed relative to the normal hydrogen electrode (NHE).

The studies on the simple macrocycles indicated that there remained problems with the oxidation from copper (I) to copper (II) (Figure 1.13) and stability to proteins (figure 1.14). Both of these issues could be addressed by introducing additional donors. This could be achieved by attaching pendant arm donors to the macrocyclic framework at the secondary amines (figure 1.15). In the studies discussed above the complex, **2**, showed the most promise and it was the one identified for this modification. Modifications of this type have been reported by Bentfeld *et al.* using related macrocycles.[50]
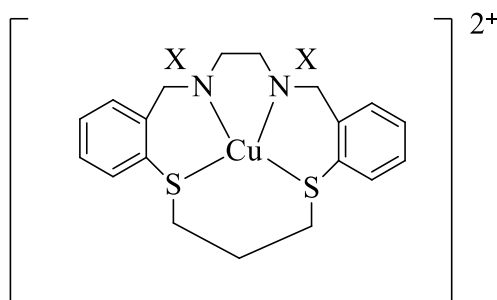
Figure 1.15: **2** with N-substitution of various pendant arms denoted by 'X' (X= $(CH_2)_nOH$ (n=2, 3), CH_2COOH).[50,51]

1.7 Aims

From studies so far, it is clear that there remain a number of obstacles to the use of copper macrocyclic compounds as contrast agents. These issues include poor redox behaviour (Figure 1.13, Table 1.3) and the lack of stability (Figure 1.14). It is however clear that it should be possible to design a copper complex which can function as an imaging agent due to its potential to redox cycle and its rate of ligand exchange equalling that of gadolinium. Consequently it has been decided to modify the parent macrocycle to improve solubility, stability and redox behaviour. There are several ways to possibly achieve this. In chapter 2 the complex has been modified to include the addition of alcohol and acetate pendant arms. The pendant arms on the macrocycles could also be modified to include a soft donor centre.

In chapter 3 electron withdrawing groups and bulky electron donating groups are introduced at various positions on the macrocycle (between the nitrogen donor atoms, between the sulfur donor atoms and on the aryl groups) to increase torsional strain in the alkyl links. This is designed to favour tetrahedral geometry and hence copper (I).

In chapter 4 softer donor systems are synthesised. Instead of the N_2S_2 system, S_4 and S_3N macrocycles are synthesised, this is also designed to promote Cu (I) formation.

In chapter 5 N_2S_2 complexes with pendant arms at the nitrogen donor position are revisited. Softer sulfur pendant arm complexes are synthesised to combat the issues with reversibility seen in chapter 2 with the oxo-based pendant arm species.

1.8 References

1. Spickett, C. M.; Smith, W. E.; Reglinski, J., *Advances in Spectroscopy: Biomedical Applications of Spectroscopy*, Vol. 25, John Wiley & Sons Ltd, Chichester, **1996**.

2. MacDonald, J.; Galley, H. F.; Webster, N. R., *British Journal of Anaesthesia*, **2003**, *90*, 221-232.

3. Pocock, G.; Richards C. D., *Human physiology: The basis of medicine*, 3 ed.; Oxford press, Oxford, **2006**.

4. Taylor, J., *Imaging in radiotherapy*, Vol. 10, Oxford press, Oxford, **1988**.

5. Weissleder,R.; Wittenberg J. W.; Harisinghani, M.G., *Primer in diagnostic imaging*, Vol. 5, Elsevier Mosby, Missouri, **2011**.

6. Webb, A., *Introduction to biomedical imaging*, John Wiley & Sons Inc, Illinois, **1995**.

7. Cotton, S., *Lanthanide and Actinide chemistry*, John Wiley & Sons Ltd, Chichester, **2006**.

8. Kaltsoyannis. N.; Scott. P., *The f elements*, Oxford University Press Inc, New York, **1999**.

9. Hieronimus, S.; Bernard, J. L.; Chevallier, P.; Chevallier, A.; Chyderiotis, G.; Fenichel, P.; Landraud, L., *Annales D Endocrinologie*, **2007**, *68*, 191-195.

10. Saeidnia, S.; Abdollahi, M., *Toxicology and Applied Pharmacology*, **2013**, *271*, 49-63.

11. Song, B.; Wu, Y. K.; Yu, M. X.; Zhao, P. Y.; Zhou, C.; Kiefer, G. E.; Sherry, A. D., *Dalton Transactions*, **2013**, *42*, 8066-8069.

12. Kattel, K.; Park, J. Y.; Xu, W.; Kim, H. G.; Lee, E. J.; Bony, B. A.; Heo, W. C.; Jin, S.; Baeck, J. S.; Chang, Y.; Kim, T. J.; Bae, J. E.; Chae, K. S.; Lee, G. H., *Biomaterials*, **2012**, *33*, 3254-3261.

13. Wilson, G. S.; Johnson, M. A., *Chemical Reviews*, **2008**, *108*, 2462-2481.

14. Dubost, J. P.; Leger, J. M.; Langlois, M. H.; Meyer, D.; Schaefer, M., *Comptes Rendus De L Academie Des Sciences Serie II*, **1991**, *312*, 349-354.

15. Botta, M., *European Journal of Inorganic Chemistry*, **2000**, *3*, 399-407.

16. Gianolio, E.; Porto, S.; Napolitano, R.; Baroni, S.; Giovenzana, G. B.; Aime, S., *Inorganic Chemistry*, **2012**, *51*, 7210-7217.

17. Jindal, A. K.; Merritt, M. E.; Suh, E. H.; Malloy, C. R.; Sherry, A. D.; Kovács, Z., *Journal of the American Chemical Society* **2010**, *132*, 1784-1785.

18. Løkling, K. E.; Fossheim, S. L.; Skurtveit, R.; Bjørnerud, A.; Klaveness, J., *Magnetic Resonance Imaging*, **2001**, *19*, 731-738.

19. Brown, J. M.; William, W. R., *Nature Reviews Cancer*, **2004**, *4*, 437-447.

20. Iwaki, S.; Hanaoka, K.; Piao, W.; Komatsu, T.; Ueno, T.; Terai, T.; Nagano, T., *Bioorganic & Medicinal Chemistry Letters*, **2012**, *22*, 2798-2802.

21. Major, J. L.; Parigi, G.; Luchinat, C.; Meade, T. J., *Proceedings of the National Academy of Sciences of the United States of America*, **2007**, *104*, 13881-13886.

22. Kasala, D.; Lin, T. S.; Chen, C. Y.; Liu, G. C.; Kao, C. L.; Cheng, T. L.; Wang, Y. M., *Dalton Transactions*, **2011**, *40*, 5018-5025.

23. Que, E. L.; New, E. J.; Chang, C. J., *Chemical Science*, **2012**, *3*, 1829-1834.

24. Auld, D. S., *Biometals*, **2009**, *22*, 141-148.

25. Lee, E. J.; Heo, W. C.; Park, J. W.; Chang, Y.; Bae, J. E.; Chae, K. S.; Kim, T. J.; Park, J. A.; Lee, G. H., *European Journal of Inorganic Chemistry*, **2013**, *16*, 2858-2866.

26. Woods, M.; Woessner, D. E.; Sherry, D. A., *Chemical Society Reviews*, **2006**, *35*, 500-511.

27. Liu, G. S.; Ali, M. M.; Yoo, B.; Griswold, M. A.; Tkach, J. A.; Pagel, M. D., *Magnetic Resonance in Medicine*, **2009**, *61*, 399-408.

28. Armitage, F. E.; Richardson, D. E.; Li, K. C. P., *Bioconjugate Chemistry*, **1990**, *1*, 365-374.

29. Kitajima, K.; Maeda, T.; Watanabe, S.; Ueno, Y.; Sugimura, K., *International Journal of Urology*, **2012**, *19*, 806-811.

30. Kueny-Stotz, M.; Garofalo, A.; Felder-Flesch, D., *European Journal of Inorganic Chemistry*, **2012**, *12*, 1987-2005.

31. Huang, Y.; Zhang, X.; Zhang, Q.; Dai, X.; Wu, J., *Magnetic Resonance Imaging*, **2011**, *29*, 554-560.

32. Hernandez, G.; Bryant, R. G., *Bioconjugate Chemistry*, **1991**, *2*, 394-397.

33. Aime, S.; Botta, M.; Gianolio, E.; Terreno, E., *Angewandte Chemie-International Edition*, **2000**, *39*, 747-750.

34. Bryant, L. H.; Hodges, M. W.; Bryant, R. G., *Inorganic Chemistry*, **1999**, *38*, 1002-1005.

35. Berg, K.; Bommer, J. C.; Winkelman, J. W.; Moan, J., *Photochemistry and Photobiology*, **1990**, *52*, 775-781.

36. Lacroix, L. M.; Delpech, F.; Nayral, C.; Lachaize, S.; Chaudret, B., *Interface Focus*, **2013**, *3*, 1-19.

37. Chertok, B.; Moffat, B. A.; David, A. E.; Yu, F.; Bergemann, C.; Ross, B. D.; Yang, V. C., *Biomaterials*, **2008**, *29*, 487-496.

38. Nasongkla, N.; Bey, E.; Ren, J.; Ai, H.; Khemtong, C.; Guthi, J. S.; Chin, S. F.; Sherry, A. D.; Boothman, D. A.; Gao, J., *Nano Letters*, **2006**, *6*, 2427-2430.

39. Bulte, J. W. M.; Douglas, T.; Witwer, B.; Zhang, S. C.; Strable, E.; Lewis, B. K.; Zywicke, H.; Miller, B.; van Gelderen, P.; Moskowitz, B. M.; Duncan, I. D.; Frank, J. A., *Nature Biotechnology*, **2001**, *19*, 1141-1147.

40. Liang, H. P.; Zhang, H. M.; Hu, J. S.; Guo, Y. G.; Wan, L. J.; Bai, C. L., *Angewandte Chemie-International Edition*, **2004**, *43*, 1540-1543.

41. Jeon, S. L.; Chae, M. K.; Jang, E. J.; Lee, C., *Chemistry European Journal*, **2013**, *19*, 4217-4222.

42. Lee, J.; Kim, H.; Kim, S.; Lee, H.; Kim, J.; Park, H. J.; Choi, E. K.; Lee, J. S.; Kim, C., *Journal of Materials Chemistry*, **2012**, *22*, 14061-14067.

43. Shkinyy, A.; Munnier, E.; Herve, K.; Souce, M.; Benoit, R.; Cohen-Jonathan, S.; Limelette, P.; Saboung, M. L.; Dubois, P.; Chourpa, I., *Journal of Physical Chemistry*, **2010**, *114*, 5850-5858.

44. Hermann, P.; Kotek, J.; Kubicek, V.; Lukes, I., *Dalton Transactions*, **2008**, 3027-3047.

45. Taylor, M. K.; Trotter, K. D.; Reglinski, J.; Berlouis, L. E. A.; Kennedy, A. R.; Spickett, C. M.; Sowden, R. J., *Inorganica Chimica Acta*, **2008**, *361*, 2851-2862.

46. Smith, D., *Metal complexes for the diagnosis of inflammatory disease*, University of Strathclyde, **2009**.

47. Constable, E. C., *Coordination Chemistry of Macrocyclic Compounds*, Oxford University Press, Oxford, **1999**.

48. Trotter, K. D.; Taylor, M. K.; Forgie, J. C.; Reglinski, J.; Berlouis, L. E. A.; Kennedy, A. R.; Spickett, C. M.; Sowden, R. J., *Inorganica Chimica Acta*, **2010**, *363*, 1529-1538.

49. Trotter, K. D.; Reglinski, J.; Robertson, K.; Forgie, J. C.; Parkinson, J. A.; Kennedy, A. R.; Armstrong, D. R.; Sowden, R. J.; Spickett, C. M., *Inorganica Chimica Acta*, **2009**, *362*, 4065-4072.

50. Bentfeld, R.; Ehlers, N.; Mattes, R., *Chemische Berichte*, **1995**, *128*, 1199-1205.

51. Sowden, R. J.; Trotter, K. D.; Dunbar, L.; Craig, G.; Erdemli, O.; Spickett, C. M.; Reglinski, J., *Biometals*, **2013**, *26*, 85-96.

Chapter 2

Copper macrocycles as putative imaging agents

2.1 Introduction

A series of copper macrocycles have been synthesised previously at Strathclyde University (chapter 1, Figure 1.11).[1,2,3] These compounds were designed to form the basis of a redox active MRI contrast agent. The redox properties and redox potentials of these species have been studied to assess their ability to respond to changes in oxidant flux. Stability studies were also conducted which show that the copper centre is removed from these macrocycles when challenged by ethylenediaminetetraacetic acid (EDTA) or bovine serum albumin (BSA).[1] These studies suggest that a further refinement in the design is required. In an attempt to increase the stability of these complexes, it was decided to extend the study and investigate the addition of pendant arms at the secondary amines (Figure 2.1). From previous work, **2** (chapter 1, Figure 1.11) was identified as being the complex which showed the most promise and consequently it was decided to focus our attention on this species.[2] Preliminary studies at Strathclyde on pendant arm complexes have been carried out and while these studies demonstrate that it was possible to attach ethanol and propanol pendant arms at the secondary amines (X = $-(CH_2)_nOH$, n = 2, 3, Figure 2.1) these complexes have not been fully characterised. As such these compounds are to be re-prepared and characterised. The range of pendant arm macrocycles was expanded to include butanol, hexanol, carboxylic acid ($-CH_2COOH$) and amine groups ($-CH_2CH_2NH_2$). The stability of the pendant arm complexes was measured against BSA to test for an increase in stability.
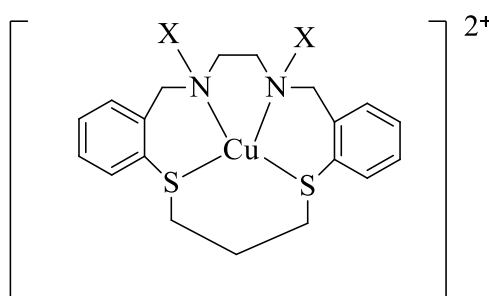
Figure 2.1: A schematic representation of **2** modified at the secondary amine, where X = $-(CH_2)_nOH$ (n= 2, 3, 4, 6), CH_2COOH and $CH_2CH_2NH_2$.

The macrocycles shown in chapter 1 (Figure 1.11), form the basis of the paramagnetic reporting centre of a copper based redox active imaging agent. Preliminary studies have

sought to explore the relaxivity of these species in comparison with that of Gd(DTPA) and copper tetrafluoroborate ($Cu(BF_4)_2$). The former is included here as it demonstrates the maximal relaxivity possible for a contrast agent and the latter is used to demonstrate the maximal effect that can be expected from copper. It should be noted that $Cu(BF_4)_2$ contains 4-6 water binding sites and the macrocycles designed here are limited to only one or two free coordination sites. Thus the performance of our complexes cannot be expected to match that of $Cu(BF_4)_2$. Our compounds fall into two categories i.e. a series of simple rings where only the ring size changes (Figure 1.11) and a series of compounds which include pendant arms which carry additional donor atoms (Figure 2.1). There is concern that to gain additional stability it is necessary to increase the coordination number of the copper from four to five and that, in turn, this will compromise relaxivity. A comparison of the data obtained from these two series of compounds will clarify this point.

2.2 Results and Discussion

2.2.1 Synthesis of pendant arm macrocycles and their copper complexes
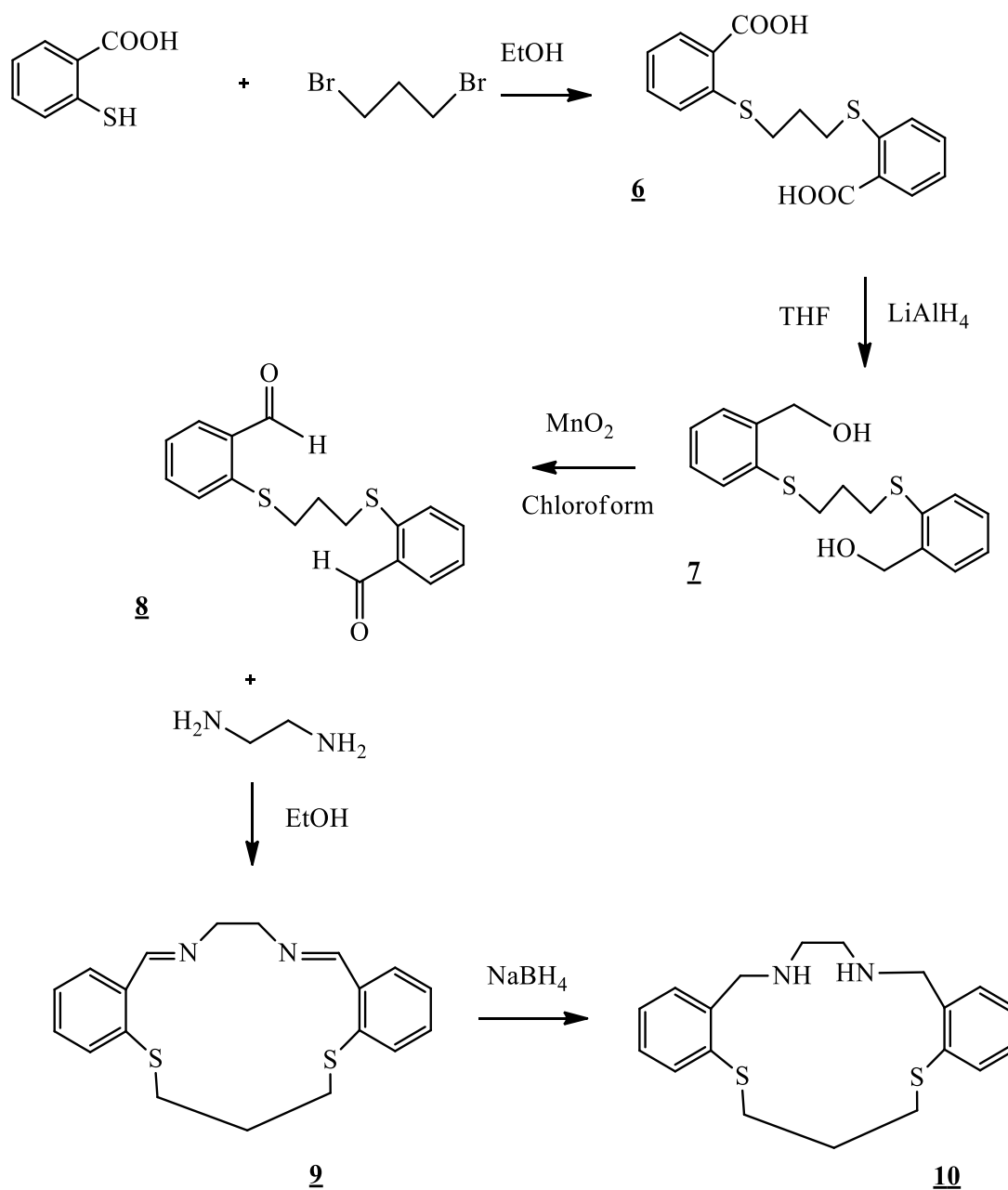
Figure.2.2: A brief schematic of the synthesis of **10**.

Previous studies on the simple macrocycles and their behaviour in oxidation/reduction chemistry and stability had identified **2** as the lead candidate for development. The synthesis of **10**, shown in outline (Figure 2.2), has been discussed extensively in previous work.[2] The

macrocycle **10**, can be produced in good yield allowing for its further modification using various functionalised haloalkanes (Figure 2.3). Typically this modification is achieved in acetonitrile under reflux using Na_2CO_3. The subsequent metal complexes were generated by treating the modified rings with copper (II) tetrafluoroborate in methanol.
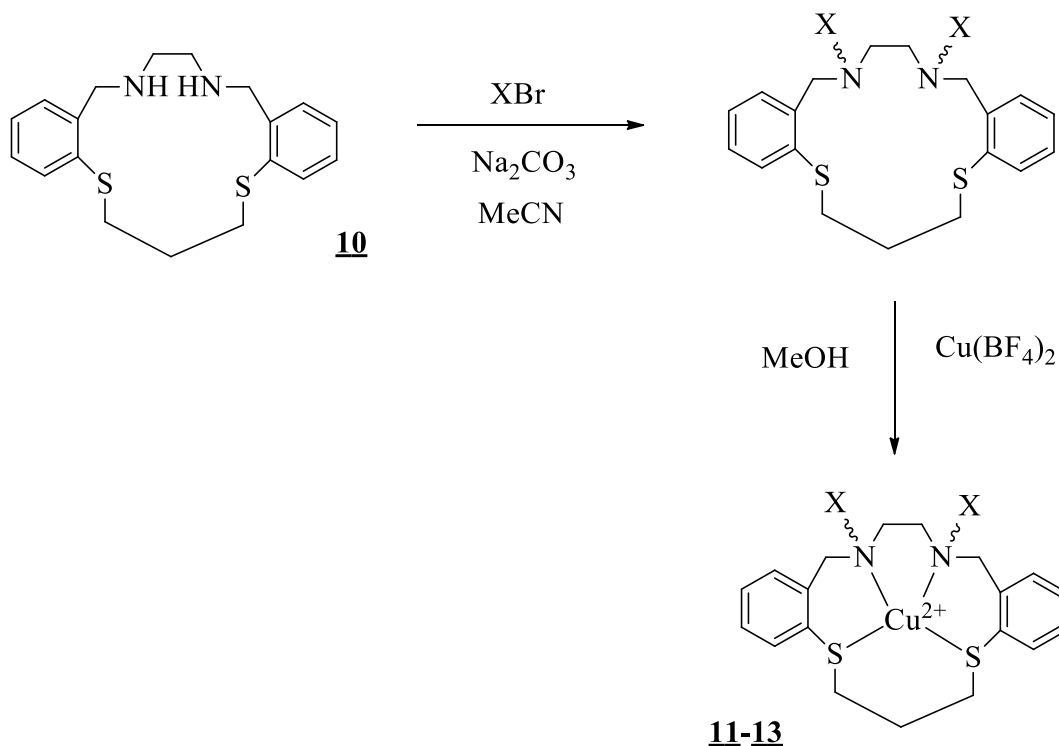
Figure 2.3: Where ∿∿ X= functionalised alkane (-CH_2CH_2OH,-$CH_2CH_2CH_2OH$, -CH_2COOH).

Mass spectrometry and elemental analysis indicated that the coupling of **10** with 2-bromoethylamine to produce a compound with amine pendant arms was unsuccessful and that the pendant arms had failed to attach. Consequently the synthesis of this motif has been abandoned. The materials obtained from the reactions where the pendant arms were a butanol and hexanol moieties produced oily materials, the purity of which could not be guaranteed. As such, they have not been included in the T_1 study. Analysis by ESI-MS and elemental analysis determined that the remaining complexes were sufficiently pure for use in NMR studies. In a previous study Smith et al.[4] was able to crystallographically characterise the propanol substituted complex **11** (Figure 2.4). This shows the complex to be five coordinate with a square pyramidal geometry at copper. The coordinated alcohol remains protonated and the complex remains a salt.
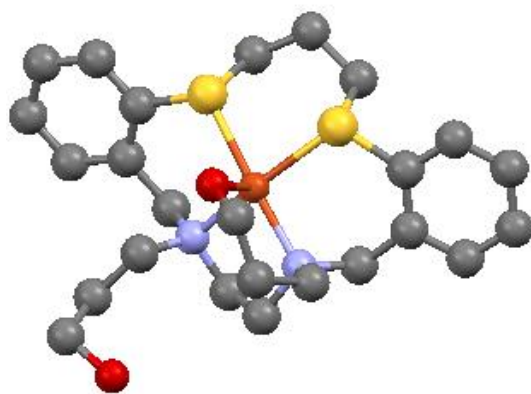
Figure 2.4: The single crystal X-ray structure of **11**. Protons have been omitted for clarity.[5]

We have, thus far, been unsuccessful in structurally characterising the two other species **12** and **13** synthesised here. However, Mattes *et al*. have been successful in structurally characterising species related to **12** and **13** which contain ethanol and carboxylate pendant arms respectively (Figure 2.5).[5,6] In these species the structures contain an ethylene backbone between the sulfur donors and a propylene backbone between the nitrogen donor atoms (the same basic skeletal frame as parent complex **5** (Figure 1.11). Similar to the complex obtained by Smith,[4] the ethanol and carboxylate compounds are a square pyramidal geometry at copper. Crucially all the complexes in this series remain cationic.[5,6] Mercury has drawn formal bonds between the six atoms closest to the copper centre, however the bond lengths suggest that not all of these contacts can be considered to be formal bonds (Table 2.1).
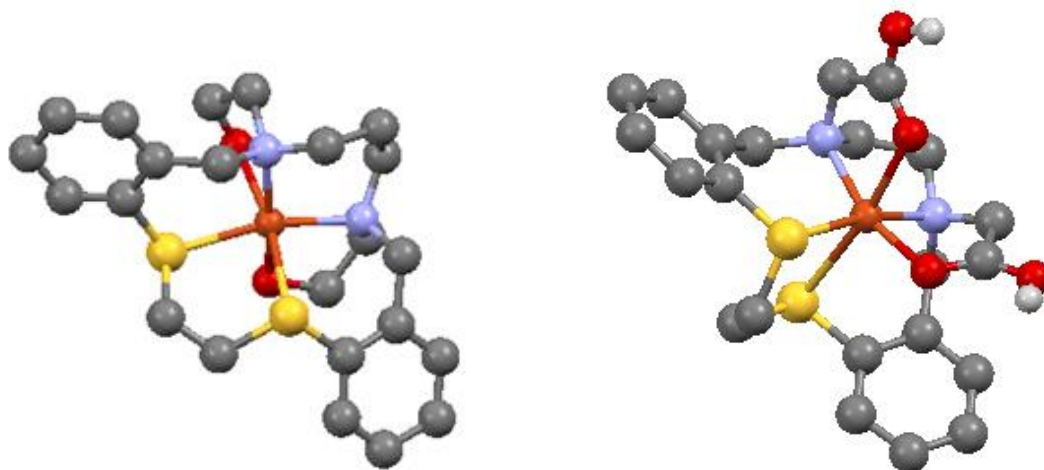
Figure 2.5: The single crystal X-ray structures of species relating to **12** (left) and species relating to **13** (right). Protons have been omitted for clarity.[5,6] No attempt has been made to edit the data set assembled from the data deposited in the CCDC database.

Table 2.1 below gives a comparison of the metrical parameters for the propanol, ethanol and carboxylate substituted complexes.[4,5,6] The relative lengths of the pendant arms can account for the geometries observed. The propanol pendant arms are long enough to allow the oxygen to gain the necessary proximity to formally bond to the copper centre. The resulting square pyramidal structure is highly stable and the macrocycle moves from the meridial plane to accommodate the new donor atom. Consequently, the second pendant arm remains uncoordinated. The resulting U.V-visible spectrum of **11** is typical of a five coordinated Cu(II) complex (Appendix 2). The ethanol pendant arm does not confer as much flexibility and the $Cu-O_1$ and $Cu-S_2$ bond lengths are markedly extended. It is thus likely that the $Cu-O_1$ and $Cu-S_2$ bonds are weaker interactions with a larger electrostatic character. Thus although it has been drawn as a 6 co-ordinate compound, the metric parameters suggest it would be better described as a 5 co-ordinate species. Similar secondary bonding interactions between copper and tetrafluoroborate have been reported for the unsubstituted copper macrocycles discussed above.[6] Finally, the lack of flexibility in the ethanol arms ensures that the macrocycle does not leave the meridial plane and if water exchange occurs a pseudo-sixth coordination site remains available.

Atom Pair	Ethanol	Propanol	Carboxylate
Cu_1-N_1	2.0615(3)	2.0440(2)	2.0029(2)
Cu_1-N_2	2.0736(2)	2.0510(2)	2.0523(3)
Cu_1-O_1	**2.3361**(3)	2.1710(2)	**2.3194**(3)
Cu_1-O_2	1.9925(2)	-	1.9757(4)
Cu_1-S_1	2.3743(3)	2.3442(7)	2.2705(2)
Cu_1-S_2	**2.7050**(3)	2.3487(8)	**2.7004**(3)

Table 2.1: A comparison of the bond lengths (Å) for the three reported copper (II) pendant arm complexes, (**2**(-R)] 2BF$_4$) where R denotes an ethanol, propanol or carboxylic acid pendant arm.[4,5,6] The numbers in bold are distances which are longer than might be expected for a formal bond to copper.

The synthesis of the two series of copper (II) complexes required for relaxation time studies is now sufficiently complete. However, prior to evaluating their potential as contrast agents, it is prudent to interrogate the stability of the pendant arm species when challenged with BSA, reducing agent and oxidising agents.

2.2.2 Compound stability tests

The compounds must be stable *in-vivo* to be used as imaging agents, it is therefore necessary to check their stability under biologically relevant conditions. This work had been carried out previously for the simple copper macrocycles.[1,2,3] From the pendant arm complexes reported here (**11**, **12** and **13**) no differences were observed in the U.V-visible (300-800 nm) and solid reflectance spectra and it would seem that the structures persist in solution. Nor were there any differences between dry and the aqueous samples (1mM, 0.1 M NaCl, 100% D$_2$O) placed in an incubator (37ºC) for a week.

2.2.3 Copper stability of the complexes

Sequestration agent stability tests were carried out on **2** and **11**-**13** using Bovine Serum Albumin (BSA) and the results compared (figure 2.6). As previously reported; as the concentration of BSA increases the charge transfer band (420 nm) derived from **2** decreases,

indicative that the macrocycle is being demetalated. In contrast for the plot obtained from the analogous experiment using **12** it is evident that there is only a marginal (<5%) loss of copper from the macrocycle. As expected the addition of a pendant arm donor has increased in stability of the copper complex. Stability tests using BSA have also been carried out on **11** and **13**. They showed similar increases in stability over the parent macrocycle **2**. These can be found in Appendix 2.
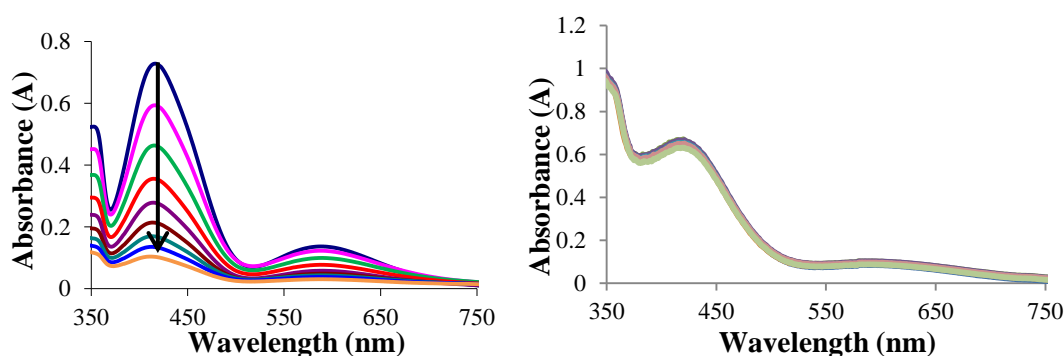
Figure 2.6: Plot of stability test of **2** (0.3 mM) (left) and **12** (0.3 mM) (right) with BSA (199mg, 1 ml) in Tris-buffer (5 mM, pH 7.4). In the stability test of compound **2** the top spectrum shows the original position of the complex prior to the addition of BSA and the bottom spectrum shows the complex after copper sequestration. Each line indicates the addition of a 5 µl aliquot of BSA. No change is observed in the spectra for compound **12** suggesting the copper is stable in the macrocycle. The band structures in the two complexes are different due to the different geometries adopted by the two complexes (planar/octahedral and square pyramidal).

2.2.4 Reduction potential of the complexes

It was necessary to test the effect of naturally occurring reducing agents (e.g. ascorbic acid) found *in-vivo* on the complexes. The parent complex **2** was tested as previously discussed (Chapter 1) as a control. The pendant arm complex **13** was also tested with biologically relevant reducing agent ascorbic acid. As before the reaction is characterised by the change in the charge transfer band at 420nm. It can be seen by the plot below (Figure 2.7) that with each aliquot of ascorbate the complex is reduced. It should be noted that although the addition of pendant arms has affected the macrocycles reduction potential, it has not shifted it

beyond the ability of ascorbate (E° 1.57 vs. NHE)[7] to act as a reducing agent. Again, this plot is typical for the treatment of all the pendant arm complexes (**11** and **12**) with reducing agents and the data for **11** and **12** can be found in Appendix 3.
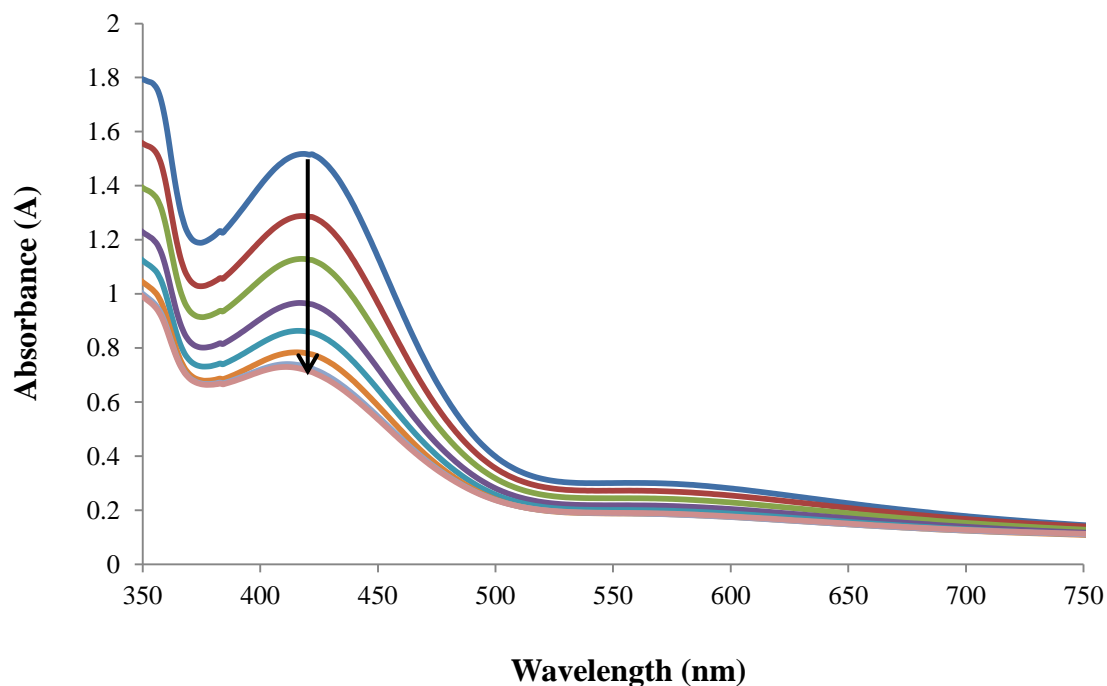
Figure 2.7: The spectrophotometric reduction plot of **13** (0.3 mM) with ascorbic acid (10 mM) in Tris-buffer (5 mM, pH 7.4) a 5 µl aliquot is added. The reduction is characterised by the absorption band at 420 nm. The top spectrum shows the original position of the complex prior to reduction and the bottom spectrum shows the complex after reduction, indicated by the direction of the arrow.

The reduction of the complexes can also be studied using ^{1}H NMR spectroscopy by analysing their effect on the T_1 relaxation time. T_1 affects the line width of the NMR spectra. Broad lines indicate a rapid relaxation and a short T_1 time, whereas narrow lines indicate a slow relaxation and a long T_1 time. Using the $-CH_2-$ resonance of the Tris-HCl buffer in H_2O we can observe the effect on the line width for **11** as the copper is reduced. Therefore line broadening was used to observe the change from paramagnetic Cu(II) to diamagnetic Cu(I) (Figure 2.8) below shows the reduction of **11** with ascorbate by the means of NMR. Seven samples of **11** were treated with an incremental varying concentration of ascorbate (0%, 20%, 40%, 60%, 80%, 100% mol/mol). The seventh spectrum (Figure 2.8 (top)) is a Tris-HCl buffer control (0.1 M NaCl in D_2O). As the copper reduces the line width of the methylene

resonance is seen to narrow. Initially there is a broad signal which equates to contrast on, as the addition of ascorbate increases the line narrows and this equates to contrast off. The study also shows that the process is stoichiometric as equal additions of ascorbate are added to give discrete and stable spectra.
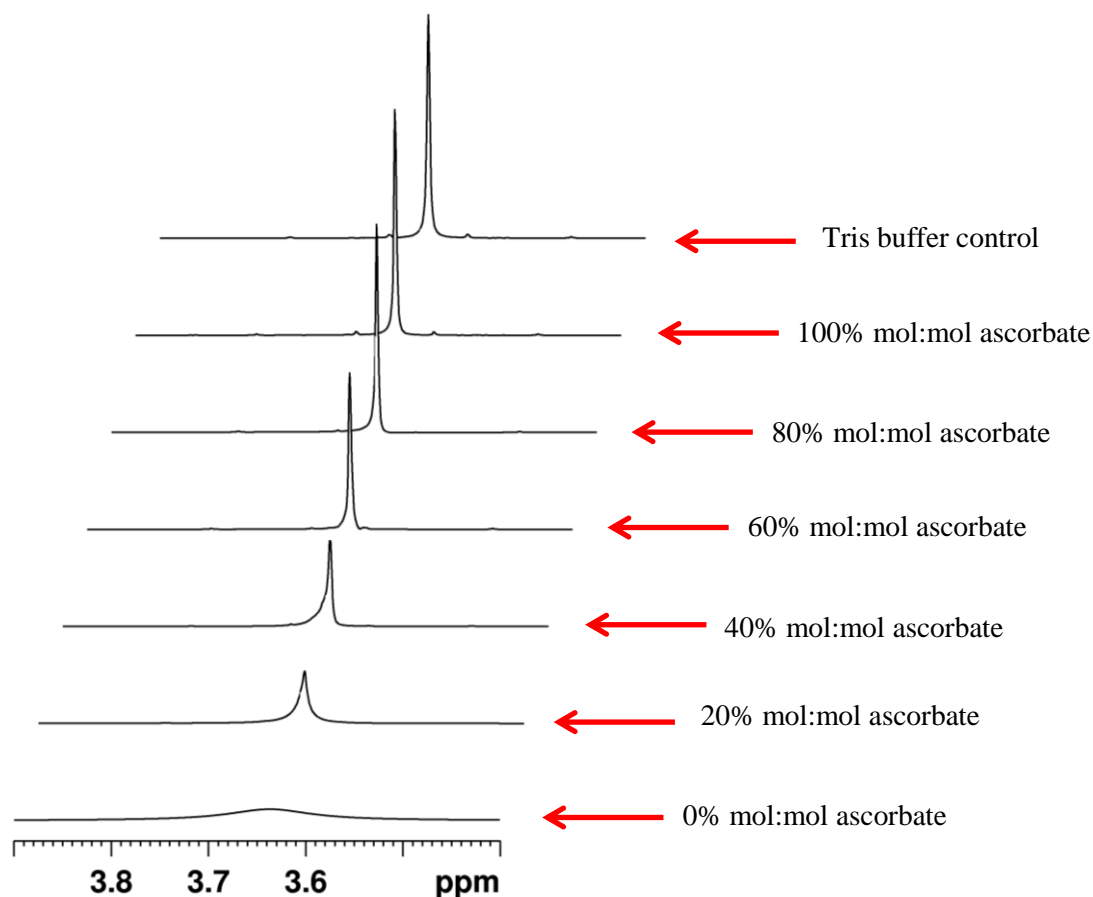
Figure 2.8: Stackplot NMR reduction of **11** stoichiometrically with ascorbate. The lowest peak represents 100% Cu (II) to 0% ascorbate, and highest represents the control Tris-buffer.

2.2.5 Oxidation potential of the complexes

It is important that the complexes synthesised are able to re-oxidise from copper (I) to copper (II) in the presence of biological oxidising agents, such as HOCl. The pendant arm complex **13** was tested using the biologically relevant oxidising agent sodium hypochlorite. Firstly each compound was reduced with ascorbate (Figure 2.8) and then treated with sodium hypochlorite to re-oxidise the complex to back to copper (II). From Figure 2.9 it can be seen

that **13** re-oxidises poorly. Only 22% of the complex is recovered once the redox cycle has been completed. This is typical for all pendant arm complexes, data for compounds **11** and **12** can be found in Appendix 3. Previous studies of the parent complexes have also shown that the compounds perform poorly in the oxidation step.[1]
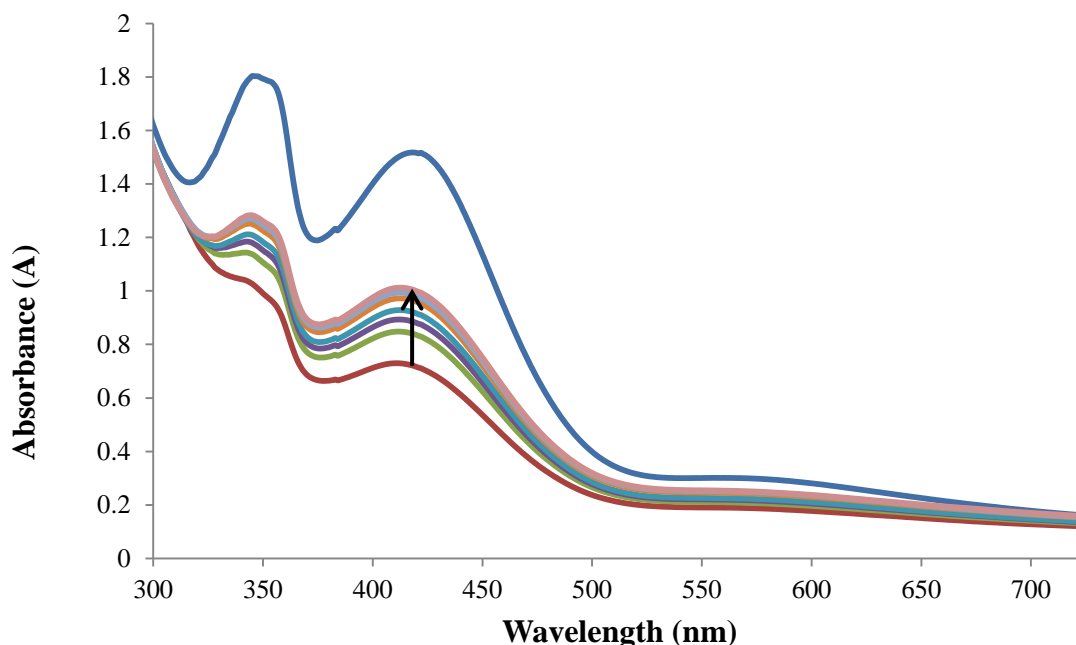
Figure 2.9: The spectrophotometric analysis of HOCl oxidation of **13**, the 100 mM solution hypochlorite in Tris-buffer (5 mM, pH 7.4) was added in 5 µl aliquots. The species being studied was generated *in-situ* using ascorbic acid as the reductant (see Figure 2.7). The top spectrum shows the original position of the complex prior to reduction and the bottom spectrum shows the complex after reduction. The spectra in the middle show the oxidation with hypochlorite as a result of 30 µl additions.

2.2.6 Electrochemistry

Cyclic voltammetry is typically used to estimate the redox potential of the complexes (see Appendix 4). The complexes were prepared as solutions (3 mM) in 0.1 M t-butylammonium tetrafluoroborate ($^tBu_4NBF_4$). This electrolyte was used as the tetrafluoroborate anion is the typical counter-ion in the copper complexes, therefore eliminating any potential exchange reactions. The voltammograms were referenced to the ferrocene/ferrocenium (Fe(III)/Fe (II)) redox couple by running a ferrocene solution under the same conditions as before and the

values for the complexes are expressed relative to the normal hydrogen electrode (NHE).[7] Cyclic voltammetry was carried out on all three species. The E° value for compound **13** was found to be 1.44 V which is within the desired biological range.[4] This is somewhat higher than the values reported for previously characterised non – pendant arm complexes (Chapter 1 Table 1.3).[2,8] It is likely that the coordination chemistry is a major factor here. The copper complexes studied previously adopted a distorted square planar geometry and the pendant arm species now adopt a square pyramidal geometry. During reduction these species will undergo a rearrangement to tetrahedral geometry, requiring a Cu-O bond to sever to satisfy the geometric preferences of copper (I). The cyclic voltammogram of **13** in the positive region is shown below (Figure 2.10) it shows the most promise out of all the complexes and shows signs of some reversibility. This is most likely due to the fact that the acetic acid group on **13** can coordinate more easily to the copper centre. The compound is not 100 % reversible so the electrochemical reversibilty is estimated from the cyclic voltammogram using i_{pc} and i_{pa} which is the peak cathodic and anodic current respectively. Cyclic voltammetry was also carried out on compounds **11** and **12**. Neither **11** nor **12** showed signs of electrochemical reversibility. The evidence in the plots to suggest that oxidation is irreversible in both cases (Figures 2.11 and 2.12).
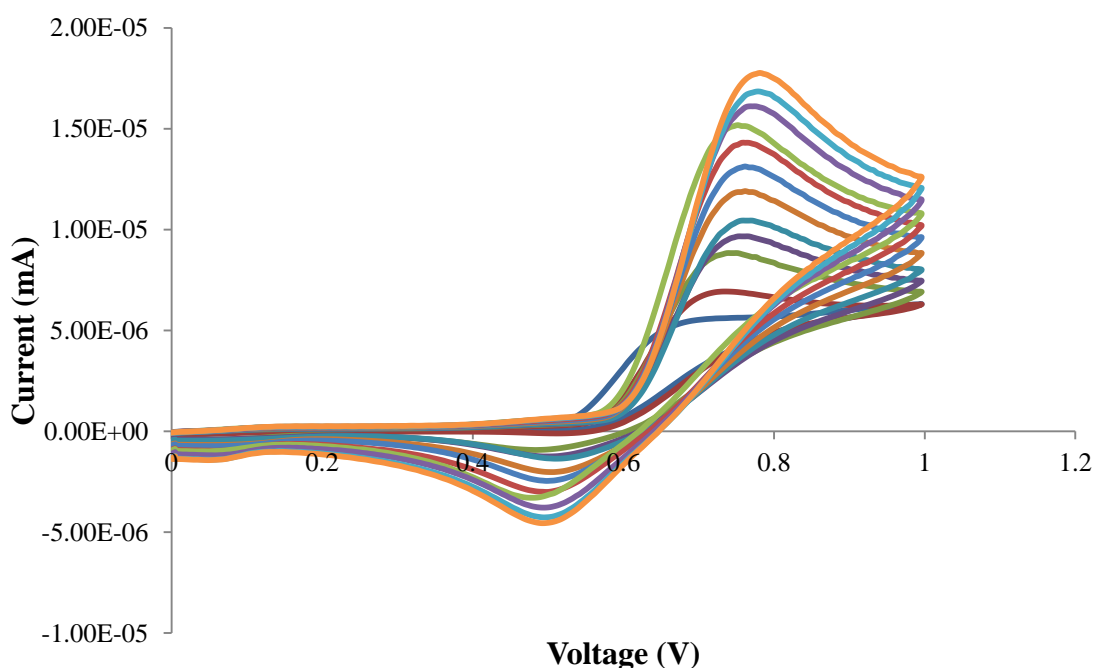
Figure 2.10: Cyclic voltammogram in the positive region of compound **13** in acetonitrile (0.1M ^{t}Bu$_4$NBF$_4$: Potential reported vs. ferrocene) recorded over a scan rate range from 10 mV-200 mVs^{-1}.

The i_{pc} vs. i_{pa} reversibility for compound **13** was calculated from the data points at 0.49V and 0.78V and found to be approximately 25%. This is in good agreement with the data found in section 2.3.4.
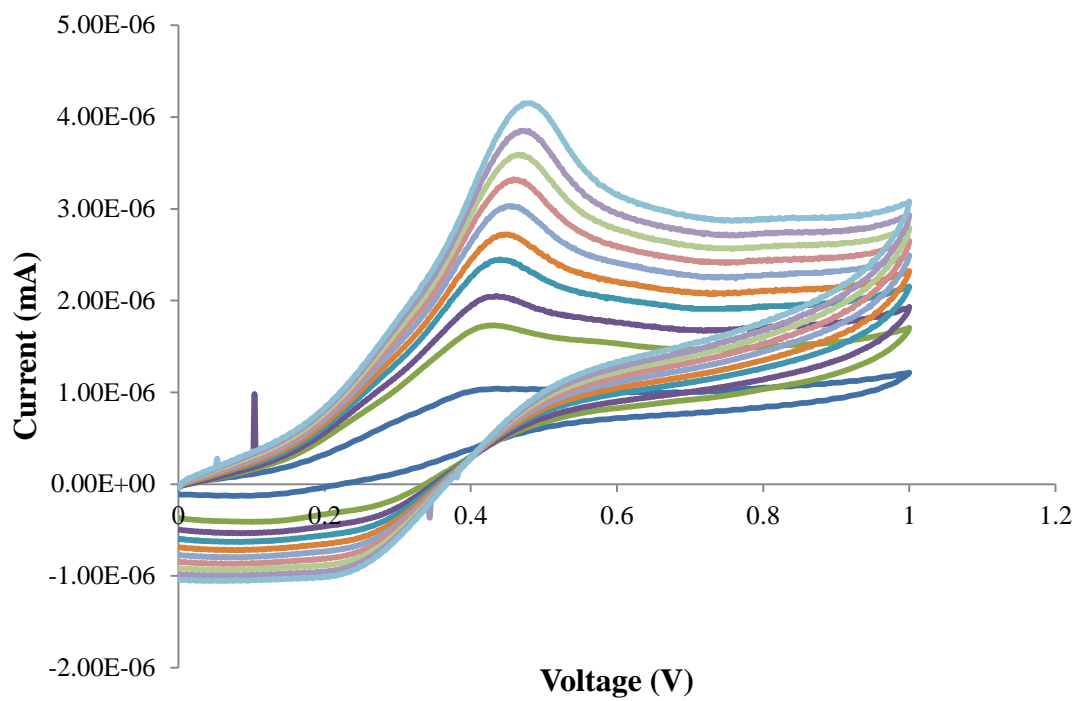
Figure 2.11: Cyclic voltammogram in the positive region of compound **12** in acetonitrile (0.1 M $^tBu_4NBF_4$: Potential reported vs. ferrocene) recorded over a scan rate range from 10 mV-200 mVs^{-1}.

Compound **12** shows no signs of electrochemical reversibility. Indeed the plot supports the position that **12** is irreversibly oxidised.
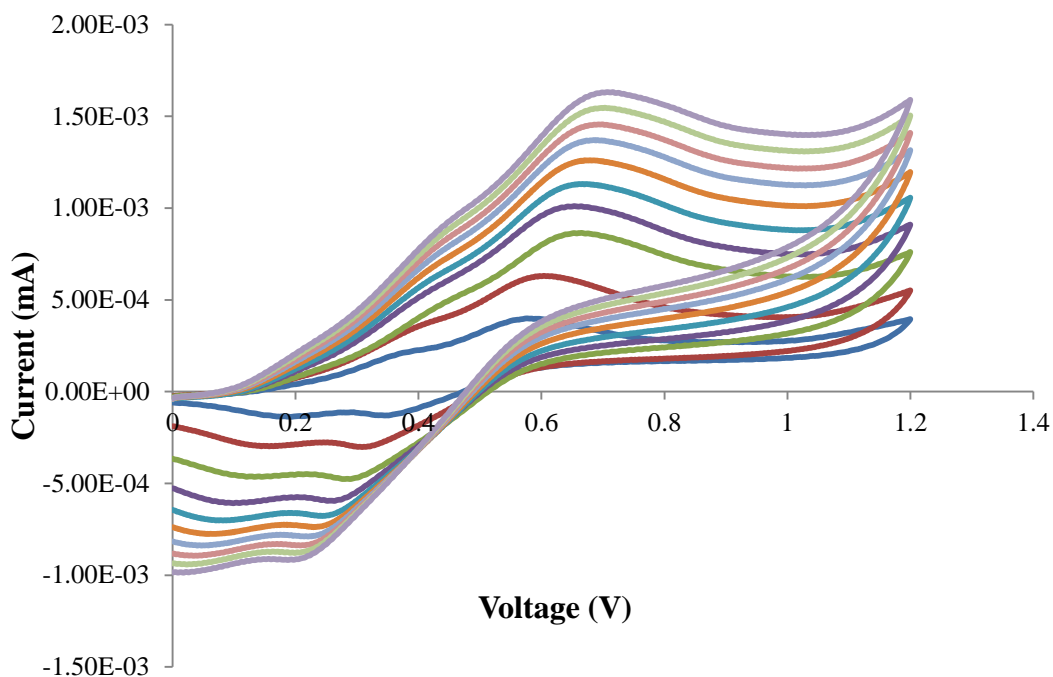
Figure 2.12: Cyclic voltammogram in the positive region of compound **11** in acetonitrile (0.1 M ^{t}Bu$_4$NBF$_4$: Potential reported vs. ferrocene) recorded over a scan rate range from 10 mV-200 mVs^{-1}.

A suitably clear plot could not be obtained at a concentration of 0.3 mM of compound **11**. A concentration of 3 mM was used to obtain the plot shown above. However, even at such high concentrations compound **11** shows little to no signs of electrochemical reversibility. Very small waves can be seen on the plot but these are very minimal and can be considered negligible or due to impurities.

2.3 Testing the ability of the complexes as contrast agents

2.3.1 Measurement of T_1 relaxation times

To assess the effect of the complexes on T_1 relaxation time and hence assess their potential as imaging agents a series of samples **11**, **12** and **13** were prepared in a range of concentrations (0.01 mM, 0.1 mM, 1 mM, 2.5 mM, 10 mM; 0.l M, NaCl in 100 % D_2O). Solutions of Gd-DTPA control and $Cu(BF_4)_2$ control were also tested under the same conditions as controls.

The T_1 relaxtion time of the water in each sample was assessed using an inversion recovery sequence (180º-τ-90º) under full automated control with a 90º pulse width of 11.5 μs. The relaxation delay varied from 1-100 s, depending on the relaxation characteristics of the sample. The intrinsic error of the magnet was found to be 3 %. This was previously calculated by running samples in triplicate and comparing the difference in T_1 times and averaging them as a percentage. The extrinsic error was found to be 8 %. This was previously calculated using 10 samples and re-shimming the machine after each run and averaging the results as a percentage.

The experiments were carried out under the following protocol: 4 transients were required for each spectrum with each experiment requiring the collection of 10-11 spectra which employed an incremental delay (τ) as defined by the list used. The interpulse delay (τ) was set between values of (0-x) s; (x = 1- 60 s depending on the relaxation characteristics of the sample). The overall experimental time ranged from 50 – 90 minutes. In order to test for the optimum experimental conditions, trial data sets were required using different interpulse delays. The range of interpulse delay settings varied from sample to sample and thus allowed for T_1 relaxation times to be measured for pure water (the longest relaxation period) together with concentrated relaxation agents (the shortest relaxation period). A plot of the signal intensity against time gives an exponential curve from which the T_1 value can be extracted. (Figure 2.13)[9]

$$I(t) = I(0) + P \text{ x } e^{t/T_1} \qquad \text{(Equation 2.1)}$$
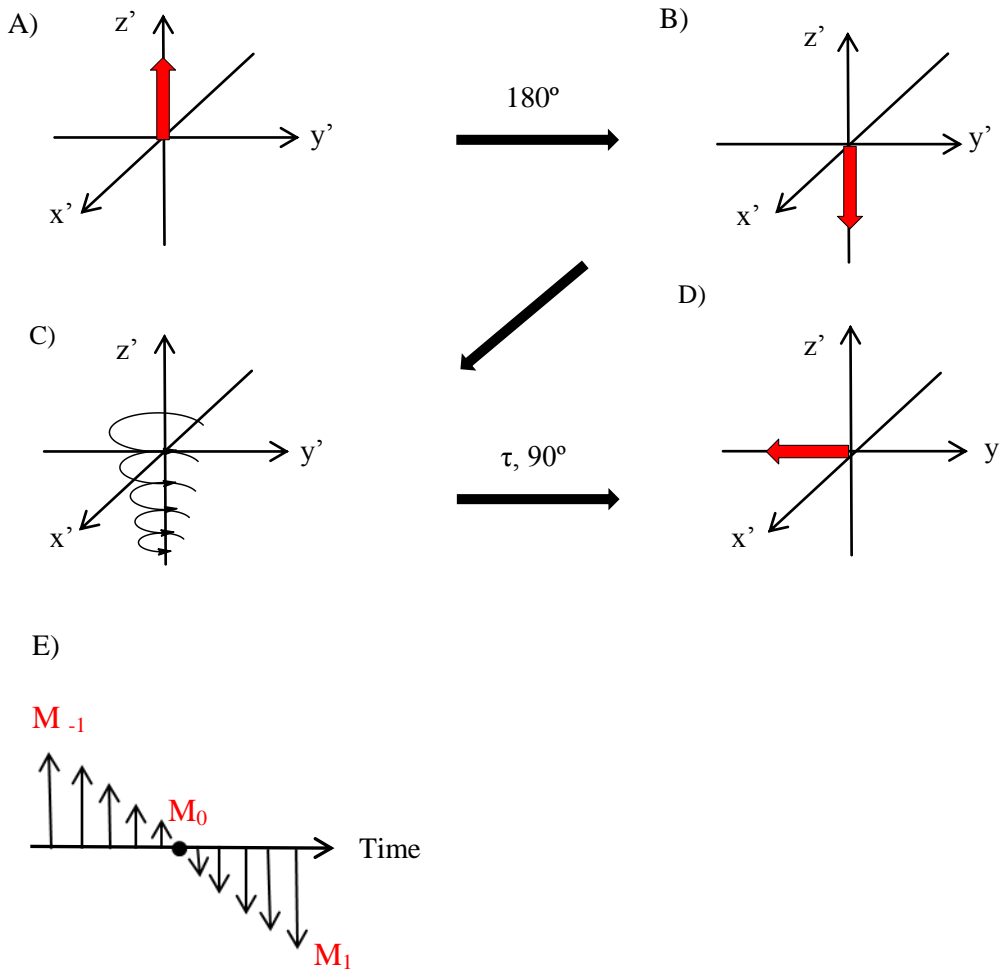
Figure 2.13: Schematic of inversion recovery sequence 180º pulse applied, leaving the system in an unstable state. Shown above is the relaxation mechanism on the z axis, below is the vector model of the mechanism. After time, τ, a 90º pulse is applied.

The application of a 180º pulse inverts the magnetisation (M) and leaves the system in an unstable state. As the excited nuclei lose their energy, they relax causing M_z to become smaller until it passes through zero, upon which it grows in size again to reach its equilibrium value. As the energy is given up to the surroundings, this change occurs along the main field axis (z), meaning that no signal will be observed by the receiver coil along the y' axis. However, after a suitable delay (τ) a 90º pulse is applied which tips the magnetisation into the xy plane allowing the population to be sampled.[9] In order to measure T_1, several 180º-τ-90º experiments are carried out, varying the length of the time delay (τ). T_1 characterises the rate at which the longitudinal component M_z' of the magnetisation vector recovers exponentially

towards its thermodynamic equilibrium (Chapter 1). A typical relaxation curve is shown in figure 2.14. The half point of the curve is where the nuclei pass through zero on the z axis, this indicates the T_1 relaxation time.
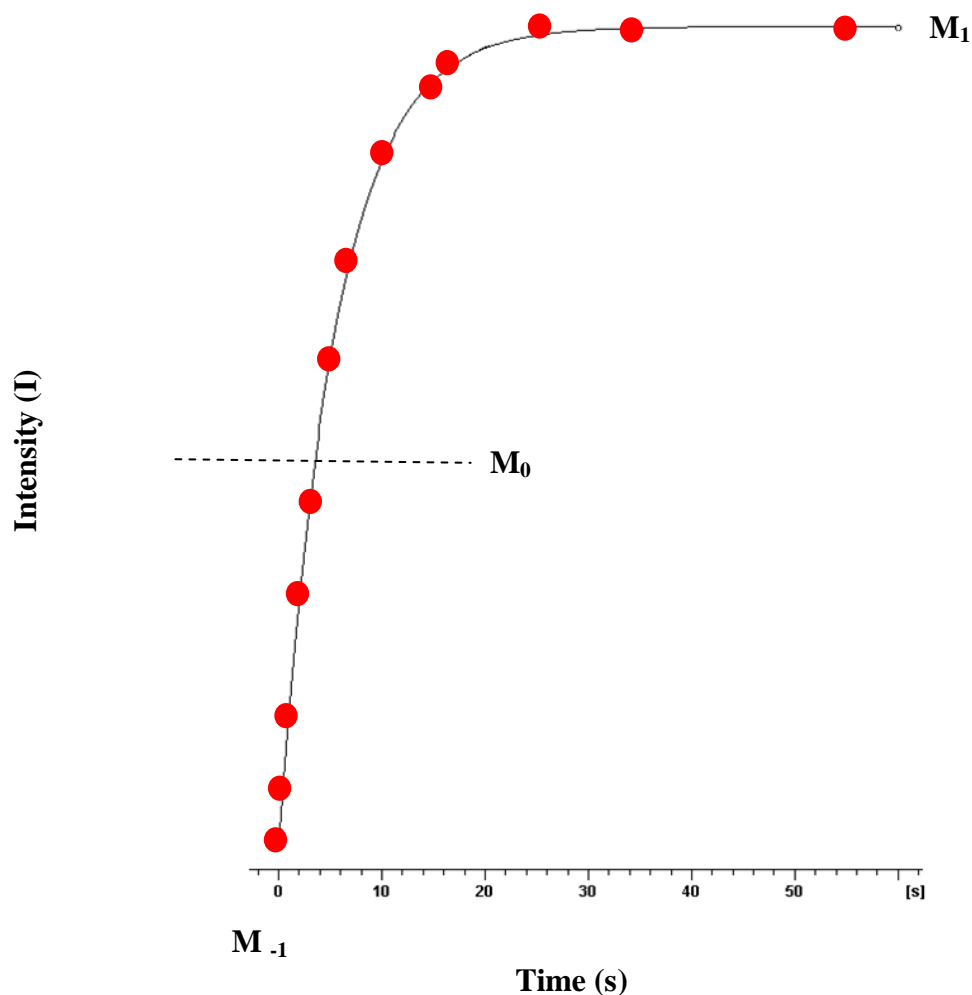
Figure 2.14: relaxation curve intensity (I vs. time(s)) for 1mM **11**. The curve is typical of all the relaxation curves recorded for the pendant arm complexes.

MRI contrast is dependent on the ability of the metal complex to reduce the relaxation time of the surrounding water. However, the T_1 relaxation rate (R_1^{obs}) is made up of 3 parameters (Equation 2.2). A diamagnetic contribution (R_1^o), a paramagnetic contribution relative to inner sphere water exchange with bulk solvent (R_{1p}^{is}) and a paramagnetic contribution relative to water molecules diffusing into the outer sphere (R_{1p}^{os}; Equation 2.3) A fourth contribution from non-bonded water in the second sphere can sometimes also be present.

$$R_1^{obs} = R_1^o + R_{1p}^{is} + R_{1p}^{os} \qquad \text{(Equation 2.2)}$$

$$R_{1p}^{is} = q[C]/(55.5(T_{1M} + \tau_M)) \qquad \text{(Equation 2.3)}$$

R_{1p}^{is} is directly proportional to the concentration, C, of the complex and is also affected by the hydration number, q, which is the number of water molecules directly co-ordinated to the metal. T_{1M} is the longitudinal relaxation time of the bound water protons, and τ_M is their residence lifetime (Equation 2.2). From Equation 2.3 we obtain a relaxivity graph. When q = 1, the plot of [C] against $1/T_1$ will theoretically produce a straight line. If the graph displays curvature a line of best fit is assigned. It is the gradient of this line which can be used to assess the effectiveness of the relaxivity of the complex. Faster relaxation is indicated by a steeper slope.

Previous work has been carried out on the simple copper (II) macrocycles and the T_1 relaxation results obtained (Table 2.2). Due to solubility problems the maximum concentration studied for each complex was 2.5 mM. This study suggests that a copper complex with suitable stability can function as an MRI contrast agent.

	T_1 Relaxation Times / s		
Conc (mM)	**2**	**4**	**5**
2.5	1.553 (84.5 %)	1.196 (88.1 %)	1.489 (85.1 %)
1.0	3.825 (61.8 %)	3.225 (67.8 %)	3.045 (69.6 %)
0.10	8.506 (15.1 %)	8.284 (17.3 %)	8.403 (16.1 %)
0.01	9.242 (7.8 %)	8.521 (15.0 %)	9.711 (3.1 %)
0.001	9.851 (1.7 %)	9.556 (4.6 %)	10.005 (0.2 %)

Table 2.2: The relaxation times of **2 4** and **5** (400 MHz, 100% D_2O, 0.1 M NaCl) at varying concentrations. Figures in brackets indicate the percentage reduction of T_1 from unbound water.[2]

From the results shown in Table 2.2 the graph shown below in Figure 2.15 was plotted. As can be seen there is very little difference between the spectra obtained for the three parent complexes.
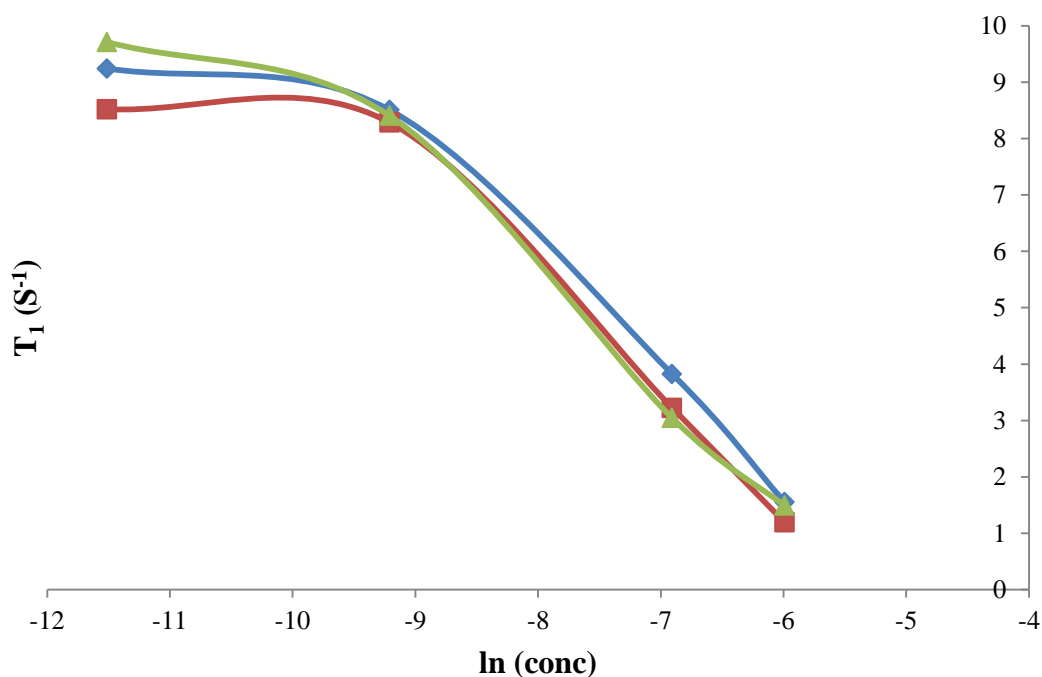
Figure 2.15: T_1 relaxation (s) vs. ln(concentration) of **2**, **4** and **5**. The compounds all have a similar performance.

2.3.2 Measurement of N-substituted macrocycles T_1 relaxation times

The nitrogen-substituted complexes were tested in a similar manner. Consistent with the procedure above (Section 2.4.1) a series of each compound (**11**, **12** and **13)** were prepared in a range of concentrations (0.01 mM, 0.1 mM, 1 mM, 2.5 mM, 10 mM, 0.l M NaCl in 100 % D_2O). Although all the complexes were studied only the data analysis of **12** is shown here (Table 2.3, Figure 2.16). The data for **11** and **13** are given in Appendix 5.

Table 2.3 shows the triplicate results obtained for **12**. From the data set the average T_1 relaxation time at each concentration can be obtained. This data is used to obtain a graph which shows how relaxation time varies with concentration (Figure 2.16). The corresponding

gradient of relaxivity obtained from the data displayed in Figure 2.16 can be calculated (Figure 2.17), where there is good agreement between the data and the line of best fit.

$T_1(1)s^{-1}$	$T_1(2)s^{-1}$	$T_1(3)s^{-1}$	ln(conc)	average T_1 (s)	Standard Deviation
1.309	1.170	1.172	-4.605	1.217	0.079
3.627	3.533	3.533	-5.992	3.564	0.054
6.209	6.197	6.310	-6.908	6.239	0.062
8.015	8.112	7.904	-9.210	8.010	0.104
9.522	9.514	9.483	-11.513	9.506	0.021

Table 2.3: T_1 relaxation data for **12** (the results are shown in triplicate (T_1 (1), (2) and (3)) for inspection; 400 MHz, 0.1M NaCl, 100% D_2O.
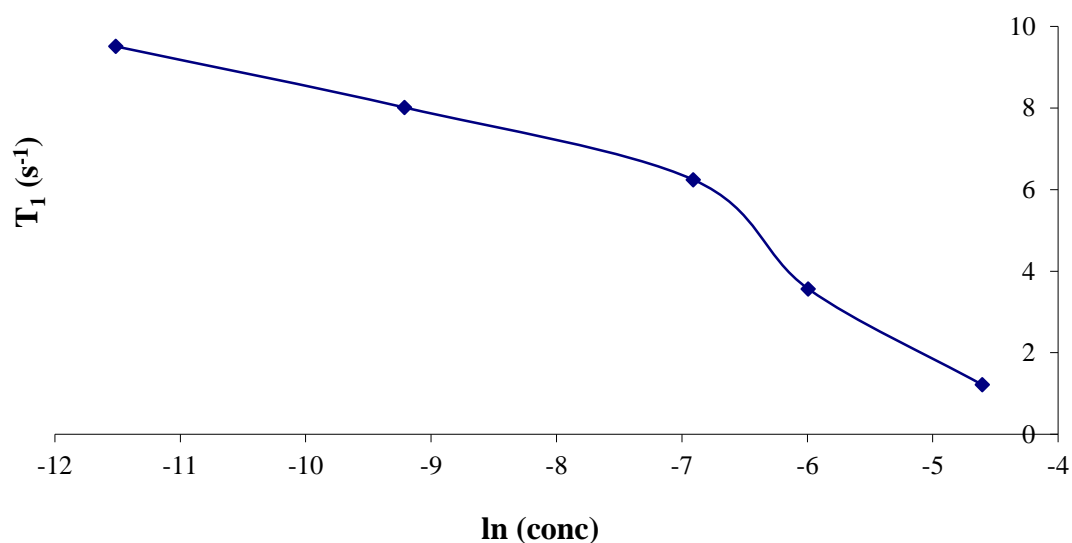
Figure 2.16: T_1 relaxation (s) vs. ln(concentration) of **12**. Line fitted by Excel.
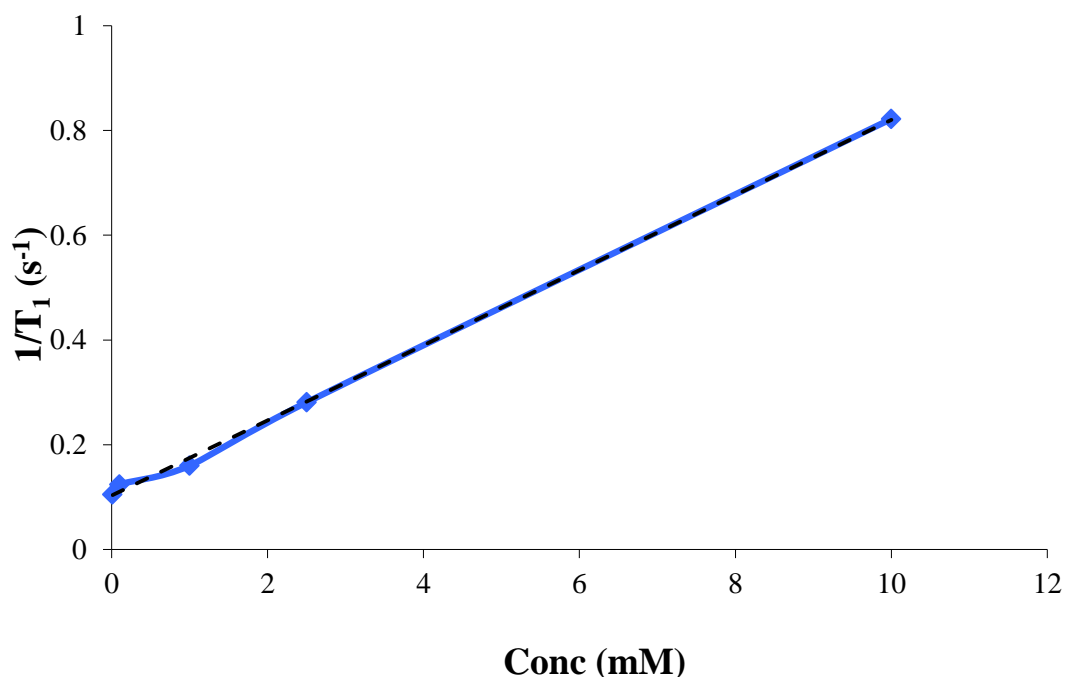
Figure 2.17: Gradient of relaxivity of **12** where y = 71.698 x + 0.1033 and R^2 = 0.9989

All the results obtained from the N-substituted complexes, as well as the controls (Gd-DTPA and $Cu(BF_4)_2$) are plotted and shown in Figure 2.18. The Gd-(DTPA) control demonstrates high relaxivity due to its 7 unpaired electrons and high magnetic moment. $Cu(BF_4)_2$ represents the maximal effect we can expect from a fully solvated copper (II) ion. Thus we calculate that the relaxivity of copper will be approximately 10 times less than current lanthanide based contrast agents.[10]

When the copper is complexed with the macrocycles, the number of available coordination sites is decreased and therefore a diminution in the relative relaxivity is expected (Figure 2.18). However, the data obtained for the N-substituted macrocycles suggest that the results derived from these complexes with higher coordination numbers are comparable with that of the unmodified macrocycles (Table 2.2, 2.3). Indeed, the addition of the pendant arms has not markedly affected the relaxivity of the compound despite the capping of the nitrogen donor atoms as can be seen in Figure 2.17 when compared with the unsubstituted parent complex (**2**). This suggests that in solution the pendant arms either exchange rapidly with solvent (water) molecules or that relaxation via hydrogen bonding with the second hydration

sphere is occurring. Thus the data obtained shows that the N-substituted macrocycles show sufficient relaxivity for use as putative imaging agents.
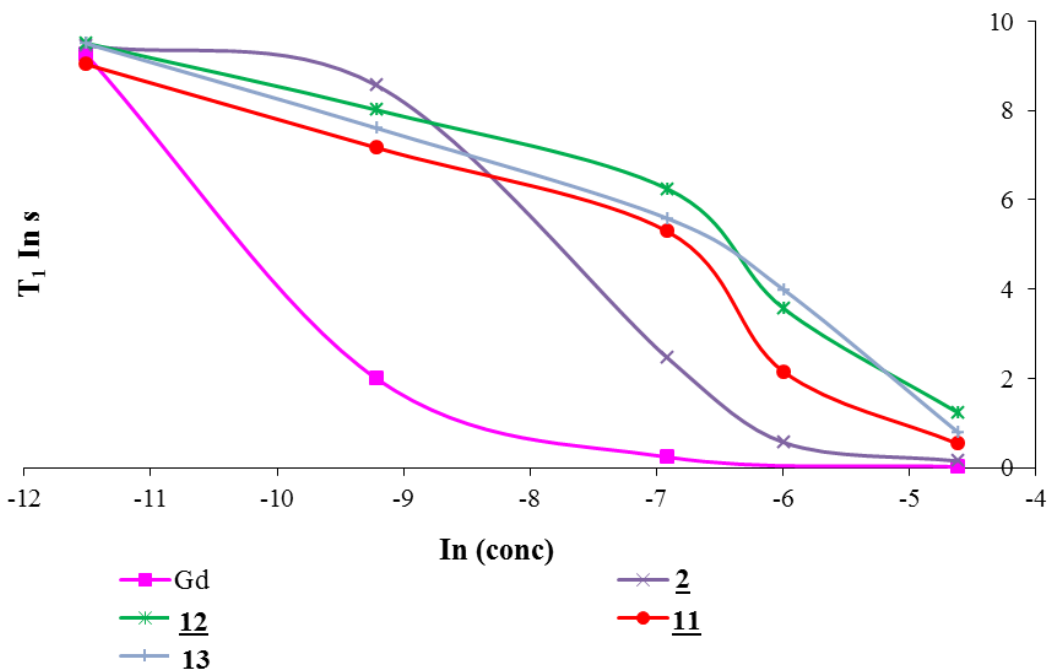
Figure 2.18: T_1 ln(s) vs. ln (concentration) plot of **2**, **11**, **12**, **13** and Gd-(DTPA). The performance is dependent on the coordination number of the copper. **2** is four coordinate: **11**, **12** and **13** are 5/6 coordinate (Figures 2.4 and 2.5).

Reference compound	Compound	Relaxivity (s^{-1} mM^{-1})
	Gd(DTPA)	4.73
Parent macrocycle	**2**	0.27 ±0.01
Pendant arm macrocycles	**11**	0.69 ±0.03
	12	0.16 ±0.02
	13	0.11 ±0.01

Table 2.4: The relaxivity of Gd(DTPA), parent compound **2** and the pendant arm complexes **11**, **12** and **13** in 0.1 M NaCl in 2H2O at 9.4 T. The solubilty of the parent macrocycle is such that it was not possible to generate a solution more concentrated than 2.5mM.

2.4 Conclusion

The aim of the chapter was to synthesise a series of copper (II) macrocyclic complexes functionalised with different pendant arms to investigate their influence on the relaxivity of water. Comparisons with previous studies on the unmodified framework allowed us to assess the effect of the presence of a fifth and or sixth donor atom which had been introduced in an attempt to increase stability and solubility and combat redox reversibility issues.

T_1 relaxation experiments and redox stability tests were carried out to identify their potential to be used as contrast agents to diagnose oxidative stress.

It can be concluded that both the solubility and stability issues have been addressed by the addition of pendant arms. The three compounds studied here are more stable than their unmodified framework. Although we can induce reduction to copper (I), the respective oxidation of the univalent forms remains non-stoichiometric. Indeed the redox potential of these species remains unfavourable. Although it has been possible to achieve additional stability with the introduction of donor arms, these species are oxygen based which unfortunately further stabilise copper (II). It might be more advantageous to study species with softer donor atoms. Thus the focus now will be to synthesise compounds with sulfur donor atoms on or in the ring.

The T_1 relaxation experiments revealed that the ethanol, propanol and carboxylic acid pendant arms all showed a relaxivity believed to be sufficient to assist in imaging oxidant production. However the redox potentials did not seem to be improved as the pendant arm complexes were very poorly re-oxidised using the biologically relevant oxidising agent, sodium hypochlorite. Previous work on the cyclic voltammetry for the propanol pendant arm complex has also revealed that the redox potential is higher than the desired range due to the alteration required to change from square pyramidal Cu(II) geometry to the tetrahedral Cu(I) geometry. In conclusion although the compounds indicate how we can increase complex stability it will not be possible to use these pendant arm complexes as the next generation of contrast agents due to poor redox potentials.

2.5 Experimental

2.5.1 General Considerations

All experiments were carried out using standard apparatus and commercially available chemicals. **2** was prepared as previously reported.[5,7] Solvents were used as supplied. Microanalysis was carried out by the Microanalysis laboratory at the University of Strathclyde. Mass Spectrometry was carried out on a ThermoFinnigan LCQ mass spectrometer with ESI ionisation, spray voltage 4.5 kV, capillary temperature 200ºC. UV/visible spectra were recorded on a Unicam UV 300 spectrometer. The spectrophotometric titrations were carried out on a Perkin Elmer Lambda 35 double beam UV/visible spectrometer running on Perkin Elmer WinLab software (version 2.85.04). T_1 relaxation experiments were measured on an AVANCE NMR spectrometer operating at a proton resonance frequency of 400 MHz. The measurements were carried out using an inversion recovery pulse sequence under full automation control with a 90º pulse width of 11.5 μs.

2.5.2 The general preparation of N-substituted macrocycles

10   **14**, **15**, **16**, **17**, **18**
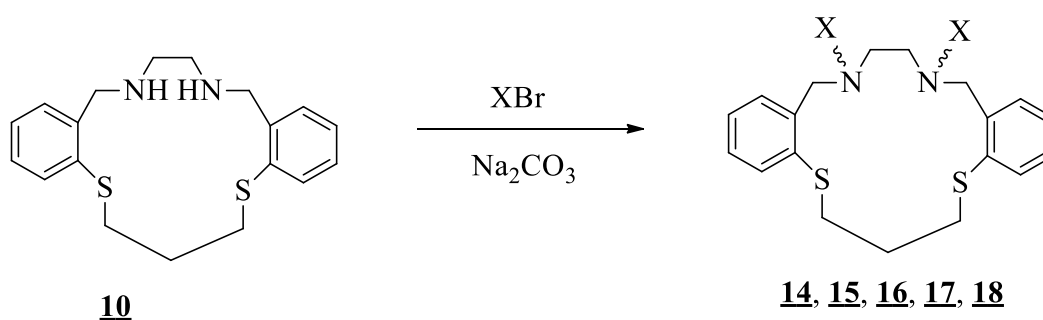
10 (1.04 g, 0.003 mol) was dissolved in acetonitrile (100 ml) and to this sodium bicarbonate (5.07 g, 0.06 mol) was added. The mixture was stirred and heated to reflux. Functionalised halo-alkanes (2-bromo-ethanol (**14**), 3-bromopropan-1-ol (**15**), 4-bromobutan-1-ol (**17**), 6-bromohexan-1-ol (**18**) and bromoacetic acid (**16**)) (2 mol equiv.) in acetonitrile (50 ml) were added dropwise overnight to the refluxing mixture. The solution was then left to cool, before

being filtered. The solvent was then removed *in vacuo,* resulting in a yellow oil. The products were used as received. Typical yields of about 70 % were obtained.

14 : ^{1}H NMR(400 MHz, CDCl$_3$; δ_H) 7.22 (m, 8H, arom), 4.72 (s, 4H, PhC**H$_2$**N-), 3.82, (t, 2H, -C**H$_2$OH**), 3.44 (t, 4H, -C**H$_2$OH**), 2.98 (m, 4H, -SC**H$_2$**-), 2.14 (s, 4H, -NC**H$_2$**), 1.98 (p, 2H, -SCH$_2$C**H$_2$**-), Mass Spec. (ESI) *m/z* 433.27 [M+H]$^+$

15 : ^{1}H NMR(400 MHz, CDCl$_3$; δ_H) 7.25(m, 8H, arom), 4.72 (s, 4H, PhC**H$_2$**N-), 3.76 (t, 2H,-C**H$_2$-OH**), 3.53 (t, 4H -C**H$_2$-OH**), 3.02 (s, 4H, -NC**H$_2$**) 2.08 (p, 4H,-CH$_2$C**H$_2$**CH$_2$OH), 1.70 (p, 2H, -SCH$_2$C**H$_2$**-), Mass Spec. (ESI) *m/z* 461.14 [M+H]$^+$

16 : ^{1}H NMR(400 MHz, CDCl$_3$; δ_H)10.24 (s, 2H,-CH$_2$COO**H**), 7.26 (m, 8H, arom), 4.74 (s, 4H, PhC**H$_2$**N-), 4.15 (s, 2H,-C**H$_2$**COOH), 3.76 (s, 4H, -NC**H$_2$**) 3.0 (t, 4H, -SC**H$_2$**-), 1.91 (p, 2H, -SCH$_2$C**H$_2$**-), Mass Spec. (ESI) *m/z* 461.13 [M+H]$^+$

17: Mass Spec. (ESI) *m/z* 488.20 [M+H]$^+$

18: Mass Spec. (ESI) *m/z* 545.33 [M]$^+$, 445.20 [M-C$_6$H$_{12}$OH]$^+$

2.5.3 Preparation of N-substituted copper(II) macrocycles

14, **15**, **16**, **17**, **18**   Cu(BF$_4$)$_2$ / MeOH   **11**, **12**, **13**, **19**, **20**
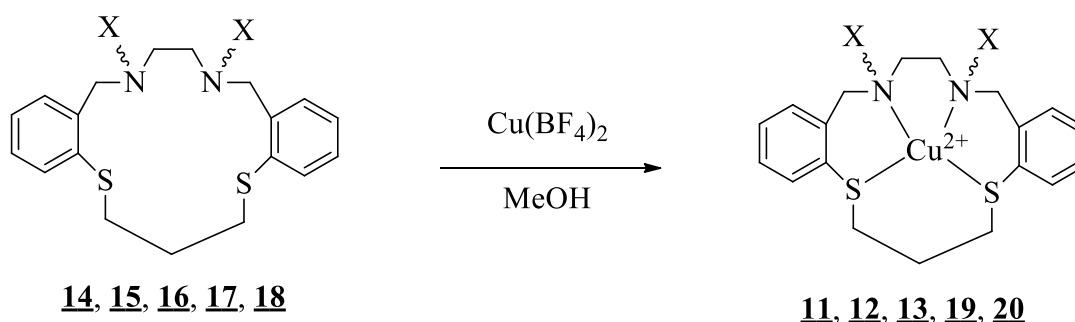
The N-substituted macrocycle was dissolved in methanol (150 ml) and treated with an equi-molar amount of Cu(BF$_4$)$_2$.6H$_2$O dissolved in methanol (10 ml). An immediate colour change from pale yellow to dark green was observed and the solution was refluxed gently overnight. The solution was cooled and filtered and the solvent removed *in vacuo* to yield a dark green

solid. The crude product was re-dissolved in the minimum amount of methanol, filtered through celite and recrystallised by vapour diffusion using diethyl ether to give a dark green powder. Typical yields of about 80% were obtained.

11: Anal. Calcd. for $C_{25}H_{36}N_2S_2O_2CuB_2F_8$: C, 43.04; H, 5.16; N, 4.02 % Found: C, 43.83; H, 5.46; N, 3.98 %. Mass Spec (ESI) *m/z* 523.20 [M]$^+$

12: Anal. Calcd. for $C_{23}H_{32}N_2S_2O_2CuB_2F_8$: C, 39.30; H, 4.41; N, 4.36 % Found: C, 39.98; H, 4.72; N, 4.57 %. Mass Spec (ESI) *m/z* 495.08 [M]$^+$, 451.13 [M-CH$_2$CH$_2$O]$^+$.

13: Anal. Calcd. for $C_{23}H_{28}N_2S_2O_4CuB_2F_8$: C, 41.94; H, 4.44; N, 3.86 % Found: C, 42.13; H, 4.42; N, 4.02 %. Mass Spec (ESI) *m/z* 523.27 [M]$^+$

19: Anal. Calcd. for $C_{27}H_{40}N_2S_2O_2CuB_2F_8$: C, 44.64; H, 5.55; N, 3.86 % Found: C, 36.72; H, 4.93; N, 3.68 %. Mass Spec (ESI) *m/z* 543.27 [M]$^+$, 471.20 [M-C$_4$H$_8$OH]$^+$

20: Anal. Calcd. for $C_{31}H_{48}N_2S_2O_2CuB_2F_8$: C, 47.87; H, 4.29; N, 3.60 % Found: C, 38.04; H, 4.28; N, 4.31 %. Mass Spec (ESI) *m/z* 607.20 [M]$^+$, 507.13 [M-C$_6$H$_{12}$OH]$^+$

Spectra could not be obtained for the copper complexes due to the paramagnetic nature of the compounds. As it was not possible to obtain suitably pure compounds for **17**, **18**, **19** and **20**, the data is here for inspection purposes only.

2.5.4 Compound stability tests

The stability of the complexes **11**, **12** and **13** were tested by placing solid samples and solutions (1 mM, 10 ml 0.1 M NaCl in distilled water) in an incubator at 37ºC and in a cupboard for a period of 1 week. The UV/visible spectrum (300-800 nm) of each sample recorded at the beginning of the experiment and again after one week to assess the degree of degradation.

2.5.5 Copper stability of the complexes

Solutions of each of the copper macrocycles (0.3 mM) and BSA (199 mg, 1 ml) were prepared in Tris-buffer (5 mM, pH 7.4). 1.0 ml of the solution of the required copper complex was placed in a 1.0 cm path length, 1.5 ml quartz cuvette and the spectrum was recorded between 300 and 800 nm against a Tris- buffer reference in a matching cuvette. The BSA solution was titrated in aliquots of 5 µl into solution. The cuvette was allowed to stand for 5 minutes at room temperature to allow the solution to come to equilibrium before the spectra was recorded. The titrations continued until no further change was observed in the spectra. Each experiment was carried out in triplicate. Although the complete spectra from each reaction was collected, the decrease in the absorbance band at 420 nm was plotted as a measure of the percentage of copper (II) form present in the solution.

2.5.6 Reduction of the complexes to copper (I)

Solutions of each of the copper macrocyclic complexes (0.3 mM) and reducing agent (10 mM ascorbic acid) were prepared in Tris-buffer (5 mM pH 7.4). 1.0 ml of the solution of the required copper complexes was placed in a 1.0 cm pathlength, 1.5 ml quartz cuvette and the spectrum was recorded between 300 and 800 nm against a tris-buffer reference placed in a matching cuvette. The reducing agent was titrated in aliquots of 5 µl into the solution. The cuvette was allowed to stand for 5 minutes at room temperature to allow the solution to come to equilibrium before the spectrum was recorded. The titrations continued until no further change was observed. Each experiment was carried out in triplicate. Although the complete spectrum from each reaction was collected the decrease in the absorbance band at 420 nm was used to characterise the reaction. Concentrations are normalised to give the percentage of Cu(II) form present in solution.

2.5.7 Reduction of 11 studied using NMR

Tris- buffer containing **11** (0.1 mM, 5 mM Tris buffer at pH 7.4) was titrated with ascorbate (0%, 20%, 40%, 60%, 80% and 100% mol/mol) into 10 ml volumetric flasks to obtain samples at varying concentrations. A control sample of Tris-HCl (0.1 M NaCl in D_2O) was

59

also prepared. The samples were transferred to a 5 mm NMR tube (507-PP). NMR measurements were carried out on Bruker DPX or AVANCE NMR spectrometers operating at a proton resonance frequency of 400 MHz.

2.5.8 Re-oxidation of the complexes to copper (II)

Solutions of each of the copper macrocyclic complexes (0.3 mM) were prepared in tris-buffer (5 mM, pH 7.4) and reduced using ascorbic acid to generate the copper (I) complex *in-situ*. 1.0 ml of the solution of the solution of the required copper complexes was placed in a 1.0 cm pathlength, 1.5 ml quartz cuvette and the spectrum was recorded between 300 and 800 nm against a tris-buffer reference placed in a matched cuvette. A 100 mM solution of sodium hypochlorite was titrated in 5 μl aliquots into the solution. The cuvette was allowed to stand for 5 minutes at room temperature to allow the solution to come to equilibrium before the spectrum was recorded. The titrations continued until no further change was observed in the spectra. Each experiment was carried out in triplicate. Although the complete spectrum from the reaction was collected the decrease in the absorbance band at 420 nm was plotted as a measurement of the percentage of the Cu(II) form present in solution.

2.5.9 Cyclic Voltammetry

Cyclic voltammetry in aqueous solution was carried out using PC driven EG&G model 263a potentiostat with PC programme Powersuite. A solution of the copper complex (0.3 mM) was prepared in acetonitrile (redistilled from calcium hydride). The electrodes were glassy carbon, platinum wire and silver wire as the working, counter and reference electrodes, respectively. All solutions were degassed with nitrogen and dissolved in acetonitrile and contained sample concentrations of the supporting electrode; NaCl (0.1 M) and $^tBu_4NBF_4$ (0.1 M) respectively. The electrolyte used contained the tetrafluoroborate anion as the typical counter-ion in the copper complexes, therefore eliminating any potential exchange reactions. NaCl was used as an electrolyte to provide a medium closer to biological conditions. The voltammograms were referenced to the ferrocene/ferrocenium (Fe(III)/Fe(II)) redox couple and the values for the complexes are expressed relative to the normal hydrogen electrode

(NHE). In the case of compound **11** a suitable plot could not be obtained at concentrations of 0.3 mM, the concentration was increased 3 mM to obtain an appropriate plot.

2.5.10 Measurement T_1 Relaxation times

Samples were prepared in 0.1M NaCl, 100% D_2O in 10 ml volumetric flask and a sample transferred to a 5 mm NMR tube (507-PP). The copper macrocycle concentrations were typically 10 mM, 2.5 mM, 1 mM, 0.1 mM and 0.01 mM respectively. Each sample was run in triplicate. A control sample of 0.1 mM NaCl in 100 % D_2O was also recorded for each experiment. The samples tested include **11**, **12** and **13**.

Relaxation measurements were carried out on Bruker DPX or AVANCE NMR spectrometers operating at a proton resonance frequency of 400 MHz. The measurements were carried out using an inversion recovery pulse sequence under full automation control with a 90º pulse width of 11.5 µs. All spectra were referenced internally to the residual proton resonance of the relevant deuterated solvent. The relaxation delay varied from 1-100 s, depending on the relaxation characteristics of the sample.

Data was transferred for remote data processing to a desktop PC, running TOPSPIN 2.1. Following Fourier transformation all data was baseline corrected and the T_1 sub-routine within TOPSPIN 2.1 carried out in order to extract the relevant T_1 values from the data.

2.6 References

1. Sowden, R. J.; Trotter, K. D.; Dunbar, L.; Craig, G.; Erdemli, O.; Spickett, C. M.; Reglinski, J., *Biometals*, **2013**, *26*, 85-96.

2. Trotter, K.D.; Reglinski, J.; Robertson, K.; Forgie, J.C.; Parkinson, J.A.; Kennedy, A.R.; Armstrong, D.R.; Sowden, R.J.; Spickett, C.M.; Berlouis, L.E.A., *Inorganica Chimica Acta*, **2010**, *363*, 1529-1538.

3. Trotter, K.D.; Reglinski, J.; Robertson, K.; Forgie, J.C.; Parkinson, J.A.; Kennedy, A.R.; Armstrong, D.R.; Sowden, R.J.; Spickett, C.M., *Inorganica Chimica Acta*, **2009**, *362*, 4065-4072.

4. Smith, D., Final year thesis, *Metal complexes for the diagnosis of inflammatory disease*, University of Strathclyde, **2009**.

5. Bentfeld, R.; Elhers, N.; Mattes, R., *Chemische Berichte*, **1995**, *28*, 1199.

6. Mattes, R.; Muhlenbrock, C.; Leeners, K.; Pyttel, C., *Zeitscrift fur Anorganische und Allegemeine Chemie*, **2004,** *630*, 722-729.

7. Buettner, G. R., *Archives of Biochemistry and Biophysics*, **1993**, *300*, 535-543.

8. Gagne, R.R.; Koval, C.A.; Lisensky, G.C., *Inorganic Chemistry*, **1980**, 19, 2854-2855.

9. Taylor, M.K.; Trotter, K.D.; Reglinski, J.; Berlouis, L.E.A.; Kennedy, A.R.; Spickett, C.M.; Sowden, R.J., *Inorganica Chimica Acta,* **2008,** *361*, 2851-2862.

10. Banwell, C.N., *Fundamentals of Molecular Spectroscopy*, 3rd Edition, McGraw-Hill Book company (UK) Ltd., Maidenhead, **1972**.

11. Fischer A.E.; Hall, L.D., *Magma*, **1994**, *2*, 203-210.

Chapter 3

Towards the synthesis of stable Cu(I) macrocycles

3.1 Introduction

The addition of donor arms to the parent macrocycle has succeeded in addressing the stability and solubility issues seen in previous studies (Chapter 2) on the unmodified framework. There is however still an issue with redox stability. All three donor arm complexes studied allow reduction to Cu(I) however the complexes are unable to achieve stoichiometric reoxidation to Cu(II). It was therefore decided to focus on producing a Cu(I) complex which responds to oxidants rather than a Cu(II) complex which responds to reductants. This could be achieved by the introduction of electron withdrawing groups onto the periphery of the macrocycle or force a change in the geometry. There are three sites which have been identified for modification shown in Figure 3.1:

Modification 1

R = electron withdrawing group on aryl rings

Modification 2

R = electron withdrawing group between nitro donors

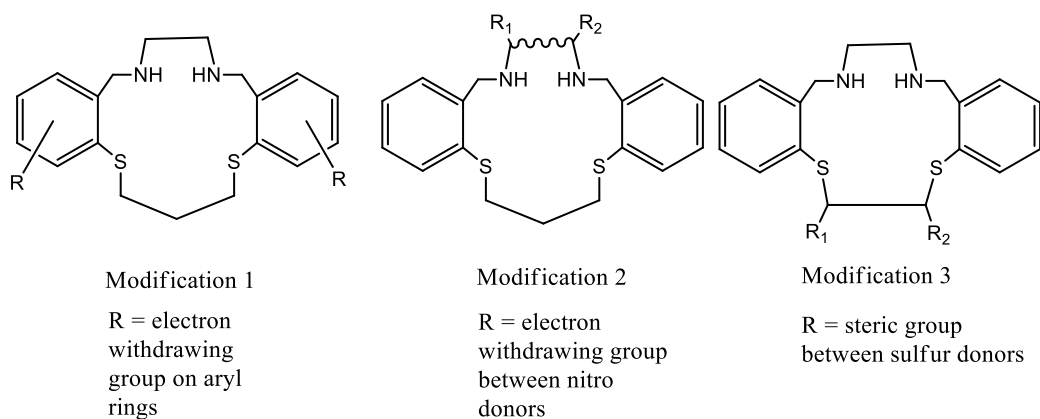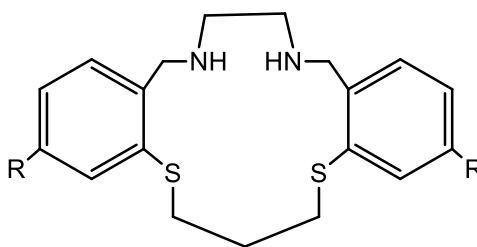Modification 3

R = steric group between sulfur donors

Figure 3.1: Sites identified suitable for the introduction of electron withdrawing groups (EWG) or bulky groups.

Modification 1 involves the addition of electron withdrawing groups (e.g F, $-NO_2$) onto the aryl rings of the original parent compound. Modification 2 involves the introducing an electron withdrawing group between the nitrogen donors (e.g diamino- benzoic acid, *o*-phenylenediamine). The third modification explores the introduction of bulky groups between the sulfur donors. It is hoped that the addition of these groups will alter the geometry of the copper to promote Cu (I) formation. Although work has not been carried out previously on the macrocycles being studied here it is known that the addition of electron withdrawing groups do have an effect on the redox properties of a macrocycle.[1] Sharma *et al.* studied the effect of ligands architecture on the structure and properties of nickel and copper complexes of amide-based ligands. Studies with the copper compounds showed that electron-

withdrawing substituents on the ring shift the compound to a lower oxidation state thus reducing the redox potential value,[1] hence the basis of this study; to produce a Cu(I) complex.
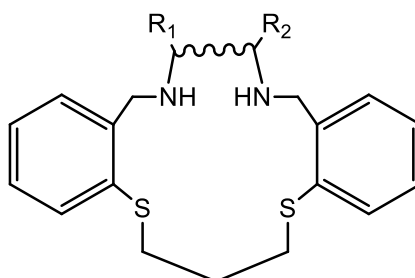
3.1.1 Modification 1

Modification 1

R on aryl rings

Figure 3.2: Where R denotes site of Modification 1.

Some preliminary work had been carried out to produce a macrocycle with an NO_2 group on the aryl rings.[2] However in previous studies the reaction was not taken to completion to produce the amine and only the imine had been synthesised. The imine, however showed signs of poor aqueous solubility. In this study the amine will be synthesised and its suitability tested.
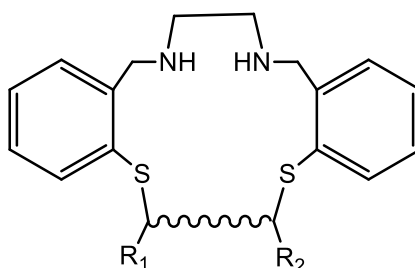
3.1.2 Modification 2

Modification 2

R between nitrogen donors

Figure 3.3: Where R denotes site of Modification 2.

There has not been a previous study into a modification between the nitrogen donors. Only studies into varying backbone lengths have been attempted. In this study the addition of different aryl compounds in the final stage of synthesis will be studied. Two simple diamino benzoic compounds have been chosen as target as they will be representative of the wider family of compounds. The introduction of *o*-phenylenediamine will allow for a simple scaffold. Benzoic acid will be introduced to add increased solubility to the compound should it be necessary.

3.1.3 Modification 3

Modification 3

R between sulfur donors

Figure 3.4: Where R denotes site of Modification 3.

There has also been no previous study into the effects of a modification between the sulfur donor atoms. This modification will start as a supervised project given to final year students to study the effect of using varying di-halo compounds with both electron donating and withdrawing effects to alter the geometry of the ring from a flat planar geometry to tetrahedral in the hope of promoting the formation of Cu(I). It has been well documented that substituting varying groups onto a ring can induce a change in geometry and promote different oxidation states.[3,4] This is demonstrated by Domagala *et. al.* where a series of copper and nickel tetraaza macrocycles are modified to alter their geometry and form unusual oxidation states (Figure 3.5).[5] This has been achieved by substituting the exocyclic nitrogen atoms with a second alkyl group to increase the deviation from planarity and induces rotation of the functional groups.[5] We have had great success forming N_2S_2 macrocycles using simple dithiols. However, it seems the use of more complex reactants i.e. substituted dithiols has yet to be explored.
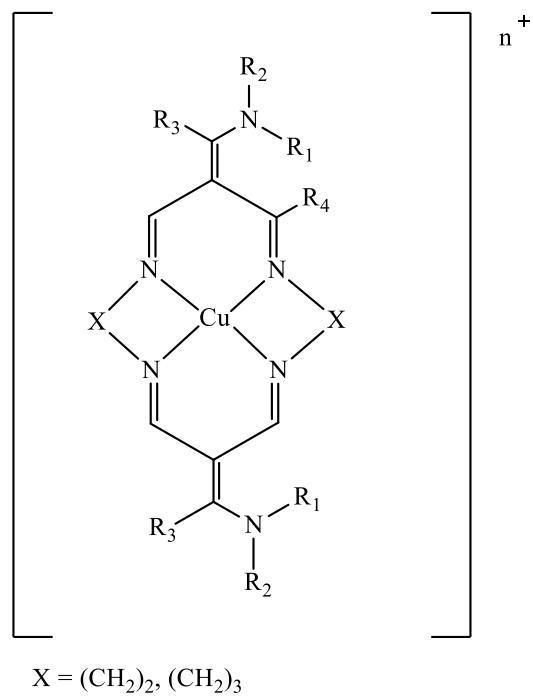
$$X = (CH_2)_2, (CH_2)_3$$

Figure 3.5: General structure of cyclidene complexes modified by Domagala *et al.*[5]

3.2 Results and discussion

3.2.1 Modification 1

The first modification was the substitution of a nitro group onto the aryl rings. As mentioned above some previous work has been carried out to produce the imine (**21/22**), in this study the completion of the synthesis to produce the amine is studied.
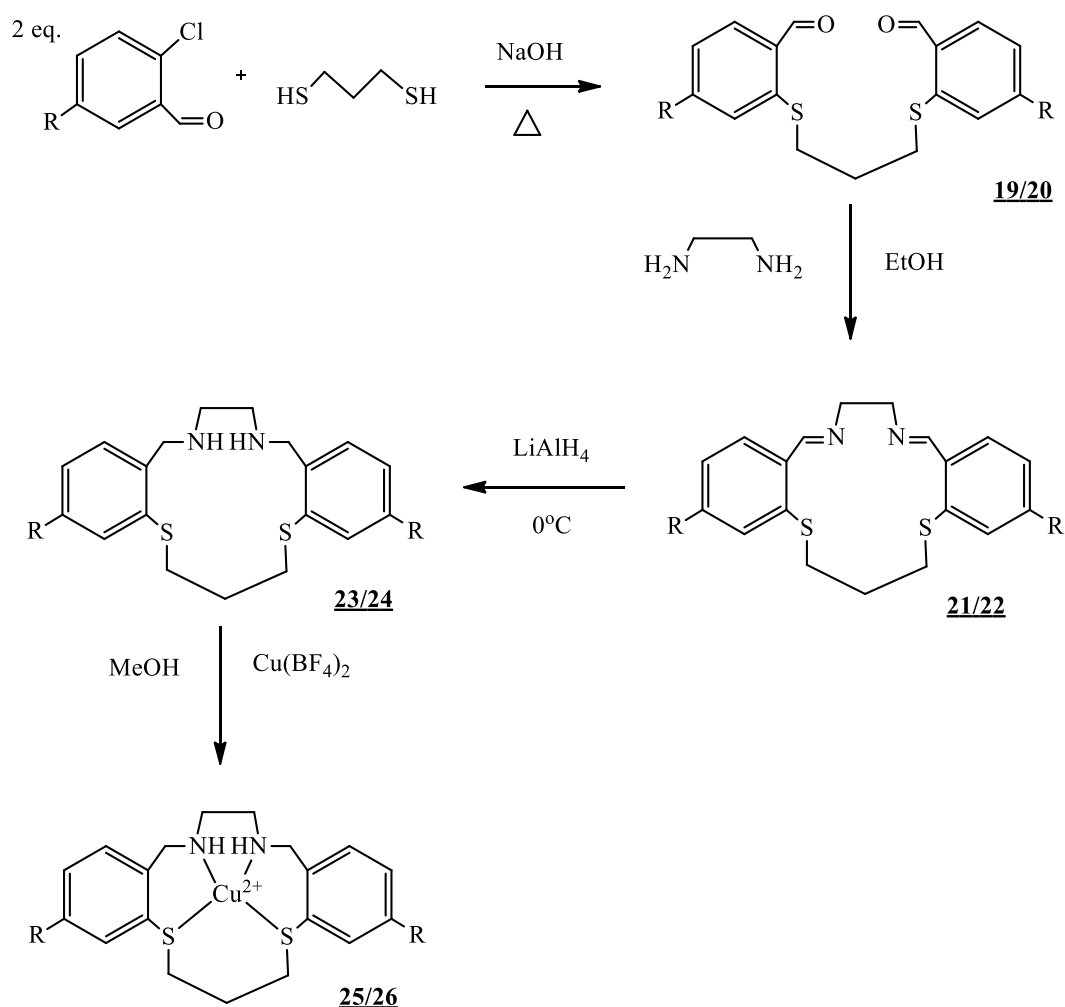
Where R = -NO$_2$, -F

Figure 3.6: Synthetic route for the formation of the aryl substituted macrocycles.

The suitable chlorobenzaldehyde was dissolved and warmed gently. A solution of 1,3-propanedithiol and NaOH was added to ethanol and water and added dropwise with a syringe to the warm solution. The solution turned bright red and a yellow precipitate formed. The mixture was refluxed for 20 hours and cooled. The yellow solid was collected by vacuum filtration and dried *in vacuo*. Ethylenediamine was added to a suspension of the substituted aldehyde in ethanol. The mixture was refluxed for 3 days to produce a yellow solution and precipitate. The solid was collected by filtration and washed with ethanol and diethyl ether and air dried. The imine was then dissolved in ethanol and placed in an ice bath to cool the solution to 0°C after which $NaBH_4$ was added over a 2 hour period. The solvent was then evaporated *in vacuo*. This mixture was then extracted in distilled water and dichloromethane and dried, the solvent was then removed *in vacuo* to yield a yellow solid. The amine was then dissolved in methanol to which $Cu(BF_4)_2$, dissolved in a small amount of methanol, was added. The mixture was refluxed and cooled. The solvent was removed *in vacuo* to yield a green oil.

Similar to previous studies with the nitro substituted imine, compound **25** showed very poor solubility, it was only slightly soluble in DMSO. This was also the case for the fluoro substituted macrocycle (compound **26**). As it was not possible to record an NMR to determine the oxidation state of the copper complexes, the μ_{eff} was measured and found to be paramagnetic for both compounds. The results for the nitro and fluoro substituted species were found to be 1.0 and 1.1 respectively. This suggests that both compounds are Cu(II).

Due to both compounds aqueous insolubility it has not possible to carry out the necessary tests to check its suitability as an imaging agent as it was not possible to obtain suitable relaxation time data. The compounds would also not dissolve in Tris-buffer to undergo both the stability and reduction/oxidation ability tests. To be a suitable candidate as a contrast agent the compound must show signs of aqueous solubility to allow for water relaxation. It was therefore decided to alter our focus to aryl acid groups to address the solubility properties.

3.2.2 Modification 2

Modification 2 was carried out in an attempt to introduce electron withdrawing groups between the nitrogen donor atoms (Figure 3.7).
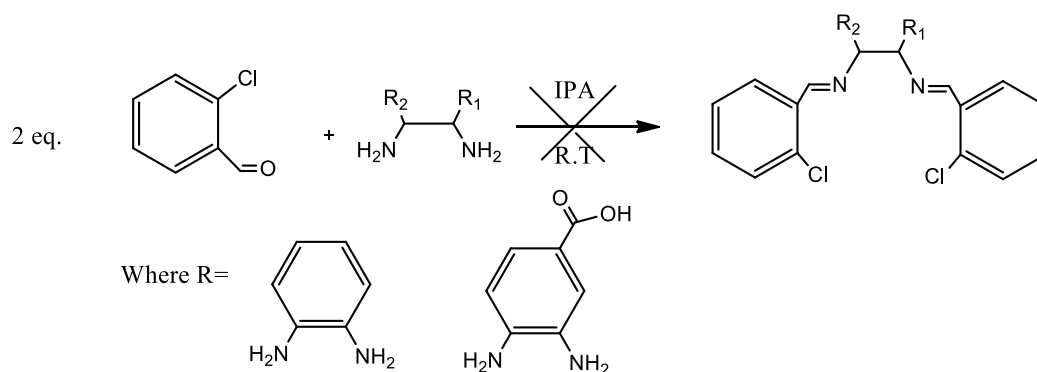

Figure 3.7: Attempted synthetic route of Modification 2 (Synthesis of **27** and **28**).

Modification 2 was attempted by stirring chlorobenzaldehyde with both *o*-phenylenediamine and 3,4-diaminobenzoic acid. Quickly it became apparent that the Schiff base complex was not progressing in line with previous syntheses. While the Schiff base was present in electrospray mass spectrometry the isolated product was predominantly the benzimidazole compound as vapour diffusion resulting in the formation of benzimidazole crystals. Bezimidazole formation is a common and well documented reaction between an aldehyde and diamino phenyl based compound and perhaps should have been taken into account when designing the experiment.[6,7] The crystal structure can be seen below in Figure 3.8. This was the resulting compound from the reaction between *o*-phenylenediamine and chlorobenzaldehyde.
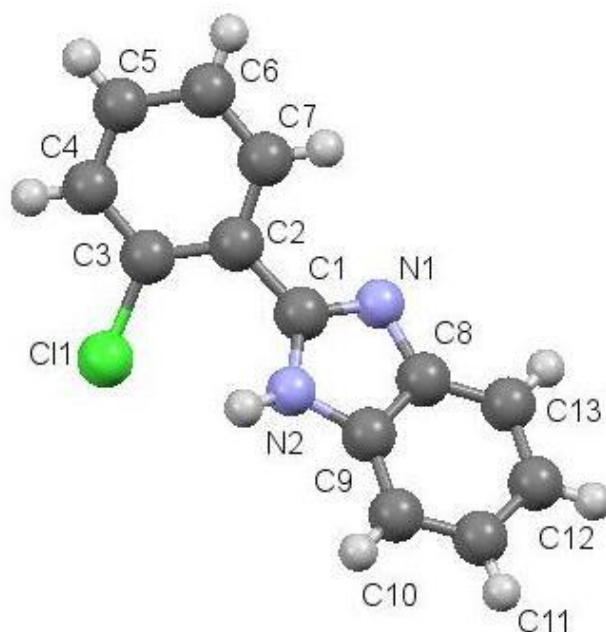
Figure 3.8: The crystal structure of closed benzimidazole compound. Thermal ellipsoids are drawn at 50% probability.

With reference to the synthetic route adopted here, each step matches the proposed reaction pathway detailed by Bahrami *et al.* except the final step where the compound is oxidised by air. The ring closure occurs due to the lack of the electron withdrawing effect on the aryl rings so the compounds sterically favours ring closure. The reaction of aldehydes with o-phenylenediamine are well documented. Figure 3.9 below describes an accepted mechanism.[8,9]
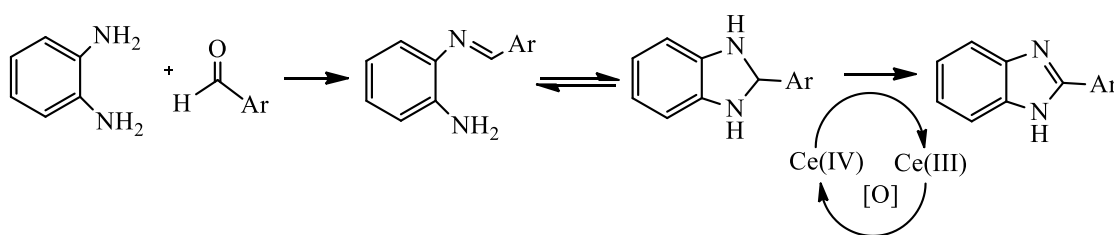

Figure 3.9: Synthetic route to form benzimidazole compound detailed by Bahrami *et al.*[8,9]

3.2.3 Modification 3

Modification 3 attempts to explore the introduction of bulky groups between the sulfur donor atoms. This was to alter the geometry of the ring in an attempt to promote Cu(I) formation. This was a supervised project given to two final year students. The dihalides used include dibromobenzene, dichlorobenzene, 2,3-dibromobutane and 2,3-dichlorobutane. All attempts proved to be unsuccessful and yielded no useable results for this study.
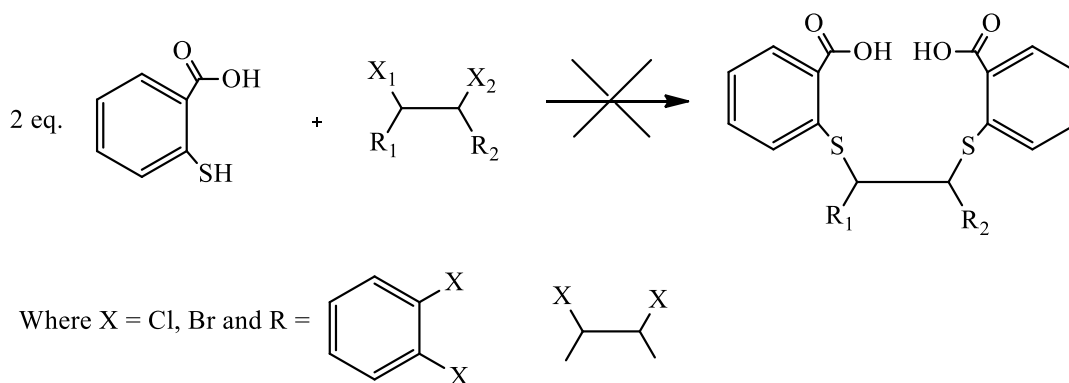

Figure 3.10: Attempted synthetic route to Modification 3.

3.2.4 Modification 1 and 2 combined

Modification 1 yielded compounds that were insoluble which made it difficult to assess their suitability which limits their value to the study, unless a functional group with imparted solubility could be included in the motif. Modification 2 did not yield the desired product due to ring closure resulting in the formation of a benzimidazole compound. Here it was thought that the absence of an electron withdrawing groups on the aryl ring of the aldehyde promoted ring closure rather than Schiff base formation. It was thought that if modification 1 and modification 2 were combined that it could be possible for the desired product to form (Figure 3.11).
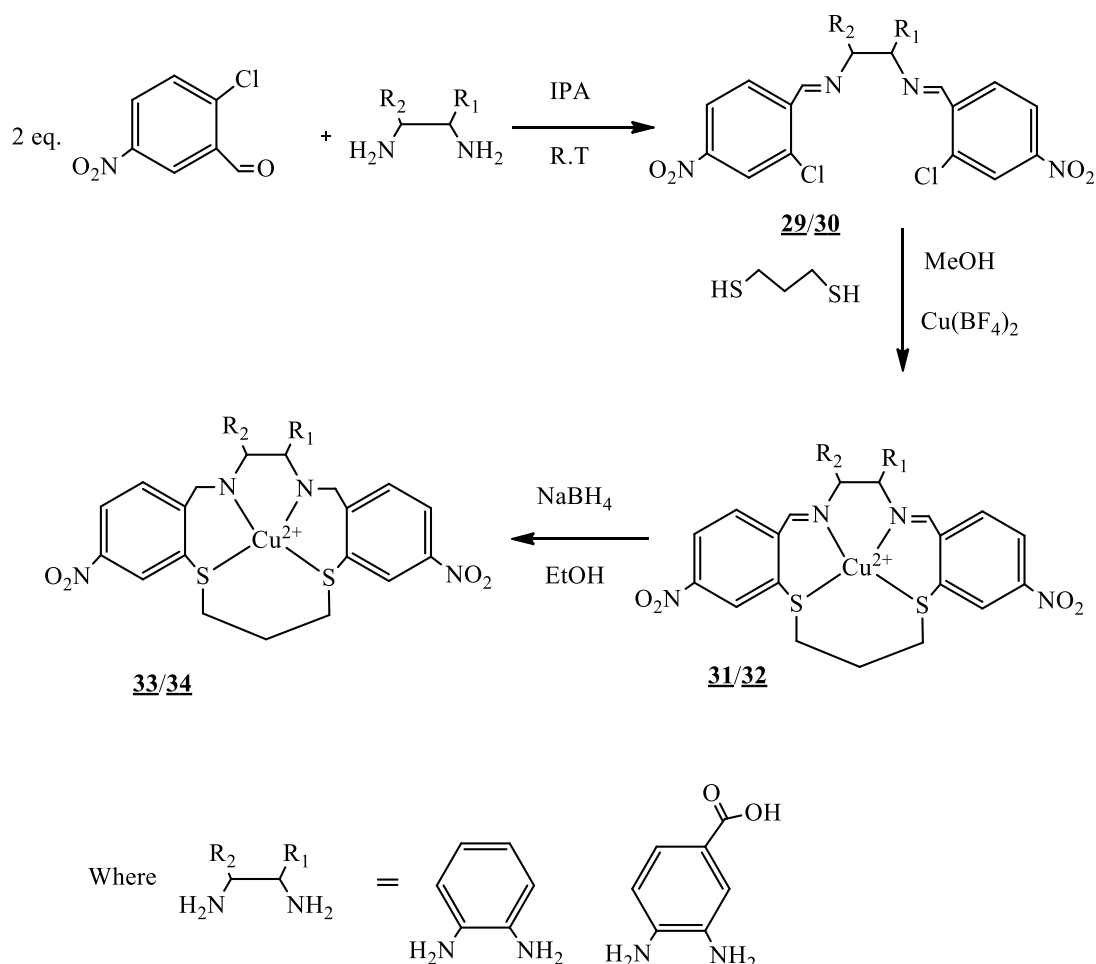

Figure 3.11: Synthesis of **33** and **34**.

5-nitro-2-chlorobenzaldehyde was dissolved in IPA to which the appropriate diamino compound was added portion-wise to the solution. The solution was then stirred at room temperature for an hour and a yellow precipitate formed. The solution was then filtered and the yellow solid collected and dried in the vacuum oven over night. The appropriate Schiff base was dissolved in methanol to which $Cu(BF_4)_2$ dissolved in a small amount of methanol was added, after which one equivalent of propanedithiol was added, the solution was refluxed for 48 hours. The solution was then filtered and removed *in vacuo* to yield a product which remained to be a green-black oil. The crude product was dissolved in distilled water and extracted with dichloromethane to yield a green-black oil. The imine was dissolved in ethanol and an excess of $NaBH_4$ was added portionwise to the solution. The solvent was then removed *in vacuo* to yield the crude product, the crude product was then dissolved in distilled water and extracted with dichloromethane and dried over anhydrous sodium sulfate and the solvent removed *in vacuo* to yield a green solid in both cases. Both products produced remained in a Cu(II) oxidation state. An acceptable microanalysis was obtained for compound **33** and as such further work was undertaken into testing its suitability. In contrast an adequate microanalysis could not be obtained for compound **34**, observations suggest that the compound was degrading when coming into contact with air.

3.2.5 Testing the suitability of 33

3.2.5.1 Electrochemistry

Cyclic voltammetry was used to estimate the redox potential of the complex as previously described in section 2.3.5. The complex was prepared as a solution (3 mM) in 0.1 M t-butylammonium tetrafluoroborate ($^{t}Bu_4NBF_4$). This electrolyte was used as the tetrafluoroborate anion is the typical counter-ion in the copper complexes, therefore eliminating any potential exchange reactions. The voltammograms were referenced to the ferrocene/ferrocenium (Fe(III)/Fe(II)) redox couple by running a ferrocene solution under the same conditions before and after the samples and subtracting this redox potential from that of the samples, the values are expressed relative to the normal hydrogen electrode (NHE). The E° value is 1.42 V which falls within the desired biological range. However the compound was found to be irreversible.
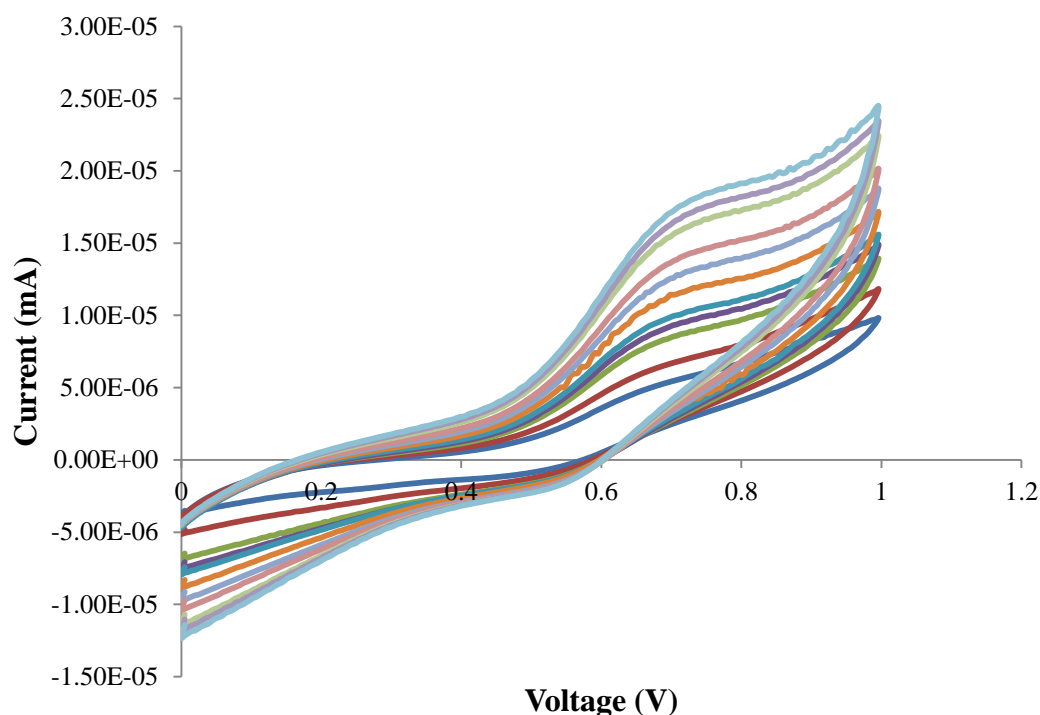

Figure 3.12: Cyclic voltammogram in the positive region of compound **33** in acetonitrile (0.1M $^{t}Bu_4NBF_4$: Potential reported vs. ferrocene) recorded over a scan rate range from 10-200mVs^{-1}.
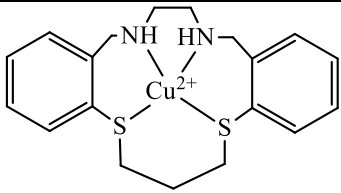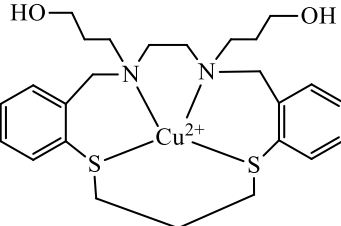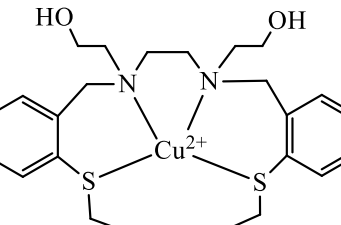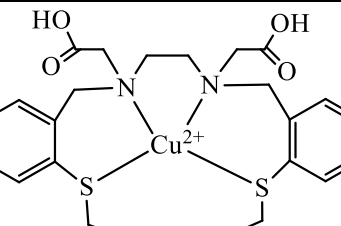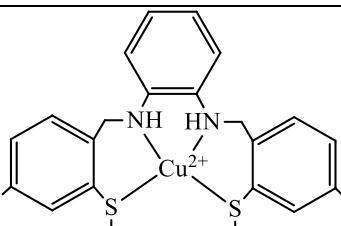
Structure	Compound	MeCN vs. NHE (V)
	2	0.85
	11	1.23
	12	1.04
	13	1.44
	33	1.42

Table 3.1: Electrochemical data for the copper macrocycles obtained by cyclic voltammetry. The complexes were analysed in acetonitrile (0.1 M ^{t}Bu$_4$NBF$_4$: Potentials recorded vs. Ferrocene at 100 mV/s). The values for the complexes are expressed relative to the normal hydrogen electrode (NHE). The data for compound **2** was adapted from Trotter *et al.* 2010.[10]

Shown above in table 3.1 are the E° value and the percentage reversibility of the parent complex (**2**), the modified N$_2$S$_2$ pendant arm complexes (**11**, **12** and **13**) and the electron

withdrawing group (EWG) complex (**33**). The desirable E° range vs. NHE is 1.2-1.5 V. From the results shown in the table it can be seen that the E° value for the original parent compound is too low at only 0.85 V. It was hoped that the modifications would increase the Eº value to fall within the desired biological range. It can be seen from the table the pendant arm complexes **11** , **13** and **33** all fall into this range. However, while the E° has risen into the desired range it can be seen that the redox reversibility (i_{pc} vs. i_{pa}) of all of these complexes has fallen. This is demonstrated in Figure 3.13.
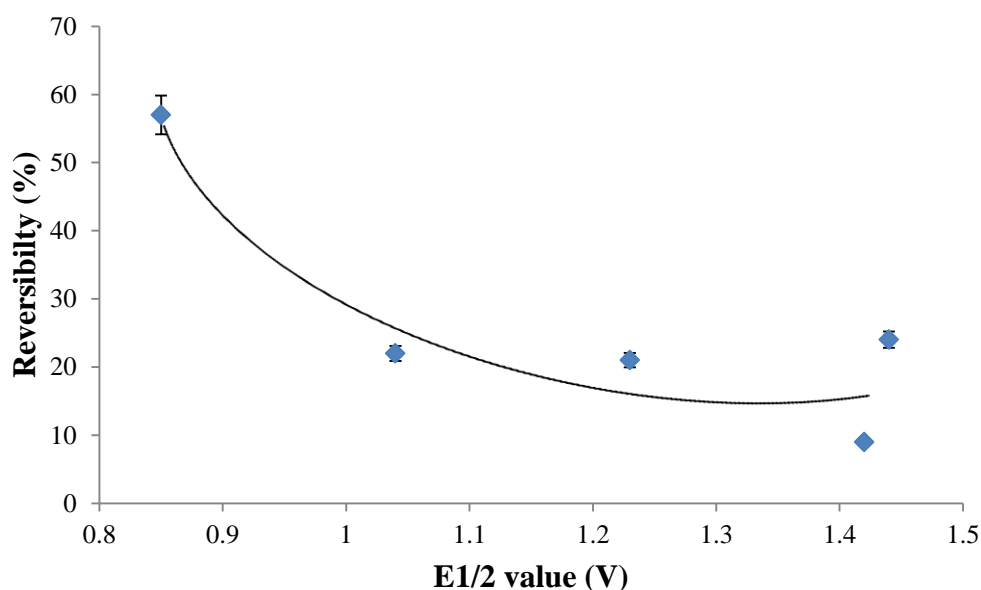

Figure 3.13: Comparison plot of reversibility (i_{pc} vs. i_{pa}) vs. E° values (compounds **2**, **11**, **12**, **13** and **33**). The initial point shows the parent compound (**2**) where the reversibility is higher but the E° value is lower than the desirable range (desirable E° value falls between 1.2 - 1.5 V). A trend can be seen where the addition of donor atom groups increases the E° but decreases the reversibility. The curve was fitted as a line of best fit by Excel.

3.2.5.2 Testing the stability

Despite the fact that compound **33** showed signs of being electrochemically irreversible it is still in our best interests to investigate the chemical reversibility of the compound as it give us a fuller insight into the behaviour of the species. As described previously in chapter 2 the compound must be stable for *in-vivo* use. Sequestration tests with BSA were carried out as previously reported on compound **33**. It also shows an increased stability over the parent complex (**2**) (Figure 3.14).
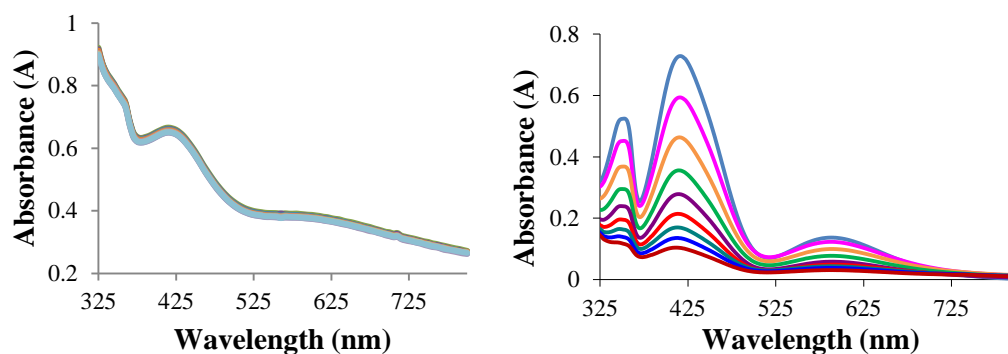

Figure.3.14: Plot of stability test of **33** (0.3 mM) (left) and **2** (0.3 mM) (right) with BSA (199 mg, 1ml in Tris-buffer 5mM, pH 7.4). In the stability test of compound **2** the top spectrum shows the original position of the complex prior to the addition of BSA and the bottom spectrum shows the complex after copper sequestration. Each line indicates the addition of a 5µl aliquot of BSA. No change is observed in the spectra for compound **33** suggesting the copper remains bound in the macrocycle. The band structures in the two complexes are different due to the different geometries adopted by the two complexes (planar (**2**) and square pyramidal (**33**)).

3.2.5.3 Testing the reduction potential

The effect of the reducing agent ascorbic acid, which is found naturally in the body was used to test compound **33**. The reaction was characterised by the charge transfer band at 420 nm (Figure 3.15).
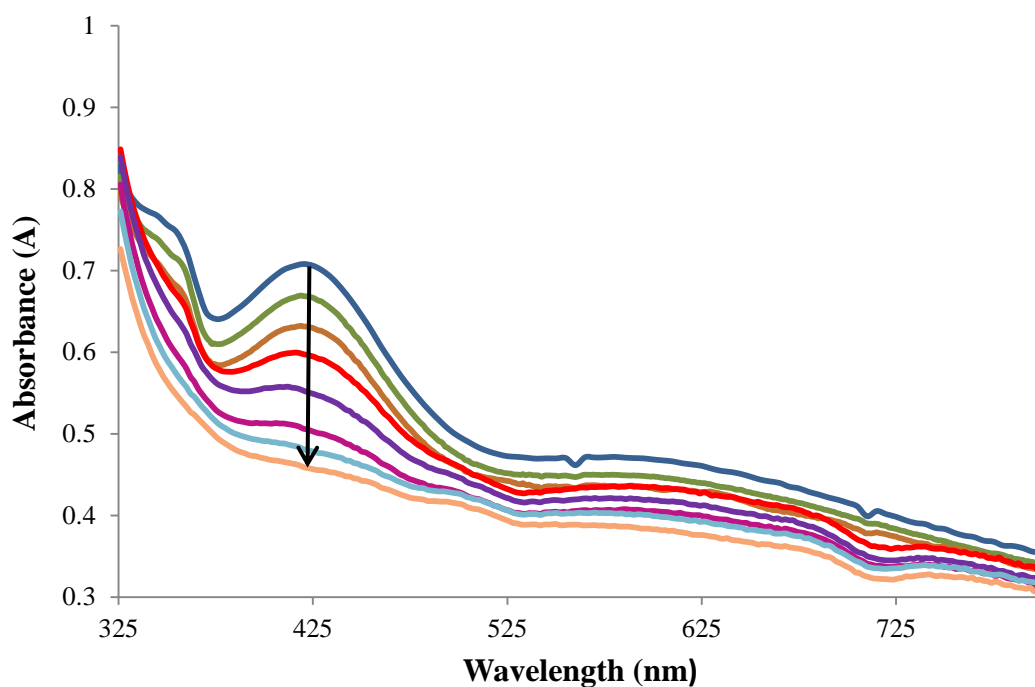

Figure 3.15: The spectrophotometric reduction plot of **33** (0.3mM) with 10mM ascorbic acid in Tris-buffer (5mM, pH7.4). Each band represents a 5µl aliquot of ascorbate (10mM). The reduction is characterised by the absorption band at 420 nm. The top spectrum shows the original position of the complex prior to reduction and the bottom spectrum shows the complex after reduction, indicated by the direction of the arrow.

As can be seen from Figure 3.15 (above) with each aliquot (5µl) of ascorbic acid the compound is reducing. It should be noted that although the addition of electron withdrawing groups has affected the macrocycles reduction potential it has not shifted beyond the ability of ascorbate to act as a reducing agent.

3.2.5.4 Testing the oxidation potential

As previously discussed in chapter 2, it is important that the complexes are able to re-oxidise from Cu(I) to Cu(II) in the presence of the biologically relevant oxidising agent sodium hypochlorite (HOCl). Complex **33** was treated with the reducing agent ascorbate (Figure 3.15) and then re-oxidation to copper (II) was attempted with sodium hypochlorite (Figure 3.16). It can be seen from the plot that similarly to the pendant arm complexes that re-oxidation is poor and a 32% conversion from Cu(I) to Cu(II) was achieved, this is more promising than the pendant arm complexes where only 22% conversion was seen. Consistent with the electrochemistry the reoxidation of the compound still remains poor.
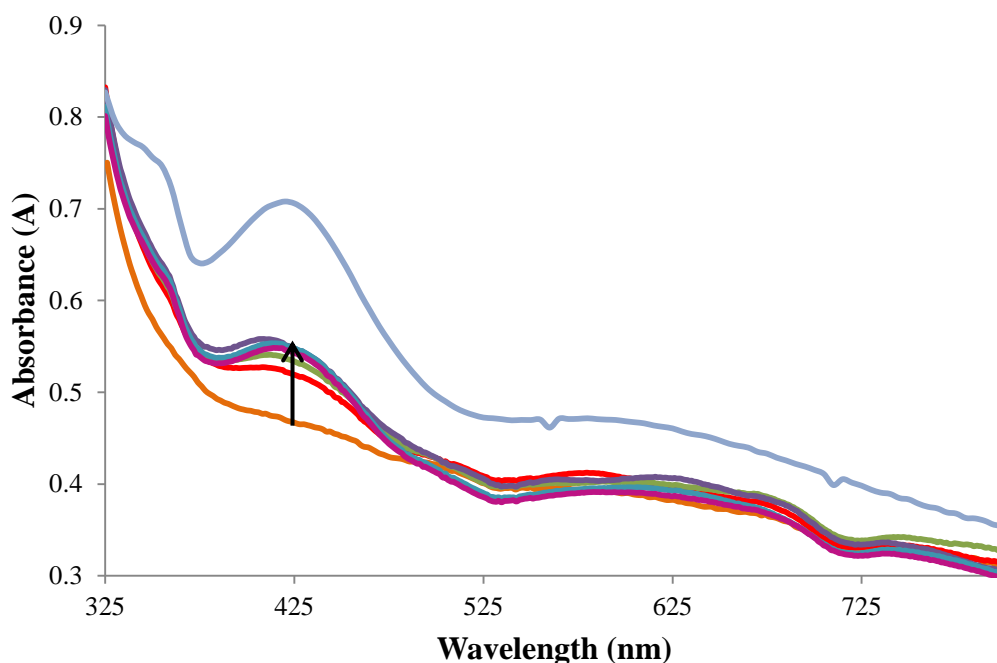

Figure 3.16: The spectrophotometric analysis of the HOCl oxidation of **33** (0.3mm). The species being studied was generated *in-situ* using ascorbic acid as the reductant. The top spectrum shows the original position of the complex prior to reduction and the bottom spectrum shows the complex after reduction. The spectra in the middle show the oxidation with hypochlorite (100mM) in Tris buffer (5mM, pH 7.4). The hypochlorite was added until no further change was observed in the spectra.

3.2.5.5 Testing the ability of the complex as a contrast agent

As discussed previously in chapter 2, to assess the effect of the complexes on the T_1 relaxation time and hence test its suitability as contrast agent **33** was prepared over a range of concentrations (0.01 mM, 0.1 mM, 1 mM, 2.5 mM, 10 mM; 0.l M, NaCl in 100% D_2O). Solutions of Gd-DTPA and $Cu(BF_4)_2$ were also tested under the same conditions as controls. The experiment was carried out as described in Chapter 2 (section 2.4.1). Table 3.2 shows the triplicate results obtained for **33** from these the average T_1 relaxation time at each concentration can be obtained. This data is used to obtain a graph which shows how relaxation time varies with concentration (Figure 3.17). The corresponding gradient of relaxivity obtained from the data displayed in Figure 3.17 can be calculated (Figure 3.18), where there is good agreement between the data and the line of best fit.

$T_1(1)s^{-1}$	$T_1(2)s^{-1}$	$T_1(3)s^{-1}$	ln(conc)	average T_1 (s)	Standard Deviation
0.813	0.864	0.854	-4.605	0.843	0.027
3.837	3.469	3.494	-5.992	3.600	0.206
6.998	6.551	6.180	-6.908	6.576	0.409
9.238	9.367	9.649	-9.210	9.418	0.210
9.072	9.438	9.221	-11.513	9.244	0.184

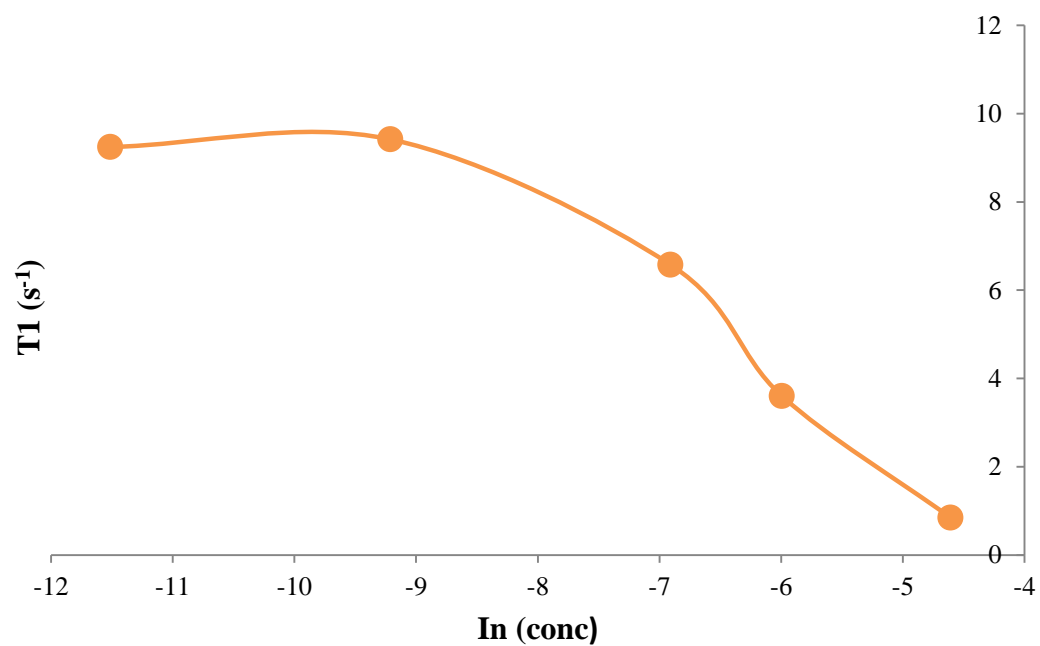Table 3.2: T_1 relaxation data for **33** (results shown in triplicate for inspection; 400 MHz,   0.1 M NaCl, 100% D_2O).

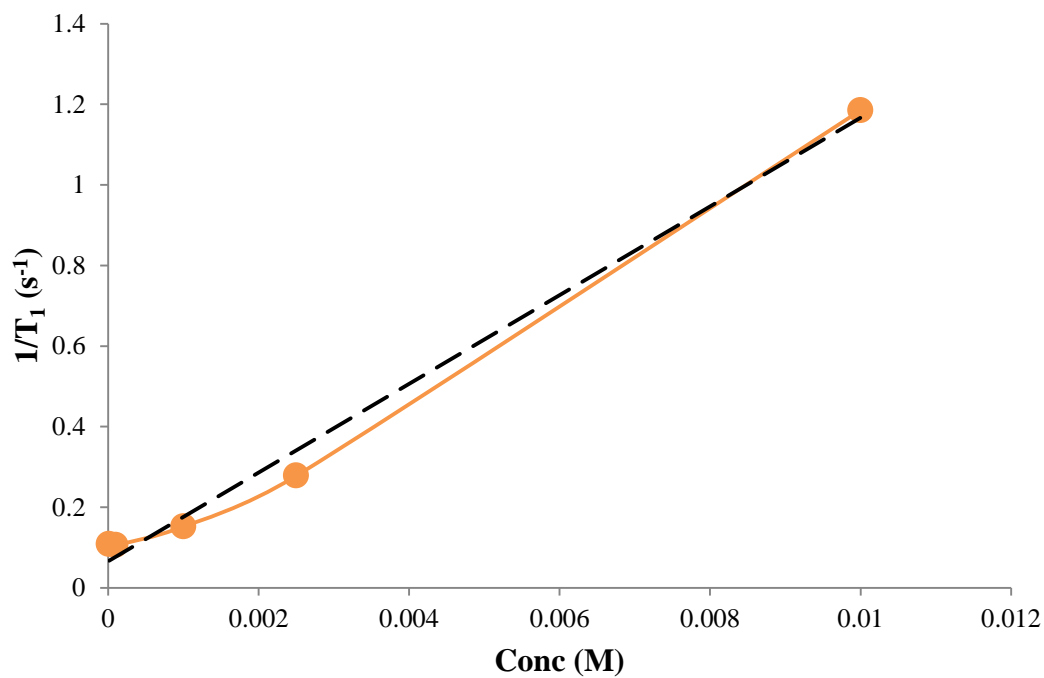Figure 3.17: T_1 relaxation (s) vs. ln(concentration) of **33**.

Figure 3.18: Gradient of relaxivity of **33** where y = 110.09 x + 0.0661 and R^2 = 0.9914.

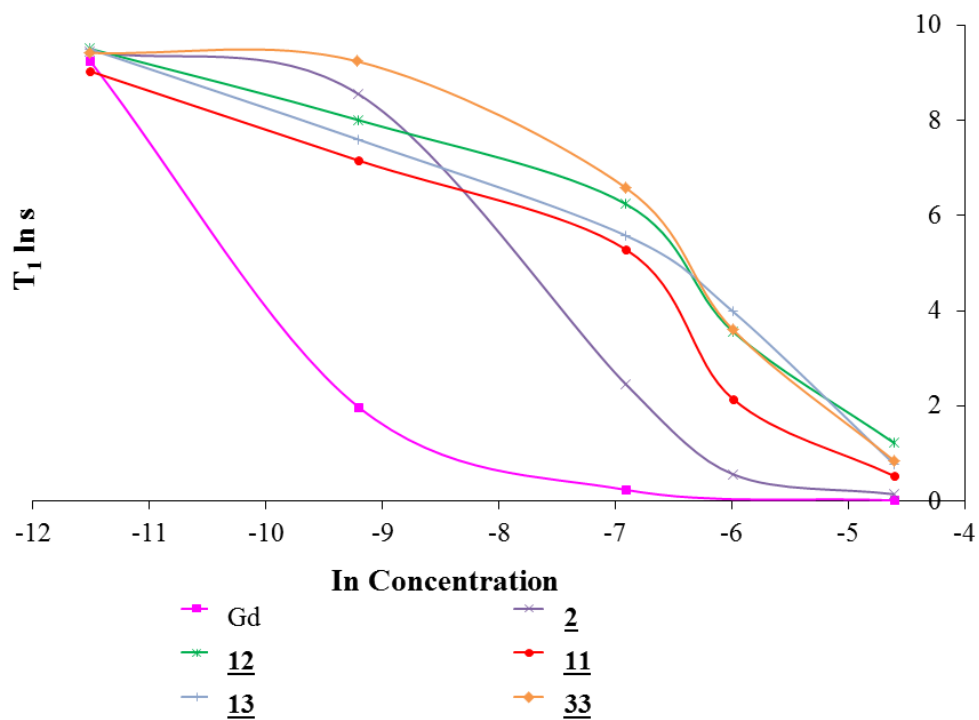Figure 3.19: T_1ln(s) vs. ln (concentration) plot of **2**, **11**, **12**, **13**, **33** and Gd-(DTPA). The performance is dependent on the coordination number of the copper. **2** is four coordinate: **11**, **12** and **13** and **33** are 5/6 coordinate (Figures 2.4, 2.5 and 3.11).

3.3 Conclusion

The aim of the chapter was to synthesise more sophisticated versions of the parent complex (**2**) with modifications at various sites on the ring in the hope it would promote copper (I) formation. This was to address the issue of poor redox stability and it was thought that Cu(I) complexes could overcome this problem as they would respond to oxidants and it would perhaps be more viable to achieve redox cycling via this method.

After further investigation, it was not possible achieve a compound with modifications between the sulfurs or between the nitrogens (*o*-phenylenediamine, diaminobenzoic acid) as it favoured ring closure to form a benzimidazole compound. The modification on the aryl groups (-NO$_2$, -F) formed a very insoluble complex in both cases. The magnetic moment of compounds was measured and it was revealed that the complexes were both Cu (II). It was therefore decided to combine the two modifications; the introduction of electron withdrawing groups on the aryl rings and between the nitrogen donors. One compound was sufficiently pure for further investigation (compound **33**).

From the results of compound **33** from the T$_1$ and stability tests it can be concluded that the compound is equally as stable and unsuitable for use as an imaging agent as the pendant arm complexes discussed in Chapter 2. The copper was not sequestered from the macrocycle in the presence of BSA. The relaxivity of compound **33** is believed to be sufficient to assist in imaging oxidant production.The complex also showed similar results to the pendant arm complexes when testing the redox ability. The complex readily reduced in the presence of ascorbate. However when the complex was treated with the biologically relevant oxidising agent sodium hypochlorite the complex only achieved 32% oxidation from Cu(I) to Cu(II). This is a 10% improvement from the pendant arm complexes which only achieved a maximum reoxidation of 22% Cu(II). The aim was to synthesise a Cu(I) complex however this has not been possible by introducing electron withdrawing and donating groups at various sites on the ring. From the results these modifications have not made a significant improvement on the chemical and electrochemical reversibility from the previous results obtained in Chapter 2. It has therefore been decided to explore different systems. The next chapter will focus on synthesising S$_4$ and S$_3$N systems in the hope they will promote Cu(I) formation.

3.4 Experimental

3.4.1 General Considerations

All experiments were carried out using standard apparatus and commercially available chemicals. Solvents were used as supplied, apart from acetonitrile, which was re-distilled over calcium hydride prior to its use in the electrochemical studies. Microanalysis was carried out by the Microanalysis laboratory at the University of Strathclyde. Mass Spectrometry was carried out on a ThermoFinnigan LCQ mass spectrometer with ESI ionisation, spray voltage 4.5 kV, capillary temperature 200ºC. UV/visible spectra were recorded on a Unicam UV 300 spectrometer. The spectrophotometric titrations were carried out on a Perkin Elmer Lambda 35 double beam UV/visible spectrometer running on Perkin Elmer WinLab software (version 2.85.04). T_1 relaxation experiments were measured on an AVANCE NMR spectrometer operating at a proton resonance frequency of 400MHz. The measurements were carried out using an inversion recovery pulse sequence under full automation control with a 90º pulse width of 11.5 µs.

3.4.2 Modification 1

3.4.2.1 Aldehyde synthesis
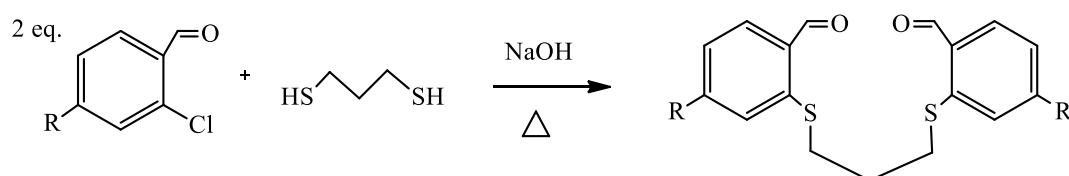
Where R= -NO$_2$ (**19**), -F (**20**)

The appropriate substituted chlorobenzaldehyde (27 mmol) was placed in a 2-necked round-bottomed flask and dissolved in 20 ml ethanol and fitted with a condenser and a warmed gently. A solution of 1,3-propane dithiol (1.35 ml, 13.5 mmol) and NaOH (1.8 g, 27 mmol) 1:1 ethanol, water was prepared with care and added portion-wise with a syringe to the warm

solution. The solution turned bright red and a yellow precipitate formed. The mixture was then refluxed for 20 hours then cooled. The yellow solid was collected by filtration, washed with water and diethyl ether and dried under vacuum. Typical yields of 90 % were obtained.

19: ^{1}H NMR (400 MHz, DMSO; δ_H) 10.12 (s, 2H, Ph-C**H**=O), 8.57 (d, 2H, arom), 8.41 (d, 2H, arom), 7.72 (d, 2H, arom), 3.12 (t, 4H, -SC**H**$_2$-), 1.83 (p, 2H, -SCH$_2$C**H**$_2$-).

20: ^{1}H NMR (400 MHz, DMSO; δ_H) 10.21 (s, 2H, Ph-C**H**=O), 7.45 (d, 4H, arom), 7.37 (d, 2H, arom), 7.32 (d, 2H, arom), 2.98 (t, 4H, -SC**H**$_2$-), 1.94 (p, 2H, -SCH$_2$C**H**$_2$-).

Electrospray or MALDI mass spectra could not be obtained due to incompatibility with the instruments.

3.4.2.2 Imine synthesis
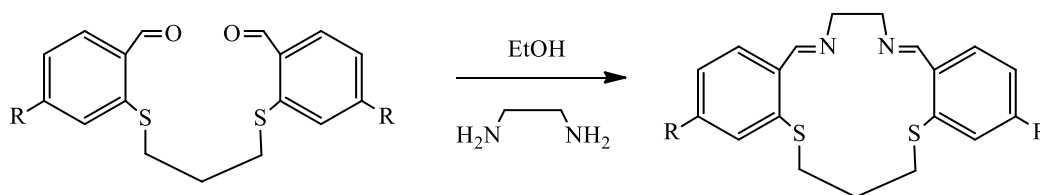
Where R= -NO$_2$ (**21**), -F (**22**)

1,2-diaminoethane (0.08 g, 1.34 mmol) was added to a suspension of the appropriate substituted aldehyde (1.34 mmol) in 125 ml ethanol. The mixture was refluxed for 24 hours producing an orange solution and precipitate. The solid was collected by filtration and washed with ethanol and diethyl ether and air dried. The solvent was evaporated in an evaporating basin and more product was obtained. Yields of 60 % were typically obtained.

21: ^{1}H NMR (400 MHz, DMSO; δ_H) 8.64 (s, 2H, -C**H**=N-), 8.51 (d, 2H, arom), 7.92 (d, 2H, arom), 7.33 (d, 2H, arom), 4.34 (s, 4H, -NC**H**$_2$-), 3.28 (t, 4H, -SC**H**$_2$-) , 1.97 (m, 2H, -SCH$_2$C**H**$_2$-), Mass Spec. (ESI) *m/z* 431 (M + H)$^+$

22: ^{1}H NMR (400 MHz, DMSO; δ_H) 8.03 (s, 2H, -C**H**=N-), 7.44 (d, 2H, arom), 7.30 (d, 2H, arom), 6.93 (d, 2H, arom), 4.67 (s, 4H, -NC**H**$_2$-), 3.16 (t, 4H, -SC**H**$_2$-) , 1.88 (m, 2H, -SCH$_2$C**H**$_2$-), Mass Spec. (ESI) *m/z* 376 (M)$^+$

3.4.2.3 Amine synthesis
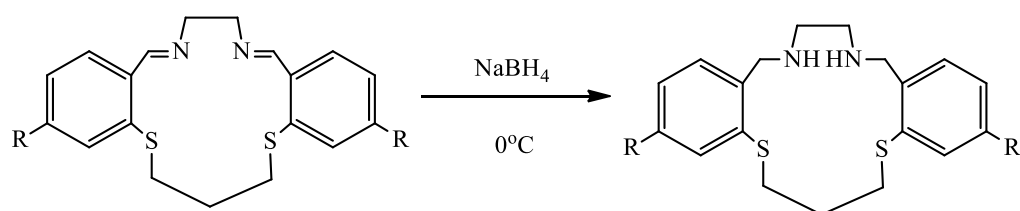
Where R= -NO$_2$ (**23**), -F (**24**)

The appropriate imine (25 mmol) was dissolved in ethanol (80 ml) and placed in an ice-bath and cooled to 0ºC. NaBH$_4$ (0.5 g) was added to the solution portion-wise over a period of 2 hours. The solution was then filtered and the solvent removed *in vacuo*. The resulting oil was redissolved in distilled water (150 ml) and extracted with dichloromethane (3 x 100 ml). The organic layers were combined and back extracted with distilled water (2 x 100 ml) and dried over anhydrous sodium sulphate. The solvent was removed *in vacuo* yielding a yellow oil. Yields of 70 % were typically obtained.

23: ^{1}H NMR(400 MHz, DMSO; δ_H) 8.49 (d, 2H, arom), 7.79 (d, 2H, arom), 7.24 (d, 2H, arom), 5.02 (s, N**H**), 4.29 (s, 4H, -NC**H**$_2$-), 3.14 (t, 4H, -SC**H**$_2$-) , 2.01 (m, 2H, -SCH$_2$C**H**$_2$) Mass Spec. (ESI) *m/z* 457 [M+Na]$^+$

24: ^{1}H NMR(400 MHz, DMSO; δ_H) 7.29 (d, 2H, arom), 7.01 (d, 2H, arom), 6.77 (d, 2H, arom), 5.17 (s, N**H**), 3.96 (s, 4H, -NC**H**$_2$-), 3.23 (t, 4H, -SC**H**$_2$-) , 1.86 (m, 2H, -SCH$_2$C**H**$_2$-), Mass Spec. (ESI) *m/z* 403 [M+Na]$^+$

3.4.2.4 Copper macrocycle synthesis
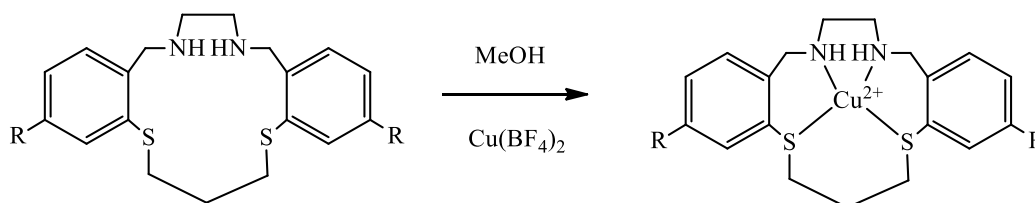
Where R= -NO$_2$ (**25**), -F (**26**)

Cu(BF4)$_2$ (0.76 g, 2.22 mol) was dissolved 10ml methanol and added to the appropriate macrocycle (**23**: 0.97 g , 2.22 mmol; **24**: 0.76 g, 2.0 mmol) was dissolved in methanol (80 ml). The mixture was refluxed for 3 hours and cooled. The solvent was removed *in vacuo* to yield a green solid. Typical yields of 70 % were obtained.
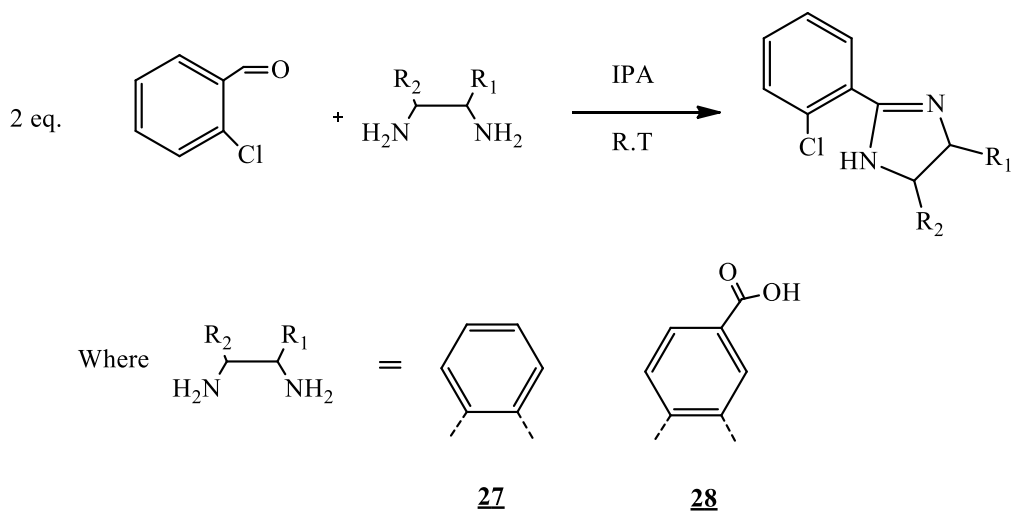
25: Anal. Calcd. for C$_{19}$H$_{22}$N$_4$O$_4$S$_2$CuB$_2$F$_8$: C, 33.97; H, 3.30; N, 8.34 % Found: C, 34.16; H, 3.24; N, 7.98 %. Mass Spec. MALDI 498 [M]$^+$

26: Anal. Calcd. for C$_{19}$H$_{22}$N$_2$S$_2$CuB$_2$F$_{10}$: C, 36.95; H, 3.59; N, 4.54 % Found: C, 36.04; H, 3.21, N, 4.97 % Mass Spec. MALDI 443 [M]$^+$

 NMR's could not be obtained due to the paramagnetic nature of the compounds.

3.4.3 Modification 2
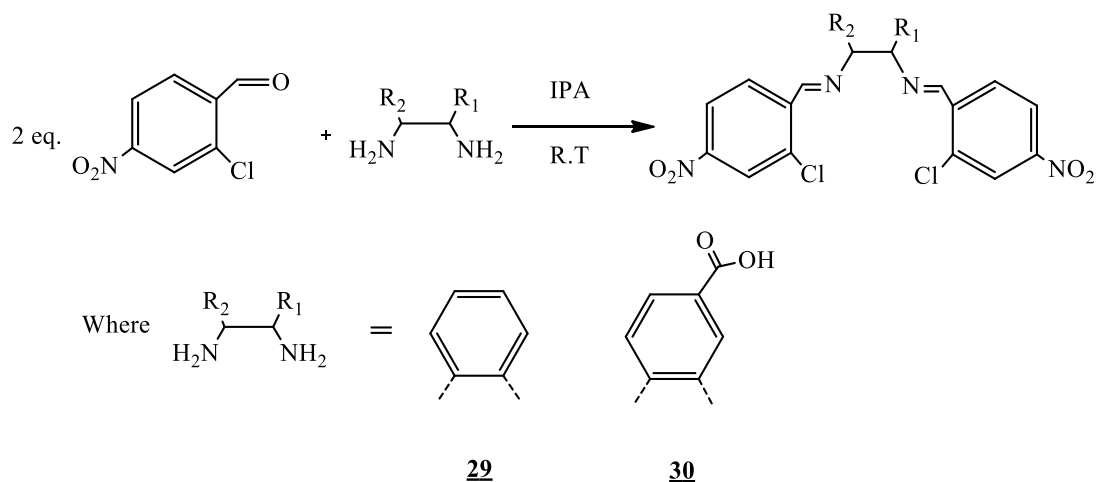
3.4.3.1 Benzimidazole formation

Where

27   28

2-chlorobenzaldehyde (1.41 g, 0.01 mol) was dissolved in IPA (40 ml) to which the appropriate diamino compound (0.01 mol) was added was added portion-wise to the solution. The solution was then stirred at room temperature for an hour and a yellow precipitate formed. The solution was then filtered and the yellow solid collected and dried in the vacuum oven over night. Typical yields of 90 % were obtained.

27: Anal. Calcd. for $C_{13}H_9N_2Cl$: C,68.28; H, 3.97; N, 12.25 % Found: C, 67.21; H, 4.63; N, 11.81 % Mass Spec. (ESI) *m/z* 229 $[M+H]^+$

28: Anal. Calcd. for $C_{13}H_9N_2O_2Cl$: C,61.66; H, 3.33; N, 10.27 % Found: C, 60.68; H, 4.11; N, 10.13 % Mass Spec. (ESI) *m/z* 273 $[M+H]^+$

3.4.4 Modification 1+2

3.4.4.1 Schiff base synthesis

5-nitro-2-chlorobenzaldehyde (1.86 g, 0.01 mol) was dissolved in IPA (40 ml) to which the appropriate diamino compound (0.01 mol) was added was added portion-wise to the solution. The solution was then stirred at room temperature for an hour and a yellow precipitate formed. The solution was then filtered and the yellow solid collected and dried in the vacuum oven over night. Typical yields of 90 % were obtained.

29: ^{1}H NMR (400 MHz, DMSO; δ_H) 8.99 (s, 2H, -**CH**=N-), 8.92 (d, 2H, arom), 8.29 (dd, 4H, arom), 7.87 (d, 2H, arom), 7.17 (d, 2H, arom), Anal. Calcd. for $C_{20}H_{12}Cl_2N_4O_4$: C, 54.20; H, 2.73; N, 12.64 % Found: C, 54.34; H, 2.60; N, 12.83 % Mass Spec. (ESI) m/z 443 [M+H]$^{+}$

30: ^{1}H NMR (400 MHz, DMSO; δ_H) 10.32 (s, H, **COOH**), 9.05 (s, 2H, -**CH**=N-), 8.95 (d, 2H, arom), 8.30 (d, 2H, arom), 7.87 (d, 2H, arom), 7.64 (d, 2H, arom), 7.14 (s, H, arom), Anal. Calcd. for $C_{21}H_{12}Cl_2N_4O_6$: C, 51.77; H, 2.48; N, 11.50 % Found: C, 52.36; H, 2.69; N, 12.06 % Mass Spec. (ESI) m/z 487 [M+H]$^{+}$

3.4.4.2 Imine synthesis
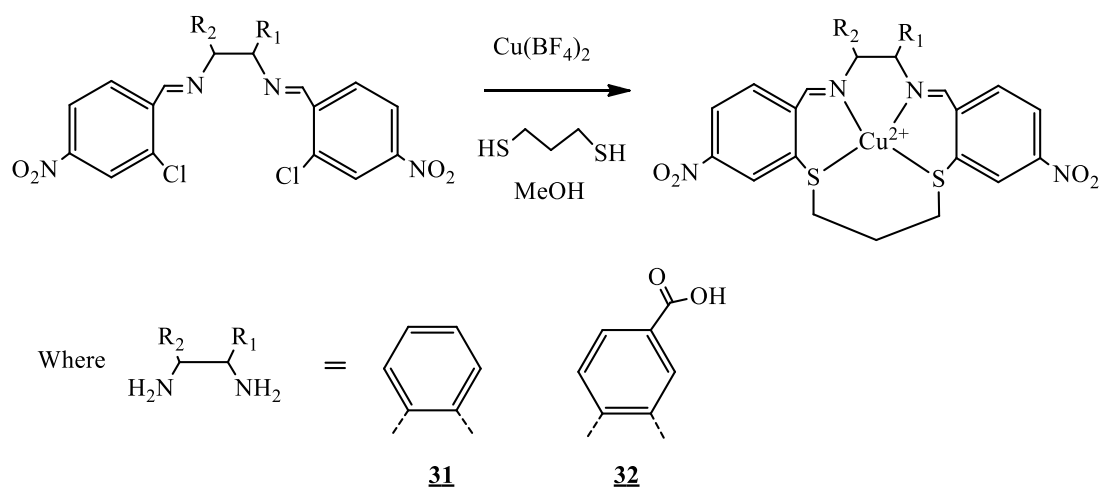
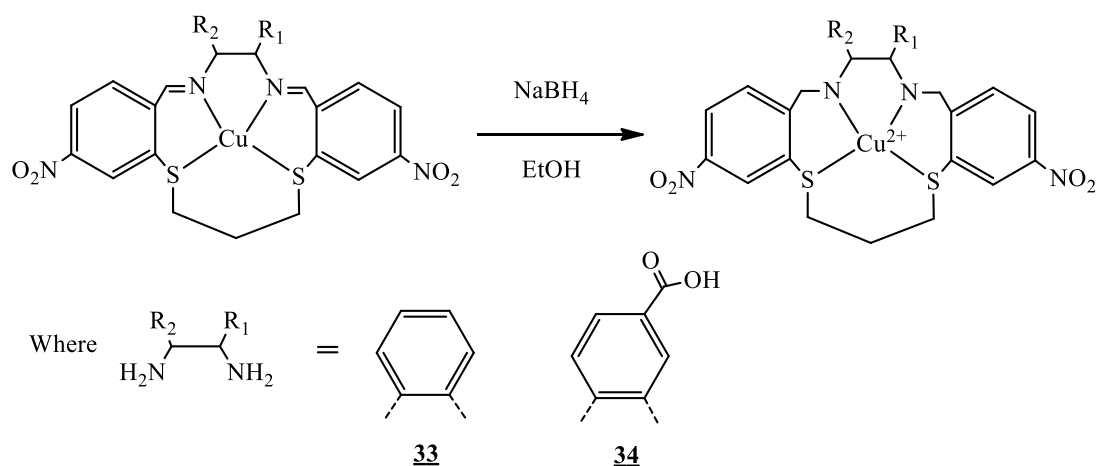

The appropriate Schiff base (10 mmol) was dissolved in dichloromethane to which Cu(BF$_4$)$_2$ (0.34 g, 10 mmol) was added. The compound was heated to reflux and then propanedithiol (0.18g, 10 mmol) was added drop-wise, the solution was subsequently refluxed for 48 hours. The solution was then filtered and removed *in vacuo* to yield a green-black oil. The crude product was dissolved in distilled water and extracted with dichloromethane to yield a green-black oil. Typical yields of 50 % were obtained.

31: Anal. Calcd. for CuC$_{23}$H$_{18}$N$_4$O$_4$S$_2$B$_2$F$_8$: C, 38.60; H, 2.53; N, 7.83 % Found: C, 40.98; H, 2.60; N, 6.59 % Mass Spec. (ESI) *m/z* 541 [M]$^+$

32: Mass Spec. (ESI) *m/z* 586 [M+H]$^+$

NMR's could not be obtained due to the paramagnetic nature of the compounds.

3.4.4.3 Amine synthesis

The appropriate imine (10 mmol) was dissolved in ethanol (100 ml) and an excess of NaBH$_4$ (1 g, 26 mmol) was added portionwise to the solution. The solvent was then removed *in vacuo* to yield the crude product, the crude product was then dissolved in distilled water and extracted with dichloromethane and dried over anhydrous sodium sulfate and the solvent removed *in vacuo* to yield a green solid.

33: Anal. Calcd. for C$_{23}$H$_{20}$N$_4$O$_4$S$_2$CuB$_2$F$_8$: C, 38.37; H, 4.42; N, 7.67 % Found: C, 39.03; H, 4.26; N, 7.59 %. Mass Spec. (ESI) *m/z* 543 [M]$^+$

34: Anal. Calcd. for C$_{24}$H$_{20}$N$_4$O$_6$S$_2$CuB$_2$F$_8$: C, 37.84; H, 2.65; N, 7.35 % Found: C, 6.41; H, 3.26; N, 1.17 % Mass Spec. (ESI) *m/z* 584 [M+H]$^+$

It was not possible to obtain a suitable microanalysis for compound **34**, the data is here for inspection only. NMR's could not be obtained due to the paramagnetic nature of the compounds.

3.4.5 Compound stability tests

The stability of the complex **33** was tested by placing the solid sample and a solution of the sample (1mM, 10 ml 0.1M NaCl in distilled water) in an incubator at 37ºC and in a cupboard for a period of 1 week. The UV/visible spectra (300-800nm) were recorded at the beginning of the experiment and again after one week to assess the degree of degradation.

3.4.6 Copper stability of the complexes

A solution of the copper macrocycle (0.3 mM) and BSA (199 mg, 1 ml) were prepared in Tris-buffer (5 mM, pH 7.4). 1.0 ml of the solution of the copper complex was placed in a 1.0 cm path length, 1.5 ml quartz cuvette and the spectrum was recorded between 300 and 800 nm against a Tris- buffer reference in a matching cuvette. The BSA solution was titrated in aliquots of 5 µl into solution. The cuvette was allowed to stand for 5 minutes at room temperature to allow the solution to come to equilibrium before the spectra was recorded. The titrations continued until no further change was observed in the spectra. Each experiment was carried out in triplicate. Although the complete spectra from each reaction was collected the decrease in the absorbance band at 420 nm was plotted as a measure of the percentage of Cu (II) form present in the solution.

3.4.7 Reduction of the complexes to copper (I)

A solution of the copper macrocyclic complex (0.3 mM) and reducing agent (10 mM ascorbic acid) were prepared in Tris-buffer (5 mM, pH 7.4). 1.0 ml of the solution of the copper complexes was placed in a 1.0 cm pathlength, 1.5 ml quartz cuvette and the spectrum was recorded between 300 and 800 nm against a Tris-buffer reference placed in a matching cuvette. The reducing agent was titrated in aliquots of 5 µl into the solution. The cuvette was allowed to stand for 5 minutes at room temperature to allow the solution to come to equilibrium before the spectrum was recorded. The titrations continued until no further change was observed. The experiment was carried out in triplicate. Although the complete spectrum from each reaction was collected the decrease in the absorbance band at 420 nm

was used to characterise the reaction. Concentrations are normalised to give the percentage of Cu(II) form present in solution.

3.4.8 Re-oxidation of the complexes to copper (II)

A solution of the copper macrocyclic complex (0.3 mM) was prepared in Tris-buffer (5 mM, pH 7.4) and reduced using ascorbic acid to generate the Cu(I) complex *in-situ.* 1.0 ml of the solution of the copper complexes was placed in a 1.0 cm pathlength, 1.5 ml quartz cuvette and the spectrum was recorded between 300 and 800 nm against a Tris-buffer reference placed in a matched cuvette. A 100 mM solution of sodium hypochlorite was titrated in 5 μl aliquots into the solution. The cuvette was allowed to stand for 5 minutes at room temperature to allow the solution to come to equilibrium before the spectrum was recorded. The titrations continued until no further change was observed in the spectra. The experiment was carried out in triplicate. Although the complete spectrum from the reaction was collected the decrease in the absorbance band at 420 nm was plotted as a measurement of the percentage of the Cu (II) form present in solution.

3.4.9 Cyclic Voltammetry

Cyclic voltammetry in aqueous solution was carried out using PC driven EG&G model 263a potentiostat with PC programme Powersuite. A solution of the copper complex (0.3mM) was prepared in acetonitrile (redistilled from calcium hydride). The electrodes were glassy carbon, platinum wire and silver wire as the working, counter and reference electrodes, respectively. All solutions were degassed with nitrogen and dissolved in acetonitrile and contained sample concentrations of the supporting electrode; NaCl (0.1 M) and $^tBu_4NBF_4$ (0.1 M) respectively. The electrolyte used was the tetrafluoroborate anion as the typical counter-ion in the copper complexes, therefore eliminating any potential exchange reactions. NaCl was used as an electrolyte to provide a medium closer to biological conditions. The voltammograms were referenced to the ferrocene/ferrocenium (Fe (III)/Fe (II)) redox couple and the value for the complex is expressed relative to the normal hydrogen electrode (NHE).

3.4.10 Measurement T_1 Relaxation times

The samples (compound **33**) were prepared in 0.1 M NaCl, 100 % D_2O in 10 ml volumetric flask and the sample was transferred to a 5 mm NMR tube (507-PP). The copper macrocycle concentrations were typically 10 mM, 2.5 mM, 1 mM, 0.1 mM and 0.01 mM respectively. The sample was run in triplicate. A control sample of 0.1 mM NaCl in 100% D_2O was also recorded for each experiment.

Relaxation measurements were carried out on Bruker DPX or AVANCE NMR spectrometers operating at a proton resonance frequency of 400 MHz. The measurements were carried out using an inversion recovery pulse sequence under full automation control with a 90º pulse width of 11.5 μs. All spectra were referenced internally to the residual proton resonance of the relevant deuterated solvent. The relaxation delay varied from 1-100 s, depending on the relaxation characteristics of the sample.

Data was transferred for remote data processing to a desktop PC, running TOPSPIN 2.1. Following Fourier transformation all data was baseline corrected and the T_1 sub-routine within TOPSPIN 2.1 carried out in order to extract the relevant T_1 values from the data.

3.5 References

1. Sharma, S. K.; Hundal, G.; Gupta, R., *European Journal of Inorganic Chemistry*, **2010**, *4*, 621-636.

2. Taylor, M. K.; *Copper complexes as putative imaging agents*, Ph.D. Thesis, University of Strathclyde, **2005**.

3. Pramanik, A.; Basu, A.; Das, G., *Polyhedron*, **2010**, *29*, 1980-1989.

4. Place C.; Zimmerman, J. L.; Mulliez, E.; Guillot, G.; Bois, C.; Chottard, J. C., *Inorganic Chemistry*, **1998**, *37*, 4030-4039.

5. Domagala, S.; Malecka, J.; Michalowicz, A.; Mames, I.; Kamienski, B.; Wozny, M.; Bilewicz, R.; Daszkiewicz, B. K.; Wozniak, K., *European Journal of Inorganic Chemistry*, **2012**, *23*, 3680-3692.

6. Venkateswarlu, Y.; Kumar, S. R.; Leelavathi, P., *Organic and Medicinal Chemistry Letters*, **2013**, **3**, 7.

7. Naeimi, H.; Alishahi, N., *Journal of Chemical Research*, **2013**, *4*, 208-209.

8. Bahrami, K.; Khodaei, M. M.; Naali, F., *Journal of Organic Chemistry*, **2008**, *73*, 6835-6837.

9. Bahrami, K.; Khodaei, M. M.; Kavianinia, I., *Synthesis,* **2007**, 417-427.

10. Trotter, K. D.; Reglinski, J.; Robertson, K.; Forgie, J. C.; Parkinson, J. A.; Kennedy, A. R.; Armstrong, D. R.; Sowden, R. J.; Spickett, C. M., *Inorganica Chimica Acta*, **2009**, *362*, 4065-4072.

Chapter 4

Donor atom substitution towards stable Cu(I) macrocycles; modification to the N_2S_2 motif

4.1 Introduction

Previous studies (Chapter 2) have shown that copper macrocycles may have some potential as redox active contrast agents. However while the N_2S_2 macrocycles support the formation of paramagnetic copper (II) complexes, the corresponding copper (I) complexes were not stable and prone to oxidation at the metal and the nitrogen donor atoms. Thus the detection of oxidants will not be stoichiometric with these complexes. In an attempt to combat the issue of N-oxidation it was decided to attach pendant arms to the nitrogen donors and while this prevented N-oxidation it also detrimentally affected the redox potential of the complex. It is evident that we need to increase the stability of the copper (I) form of this species. In an attempt to achieve this it has been decided to completely replace the nitrogens in the macrocycle with sulfurs and synthesize a much softer, cyclic S_4-thioether copper complex. There are relatively few reports on copper complexes of tetradentate thioether macrocycles. However these do support the hypothesis that it should be possible to isolate copper (I) compounds. Shown is a very simple complex reported by Glick *et al.*[1] (Figure 4.1) of a copper (I) thioether macrocyclic species.
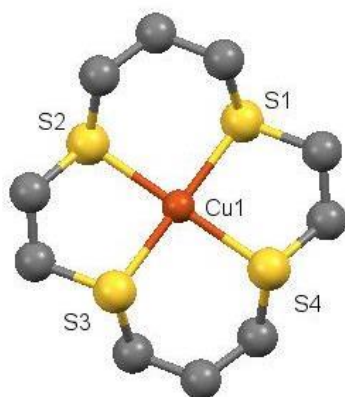
Figure 4.1: Copper 1,4,8,11-tetrathiacyclotetradecane [Cu(TTCD)]$^+$ cation reported by Glick *et al.*[1] The complex is square planar. The structure has been re-drawn from the cif file deposited in the CSD database. Protons and tetrafluoroborate anion are omitted for clarity.

From the metrical parameters for [Cu(TTCD)]$^+$ it can be seen that the complex exhibits great symmetry. The bond lengths between adjacent sulfurs are identical (2.309 Å, 2.296 Å) and that the *trans* S-Cu-S bond angles are both 180º confirming the planar nature of the complex.[1] Although this complex demonstrates the stability of the desired macrocycle, the simple nature of the ring limits the possible uses of the compound. We have consequently opted to maintain

our basic organic skeleton (Figure 4.2) as we anticipate using the aromatic groups to allow us to control properties such as solubility and toxicity. Kakos *et al*. studied the effect of the stability of the parent compound [Cu(TTCD)]$^+$ and modified versions with the addition of cyclic groups.[2,3] The addition of aryl groups (cyclopentadiene) to the parent macrocycle showed that in general there was an increase in stability. Thus the aim of this study is to synthesise the complex shown (figure 4.2) as a representative example of the thioether macrocycles. It is hoped that this macrocycle will promote copper (I) formation and show a greater redox stability than the previous N_2S_2 macrocycle.
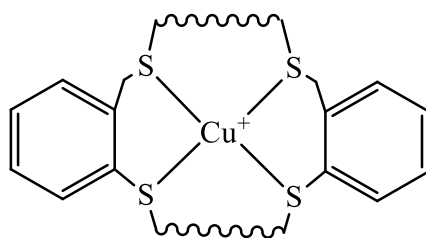
Figure 4.2: Diagrammatic representation of the target copper complex: [Cu(I)$S_{xu}S_{xl}$]$^+$.

Rorabacher and Ochrymowycz have synthesised a series of open chain Cu(I)/Cu(II) S_3N and N_2S_2 macrocycles as well as S_4 macrocycles [4,5,6] (Figure 4.3). These studies have included an investigation of the redox potential and electron transfer rates of a series of macrocycles of interest to this project (Figure 4.4).

[14]ane S4-a   [14]ane S4-b

[14]ane NS3-a   [14]ane NS3-b
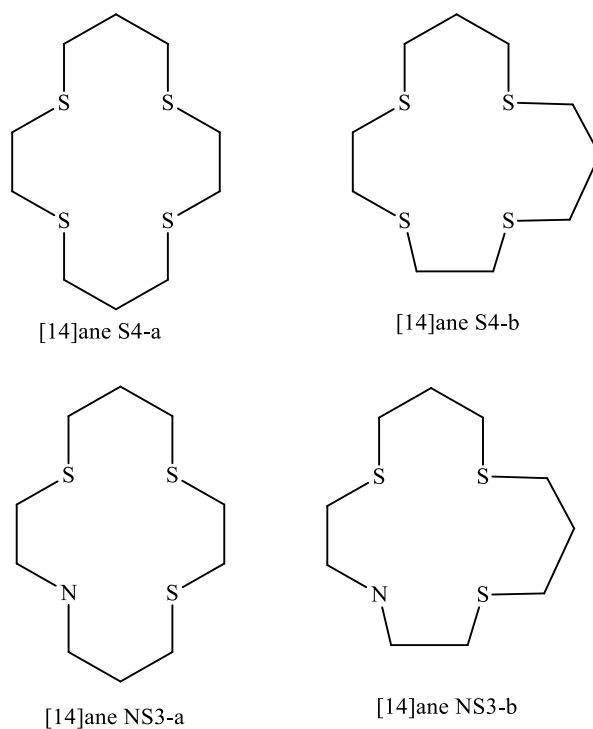
Figure 4.3: Chem draw structure of S_4 and S_3N systems involved in study by Rorabacher et.al.[5]
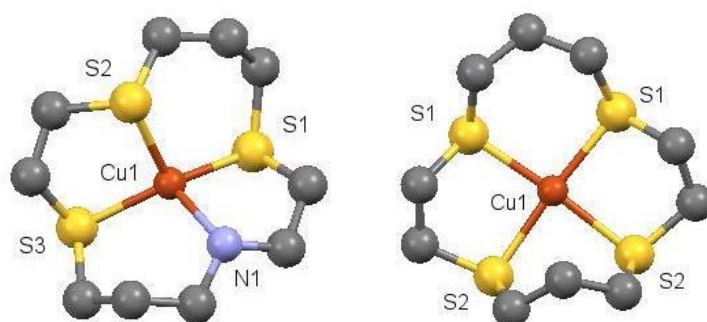
Figure 4.4: Copper 1,4,10-trithia-7-azacyclotridecane ([Cu[14]ane-S_3N-a], left) and copper 1,4,8,11-tetrathiacyclotetradecane ([Cu[14]ane-S_4-a], right). The complexes are square planar. The structure has been re-drawn from the cif file deposited in the CSD database. Protons and perchlorate anions are omitted for clarity in both cases.[3,4]

In aqueous solution at 25°C the Cu(I) and Cu(II) S_4 systems (figure 4.4) showed reversible behaviour at slower scan rates.[7] The investigation of the electron transfer pathways of Cu(I)/Cu(II) S_4 and S_3N macrocycles supports a dual pathway 'square scheme' mechanism in which changes in the coordination geometry occur sequentially rather than concertedly with

the electron transfer step. The different coordination geometries preferred by Cu(II) (square planar) and Cu(I) (tetrahedral) imply the reduction and oxidation of the complexes involve significant structural changes. Rorabacher's studies suggest that the S_3N system showed greater promise with electrochemically reversible characteristics.[5] Despite this we have initially chosen to focus our attention on our related S_4 systems as this will better identify our limiting conditions.

Pathway A

Cu(II)L (O) ⇌ Cu(I)L (P)

KOQ   KRP

Cu(II)L (Q) ⇌ Cu(I)L (R)
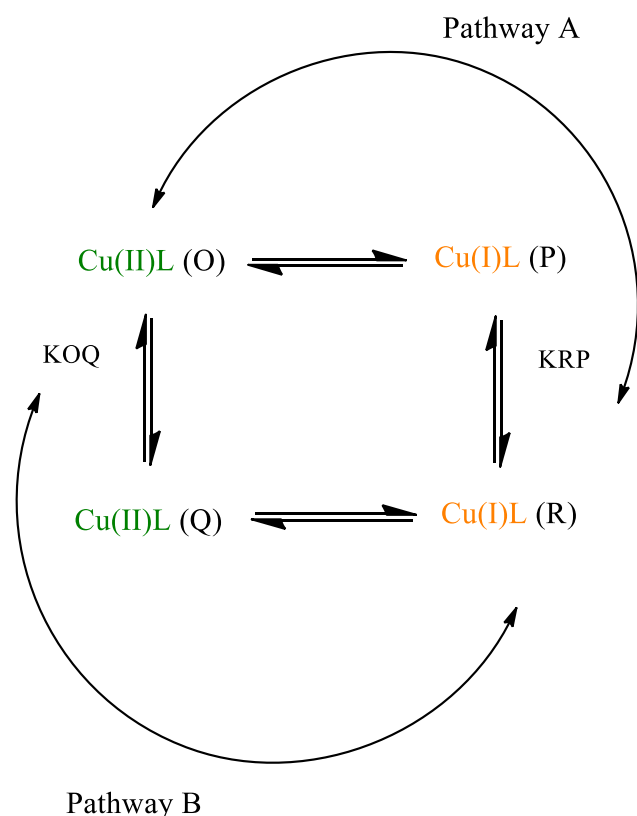
Pathway B

Figure 4.5: Dual pathway square scheme for electron transfer reaction involving Cu(I/II) tetrathiaether complexes. The species labelled **O** and **R** are the stable form of the Cu(II) and Cu(I) forms, respectively, while **P** and **Q** represent metastable intermediate species which are presumed to involve geometries resembling the stable form of the opposite oxidation state. The horizontal reaction represents electron transfer and the vertical reactions represent conformational changes.

The geometries of the intermediate species in the dual pathway scheme (Figure 4.5) have remained a matter of speculation. Studies suggest that **O** ⇌ **Q** and **P** ⇌ **R** transformations may represent changes in the conformation of the coordinated macrocycle involving donor atom inversion.[8] Bosnich *et al.* were the first to note that macrocycles with alternating ethylene and propylene backbones could form metal ion complexes with five

distinct ligand conformations if the donor atoms are tetrahedral when coordinated.[9] These five conformers are distinguished by the orientations of the coordinated donor atoms. Conformer I is when the lone pair electrons on all four sulfur donor atoms are orientated on the same side of the S_4 plane (RSRS or + + + +) this results in an overall 'boat' conformation, conformation II (RRRS or + - ++) for any inter-conversion between the various conformers, conformation II must serve as an intermediate species if it is assumed that the donor atom inversions occur at the one time rather than in a concerted matter. There are three other conformations (Conformation III (RRSS or + - - +), conformation IV (RSSR or + + - -) and conformation V (RRRR or + - + -)). These conformations only differ in the positioning of the lone pairs.[8] This behaviour is seen in the structural chemistry these species. For example in the solid state [Cu (II)[14]ane S_4-a](ClO$_4$)$_2$ exists as conformer III. Comparative studies suggest [Cu(II)[14]ane S_3N-a] adopts the same conformer. In contrast, the crystal structure of [Cu(II)([14]ane S_3N-b)H$_2$O](ClO$_4$)$_2$ is found to adopt a structure consistent with conformer II. The crystal structure obtained for [Cu(I)[14]ane S_3N-a](ClO$_4$)[5] shows the ligand to be consistent with conformer V. The same conformer has also been found in the Cu (I) complexes formed with two substituted versions of Cu(II)[14]ane S_4 where the ethylene bridges have been replaced with 1,2-cyclohexane[10] and 1,2-cyclopentane[11]. The Cu (I) substituted systems are the closest comparison to the target macrocycles in this study, and while it is tempting to suggest that the species being synthesised here will adopt the structure of conformer V, the planar aromatic present in our compound may heavily influence this.

The aim of this work was to synthesise and characterise a representative member of the S_4-thioether macrocycles and make chemical comparisons with the N_2S_2 systems discussed earlier.

4.2 Results and discussion

4.2.1 Synthesis of 36
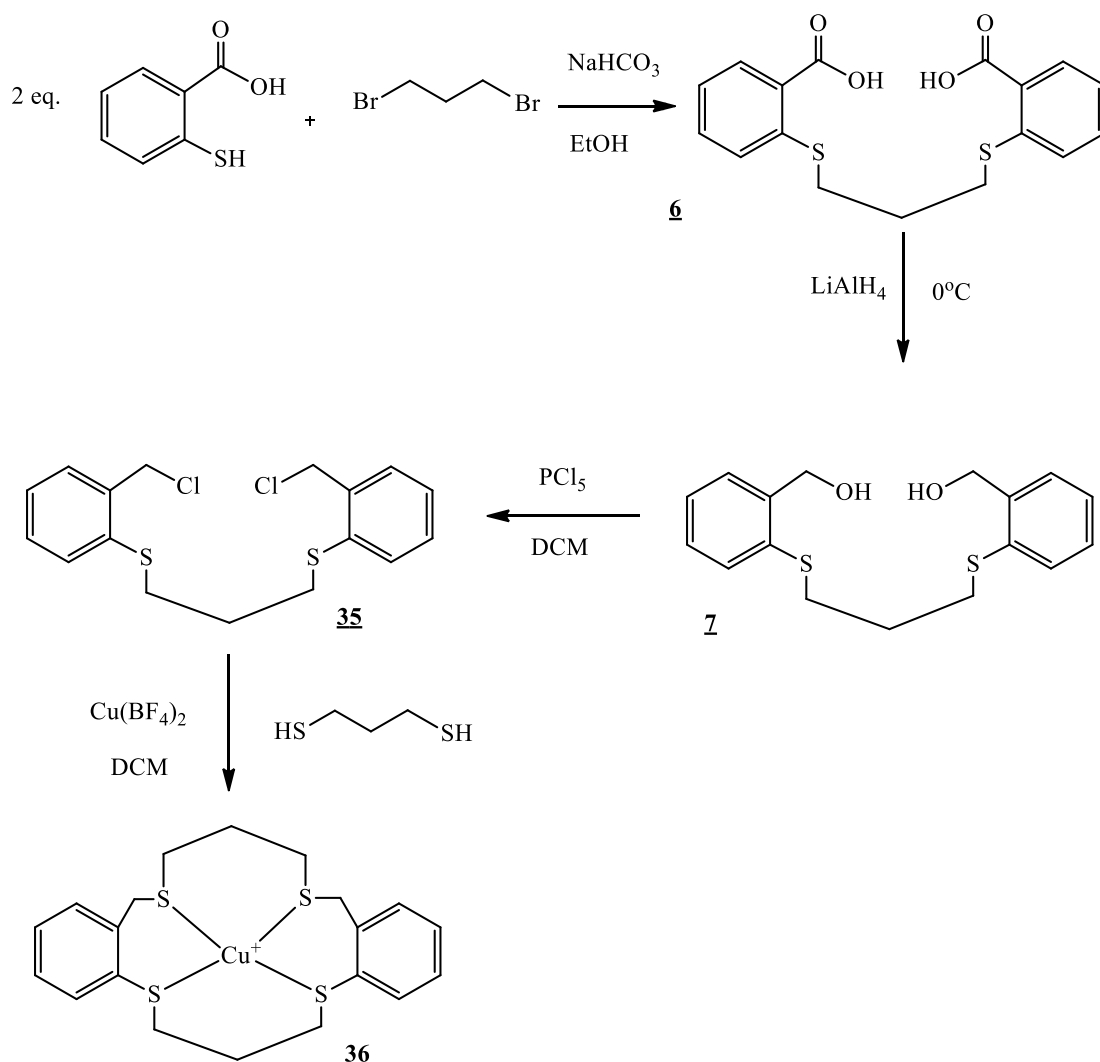
Figure 4.6: Synthetic route to produce compound **36**.

The synthesis of compound **36** parallels that of the N_2S_2 macrocycle in the initial synthetic steps. Once **7** was prepared the compound was chlorinated with PCl_5 in dichloromethane to produce compound **35**. $Cu(BF_4)_2$ and propane dithiol were added to **35** to close the ring and metallate the centre. The product was isolated as a waxy yellow solid and characterised using mass spectrometry, NMR and microanalysis. This data supports the formulation of the complex as a copper (I) complex. The complex was of suitable quality for electrochemical analysis.

The same synthesis was attempted with varying backbone lengths but these did not yield any suitable results. It was therefore decided to try a different approach to the synthesis of this family of macrocycles i.e. those included a mix of propyl and ethyl backbones, including the S_3N macrocycle based on cysteamine.

4.2.2 Electrochemistry

Cyclic voltammetry was used to estimate the redox potential of the complex as previously described in 2.3.5. The complex (**36**) was prepared as a solution (3 mM) in 0.1 M t-butylammonium tetrafluoroborate (${}^{t}Bu_4NBF_4$). This electrolyte was used as the tetrafluoroborate anion is the typical counter-ion in the copper complexes, therefore eliminating any potential exchange reactions. The voltammograms were referenced to the ferrocene/ferrocenium (Fe(III)/Fe(II)) redox couple by running a ferrocene solution under the same conditions before and after the samples and subtracting this redox potential from that of the samples, the values are expressed relative to the normal hydrogen electrode (NHE).
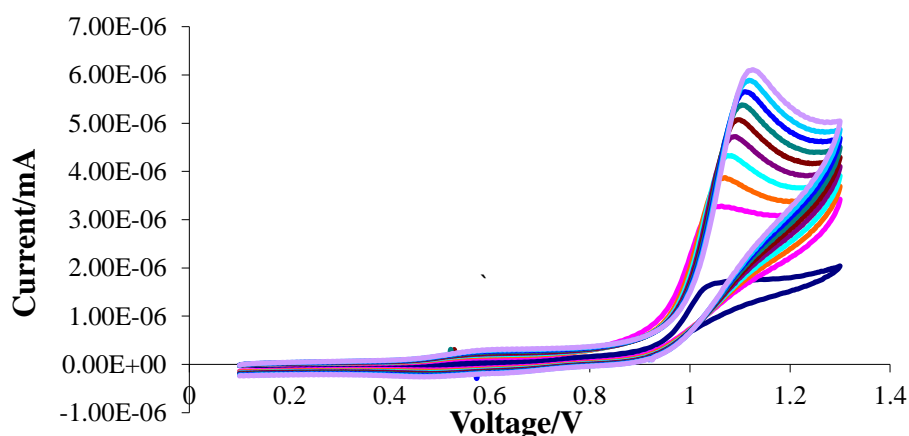
Figure 4.7: The cyclic votammogramm for **36** in acetonitrile at scan rates varying from 50 mVs^{-1} to 500 mVs^{-1}.

A direct comparison with the ferrocene standard (Appendix 4) indicate that the process is a one electron oxidation i.e. the successful oxidation of the Cu(I) complex to Cu(II), however

there is no reverse wave indicating the complex does not reduce. The E^o value was calculated to be 1.28 V (vs. NHE). Cyclic voltammetry suggests that the complex shows signs of electrochemical irreversibility. However, this issue may resolve itself with a larger or smaller ring which, according to Rorabacher *et. al.* may allow more rapid conformational changes.[9] As such further work will be carried out on the synthesis of alternative compounds with varying backbone lengths.

4.2.3 Alternative synthetic route to S$_4$ systems

The synthesis described in section 4.2.1 only produced one S$_4$ system. It was therefore decided to try an alternative method which involved chlorinating the acid instead of the alcohol which would leave a ketone still attached. It was thought that the oxygens would provide some stability to the rings during cyclisation.
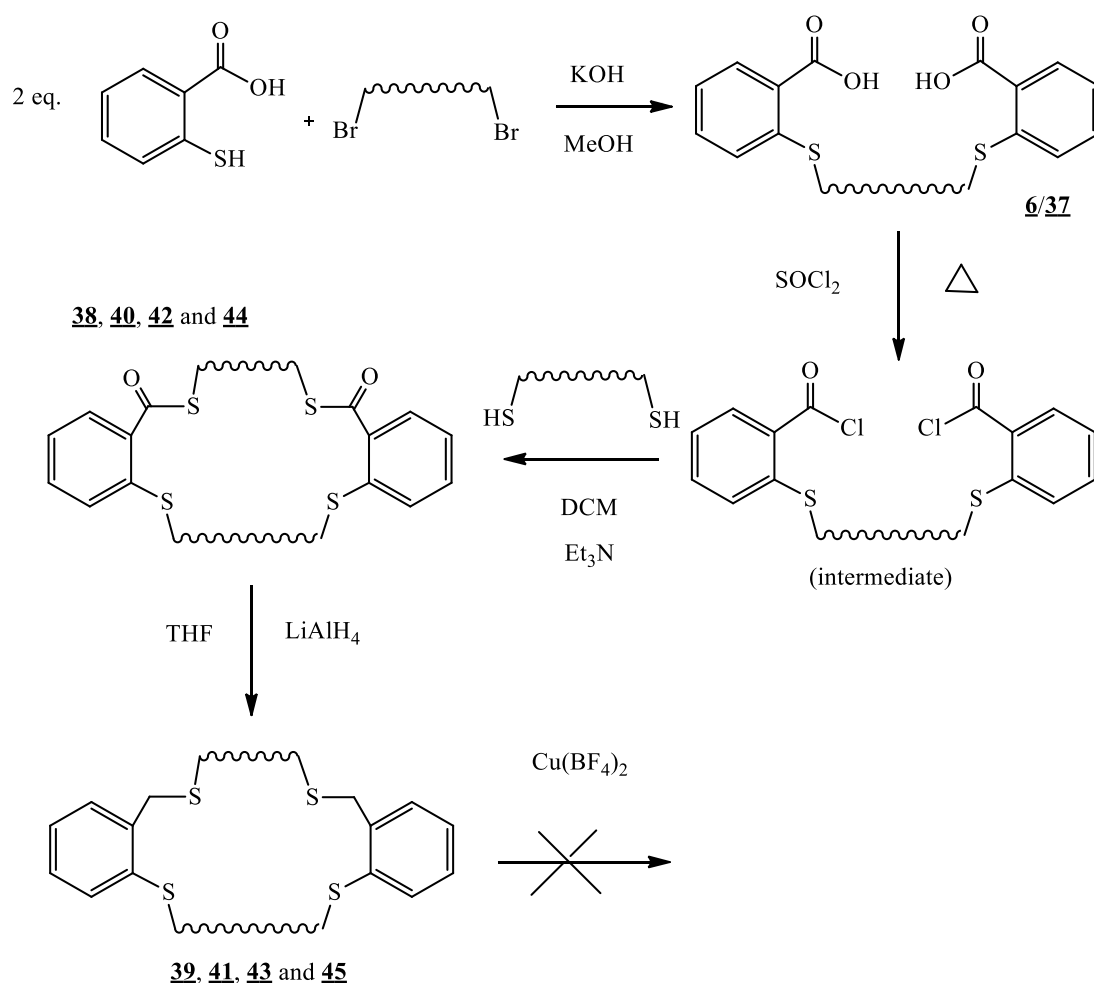
Figure 4.8: Alternative synthetic route to S_4 system.

6 and **37** were synthesised as previously reported, the dibromo backbone lengths include both the propyl and ethyl. In contrast to the synthetic route shown in Figure 4.6, the acid is not reduced to the alcohol as its thought that the oxygens would have a stabilising effect and would promote ring closure in smaller backbone lengths. The carboxylate is chlorinated by refluxing in thionyl chloride for an hour to produce an intermediate acyl chloride. The intermediate is then dissolved in dichloromethane and triethylamine to which the appropriate dithiol and triethylamine is added. This produced a yellow solid. The addition of copper to the centre of the ligand was attempted, this proved to be unsuccessful in all cases. A crystal structure of a macrocycle (compound **38**) was isolated (Figure 4.9). In contrast to the crystal structure reported by Glick *et al.*[Cu(TTCD)]$^+$ (Figure 4.1) it can be seen that the ring is not planar, this could be due to the inflexibility of aryl rings which lie in close proximity to the ketonic oxygens. As can be seen from figure 4.9 the ring is puckered. This is an undesirable

shape for the bonding of copper to the macrocyclic centre and it is unsurprising that the copper complex could not be formed.
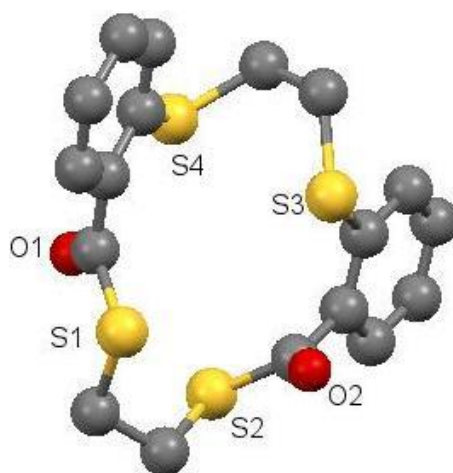
Figure 4.9 The X-ray crystal structure of compound **38**. The hydrogens have been omitted for clarity.

The oxygens were removed using LiAlH$_4$ in the hope that this would alter the shape of the ring to afford a better flexibility and allow for a copper to bond at the centre of the macrocycle. Despite this modification, mass spectrometry and microanalysis confirmed that even in the absence of the oxygens the copper did not bind to the macrocycle. This was a contrast to compound **36** and it was not fully understood why this was the case. It was therefore decided to perform DFT analysis (*vide infra*) to better understand the bonding interactions between copper and the sulfurs present in the rings.

4.2.4 Synthesis of S$_3$N system

Previously both N$_2$S$_2$ and S$_4$ macrocycles have been synthesised, it was therefore decided to synthesise an S$_3$N as it would open up the possibility of adding one pendant arm group at the nitrogen position. The S$_3$N system was attempted using the same synthesis described in figure 4.6 where the dithiol was replaced with cysteamine, however the cysteamine did not couple with the chlorinated intermediate and the ring failed to close. The synthesis was then altered to a similar manner as described in Figure 4.8, where the dithiol was again replaced with cysteamine. This yielded more positive results where both the ring with the ketonic oxygens

present was formed as well as the reduced ring without oxygens. However, similarly to the attempts to introduce a copper centre to the S_4 systems, the S_3N system (**47**) would not metallate.
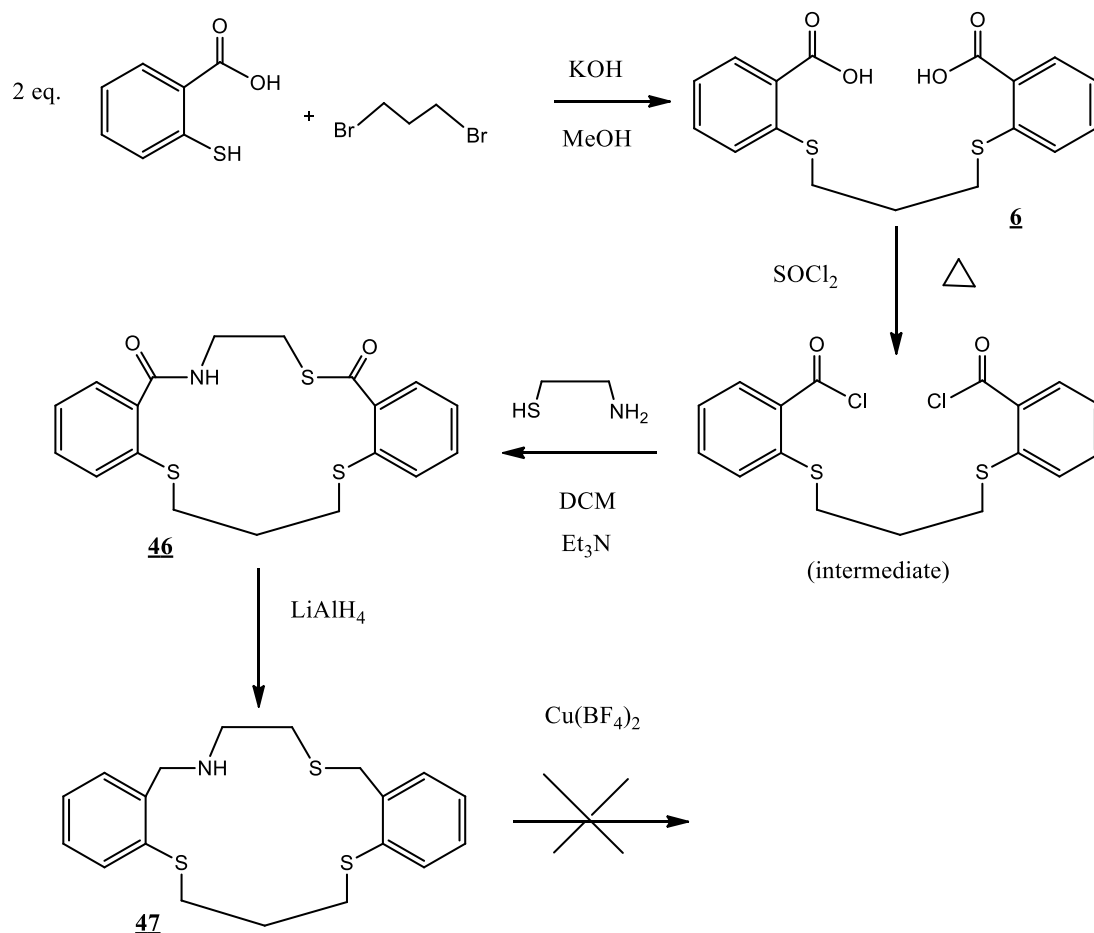
Figure 4.10: The synthetic route of S_3N macrocycle **47**.

4.2.5 DFT investigation

4.2.5.1 Copper positioning

As discussed in section 4.2.3 it has proved difficult to prepare copper complexes of these S_4 macrocycles. In an attempt to better understand the underlying chemistry, it was decided to perform rudimentary restricted density functional theory (DFT) calculations using the Gaussian 09 program on the desired compounds [13,14,15]. The investigation includes the S_4 macrocycles discussed above (compounds **39**, **41**, **43** and **45**) and their desired interaction with copper. The XRD data for the analogous N_2S_2 macrocycles (CCDC 738882, 738885, 738886 and CSD 591132) were used to generate the desired motif replacing the two secondary amines with two thio-ethers. These modified species were then optimised. Once the structures had refined a copper atom was introduced into the centre of each of the rings. The complexes formed "in silico" were further optimised and then subjected to frequency analysis. The tables give the initial starting position of the copper and the subsequent position of the copper after undergoing optimisation and frequency analysis. In all cases the copper remains within the macrocyclic pocket. However, with further optimisation many of the Cu-S bond distances fall outside that expected for a formal copper-sulfur bond (2.40 Å). This initial finding would be that copper is reluctant to go four coordinate in these systems.

The initial model placed the copper equidistant from all four sulfurs. This positioning may have given rise to the product obtained. Thus the calculations were conducted again except that the copper was moved to various positions to generate models which had the copper in a two or three coordinate environment.
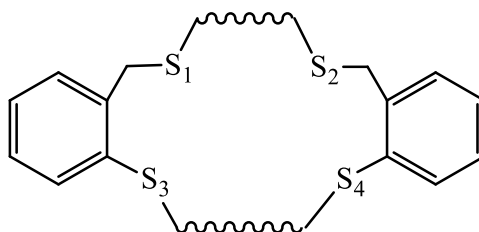
Figure 4.11: Schematic illustrating theoretical numbering system of sulfur atoms for use in understanding the Cu-S bonding positions used in DFT calculations.
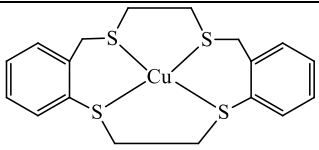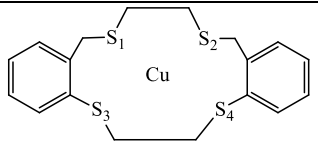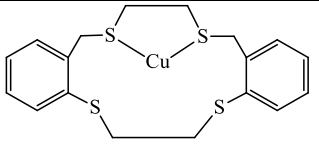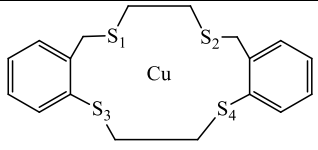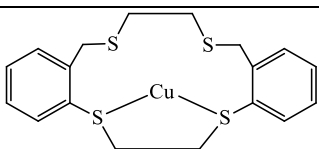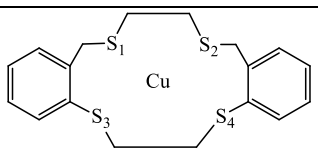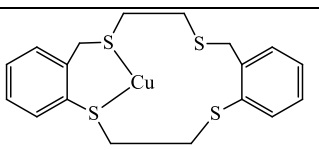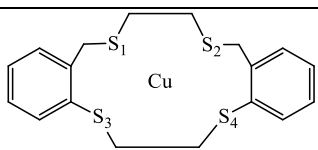
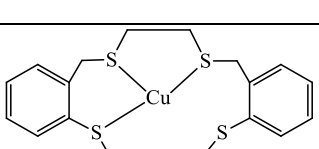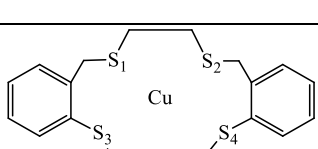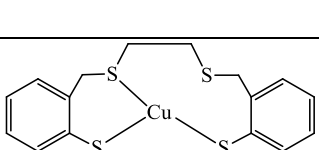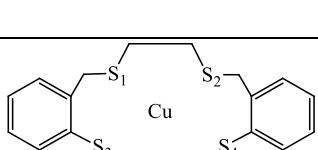| Initial Structure	Optimised Structure	Cu-S bond distance (Å)		Energy (A.U)
		S_1	2.390	-3931.29940953
		S_2	2.383	
		S_3	2.402	
		S_4	2.400	
		S_1	2.389	-3931.29940942
		S_2	2.383	
		S_3	2.402	
		S_4	2.400	
		S_1	2.383	-3931.29940935
		S_2	2.390	
		S_3	2.399	
		S_4	2.403	
		S_1	2.388	-3931.29940939
		S_2	2.383	
		S_3	2.403	
		S_4	2.399	
		S_1	2.390	-3931.29940882
		S_2	2.380	
		S_3	2.405	
		S_4	2.399	
		S_1	2.289	-3931.29940942
		S_2	2.383	
		S_3	2.403	
		S_4	2.399	

Table 4.1: Results of DFT calculations of compound **39** where copper is introduced at various starting positions on the ring. Bonding has been predicted by Gaussview5[16] after compounds undergo optimisation and frequency analysis. The lines shown depict Cu-S distance which fall below 2.4 Å which signify the potential for a formal bond. Irrespective of the starting position of the calculation the final structures are the same (±6.28 cal/mol) i.e a copper loosely held within the cavity generated by the macrocycle.
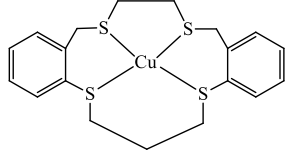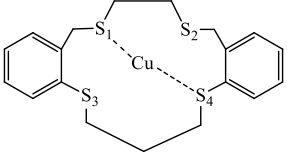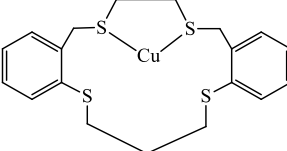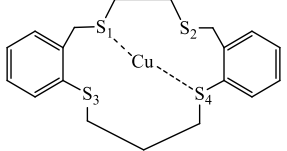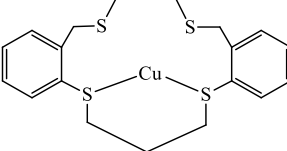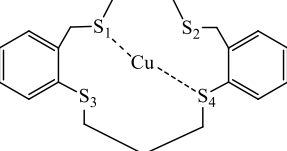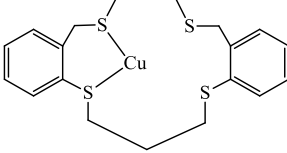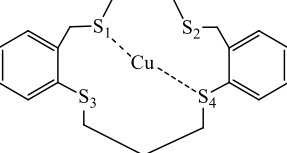
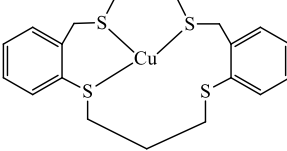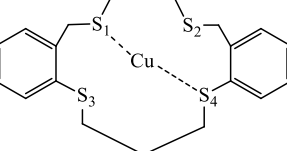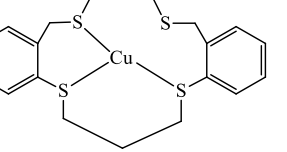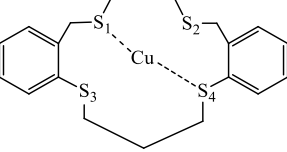| Initial Structure	Optimised Structure	Cu-S bond distance (Å)		Energy (A.U)
		S_1	2.243	-3970.62027630
		S_2	2.655	
		S_3	2.862	
		S_4	2.239	
		S_1	2.243	-3970.62027672
		S_2	2.645	
		S_3	2.868	
		S_4	2.238	
		S_1	2.238	- 3970.6197676
		S_2	3.155	
		S_3	2.556	
		S_4	2.243	
		S_1	2.243	- 3970.6197677
		S_2	3.155	
		S_3	2.556	
		S_4	2.238	
		S_1	2.243	-3970.62027676
		S_2	2.867	
		S_3	2.649	
		S_4	2.238	
		S_1	2.258	-3970.61782674
		S_2	2.914	
		S_3	2.567	
		S_4	2.284	

Table 4.2: Results of DFT calculations of compound **41** where copper is introduced at various starting positions on the ring. Bonding has been predicted by Gaussview5[16] after compounds undergo optimisation and frequency analysis. The lines shown depict Cu-S distance which fall below 2.4 Å which signify the potential for a formal bond. There is a slight energy difference in the structures (1.54 kcal/mol) which can be attributed to differences in the conformation of the rings. The refined final structures are the same i.e. the copper sits *trans* didentate within the cavity generated by the macrocycle.

Table 4.2 suggests that there are three structures available with comparable energies, these structure have lower energies and were found to be in the boat conformation. The table also shows that there are three structures with higher energies. The highest energy conformation was found to have an energy difference of 1.54 kcal/mol and this structure was in the chair conformation. There are also two structures which appear to be much more planar and the slight energy difference between these and the lowest energy (boat) conformation was found to be 0.32 kcal/mol. The reorganisation of the boat/chair conformation of related copper macrocycles has been discussed previously in N_2S_2 systems. Trotter *et. al.* studied the kinetic and thermodynamic behaviour of the chair/boat flip and found that the reaction to be facile with only minor energy differences between the two forms.[17,18] As the position of the copper in the final calculated structures is not "different" it was not thought necessary to further study the conformational variances of this system further.
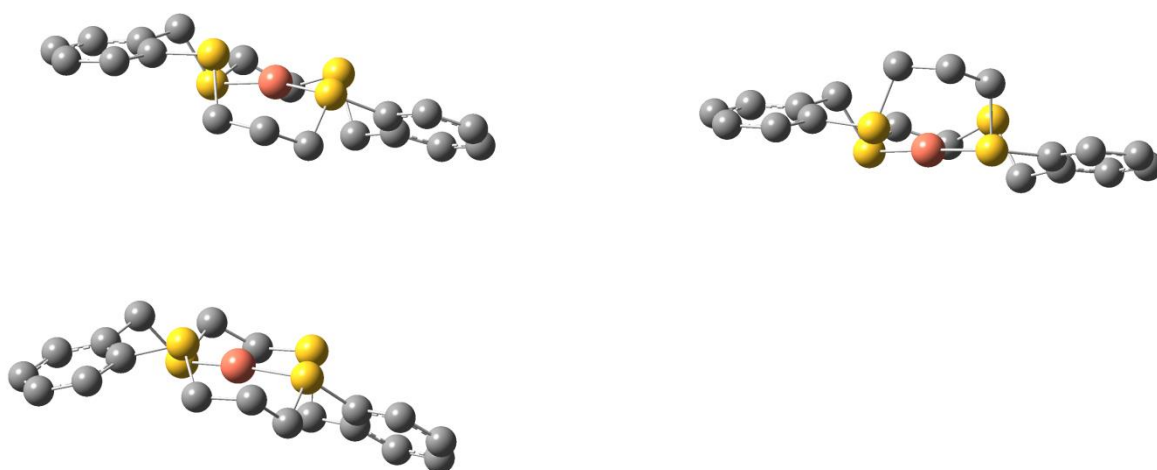

Figure 4.12: Optimised structures obtained from final DFT calculations for compounds **41**. The lowest energy structure has optimised to a boat conformation where the propyl backbone is below the aryl rings (top left) and the highest energy structure has optimised to a chair conformation where the propyl backbone is above the aryl rings (top right). The energy difference between the two structures (1.54 kcal/mol) can be attributed to the differences in conformations. The third conformation is also shown (bottom left), and this is a slightly higher energy conformation all be it by 0.32 kcal/mol.
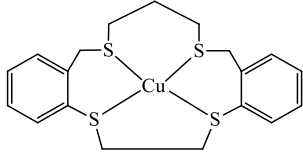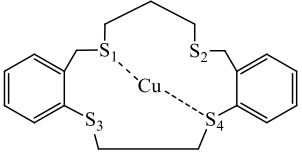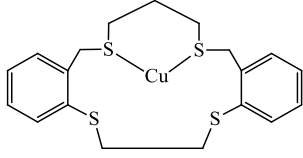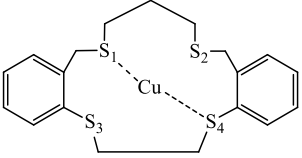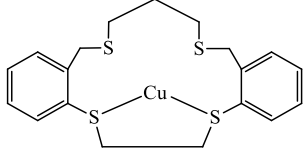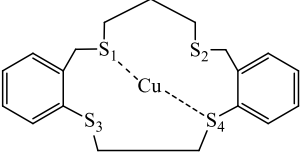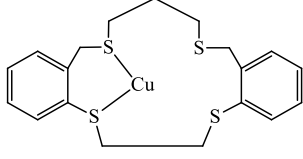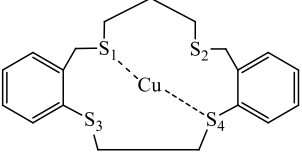
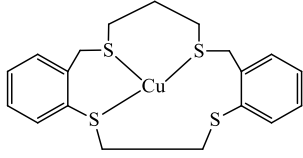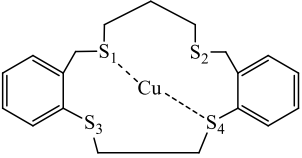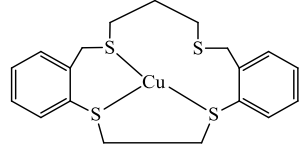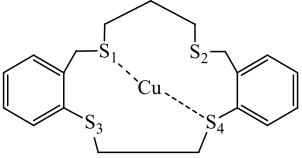| Initial Structure	Optimised Structure	Cu-S bond distance (Å)		Energy (A.U)
		S_1	2.216	- 3970.62118893
		S_2	2.405	
		S_3	3.565	
		S_4	2.225	
		S_1	2.216	-3970.62118900
		S_2	2.405	
		S_3	3.566	
		S_4	2.225	
		S_1	2.231	- 3970.61875587
		S_2	3.312	
		S_3	2.485	
		S_4	2.235	
		S_1	2.225	- 3970.62118884
		S_2	2.405	
		S_3	3.566	
		S_4	2.216	
		S_1	2.230	- 3970.61875577
		S_2	3.312	
		S_3	2.485	
		S_4	2.234	
		S_1	2.225	-3970.6211884
		S_2	3.670	
		S_3	2.404	
		S_4	2.216	

Table 4.3: Results of DFT calculations of compound **43** where copper is introduced at various starting positions on the ring. Bonding has been predicted by Gaussview5[16] after compounds undergo optimisation and frequency analysis. The lines shown depict Cu-S distance which fall below 2.4 Å which signify the potential for a formal bond. There is a slight energy difference in the structures (1.53 kcal/mol) which can be attributed to differences in the conformation of the rings. The refined final structures are the same i.e. the copper sits *trans* didentate within the cavity generated by the macrocycle.
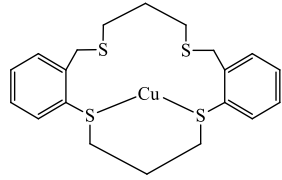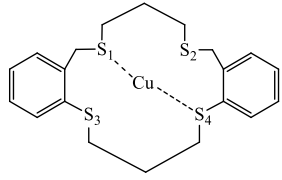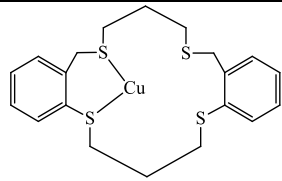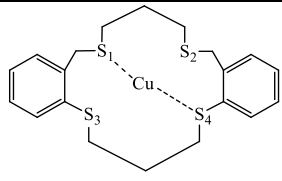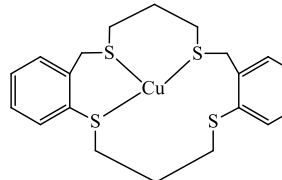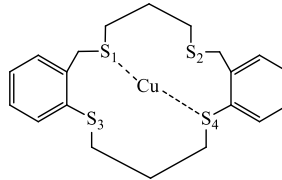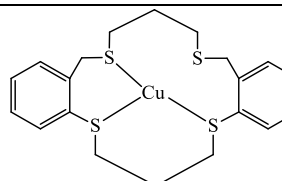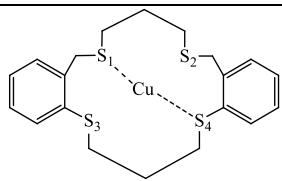
Initial Structure	Optimised Structure	Cu-S bond distance (Å)		Energy (A.U)
		S_1	2.223	-4009.94747699
		S_2	2.429	
		S_3	3.754	
		S_4	2.243	
		S_1	2.233	-4009.94458428
		S_2	2.450	
		S_3	3.512	
		S_4	2.223	
		S_1	2.243	-4009.94747737
		S_2	2.450	
		S_3	3.512	
		S_4	2.223	
		S_1	2.223	-4009.94747716
		S_2	2.428	
		S_3	3.753	
		S_4	2.243	
		S_1	2.233	-4009.94458435
		S_2	2.450	
		S_3	3.511	
		S_4	2.223	
		S_1	2.230	-4009.94292953
		S_2	2.626	
		S_3	3.201	
		S_4	2.223	

Table 4.4: Results of DFT calculations of compound **45** where copper is introduced at various starting positions on the ring. Bonding has been predicted by Gaussview5[16] after compounds undergo optimisation and frequency analysis. The lines shown depict Cu-S distance which fall below 2.4 Å which signify the potential for a formal bond. There is a slight energy difference in the structures (2.85 kcal/mol) which can be attributed to differences in the conformation of the rings. The refined final structures are the same i.e. the copper sits *trans* didentate within the cavity generated by the macrocycle.
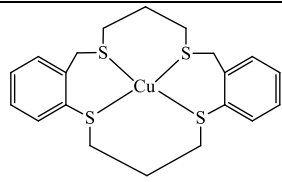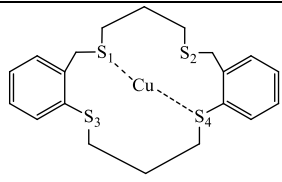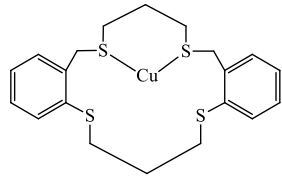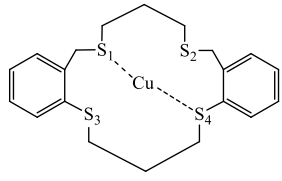
The energy difference in compound **43** (1.53kcal/mol) and **45** (2.85 kcal/mol) can again be attributed to the change between the boat/chair conformations, similar to compound **41** (figure 4.12). The compound with the lowest energy is again the boat conformation.

The results obtained (Figure 4.12) indicate that in the absence of additional donors there is a preference for a didentate configuration in every case (compounds **41**, **43** and **45**) apart from compound **39** where the copper sits in a pocket in the middle of the ring. The alteration in structure probably arises from the change in ring size. **39** is the smallest of the rings and most likely generates a more confined pocket. It is likely that the copper has found a potential energy minimum equidistant from the donors. A larger ring affords more flexibility and as such the formation of formal interactions with the lone pairs on the thio-ethers.
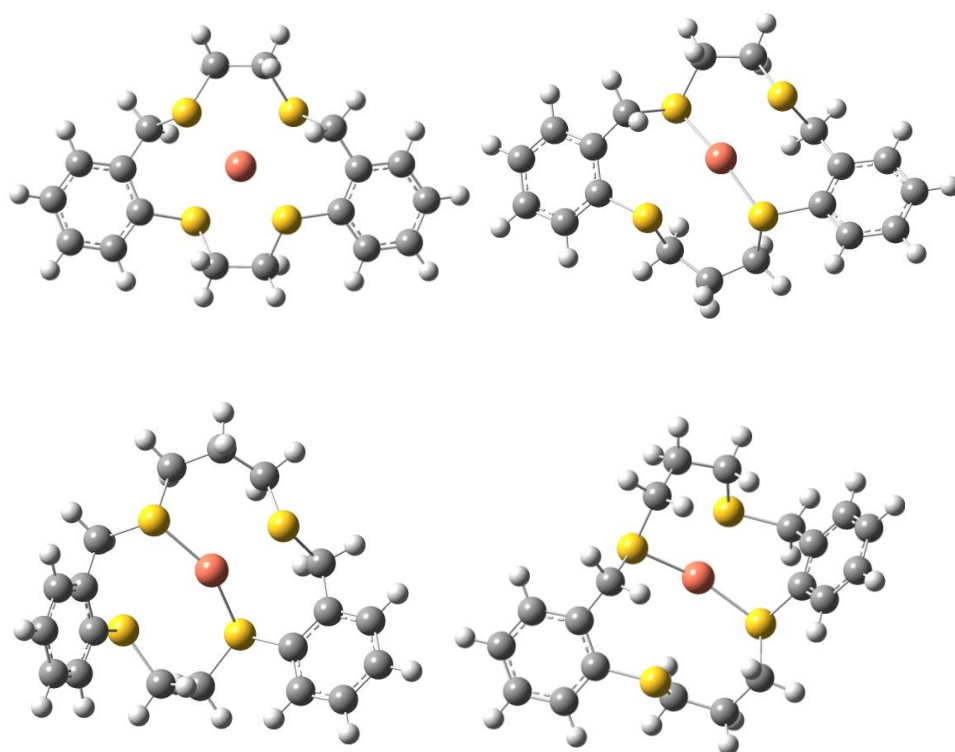

Figure 4.13: Gaussian output file of lowest energy optimised structures of S_4 systems with copper atom. **39** (top left), **41** (top right), **43** (bottom left) and **45** (bottom right).

The study above had placed the copper at various positions within the ring. For completeness it was decided to also place the copper atom on external sites to investigate if it migrated into the ring or not. Thus a copper atom is introduced at the exo and endo positions on one sulfur to see if there was a preference for interactions with the adjacent sulfurs and the centre of the ring. In these studies the single copper was introduced as shown at either of the two positions in Figure 4.14.
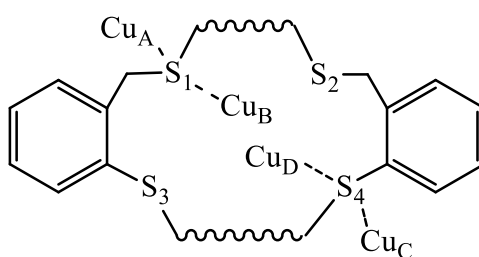
Figure 4.14: Schematic illustrating theoretical numbering system of sulfur atoms for use in understanding the Cu-S bonding at the exo and endo positions used in DFT calculations. Where the sulfurs are numbered ($S_1 - S_4$) for identification and the exo positions (Cu_A and Cu_C) and endo positions (Cu_B) and Cu_D) are lettered for identification.

As expected the results obtained show that when the copper is introduced at the endo position (Cu_B and Cu_D) at both upper and lower sulfurs (S_1 and S_4), the copper has a preference to bond in the manner seen in the first set of calculations (Table 4.1 – 4.4, Figure 4.12). However, when the copper is placed on an exo position (Cu_A and Cu_C) it optimises to the centre of the ring in most cases except for three isolated incidences. In these cases the copper formally bonded in an unexpected manner. (All tables with structures and values can be found in Appendix 6 for inspection).

The results obtained from the analysis of compound **39**, introducing the copper at the exo positon indicates that the copper does not migrate into the ring but remains attached to just one of the sulfur atoms. In both cases of the introduction of copper at the exo positions (Cu_A

and Cu$_C$) Gaussian optimised the copper to attach to the aryl ring as well (Figure 4.15). The bond length is a feasible length however it is unlikely that structures obtained for either exo position copper optimisation calculation would form as the energy required is much higher than the optimised structures in Table 4.1.
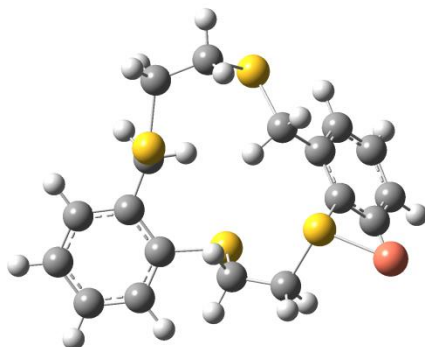
Figure 4.15: Predicted optimised structure of compound **39** after introduction of copper on exo positions (Cu$_A$ and Cu$_C$), where the copper has bonded to the aryl ring. Note that the energy required to achieve this structure (+ 62.12 kcal/mol) is much more than the lowest energy optimised structure found in Table 4.1.

Additional solutions were identified for compound **41** which has the copper *cis* didentate rather than *trans* after introducing the copper at the exo position Cu$_C$ on S$_4$. The energy required to achieve this structure is much larger that the energy of any optimised structure shown in Table 4.2.
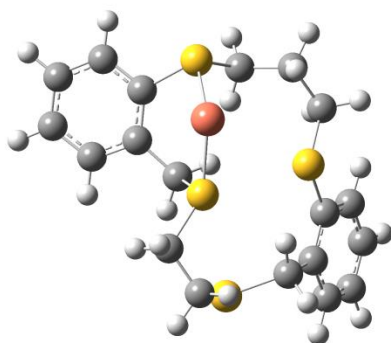

Figure 4.16: Predicted optimised structure of compound **41** after introduction of copper at exo position (Cu$_C$). Gaussian has optimised the copper in the *cis* didentate position. Note that the energy required to achieve this structure (+ 32.89 kcal/mol) is much more than the lowest energy optimised structure found in Table 4.2.

The results obtained (Appendix 6) from introducing the copper on the exo positon Cu_A for compound **43** show that the copper does not coordinate within the ring and remains attached to just one of the sulfur atoms (Figure 4.16). The energy required to achieve this structure is also much larger that the energy of any optimised structure shown in Table 4.3.
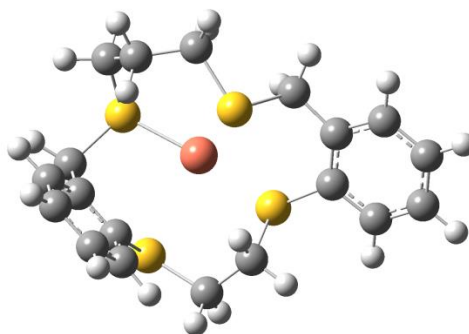
Figure 4.17: Predicted optimised structure of compound **43** after copper is introduced at exo position (Cu_A). Gaussian has optimised the copper to attach to only one sulfur donor atom. Note that the energy required to achieve this structure (+ 6.52 kcal/mol) is much more than the lowest energy optimised structure found in table 4.3.

4.2.5.3 Introduction of water

The DFT calculations performed suggest that it might be possible for copper to form sulfur macrocycles in all cases but with differing coordination numbers and bond strengths. However the computational studies are not in good agreement with the synthetic studies. In an attempt to harmonise these two approaches it was decided to introduce water molecules to the compounds formed "in silico" and see if the copper preferentially coordinates to the water. A model was constructed which had a copper atom attached to a sulfur on an exo position, Cu_A (Figure 4.14). This was used to further produce four species in which the number of water molecules introduced was varied from one to four. The waters and sulfur donor were arranged in a regular manner around the copper centre. The systems were allowed to optimise and the energy for each system containing a varying numbers of water molecules calculated (Figure 4.18). All energies have been normalised by including the corresponding energy of water to balance the stoichiometry of the reaction (Equation 4.1). The relative energies of the four ligands and their hydration states is given in Figure 4.18. The system of lowest energy was found to be the hydrate copper (II) cation and the uncoordinated

macrocycle and the energy of the other species in the reactions have been normalised (macrocycle specific) to these species. The values are only comparible within individual systems as they all contain a different number of atoms, except in the case of compounds **41** and **43** which are isomers.

$$[Cu(OH_2)_4]^{2+} + L \leftrightarrow [Cu(OH_2)_xL]^{2+} \qquad \text{(Equation 4.1)}$$

The data clearly shows that the reaction (Equation 4.1) lies to the left i.e. the lowest energy of the system is achieved by a hydrated copper ion and a discreet ligand. The can been seen below in Figure 4.18.
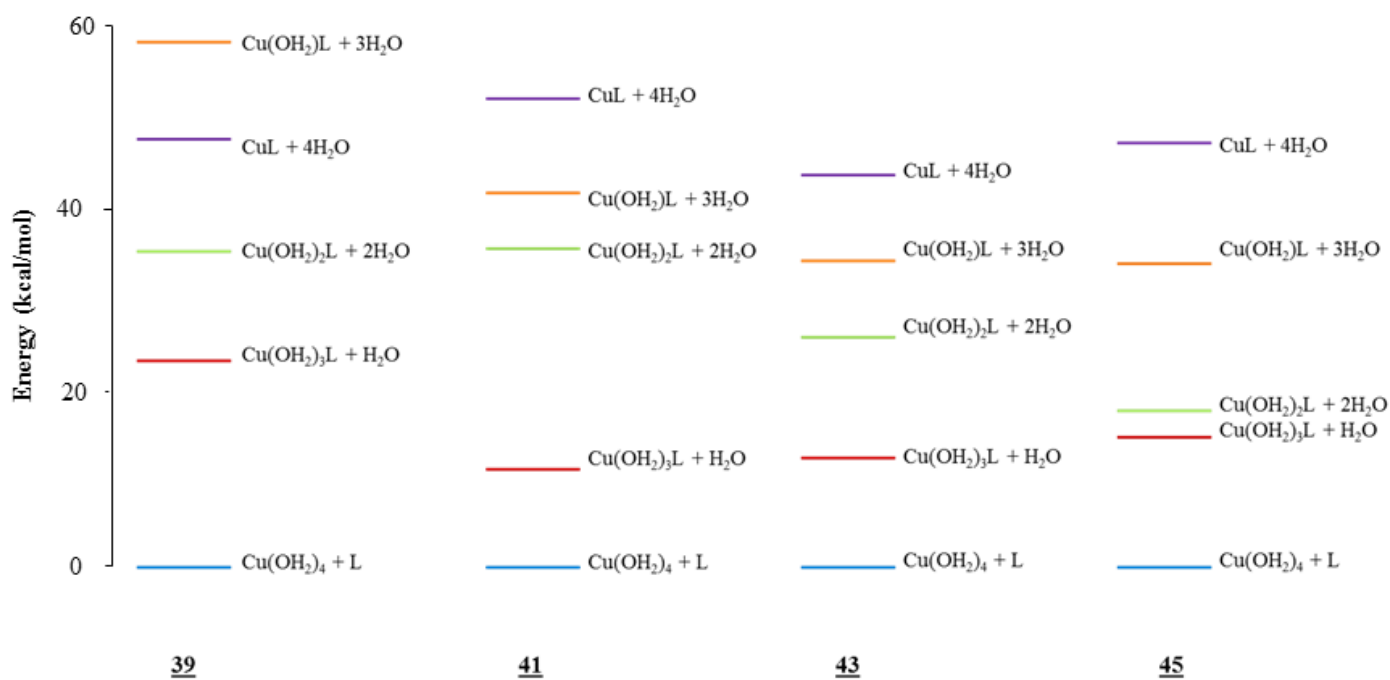
Figure 4.18: The comparison of energy values obtained from optimised DFT calculations (kcal/mol) of ligands (**39**, **41**, **43** and **45**) with water molecules (varying from 1-4) and the lowest energy value obtained from the optimisation of each ligand without water present (where L= ligand). Note that only the energy between the same compounds are comparable. All compounds have been normalised to corresponding $Cu(OH_2)_4 + L$ for use in this figure.

The calculations suggest that these copper complexes will have insufficient stability for use in aqueous solution and are broadly supportive of previous problems isolating these species from donor solvents. We were successful isolating compound **45** by the method discussed in 4.2.1. In retrospect, it is thought that the longer backbone length affords this compound more flexibility than the others which have been studied. The DFT studies suggest that greater success might be had by moving to anhydrous conditions and it was decided to try the alternative synthesis shown in section 4.2.3 using the same method employed in Figure 4.8 but substituting DCM for dry THF.

The results obtained from the synthesis were inconclusive. The elemental analysis obtained did not suggest the compound was suitably pure and it was not possible to obtain a satisfactory mass spectrum of the compound using methanol or acetonitrile. Both are coordinating solvents and could therefore sequester the already fragilely bonded copper; hence the inconclusive nature of the result. This method of synthesis was therefore deemed unsuccessful and the only synthetic route which afforded any success in the formation of a complex was by introducing the copper to the macrocycle prior to ring closure as described in section 4.2.1. However, this does not afford a general synthesis allowing the formation of a single product only.

4.3 Conclusions

The main aim of this study was to synthesise an S_4 macrocyclic copper complex and investigate its electrochemical properties such that we could investigate its potential as the basis of a redox active contrast agent to diagnose oxidative stress.
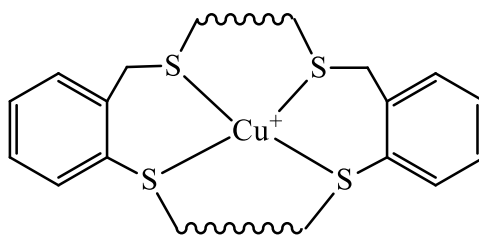

Figure 4.20: Schematic illustrating the target Cu S_4 complexes.

It was attempted to synthesis a series of copper S_4 complexes with varying backbone lengths. This included a propyl/propyl backbone, an ethyl/ethyl backbone, and two propyl/ethyl backbone compounds. Synthetic attempts to produce all the target complexes fell short and after attempting all possible synthetic routes the only compound that was obtained was compound **36** which contained a propyl/propyl backbone.

A series of DFT calculations were conducted in an attempt to better understand the reason behind the difficulty in synthesising the other complexes. Firstly all of the S_4 ring systems were optimised. The copper was then introduced at different positions on the ring and underwent optimisation and frequency calculations. From this the lowest energy system was obtained and the bonding explored using Gaussview5[16]. The general trend in all of the systems (**41**, **43** and **45**) was for *trans* bonding between S-Cu-S apart from compound **39** where the copper optimised to a pocket in the middle of the ring. In this instance the calculations did not support the formation of a formal bonding between the copper and sulfurs.

As the computational and experimental results were in disagreement it was decided to study the effect of sequentially introducing water molecules into the system. From the results

obtained it can be concluded that in a more complex system the copper would preferentially bond to water rather than the macrocycle. The exception was compound **45** where the calculations suggested that a complex might form under anhydrous conditions. A final attempt was made to synthesise compound **45** using dry THF in the hope it would form a stable copper complex. Sadly the synthesis was not successful. It can therefore be concluded that the only CuS_4 macrocycle i.e compound **36** which is thought to be stable due to the flexibility afforded by the longer backbone length. It can also be concluded that the only successful synthetic route to obtaining the target molecule is to introduce the copper prior toring closure. Finally from the results acquired from cyclic voltammetry it can be concluded that these compounds do not possess the reversibility characteristic necessary for use as a redox active imaging agent and as such the chemical effort required to solve the synthetic problems will only have academic value.

4.4 Experimental

4.4.1 General considerations

All experiments were carried out using standard apparatus and commercially available chemicals. Solvents were use as supplied, apart from acetonitrile, which was re-distilled over calcium hydride prior to its use in the electrochemical studies. Microanalysis was carried out by the Microanalysis laboratory at the University of Strathclyde. Mass Spectrometry was carried out on a ThermoFinnigan LCQ mass spectrometer with ESI ionisation, spray voltage 4.5 kV, capillary temperature 200ºC.

4.4.2.1 The preparation of 35
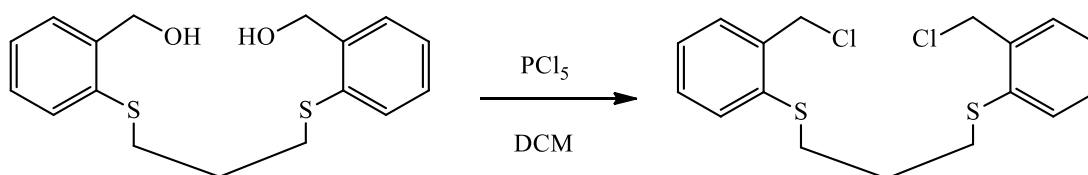
The ligand preparation as far as **7** was as previously reported in 2.2.1. **7** (2.5g, 0.0078 mol) was added to dry dichloromethane to which PCl$_5$ (3.0g, 0.014 mol) was added. The mixture was stirred and heated to reflux overnight. The solution was left to cool and then filtered. The solvent was removed *in vacuo* to yield the crude product. This was then redissolved in distilled water (150 ml) and extracted with dichloromethane (3 x 100 ml). The organic layers were combined and back extracted with distilled water (2 x 100 ml) and dried over anhydrous sodium sulfate. The solvent was removed *in vacuo* to yield a waxy yellow oil.

35: Mass Spec (ESI) *m/z* 357.14 [M]$^+$

An NMR could not be obtained due to the poor solubility of the compound.

4.4.2.2 The preparation of 36
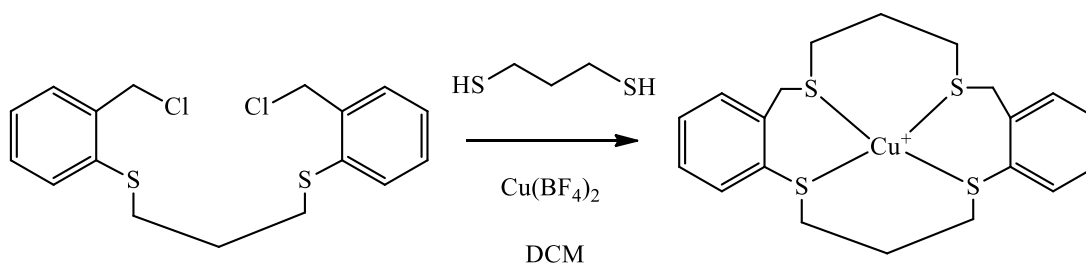
Compound **35** (2.27 g, 0.0063 mol) was dissolved in methanol (150 ml) to which Cu(BF$_4$)$_2$ (0.98g, 0.0041 mol) in methanol (10 ml) was added and the mixture was heated. The solution was then treated dropwise over 2 hours with 1,3-propanedithiol (1.08g, 0.01 mol) and stirred and refluxed overnight. The solution was then left to cool and the solvent removed *in vacuo* to form a yellow solid. The resulting solid was redissolved in distilled water (150 ml) and extracted with dichloromethane (3 x 100 ml). The organic layer were combined and back extracted with distilled water (2 x 100 ml) and dried over anhydrous sodium sulfate. The solvent was removed *in vacuo* to yield a waxy yellow oil.

36: Anal. Calcd. for C$_{19}$H$_{24}$S$_4$CuBF$_4$**:** C, 44.23; H, 5.86; S, 23.22 % Found: C, 44.77; H, 5.31; S, 18.40 % , ^{1}H NMR (400 MHz, CDCl$_3$; δ$_H$) 7.42 (d, 2H ,arom),7.36 (d, 2H, arom), 7.24 (m, 4H, arom), 3.06 (t, 4H, -SC**H**$_2$-), 3.44 (t, 4H, -C**H**$_2$-), 2.19 (s, 4H, -SC**H**$_2$-), 1.97 (p, 2H, -SCH$_2$C**H**$_2$-). Mass Spec (ESI) *m/z* 464.63 [M+Na]$^+$

Note that the sulfur does not combust efficiently in the presence of copper during elemental analysis.

4.4.3.1 The general preparation of S₄O₂ ligands

The preparation of **6** has been discussed previously in section 2.2.1. The preparation of the acid with the ethyl backbone (**37**) is made in the same manner using 1,2- dibromoethane.
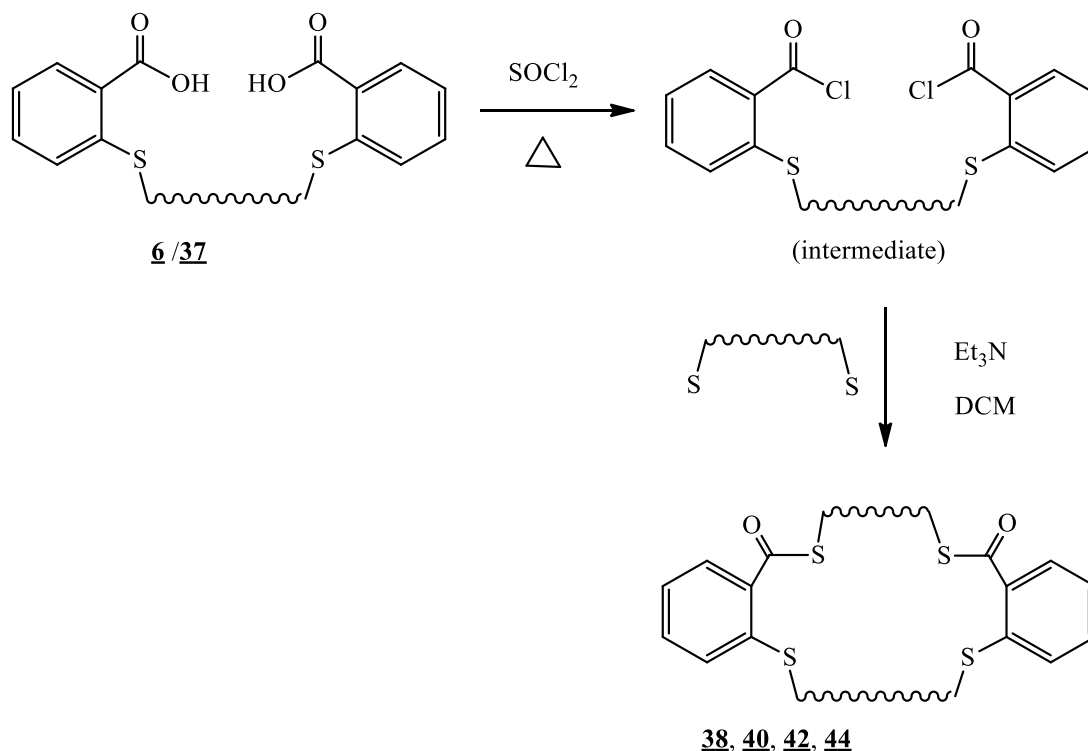
The appropriate acid (**6**/**37**) (0.0075 mol) was dissolved in thionyl chloride (20 ml) and gently heated to reflux for 1 hour under a stream of nitrogen. The thionyl chloride was removed by distillation to yield a yellow solid. The chlorinated intermediate (0.0075 mol) was dissolved in dichloromethane (450 ml) with triethylamine (1.515 g, 0.015 mol) and heated. The appropriate dithiol (0.0075 mol) was then added dropwise. After the addition was complete the mixture was refluxed for 24 hours. The solution was then allowed to cool before being filtered. The solvent was removed *in vacuo* to yield a yellow solid. The solid was then sonicated for 30 minutes in water (200 ml) to remove any traces of residual triethylamine. The compound was then vacuum filtered and a yellow solid collected. This was then dried under vacuum for 3 hours. A yellow solid was obtained.

38: ^{1}H NMR (400 MHz, CDCl$_3$; δ_H) 7.28 (m, 8H, arom), 3.52 (s, 2H, -SC**H**$_2$-), 3.14(s, 2H, -SC**H**$_2$-), Mass Spec. (ESI) *m/z* 393 [M+H]$^+$

40: ^{1}H NMR (400 MHz, CDCl$_3$; δ_H) 7.37 (m, 8H, arom), 3.16 (s, 2H, -SC**H**$_2$-), 2.68 (t, 2H, -SC**H**$_2$-), 1.43 (p, 2H, -SCH$_2$C**H**$_2$), Mass Spec. (ESI) *m/z* 429 [M+Na]$^+$

42: ^{1}H NMR (400 MHz, CDCl$_3$; δ_H) 7.32 (m, 8H, arom), 3.21 (s, 2H, -SC**H**$_2$-), 2.92 (t, 2H, -SC**H**$_2$-), 1.94 (p, 2H, -SCH$_2$C**H**$_2$),Mass Spec. (ESI) *m/z* 405 [M-H]$^+$

44: ^{1}H NMR (400 MHz, CDCl$_3$; δ_H) 7.45 (m, 8H, arom), 2.97 (t, 2H, -SC**H**$_2$-), 2.59 (t, 2H, -SC**H**$_2$-), 1.94 (p, 2H, -SCH$_2$C**H**$_2$), 1.34 (p, 2H, -SCH$_2$C**H**$_2$), Mass Spec. (ESI) *m/z* 421 [M+H]$^+$

4.4.3.2 The general preparation of the S$_4$ macrocycles

38, **40**, **42**, **44**   LiAlH$_4$ / THF   **39**, **41**, **43**, **45**
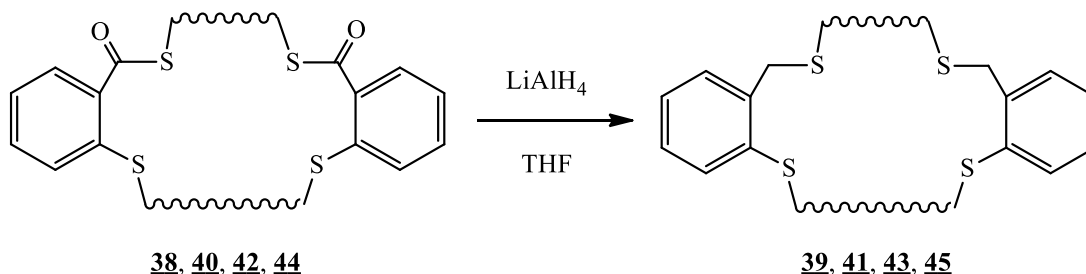
The appropriate S$_4$O$_2$ macrocycle (0.0075 mol) was dissolved in dry THF (150 ml) under a stream of nitrogen. The round bottomed flask was then placed in an ice bath and cooled to 0°C. Four equivalents of LiAlH$_4$ was added to the solution portion wise over a period of 2 hours. After the addition was complete the mixture was refluxed overnight. The solution was then allowed to cool before the addition of methanol (200 ml) and distilled water (20 ml) to produce a white gel, the solution was then vacuum filtered. The solvent was removed *in vacuo* to yield a yellow oil. The resulting solid was redissolved in distilled water (150 ml) and extracted with dichloromethane (3 x 100 ml). The organic layer were combined and back

extracted with distilled water (2 x 100 ml) and dried over anhydrous sodium sulfate. The solvent was removed *in vacuo* to yield a yellow-orange solid.

39: Anal. Calcd. for $C_{18}H_{20}S_4$**:** C, 59.29; H, 5.53 % Found: C, 59.54; H, 5.37 % , ^{1}H NMR (400 MHz, CDCl$_3$; δ_H) 7.18 (m, 8H, arom), 3.59 (s, 4H, arom-C**H**$_2$-S-), 2.89 (s, 2H, -SC**H**$_2$-), 2.62(s, 2H, -SC**H**$_2$-), Mass Spec (ESI) *m/z* 364.85 [M]$^+$

41: Anal. Calcd. for $C_{19}H_{22}S_4$**:** C, 60.27; H, 5.86 % Found: C, 59.94; H, 5.72 % , ^{1}H NMR (400 MHz, CDCl$_3$; δ_H) 7.36 (m, 8H, arom), 3.34 (s, 4H, arom-C**H**$_2$-S-) 2.76 (s, 2H, -SC**H**$_2$-), 2.51 (t, 2H, -SC**H**$_2$-), 1.76 (p, 2H, -SCH$_2$C**H**$_2$), Mass Spec (ESI) *m/z* 378.60 [M]$^+$

43: Anal. Calcd. for $C_{19}H_{22}S_4$**:** C, 60.27; H, 5.86 % Found: C, 60.51; H, 5.61 %, ^{1}H NMR (400 MHz, CDCl$_3$; δ_H) 7.30 (m, 8H, arom), 3.29 (s, 4H, arom-C**H**$_2$-S-) 2.89 (s, 2H, -SC**H**$_2$-), 2.66 (t, 2H, -SC**H**$_2$-), 1.92 (p, 2H, -SCH$_2$C**H**$_2$), Mass Spec (ESI) *m/z* 380.33 [M+H$_2$]$^+$

45: Anal. Calcd. for $C_{20}H_{24}S_4$**:** C, 61.18; H, 6.16 % Found: C, 60.97; H, 6.11 % , ^{1}H NMR (400 MHz, CDCl$_3$; δ_H) 7.25 (m, 8H, arom), 3.52 (s, 4H, arom-C**H**$_2$-S-) 2.82 (t, 2H, -SC**H**$_2$-), 2.43 (t, 2H, -SC**H**$_2$-), 1.88 (p, 2H, -SCH$_2$C**H**$_2$), 1.47 (p, 2H, -SCH$_2$C**H**$_2$) Mass Spec (ESI) *m/z* 416.0 [M+Na]$^+$

4.4.4.1 The preparation of the S₃NO₂ macrocycle

(intermediate)

46
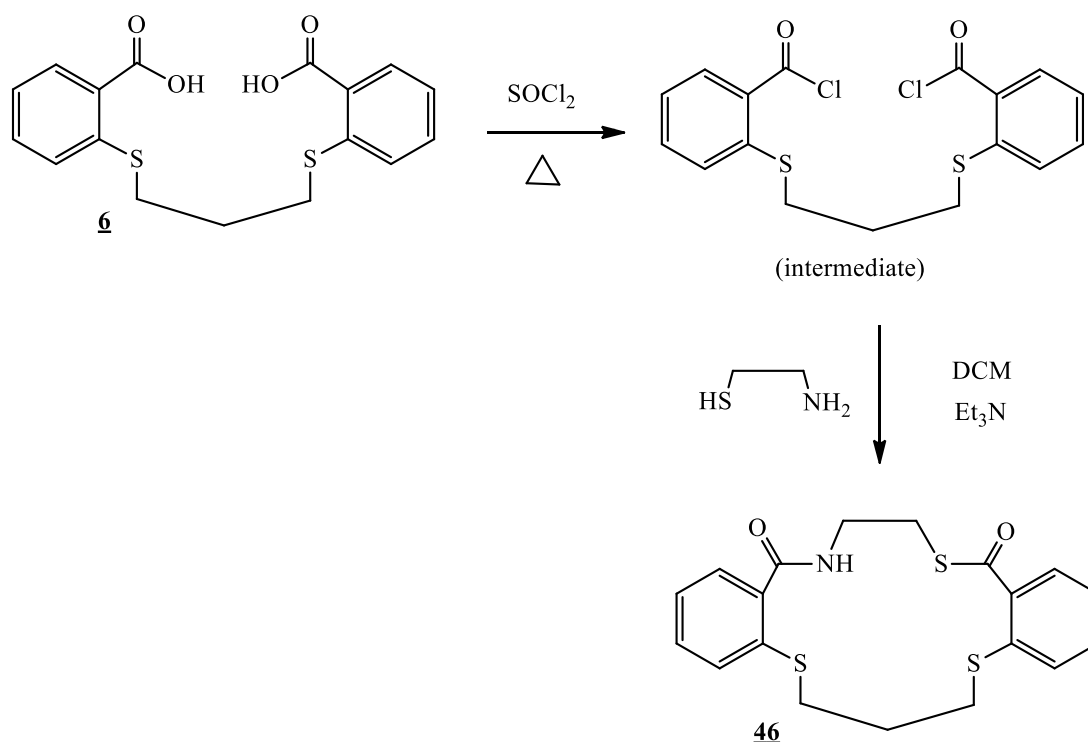
The synthesis of the S_3NO_2 system is similar to the synthesis described for the S_4O_2 systems. In place of dithiol compounds, cysteamine (0.58 g, 0.0075 mol) was used.

46: ^{1}H NMR (400 MHz, CDCl₃; δ_H) 7.34 (m, 8H, arom), 3.29 (s, 2H, -SCH₂-), 2.59 (t, 2H, -SCH₂-), 1.83 (s, NH), 1.34 (p, 2H, -SCH₂CH₂), Mass Spec. (ESI) *m/z* 390 [M+H]⁺

4.4.4.2 The preparation of the S$_3$N macrocycle
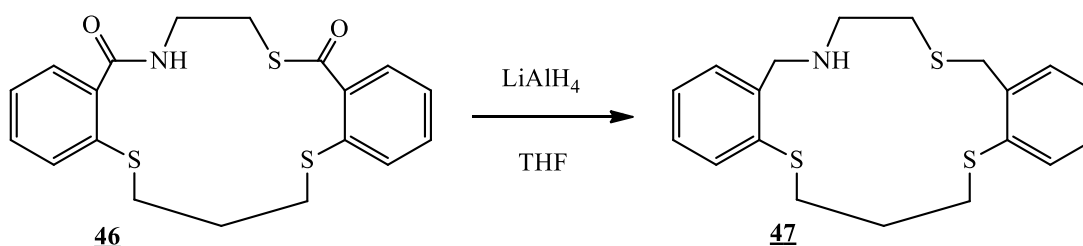
The synthesis of the S$_3$N system mirrors that of the S$_4$ system described in section 4.4.3.2.

47: Anal. Calcd. for C$_{19}$H$_{22}$NS$_3$: C,63.29; H,6.15 ; N, 3.88 %   Found: C,61.94; H, 6.80, N; 4.02 %, ^{1}H NMR (400 MHz, CDCl$_3$; δ_H) 7.29 (m, 8H, arom), 3.56 (s, 2H, arom-**CH**$_2$-S), 3.16 (s, 2H, arom-**CH**$_2$-NH-), 2.94 (t, 2H, -NH-**CH**2-), 2.74 (t, 2H, -S-**CH**$_2$-), 2.49 (t, 2H, -S**CH**$_2$-), 1.98 (s, N**H**), 1.47 (p, 2H, -S**CH**$_2$**CH**$_2$), Mass Spec. (ESI) *m/z* 383 [M+H]$^+$

4.4.5 Cyclic Voltammetry

Cyclic voltammetry in aqueous solution was carried out using PC driven EG&G model 263a potentiostat with PC programme Powersuite. A solution of the copper complex (3mM) was prepared in acetonitrile (redistilled from calcium hydride). The electrodes were glassy carbon, platinum wire and silver wire as the working, counter and reference electrodes, respectively. All solutions were degassed with nitrogen and contained sample concentrations 4 x 10^{-3} M acetonitrile, together with the supporting electrode; NaCl (0.1M) and ^{t}Bu$_4$NBF$_4$ (0.1M) respectively. This electrolyte was used as the tetrafluoroborate anion is the typical counter- ion in the copper complexes, therefore eliminating any potential exchange reactions. NaCl was used as an electrolyte to provide a medium closer to biological conditions. The voltammograms were referenced to the ferrocene/ ferrocenium (Fe(III)/Fe(II)) redox couple as is accepted practice by running a ferrocene solution under the same conditions before and the values are expressed relative to the normal hydrogen electrode (NHE).

4.4.6 DFT calculations

Calculations were performed using Gaussian 09 program.[13] The molecular species were subjected to geometry optimisation at the DFT level RB3LYP[14,15] using using a 6-311G basis set. The optimised species were subjected to a frequency analysis. Geometry optimisations were performed with no symmetry constraints and vibrational mode analysis used to confirm the ground state. Initial geometries were taken from the single crystals XRD structures previously reported.

4.5 References

1. Glick, M. D.; Gavel, D. P.; Diaddrio, L. L.; Rorabacher, D. B.; *Inorganic Chemistry*, **1976**, *15*, 1190 – 1193.

2. Kakos, S. H.; Dressel, L.T.; Bushendorf, J. D.; Kotarba, C. P.; Wijentunge, P.; Kulatilleke, C. P.; McGillirary, M. P.; Chacka, G.; Heeg, M. G.; Ochrymowycz, L. A.; Rorabacher, D. B., *Inorganic Chemistry*, **2006**, *45*, 923-934.

3. Sokol, L. S. W. L.; Ochrymowycz, L. A.; Rorabacher, D. B., *Inorganic Chemistry*, **1981**, *20*, 3189-3195.

4. Galijasevic, S.; Krylova, K.; Koenigbauer, M. J.; Jaeger, G. S.; Bushendorf, J. D.; Heeg, M. J.; Ochrymowycz, L. A.; Taschner, M. J.; Rorabacher, D. B., *Dalton Transactions,* **2003**, 1577-1586.

5. Bernardo, M. M.; Heeg, M. J.; Schroeder, R. R.; Ochrymowycz, L. A.; Rorabacher, D. B., *Inorganic Chemistry*, **1992**, *31*, 191-198.

6. D. B. Rorabacher, M. J. Martin, M. J. Koenigbauer, M. Malik, R. R. Schroeder, J. F. Endicott, L. A. Ochrymowycz, *Biochemical Inorganic Perspective*, **1983**, 167-202.

7. Bernardo, M. M.; Robandt, P. V.; Schroeder, R. R.; Rorabacher, D. B., *Journal of the American Chemical Soc*iety, **1989**, *111*, 1224-1231.

8. Villeneuve, N. M.; Schroeder, R. R.; Ochrymowycz, L. A.; Rorabacher, D. B., *Inorganic Chemistry*, **1997**, *36*, 4475-4483.

9. Bosnich, B.; Poon C. K.; Tobe, M. L., *Inorganic Chemistry*, **1965**, *4*, 1102–1108.

10. Salhi, C. A.; Yu, Q.; Heeg, M. J.; Villeneuve, N. M.; Juntunen, K. L.; Schroeder, R. R.; Ochrymowycz, L. A.; Rorabacher, D. B., *Inorganic Chemistry*, **1995**, *34*, 6053–6064.

11. Wijetunge, P.; Kulatilleke, C. P.; Dressel, L. T.; Heeg, M. J.; Ochrymowycz, L. A.; Rorabacher, D. B., *Inorganic Chemistry*, **2000**, *39*, 2897–2905.

12. Habata, Y.; Noto, K.; Osaka, F., *Inorganic Chem*istry, **2007**, *46*, 6529-6534.

13. Gaussian 09, Revision D.01, Frisch, M. J.; Trucks, G. W.; Schlegel, H. B.; Scuseria, G. E.; Robb, M. A.; Cheeseman, J. R.; Scalmani, G.; Barone, V.; Mennucci, B.; Petersson, G. A.; Nakatsuji, H.; Caricato, M.; Li, X.; Hratchian, H. P.; Izmaylov, A. F.; Bloino, J.; Zheng, G.; Sonnenberg, J. L.; Hada, M.; Ehara, M.; Toyota, K.; Fukuda, R.; Hasegawa, J.; Ishida, M.; Nakajima, T.; Honda, Y.; Kitao, O.; Nakai, H.; Vreven, T.; Montgomery, J. A., Jr.; Peralta, J. E.; Ogliaro, F.; Bearpark, M.; Heyd, J.

J.; Brothers, E.; Kudin, K. N.; Staroverov, V. N.; Kobayashi, R.; Normand, J.; Raghavachari, K.; Rendell, A.; Burant, J. C.; Iyengar, S. S.; Tomasi, J.; Cossi, M.; Rega, N.; Millam, M. J.; Klene, M.; Knox, J. E.; Cross, J. B.; Bakken, V.; Adamo, C.; Jaramillo, J.; Gomperts, R.; Stratmann, R. E.; Yazyev, O.; Austin, A. J.; Cammi, R.; Pomelli, C.; Ochterski, J. W.; Martin, R. L.; Morokuma, K.; Zakrzewski, V. G.; Voth, G. A.; Salvador, P.; Dannenberg, J. J.; Dapprich, S.; Daniels, A. D.; Farkas, Ö.; Foresman, J. B.; Ortiz, J. V.; Cioslowski, J.; Fox, D. J. Gaussian, Inc., Wallingford CT, **2009**.

14. Becke, A. D., *Journal of Chemical Physics*, **1993**, *98*, 5648-5652.

15. Lee, C.; Yang, W.; Parr, R. G., *Physical Review B*, **1988**, *37*, 785-789.

16. GaussView, Version 5, Dennington, R.; Keith, T.; Millam, J. *Semichem Inc.*, Shawnee Mission KS, **2009**.

17. Trotter, K. D.; Reglinski, J.; Robertson, K.; Forgie, J. C.; Parkinson, J. A.; Kennedy, A. R.; Armstrong, D. R.; Sowden, R. J.; Spickett, C. M., *Inorganica Chimica Acta*, **2009**, *362*, 4065-4072.

18. Rodgers, G. E., *Introduction to coordination, solid state, and descriptive inorganic chemistry*, 1st ed.; McGraw-Hill Inc., New Jersey, **1994**.

Chapter 5

The attachment of soft donor pendant arms on the N$_2$S$_2$ macrocycles

5.1 Introduction

The alteration of donor atoms in the initial macrocycles (Chapters 1, 2 and 3) from N_2S_2 to S_3N and S_4 systems (Chapter 4) have generated compounds that do not have a high enough stability in water and are thus unsatisfactory for use as putative imaging agents. It has therefore been decided to return to the modified N_2S_2 system (Chapters 2, 3) as these species had shown some promise in terms of stability (section 2.3.2), solubility, performance with biologically relevant reducing agents (section 2.3.4) and T_1 relaxation behaviour (section 2.4.2). A solution to the issues of the complexes ability to re-oxidise and problems with their electrochemical reversibility is still thought to centre on increasing the sulfur density at the metal centre. As such an attempt is to be made to increase the number of sulfur donors on the macrocycle by placing them at the terminus of the pendant arms attached to the secondary amines (Figure 5.1).
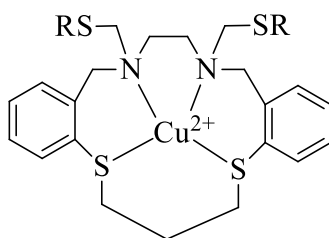

Figure 5.1: A schematic representation of **2** modified at the secondary amine with the attachment of sulphur based pendant arms (SR) is shown. (R = -SH and –S-Ph).

There is much literature reporting the synthesis and use of copper N_4 macrocyclic systems with thiol pendant arms (Figure 5.2). The main uses include bi-functional chelating agents which can be used in Positron Emission Tomography (PET) imaging and targeted radiotherapy.[1] Sevcikova *et al.* found that the addition of thiol pendant arms to these species is stable for *in-vivo* use and increases the kinetic inertness and it is believed that this is due to the thiol group binding weakly to the metal ion. They have reported these features are suitable for the utilisation of conjugating to target molecules.[1] A similar tetraazamacrocycle was reported by Lacerda *et al.*[2] They reported a ligand which introduced carboxylate pendant arms on the remaining nitrogens (Figure 5.2). The study found the ligand, when coupled with a range of lanthanides was found to be stable when tested with the biologically relevant agents including cysteine and glutathione and at biological pH ranges.
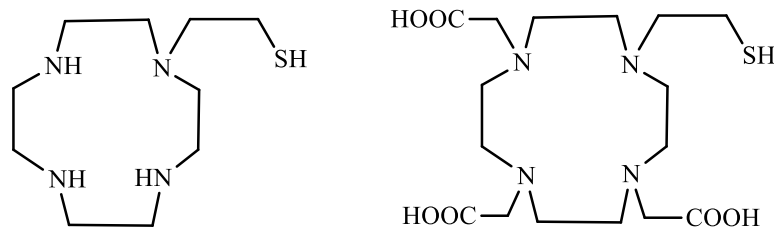
Figure 5.2: A schematic representation of the tetraaza macrocycle with a thiol pendant arm reported by Sevcikova *et al.*[1] (left) and Lacerda *et al.*[2] (right).

There has also been a number of reports on the addition of nitrogen and oxygen pendant arms to N_2S_2 systems for the labelling of peptides and antibodies with copper.[3,4] The use of oxygen and nitrogen based pendant arms have also previously been investigated for use in this study (Chapter 2) and proved to be unsuitable. There is, however, only a very limited amount of literature reported in N_2S_2 macrocycles with sulfur based pendant arms.

There has been no previous work into the specific macrocycles which are being synthesised and studied in this chapter. It is hoped that the addition of sulfur donor atoms will also have increased biological stability similar to the tetraaza macrocycles shown in Figure 5.2. It is also hoped that an increase in water stability can be seen, as well as increased reversibility resulting in a compound which would be suitable for *in-vivo* use for the detection of oxidative stress.

5.2 Results and Discussion

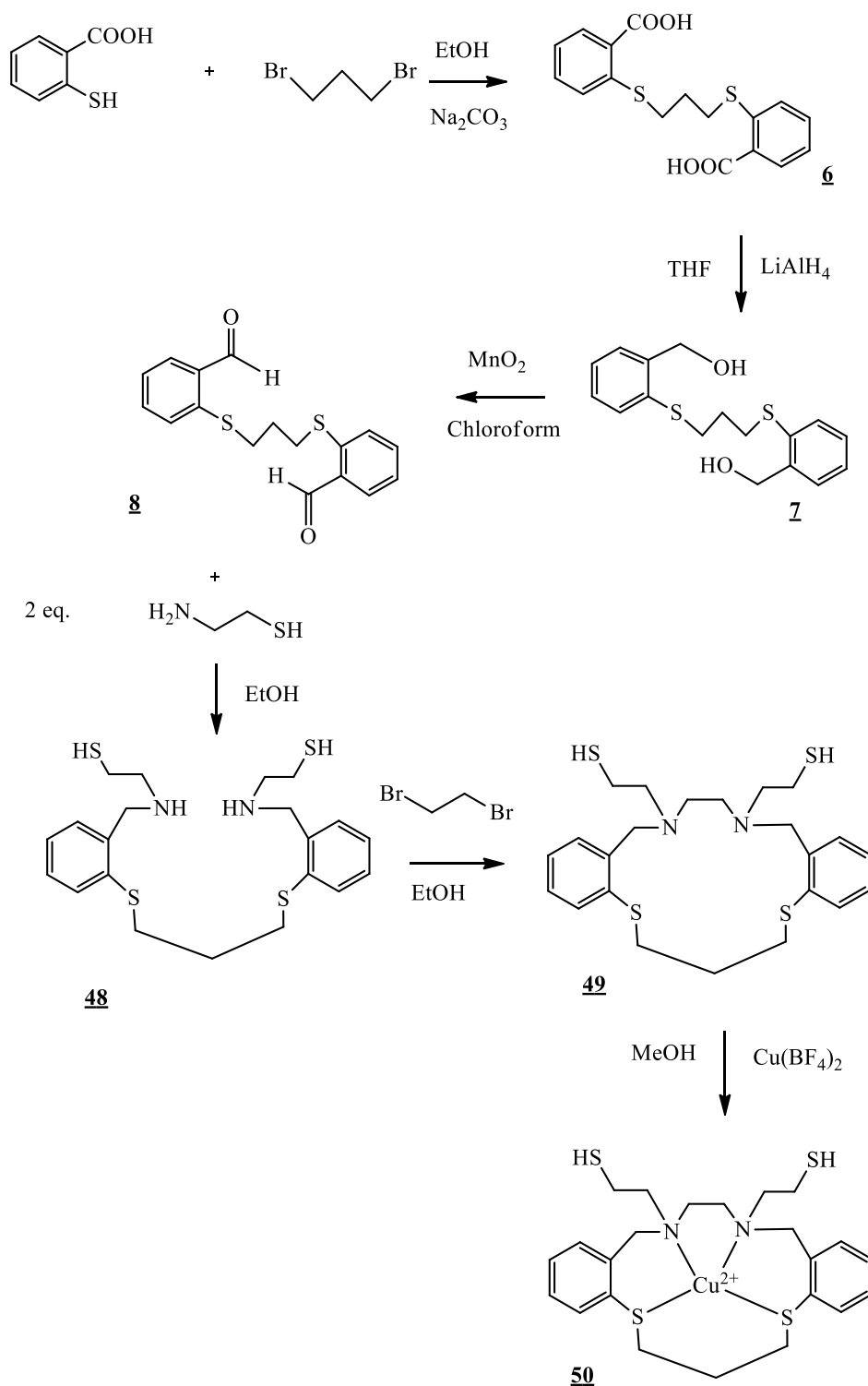## 5.2.1 Synthesis of thiol pendant arm complex

Figure 5.3: Synthesis of complex **50**.

As previously discussed in section 2.2.1, compound **2** was identified as a lead candidate for development. However the attachment of thiol pendant arms using compound **2** would require the use of sulfur mustards; a class of cytotoxic vesicant chemical warfare agents.[5] Another reason for not using mustards as a synthetic route is the coupling of the halogenated amine pendant arm (chapter 2) was unsuccessful and due to the similar nature of the compound it was postulated that there was a significant possibility that a reaction involving 1-chloro 2- thioethane would most likely also be unsuccessful. It was therefore decided to take a different approach to the incorporation of the thiol pendant arms into the desired motif and in doing so, arrive at compound **50** (Figure 5.3). A route was devised where by cysteamine is coupled with the aldehyde (compound **8**) effectively incorporating the pendant arms prior to ring closure using dibromoethane. The synthesis to produce **8** has been discussed extensively in previous work.[5] Once the macrocycle was ring closed the copper can be inserted by the addition of $Cu(BF_4)_2$.

It can be demonstrated by mass spectrometry and NMR that the ligand (**49**) has formed. Despite the introduction of copper into the system it generated a green compound, after closer inspection of the spectroscopic data it suggested that the copper was not bound in the expected manner, i.e. within the macrocycle. Instead mass spectrometry (993 $[M+H]^+$) and microanalysis (see section 5.4.4) suggest the empirical formula for the new complex was CuL_2 (L = macrocycle) i.e. two macrocycles were bound to one copper. This arrangement has been observed previously by Trotter *et al.* [5] in the development of the parent macrocyclic systems (Figure 5.4).
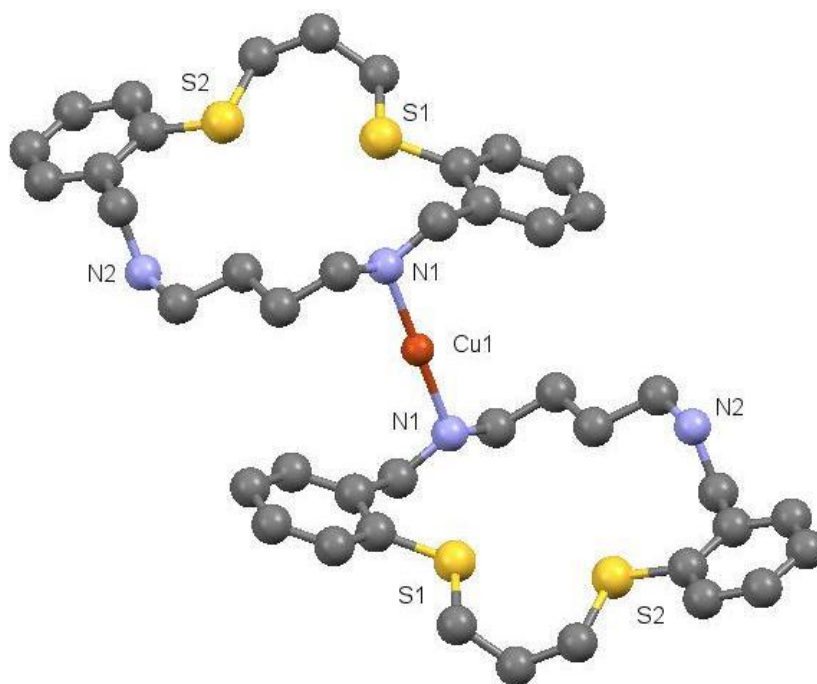
Figure 5.4: Molecular structure of macrocycle with copper in exo position, where incorporation of the metal within the ring or between donors is no longer favoured.[5] Protons and the tetrafluoroborate anion have been omitted for clarity.

Due to the fact that copper would not coordinate at an endo position within the macrocycle under standard conditions, it is believed that the desired complex could only be achieved under anhydrous conditions. However this method was used in chapter 4 and proved to be unsuccessful as the copper was weakly bound to the macrocycle and was sequestered from the ring in the presence of water. This would deem the compound unsuitable for *in-vivo* use as it must have a high water stability. Instead of copper, it was decided to use nickel as an alternative as it has a higher coordination number and thus more likely to attach to both the nitrogen and sulfur. Mass spectrometry results suggest that a nickel did coordinate to the ring (523 [M]$^+$). A suitably clean elemental analysis or crystal structure could not be obtained, it was therefore not possible to investigate this compound further. It was decided that this system is not suitable for use as a contrast agent and any further work has currently been abandoned.

5.2.2 Synthesis of thio-ether pendant arm complex

As the synthesis of a copper macrocycle with thiol pendant arms failed to give the desired product, it was decided to investigate the attachment of a thio-ether pendant arm instead. A protected mustard group was found in the form of 2-bromoethyl phenyl sulfide. The MSDS data on this species identified it as a "safe mustard" compound and as such it was possible to return to the original synthesis for pendant arm attachment which was first explored in chapter 2 (Figure 2.3) i.e. attaching the thio-ether to the macrocycle.
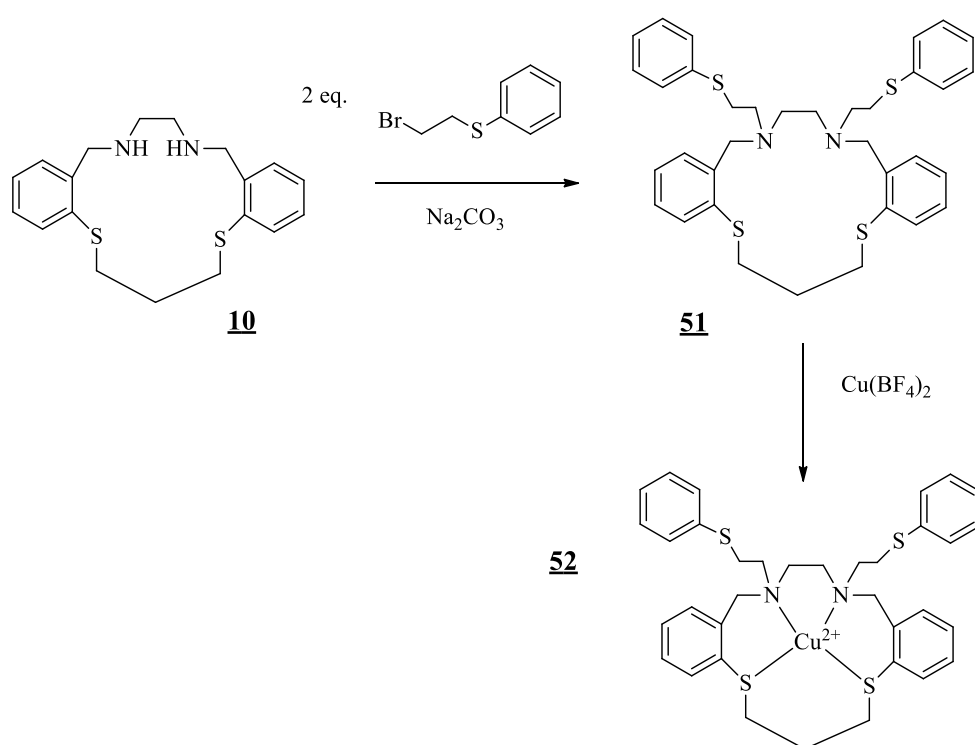
Figure 5.5: Synthesis of **52**.

The synthesis of **10** has been discussed extensively in previous work.[5] Compound **10** was coupled with two equivalents of 2-bromoethyl phenyl sulfide and $Cu(BF_4)_2$ was consequently added to metallate the ring. Analysis by ESI-MS and elemental analysis determined that the complex was sufficiently pure for use in further studies.

A similar structure to **52** has been previously reported by Funkemeier *et al.* with nitrogen donor pendant arms.[6] This literature outlines the attachment of 2-chloromethyl pyridine to the same parent macrocycle (**2**) as used in this study. A crystal structure was obtained (Figure 5.6) which clearly shows that the nitrogens in the pendant arms coordinate to the copper centre. It is believed that this also occurring with the sulfur on the pendant arms (compound **52**) in this study.
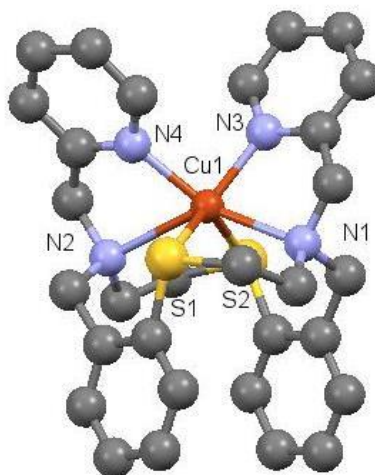

Figure 5.6: Molecular structure of methyl pyridine pendant arm structure. It can be seen that the nitrogens on the pendant arms are coordinating to the copper centre. Protons and perchlorate anions have been omitted for clarity.[6]

Atom pair	Bond distance (Å)
Cu-N$_1$	2.26 (1)
Cu-N$_2$	2.55 (1)
Cu-N$_3$	**1.98 (1)**
Cu-N$_4$	**2.00 (1)**
Cu-S$_1$	2.43 (4)
Cu-S$_2$	2.70 (4)

Table 5.1: Bond lengths of compound reported by Funkemeier *et al.*[6] It can be seen from the bond lengths reported for that of the nitrogens on the pendant arms (in bold) that they are formally bonded to the copper centre of the macrocycle.

5.2.3 Compound stability test

The desired compound must be stable *in-vivo* to be used as imaging agents, it is therefore necessary to check its stability under biologically relevant conditions. This work had been carried out previously for the simple copper macrocycles.[1,2,3] From the pendant arm complex reported here (**52**) no differences were observed between the U.V-visible (300-800 nm) and solid reflectance spectra and it would seem that the structures shown above persist in solution. Nor were there any differences between dry and the aqueous samples (1mM, 0.1NaCl, 100 % D_2O) placed in an incubator (37ºC).

5.2.4 Copper stability of the complex

Sequestration agent stability tests were carried out on **2** and **52** using Bovine Serum Albumin (BSA) and the results compared (figure 5.6). As previously reported; as the concentration of BSA increases the charge transfer band (420 nm) derived from **2** decreases, indicative that the macrocycle is being de-metalated. In contrast for the plot obtained from the analogous experiment using **52** it is evident that there is no loss of copper from the macrocycle. As expected the addition of a pendant arm donor has increased the stability of the copper complex.
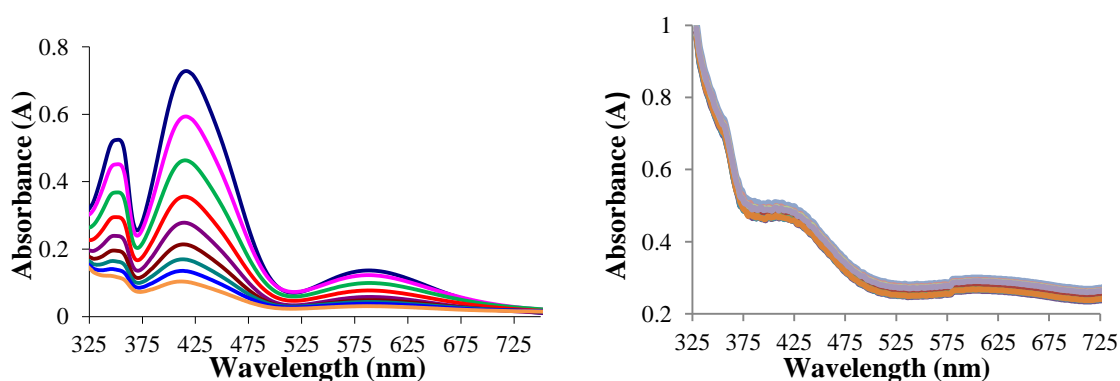
Figure 5.6: Plot of stability test of **2** (left) and plot of stability test of **52** (right) with BSA (10mM) in Tris buffer (5mM, pH 7.4). The band structures in the two complexes are different due to the different geometries adopted by the two complexes (planar/octahedral and square pyramidal).

5.2.5 Reduction potential of the complexes

It was necessary to test the effect of naturally occurring reducing agents found *in-vivo* on the complexes. The parent complex **2** was tested as previously discussed (Chapter 1). The pendant arm complex **52** was also tested with biologically relevant reducing agent ascorbic acid. As before (Chapter 2) the reaction is characterised by the charge transfer band at 420 nm. It can be seen by the plot below (Figure 5.7) that with each aliquot of ascorbate the complex is reduced. It should be noted that although the addition of pendant arms has affected the macrocycles reduction potential, it has not shifted it beyond the ability of ascorbate to act as a reducing agent.
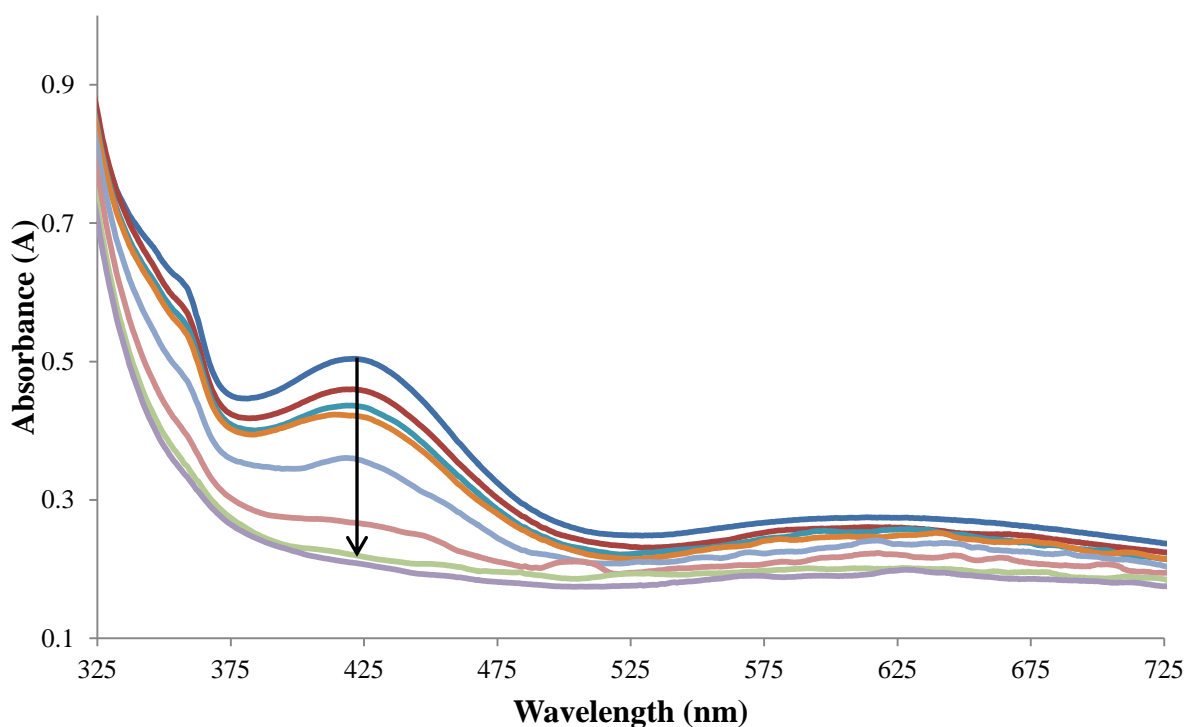
Figure 5.7: Reduction plot of **52** (0.3 mM) with ascorbate (10 mM) in Tris buffer (5 mM, pH 7.4). The reduction is characterised by the absorption band at 420 nm. The top spectrum shows the original position of the complex prior to reduction and the bottom spectrum shows the complex after reduction, indicated by the direction of the arrow.

5.2.6 Oxidation potential of the complexes

It is important that the complexes are able to re-oxidise from copper (I) to copper (II) in the presence of biological oxidising agents, such as HOCl. Complex **52** was tested using the biologically relevant oxidising agent sodium hypochlorite. Firstly the compound was reduced with ascorbate (Figure 5.7) it was then treated with sodium hypochlorite to reoxidise the complex to back to copper (II). From the plot below it can be seen that **52** has reoxidised, achieving 92.2% recovery of the complex once the redox cycle has been completed. Previous work has also shown that it is not at all possible to re-oxidise the parent complexes [6] and the previous pendant arm complexes (**11**, **12** and **13**) only achieved ~20% recovery (section 2.3.4).
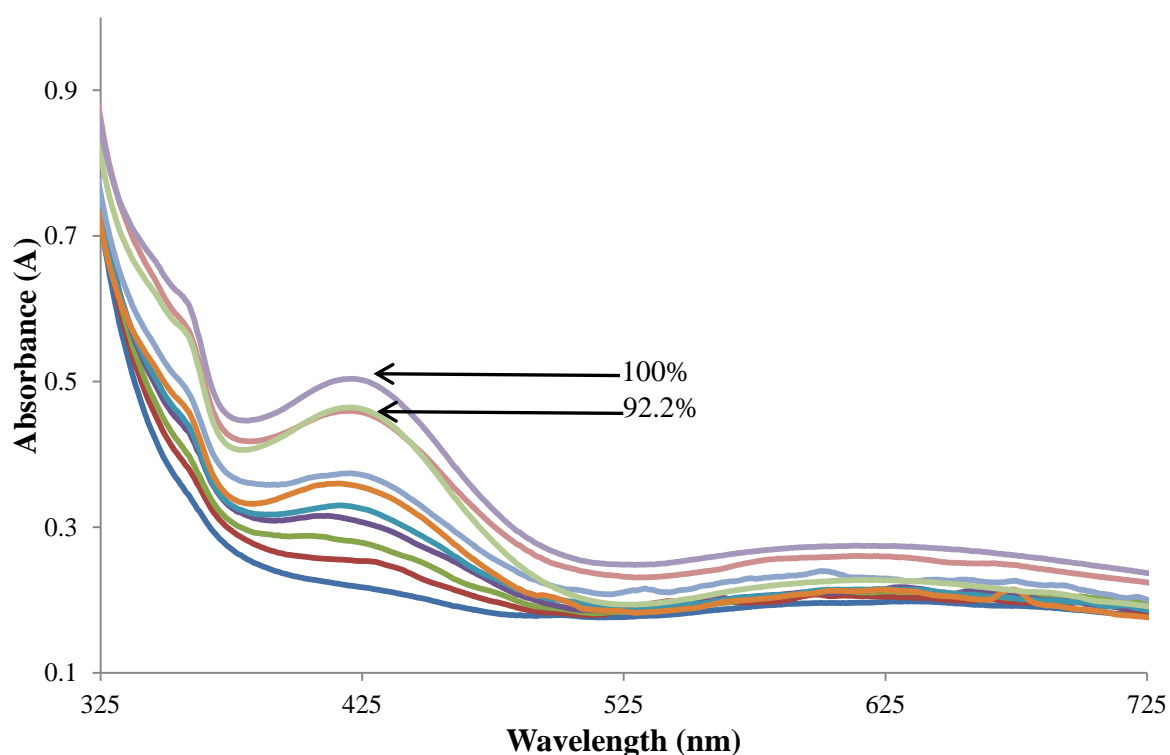
Figure 5.8: The spectrophotometric analysis of the HOCl oxidation of **52** (0.3 mM). The species being studied was generated *in-situ* using ascorbic acid as the reductant. The top pink spectrum (see arrow) shows the original position of the complex prior to reduction and the bottom spectrum shows the complex after reduction. The blue spectra (see arrow) shows the oxidation with hypochlorite as a result of 50 μl additions of hypochlorite (100 mM) in Tris buffer (5 mM, pH 7.4).

5.2.7 Electrochemistry

Cyclic voltammetry is typically used to estimate the redox potential of the complex (see Appendix 4). Complex **52** was prepared as a solution (4 mM) in 0.1 M t-butylammonium tetrafluoroborate ($^tBu_4NBF_4$). This electrolyte was used as the tetrafluoroborate anion is the typical counter-ion in the copper complexes, therefore eliminating any potential exchange reactions. The voltammogram was referenced to the ferrocene/ferrocenium (Fe(III)/Fe(II)) redox couple as is accepted practice by running a ferrocene solution under the same conditions before and after the samples and subtracting this redox potential from that of the samples.[7] From the cyclic voltammogram obtained (Figure 5.9) it can be seen that the compound shows signs of electrochemical reversibility. The E^o value obtained was 1.28 V (vs. NHE) which falls within the desired biological range.
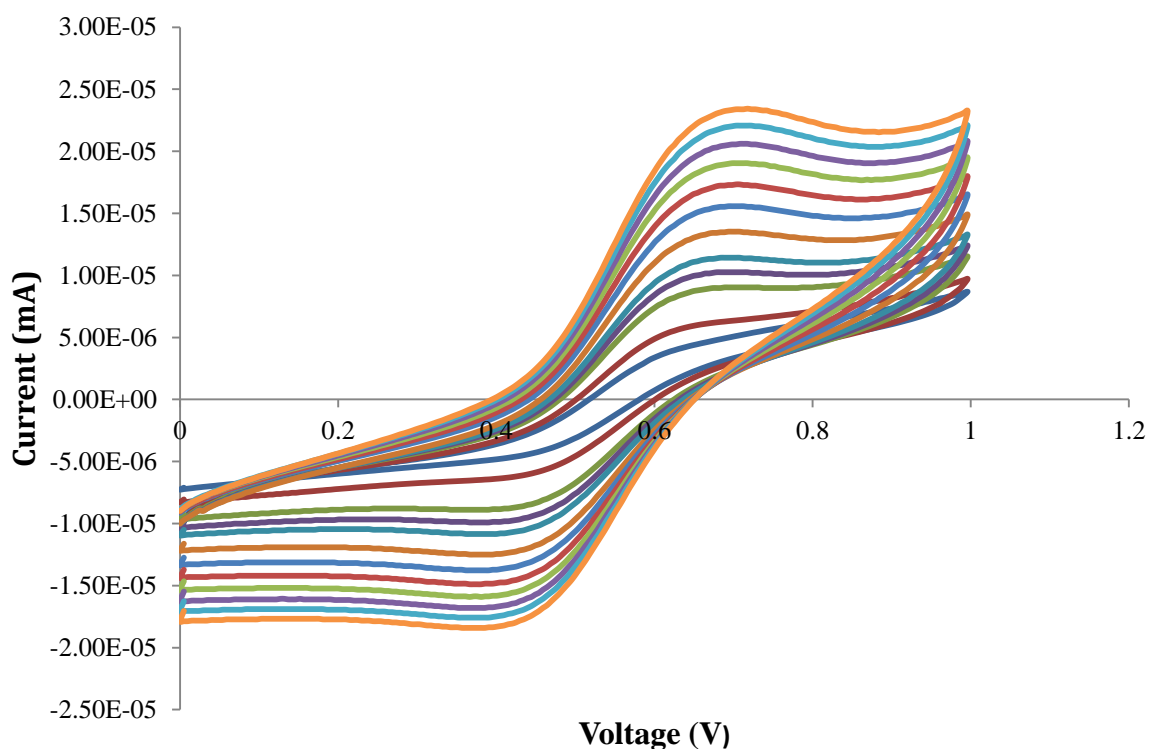
Figure 5.9: Cyclic voltammogram in the positive region of compound **52** in acetonitrile (0.1 M $^tBu_4NBF_4$: Potential reported vs. ferrocene) recorded over a scan rate range from 10 mV-200 mVs^{-1}.

The percentage electrochemical reversibility for compound **52** was calculated from the data points at 0.40 and 0.71V (i_{pc} vs. i_{pc}) and found to be approximately 79 %. This electrochemical reversibility is found to be slightly lower than the percentage reversibility found in section 5.3.4. This is a vast improvement from the previously tested compounds. The maximum percentage electrochemical reversibility for the pendant arm complexes was found to be 25% (i_{pc} vs. i_{pc}) (compound **13**) and an improvement on the parent complex (**2**) which was found to be 57% (i_{pc} vs. i_{pc}).

5.2.8 Measurement of N-substituted macrocycles T_1 relaxation times

The N-substituted complex was tested in a similar manner as described in chapter 2. As previously described (section 2.4.1) compound **52** was prepared in a range of concentrations (0.01 mM, 0.1 mM, 1 mM, 2.5 mM, 10 mM, 0.l M NaCl in 100 % D_2O).

Table 5.1 shows the triplicate results obtained for **52** from these the average T_1 relaxation time at each concentration can be obtained. This data is used to obtain a graph which shows how relaxation time varies with concentration (Figure 5.10). The corresponding gradient of relaxivity obtained from the data displayed in Figure 2.13 can be calculated (Figure 5.11), where there is good agreement between the data and the line of best fit.

$T_1(1)s^{-1}$	$T_1(2)s^{-1}$	$T_1(3)s^{-1}$	In (conc)	average T_1 (s)	Standard Deviation
0.677	0.748	0.549	-4.605	0.658	0.101
2.071	1.575	1.237	-5.992	1.626	0.422
2.291	2.296	2.356	-6.908	2.314	0.036
6.040	5.980	4.773	-9.210	5.581	0.744
7.226	7.524	7.137	-11.513	7.296	0.203

Table 5.1: T_1 relaxation data for **52** (results shown in triplicate for inspection; 400 MHz, 0.1M NaCl, 100% D_2O).
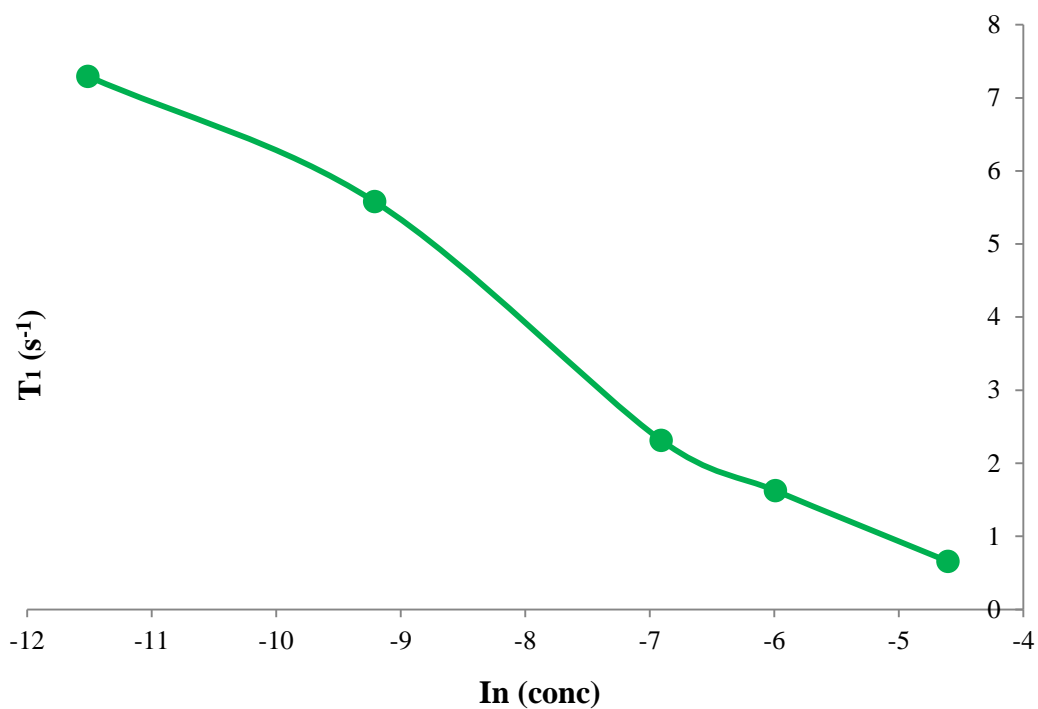
Figure 5.10: T_1 relaxation (s) vs. ln(concentration) of **52**. Curve fitted by Excel.
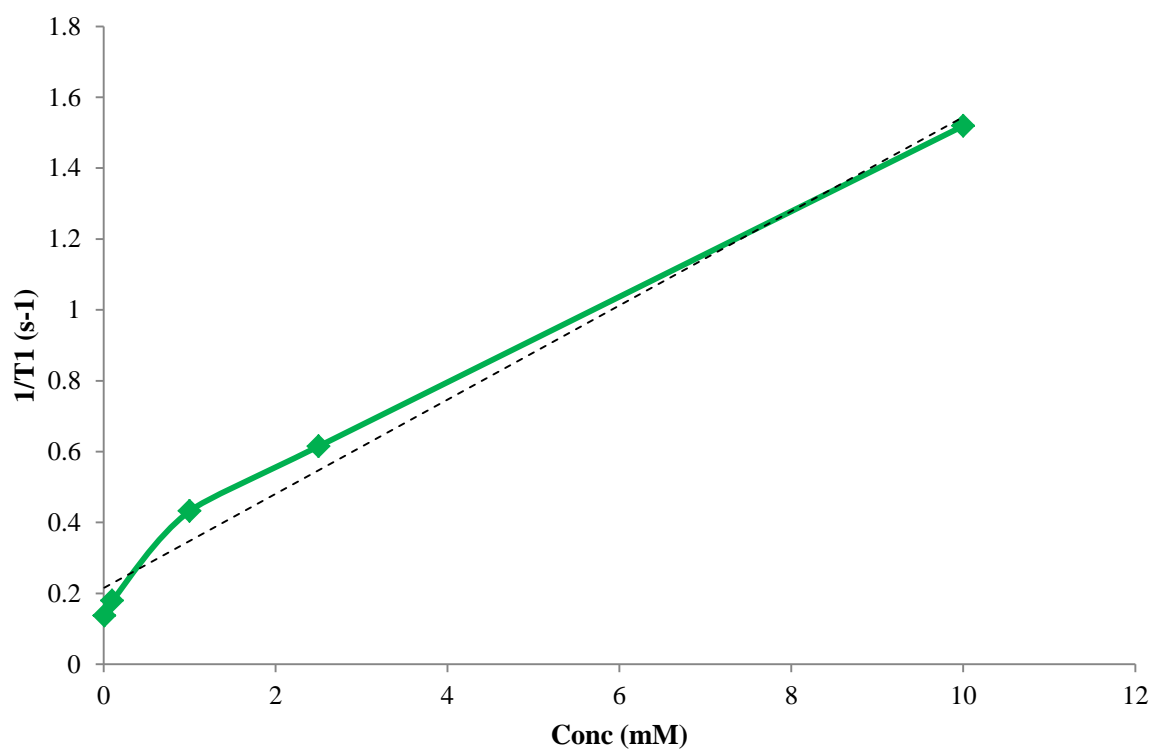
Figure 5.11: Gradient of relaxivity of **52** where y = 132.94 + 0.2147 and R^2 = 0.9834.

When the copper is complexed with the macrocycles, the number of available coordination sites is decreased and therefore a diminution in the relative relaxivity is expected (Figure 5.12). However, the data obtained for the N-substituted macrocycles suggest that the results derived from these complexes with higher coordination numbers are comparable with that of the unmodified macrocycles (Table 2.2, 5.1). Indeed, the addition of the pendant arms has not markedly affected the relaxivity of the compound despite the capping of the nitrogen donor atoms. This suggests that in solution the pendant arms either exchange rapidly with solvent (water) molecules or that relaxation via hydrogen bonding with the second hydration sphere is occurring similarly to the other pendant arm complexes tested (Figure 2.15 and Appendix 5) Thus the data obtained shows that the N-substituted macrocycle shows sufficient relaxivity for use as putative imaging agents.
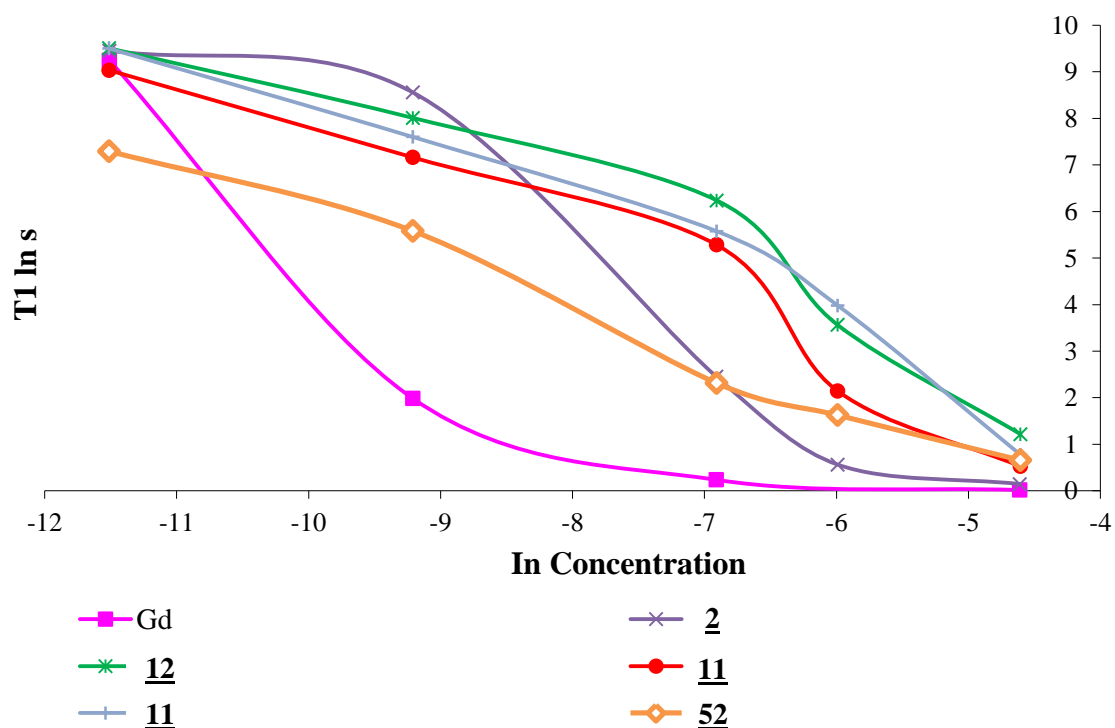
Figure 5.12: $T_1 \ln(s)$ vs. ln(concentration) plot of **2**, **11**, **12**, **13**, **52**, Gd-(DTPA) and Cu(BF$_4$)$_2$. Curve fitted by Excel.

5.3 Conclusions

The aim of the chapter was to introduce sulfur at the N-substituted position to investigate its influence on the relaxivity of water. Comparisons with previous studies on the unmodified framework (Chapter 1), alcohol and carboxylate pendant arm complexes (Chapter 2) allowed us to assess the effect of introducing sulfur pendant arms at the nitrogen to increase stability and solubility and combat redox reversibility issues. The thiol pendant arm complex (**50**) was identified as being unsuitable due to its preference of forming a complex with two macrocycles bound to one copper in the exo position.

T_1 relaxation experiments and redox stability tests were carried out to identify the potential of the phenyl sulfide pendant arm complex to be used as contrast agents to diagnose oxidative stress. From the results obtained it can be concluded that the electrochemical reversibility of the compound has greatly increased from only 20 % in previous pendant arm complexes (~25% for compound **13**) to approximately 80 %.

It can be concluded that compound **52** shows both good stability and solubility. The previous issues with redox reversibility (chapter 2) shows a large increase in the recovery of Cu(II) using the biologically relevant agent sodium hypochlorite. The result was obtained after inducing an *in-vivo* reduction to Cu(I) using ascorbic acid. The previous pendant arm complexes (**11**, **12** and **13**) only achieved ~20 % recovery whereas compound **52** shows an increased recovery of approximately 90 % Cu(II).

The T_1 relaxation experiments revealed that the phenyl sulfide pendant arm complex showed a relaxivity believed to be sufficient to assist in imaging oxidant production. Cyclic voltammetry has also revealed that the complex shows signs of electrochemical reversibility within the desired biological range (1.28 vs. NHE). In conclusion the compound shows much promise for use as a redox sensitive imaging agent.

5.4 Experimental

5.4.1 General Considerations

All experiments were carried out using standard apparatus and commercially available chemicals. **2** was prepared as previously reported.[5,7] Solvents were used as supplied. Microanalysis was carried out by the microanalysis laboratory at the University of Strathclyde. Mass Spectrometry was carried out on a ThermoFinnigan LCQ mass spectrometer with ESI ionisation, spray voltage 4.5 kV, capillary temperature 200ºC. UV/visible spectra were recorded on a Unicam UV 300 spectrometer. The spectrophotometric titrations were carried out on a Perkin Elmer Lambda 35 double beam UV/visible spectrometer running on Perkin Elmer WinLab software (version 2.85.04). T_1 relaxation experiments were measured on an AVANCE NMR spectrometer operating at a proton resonance frequency of 400 MHz. The measurements were carried out using an inversion recovery pulse sequence under full automation control with a 90º pulse width of 11.5 μs.

5.4.2 The preparation of 48

8 (1.34 g, 4.2 mmol) was dissolved in ethanol (150 ml) and to this sodium bicarbonate (5.60 g, 0.067 mol) was added. The mixture was stirred and heated to reflux. To this cysteamine (0.65 g, 8.4 mmol) in ethanol (50 ml) was added dropwise overnight to the refluxing mixture. The solution was left to cool, before being filtered. The solvent was removed *in vacuo* to yield a yellow oil. A yield of 87 % was achieved.

48 : [^1]H NMR(400 MHz, DMSO; δ_H) 7.56 (m, 4H, arom), 7.18 (m, 4H, arom), 3.15 (s, 4H, PhC**H**₂N-) 2.95 (t, 4H, -SC**H**₂-), 2.73 (t, 4H, -CH₂C**H**₂SH), 2.50 (t, 4H, -C**H**₂CH₂SH), 1.81 (p, 2H, -SCH₂C**H**₂-),1.61 (s, 2H, -CH₂S**H**), Mass Spec. (ESI) *m/z* 439 [M+H]⁺ , 461 [M+Na]⁺

5.4.3 The preparation of 49

48

49
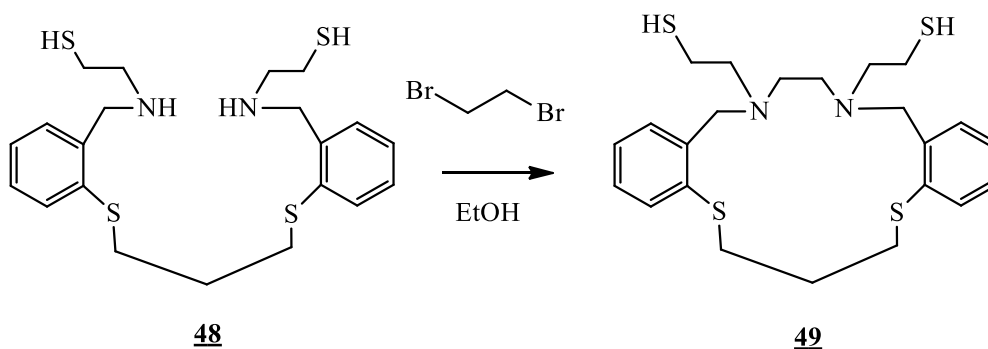
48 (1.6 g, 3.7 mmol) was dissolved ethanol (450 ml) to this dibromoethane (0.69 g, 3.7 mmol) was added dropwise. Once the addition was complete the solution was stirred and heated to reflux overnight. The solution was then left to cool then subsequently filtered. The solvent was then removed *in vacuo,* resulting in a yellow oil. A yield of 74 % was achieved.

49 : [^1]H NMR (400 MHz, DMSO; δ_H) 7.92 (m, 4H, arom), 7.33 (m, 4H, arom), 3.17 (s, 4H, PhC**H**₂N-), 2.95 (t, 4H, -SC**H**₂-), 2.79 (t, 4H, -CH₂C**H**₂SH), 2.53 (t, 4H, -C**H**₂CH₂SH), 2.29 (s, 4H, -NC**H**₂), 2.07 (p, 2H, -SCH₂C**H**₂-),1.83 (s, 2H, -CH₂S**H**), Mass Spec. (ESI) *m/z* 465 [M+H]⁺

5.4.4 The preparation of 50
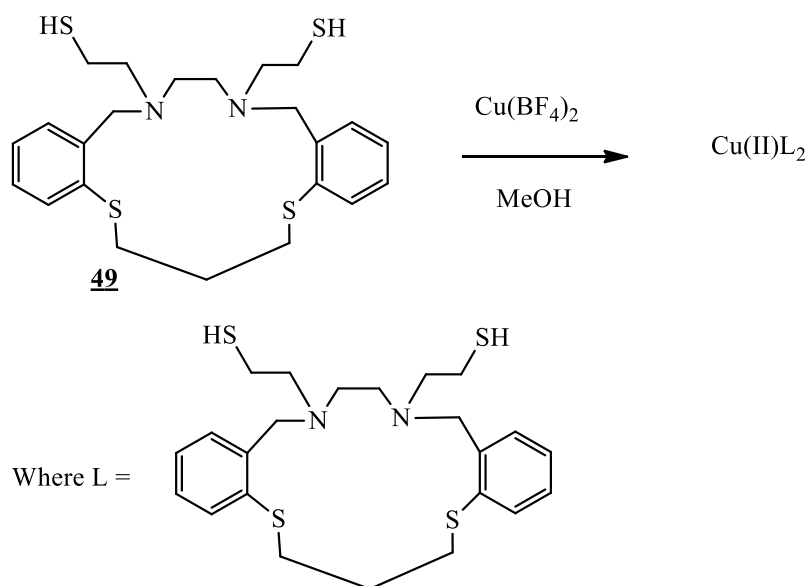
The thiol pendant arm complex (0.5 g, 1.07 mmol) was dissolved in methanol (150 ml) and treated with an equi-molar amount of $Cu(BF_4)_2.6H_2O$ dissolved in methanol (10 ml). An immediate colour change from pale yellow to light green was observed and the solution was refluxed gently overnight. The solution was cooled and filtered and the solvent removed *in vacuo* to yield a light green solid. The crude product was re-dissolved in the minimum amount of methanol, filtered through celite and recrystallised by vapour diffusion using diethyl ether to give a light green powder. The copper did not bind in a typical manner, electrospray mass spectrometry and microanalysis suggests two of the macrocycles have bound to one copper at the exo position.

50: Anal. Calcd. for $C_{46}H_{64}N_4S_8CuB_2F_8$: C, 47.36; H, 5.53; N, 4.80 % Found: C, 47.64; H, 5.68; N, 4.51 %. Mass Spec (ESI) *m/z* 992.94[M+H]$^+$

An NMR could not be obtained due to the paramagnetic nature of the compound.

5.4.5 The preparation of 51
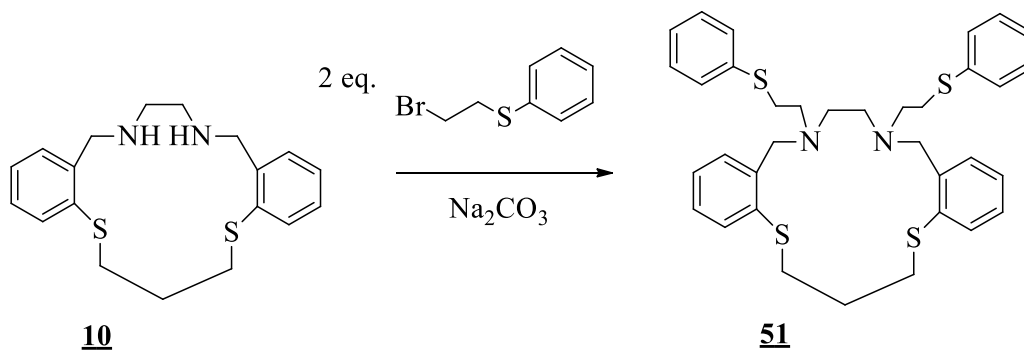
10 (1.04 g, 3.01 mmol) was dissolved in acetonitrile (150 ml) and to this sodium bicarbonate (5.07 g, 0.06 mol) was added. The mixture was stirred and heated to reflux. 2-bromoethyl phenyl sulfide (1.31 g, 6.02 mmol) in acetonitrile (50 ml) was added dropwise overnight to the refluxing mixture. The solution was then left to cool, before being filtered. The solvent was then removed *in vacuo,* resulting in a yellow oil. A yield of 64 % was obtained.

51 : ^{1}H NMR (400 MHz, DMSO; δ_H) 7.39 (m, 10H, arom), 7.33 (m, 4H, arom), 7.24 (m, 4H, arom), 3.65 (s, 4H, PhC**H**$_2$N-), 3.58 (t, 4H, -NC**H**$_2$CH$_2$S-), 3.40 (t, 4H, -S-C**H**$_2$-), 3.02 (t, 4H, -NCH$_2$C**H**$_2$S-), 2.09 (s, 4H, -NC**H**$_2$), 1.82 (p, 2H, -SCH$_2$C**H**$_2$-), Mass Spec. (ESI) *m/z* 617.13 [M+H]$^+$

5.4.6 The preparation of 52

51   Cu(BF$_4$)$_2$ **52**
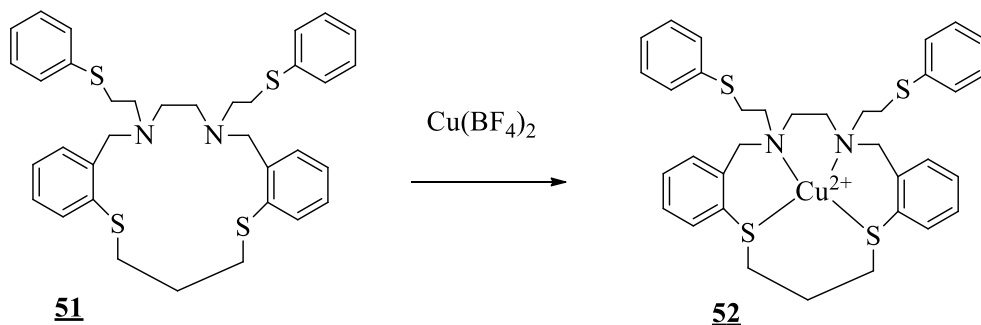
The pendant arm complex (1 g, 1.47 mmol) was dissolved in methanol (150 ml) and treated with an equi-molar amount of Cu(BF$_4$)$_2$.6H$_2$O dissolved in methanol (10 ml). An immediate colour change from pale yellow to dark green was observed and the solution was refluxed gently overnight. The solution was cooled and filtered and the solvent removed *in vacuo* to yield a dark green solid. The crude product was re-dissolved in the minimum amount of methanol, filtered through celite and recrystallised by vapour diffusion using diethyl ether to give a dark green powder.

52: Anal. Calcd. for C$_{35}$H$_{40}$N$_2$S$_4$CuB$_2$F$_8$: C, 49.22; H, 4.68; N, 3.28 % Found: C, 49.67; H, 4.79; N, 3.11 %. Mass Spec (ESI) *m/z* 679 [M]$^+$, 543 [M-C$_9$H$_{12}$S]$^+$

An NMR could not be obtained due to the paramagnetic nature of the compound.

5.4.7 Compound stability tests

The stability of complex **52** was tested by placing solid samples and solutions (1 mM, 10 ml 0.1 M NaCl in distilled water) in an incubator at 37ºC and in a cupboard for a period of 1 week. The UV/visible spectrum (300-800 nm) were recorded at the beginning of the experiment and again after one week to assess the degree of degradation.

5.4.8 Copper stability of the complexes

Solution of the copper macrocycle (0.3 mM) and BSA (199 mg, 1 ml) was prepared in Tris-buffer (5 mM, pH 7.4). 1.0 ml of the required copper complex was placed in a 1.0 cm path length, 1.5 ml quartz cuvette and the spectrum was recorded between 325 and 800 nm against a Tris- buffer reference in a matching cuvette. The BSA solution was titrated in aliquots of 5 μl into solution. The cuvette was allowed to stand for 5 minutes at room temperature to allow the solution to come to equilibrium before the spectra was recorded. The titrations continued until no further change was observed in the spectra. Each experiment was carried out in triplicate. Although the complete spectra from the reaction was collected the decrease in the absorbance band at 420 nm was plotted as a measure of the percentage of copper (II) form present in the solution.

5.4.9 Reduction of the complexes to copper (I)

A solution of the copper macrocyclic (0.3 mM) complex and reducing agent (10 mM ascorbic acid) was prepared in Tris-buffer (5 mM, pH 7.4). 1.0 ml of the solution of the complexes was placed in a 1.0 cm pathlength, 1.5 ml quartz cuvette and the spectrum was recorded between 325 and 800 nm against a tris-buffer reference placed in a matching cuvette. The reducing agent was titrated in aliquots of 5 μl into the solution. The cuvette was allowed to stand for 5 minutes at room temperature to allow the solution to come to equilibrium before the spectrum was recorded. The titrations continued until no further change was observed. Each experiment was carried out in triplicate. Although the complete spectrum from each reaction was collected the decrease in the absorbance band at 420 nm was used to

characterise the reaction. Concentrations are normalised to give the percentage of Cu(II) form present in solution.

5.4.10 Re-oxidation of the complexes to copper (II)

Solution of the copper macrocyclic complex (0.3 mM) was prepared in tris-buffer (5 mM, pH 7.4) and reduced using ascorbic acid to generate the copper (I) complex *in-situ.* 1.0 ml of the required copper complex was placed in a 1.0 cm pathlength, 1.5 ml quartz cuvette and the spectrum was recorded between 250 and 800 nm against a tris-buffer reference placed in a matched cuvette. A 100 mM solution of sodium hypochlorite was titrated in 5 μl aliquots into the solution. The cuvette was allowed to stand for 5 minutes at room temperature to allow the solution to come to equilibrium before the spectrum was recorded. The titrations continued until no further change was observed in the spectra. Each experiment was carried out in triplicate. Although the complete spectrum from the reaction was collected the decrease in the absorbance band at 420 nm was plotted as a measurement of the percentage of the Cu(II) form present in solution.

5.4.11 Cyclic Voltammetry

Cyclic voltammetry in aqueous solution was carried out using a PC driven EG&G model 263a potentiostat with PC programme Powersuite. A solution of the copper complex (0.002 mol dm^{-3}) was prepared in acetonitrile (redistilled from calcium hydride). The electrodes were glassy carbon, platinum wire and silver wire as the working, counter and reference electrodes, respectively. All solutions were degassed with nitrogen and dissolved in acetonitrile and contained sample concentrations of the supporting electrode; NaCl (0.1 M) and ^{t}Bu$_4$NBF$_4$ (0.1 M) respectively. The electrolyte used was the tetrafluoroborate anion as the typical counter-ion in the copper complexes, therefore eliminating any potential exchange reactions. NaCl was used as an electrolyte to provide a medium closer to biological conditions. The voltammograms were referenced to the ferrocene/ferrocenium (Fe(III)/Fe(II)) redox couple and values expressed relative to the normal hydrogen electrode (NHE).

5.4.12 Measurement T$_1$ Relaxation times

The sample was prepared in 0.1M NaCl, 100 % D$_2$O in 10 ml volumetric flask and a sample transferred to a 5 mm NMR tube (507-PP). The copper macrocycle concentrations were typically 10 mM, 2.5 mM, 1 mM, 0.1 mM and 0.01 mM respectively. Each sample was run in triplicate. A control sample of 0.1 mM NaCl in 100 % D$_2$O was also recorded for each experiment.

Relaxation measurements were carried out on Bruker DPX or AVANCE NMR spectrometers operating at a proton resonance frequency of 400 MHz. The measurements were carried out using an inversion recovery pulse sequence under full automation control with a 90º pulse width of 11.5 µs. All spectra were referenced internally to the residual proton resonance of the relevant deuterated solvent. The relaxation delay varied from 1-100 s, depending on the relaxation characteristics of the sample.

Data was transferred for remote data processing to a desktop PC, running TOPSPIN 2.1. Following Fourier transformation all data was baseline corrected and the T$_1$ sub-routine within TOPSPIN 2.1 carried out in order to extract the relevant T$_1$ values from the data.

5.5 References

1. Sevcikova, R.; Lubal, P.; Campello, M. P. C.; Santos, I., *Polyhedron*, **2013**, *62*, 268-273.

2. Lacerda, S.; Campello, M. P.; Marques, F.; Gano, L.; Kubicek, V.; Fouskova, P.; Toth, E.; Santos, I., *Dalton Transactions*, **2009**, *23*, 4509-4518.

3. Lui, S., *Advanced Drug Delivery Reviews*, **2008**, *60*, 1347.

4. Wadas, T. J.; Wong, E. H.; Weisman, G. R.; Anderson, C. J., *Chemical Reviews*, **2010**, *110*, 2858-2902.

5. Wu, H. C.; Bayley, H., *Journal of the American Chemical Society*, **2008**, *130*, 6813-6819.

6. Funkemeier, D.; Mattes, R., *Journal of the Chemical Society, Dalton Transactions*, **1993**, 1313-1319.

7. Lui, J. Y.; Powell, K. L.; Thames, H. D.; MacLeod, M. C.; *Chemical Research in Toxicology*, **2010**, *23*, 488-496.

8. Lacerda, S.; Campello, M. P.; Santos, I. C.; Santos, I.; Delgado, R., *Polyhedron*, 2**007**, *26*, 3763-3773.

9. Trotter, K.D.; Reglinski, J.; Robertson, K.; Forgie, J.C.; Parkinson, J.A.; Kennedy, A.R.; Armstrong, D.R.; Sowden, R.J.; Spickett, C.M.; Berlouis, L.E.A., *Inorganica Chimica Acta*, **2010**, *363*, 1529-1538.

10. Sowden, R. J.; Trotter, K. D.; Dunbar, L.; Craig, G.; Erdemli, O.; Spickett, C. M.; Reglinski, J., *Biometals*, **2013**, *26*, 85-96.

11. Gagne, R.R.; Koval, C.A.; Lisensky, G.C., *Inorganic Chemistry*, **1980**, 19, 2854-2855.

Chapter 6

Final Conclusions

The initial aim of this project was to build on existing research which focuses on the design of an *in vivo* oxidant sensors, which could be used as an MRI contrast agents for the early detection of oxidative stress, a common indicator of inflammatory disease. The design of such a compound involves the presence of a metal centre with two available oxidation states. The complex should preferably be prepared in the reduced form. The compound should have an oxidation potential similar to that of biologically relevant oxidants, (e.g hydrogen peroxide, hydroxyl radicals, superoxide, hypochlorite), shifting from a diamagnetic to a paramagnetic species without releasing the metal. For contrast purposes, a vacant coordination site is required for water exchange at the paramagnetic transition metal centre. The desired complex should also be water soluble in aqueous solution and be stable at physiological pH.

Copper was chosen as the metal, as it is diamagnetic in its reduced form (Cu(I), d^{10}) and paramagnetic in its oxidised form (Cu(II), d^9). A macrocyclic parent ligand containing N_2S_2 donor atoms had been identified in previous studies as showing potential for use with modified pendant arms attached at the nitrogens. Pendant alcohol groups were already present in commercially available contrast agents. There had been some preliminary work into the addition of alcohol pendant arms, however, these species had not been fully characterised in the past. Therefore the initial task was the synthesis of a range of pendant arm complexes including alcohol (ethanol, propanol, butanol and hexanol), acetic acid and amine functionalised arms.
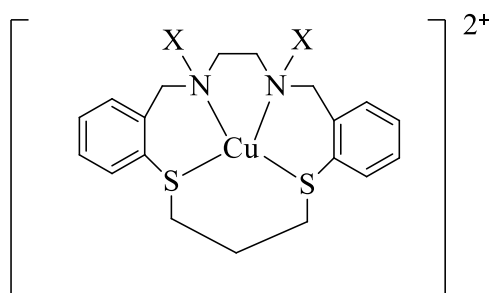
Figure 6.1: A schematic representation of **2** modified at the secondary amine, where X = -$(CH_2)_nOH$ (n=2, 3,4,6), CH_2COOH and $CH_2CH_2NH_2$.

The attachment of bromoethylamine, 4-bromobutanol and 6-bromohexanol pendant arms did not generate suitably clean products and these were abandoned. The ethanol, propanol and acetic acid pendant arm complexes were successfully synthesised and the stability and electrochemistry interrogated. Compound **13** had a redox potential of 1.44V (vs. NHE) which fell into the desired biological range and showed signs of electrochemical reversibility. Compounds **11** and **12** showed signs of irreversible oxidation which would suggest they are unsuitable as redox sensors of oxidative stress.

The magnetic properties of these species, including their parent (secondary amine) macrocycles were investigated, specifically their ability abilities to enhance the T_1 relaxation of water. As it is the copper (II) form of the complexes which would exist in regions of oxidative stress it is possible to measure their effect on the relaxation of water and hence their ability to generate contrast. It was found that the Cu(II) pendant arm complexes all displayed similar relaxation characteristics. Furthermore the addition of the pendant arms has not markedly affected the relaxivity of the compounds. This suggests that in solution the pendant arms either exchange rapidly with solvent (water) molecules or that relaxation via hydrogen bonding with the second hydration sphere is also occurring. Thus the data obtained shows that the N-substituted macrocycles show sufficient relaxivity for use as putative imaging agents.
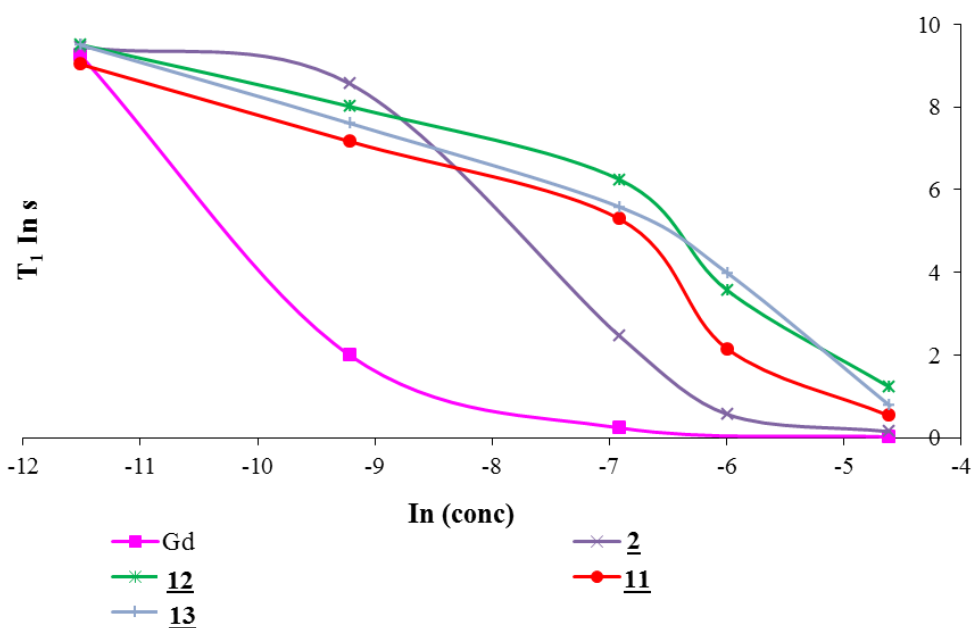
Figure 6.2: T_1ln(s) vs. ln (concentration) plot of **2**, **11**, **12**, **13** and Gd-(DTPA). The performance is dependent on the coordination number of the copper. **2** is four coordinate: **11**, **12** and **13** are 5/6 coordinate (Figures 2.4 and 2.5).

The pendant arm complexes were treated with biological reductants and oxidants to determine their chemical reversibility and it was found that despite their reduction with ascorbic acid, upon reoxidation, only 22% of the copper (II) complex was recovered in each case. It has been identified that further modifications need to be made in order to fine tune the biological redox potentials and relaxation characteristics. This could be achieved by placing electron withdrawing groups at judicious points on the macrocycle in the hope that it encourages full reoxidation to copper (II) following treatment with reductants. It is thought this could be achieved by promoting Cu(I) formation. The sites identified for the introduction of electron withdrawing groups (EWG) and bulky electron donating groups (EDG) are shown below.

Modification 1
R on aryl rings

Modification 2
R between nitro donors

Modification 3
R between sulfur donors
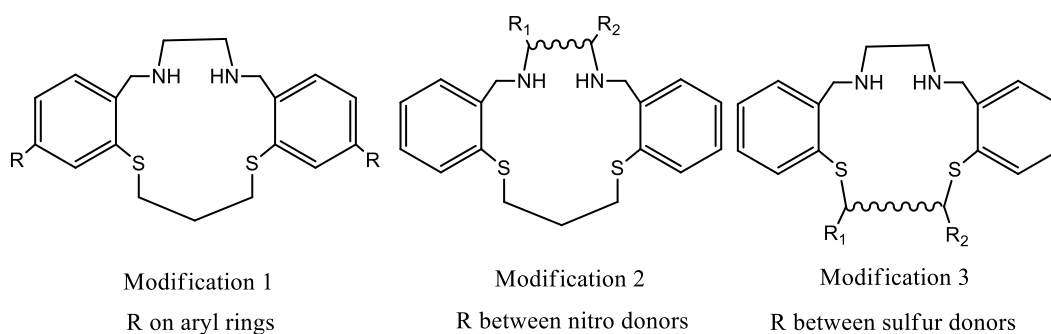
Figure 6.3: Sites identified as suitable for the introduction of electron withdrawing groups

It was not possible to achieve any results for Modification 3. Modification 2 resulted in ring closure to form a benzimidazole compound. Modification 1 was successful, however, it generated a highly insoluble compound. The combination Modification 1 and 2 as it was, however, successful giving rise to compound **33**. Sadly this was also copper (II). Significantly this modification did not make a substantial improvement to the chemical behaviour of the macrocycle and it was decided to explore S_4 and S_3N systems and a source of Cu(I) compounds (Figure 6.4).
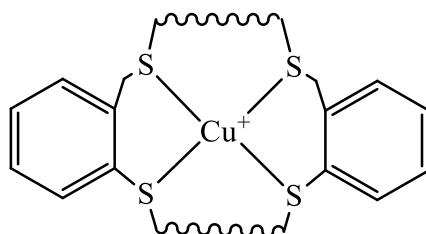
Figure 6.4: Diagrammatic representation of the target copper complex: $[Cu(I)S_{xu}S_{xl}]$

The attempts to produce complexes in this area were only modestly successful. It was only possible to isolate on compound (**36**) which contained two propyl backbones. A series of DFT calculations were run to try to better understand the reason behind the difficulty in synthesising the other complexes. DFT calculations on these systems helped explain the difficulty with the isolation of these compounds. Compound **36** was of great value as using this species it was possible to show that despite being Cu(I) does not possess the appropriate redox properties and aqueous stability. As a result of these studies it was decided to return to the modified N_2S_2 systems in an attempt to increase sulfur donor density by incorporating sulfur donors onto the pendant arms (Figure 6.5).

165
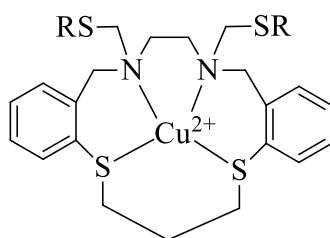
Figure 6.5: A schematic representation of the parent macrocycle **2** showing the site of the attachment of sulphur based pendant arms (SR) is shown. (R = -SH and –S-Ph).

A representative compound (**52**) in this class was produced. Its redox potential (1.28 V vs. NHE) falls in the desired range and in contrast to the previous compounds produced it shows good reversibility (~90 %) and its relaxivity in commensurate with the unmodified macrocycles which is the best that can be expected. Crucially the re-oxidation in non-stoichiometric and the compound requires a 10 fold excess of oxidant to respond.

Despite the significant improvements which have been made to the sensing motif, it is clear that the complexes still have issues regarding their use as MR imaging agents. An increase in relaxivity would be needed and as such future work might explore the combination of the macrocyclic motif developed here with a gadolinium centre. Unless the issue of stoichiometry is unresolved the sensor will only be able to work in a rudimentary (On/Off) mode. If the issues of relaxivity cannot be resolved then it might be prudent to explore the use of these macrocycles in positron emission tomography (PET) imaging.

Appendices

Appendix 1

Donor atoms & Macrocycles

Ligands are divided into two major subdivisions, hard and soft:

- Nitrogen (N), sulfur (S), phosphorous (P) and arsenic (As) which coordinate to polarisable heavy/ transition metals.

- Ethers (O) which coordinate to high charge density alkali/ alkaline earth metals.

As copper is a transition metal, it falls into the former category. The structure of the ligand and choice of donor atoms have a significant effect, in that they will determine the way in which the metal is coordinated, and for macrocycles, the cavity size and the degree to which the metal is retained, as well as influencing the redox potential.

Nitrogen

Nitrogen features strongly in macrocyclic chemistry due to its synthetic flexibility. Numerous macrocycles consisting of nitrogen donor atoms have been prepared, with varying numbers of nitrogen donors and ring sizes. The majority contain four donors and these are termed tetraazamacrocycles. The nitrogens offer the potential for the ligand to be anionic (by deprotonation of N), neutral or cationic (by protonation of N), although the latter is less common. Aza-macrocycles are found in nature, for example porphyrins.

Sulfur

Sulfur is a softer donor than nitrogen, but complexes with only sulfur donors are less common due to lack of synthetic ease. However, thiacrown ethers are known to offer interesting and diverse coordination chemistry as they can bind metal ions more strongly than mono- or bi-dentate thioethers. The sulfur lone pairs tend to orientate out of the macrocyclic cavity and then undergo a substantial conformation change to coordinate metal ions.

Mixed Donor Systems

Mixed donor systems bring together the properties of two or more donor atoms into the macrocycle and broaden the applicability of the ligand by offering different bonding preferences, which allows selectivity in metal ion binding.

Cavity Size

A key property of macrocycles is the cavity size. Physically, this can be imagined as being the space a metal ion can occupy. The most straightforward way to determine the cavity size is by estimating the cavity radius by measuring the distance between the nuclei of the diagonally opposite donor atoms in the macrocycle. This is most commonly achieved by using molecular or computational models, or by taking direct measurements of solid-state structures. Results can then be compared to the metal ion radii to identify which would be suitable for complexation.

The key point is the cavity must be the ideal size to complex the metal appropriately. If this is not the case then a number of things may happen; few or none of the donor atoms can coordinate to the metal, the macrocycle may undergo a conformational change to incorporate the metal, the metal may coordinate and lie in a different geometry out with the cavity, or the metal may bind weakly. In terms of contrast agents, the latter is of particular significance. If the metal is only weakly or partially bound to the macrocycle, it is likely that the synthesised complex will have low stability, indicating a high possibility of the metal ion being lost from the complex.

Appendix 2

Bovine Serum Albumin (BSA) stability test data for N-substituted macrocycles

Stability test of compound **11** with BSA:
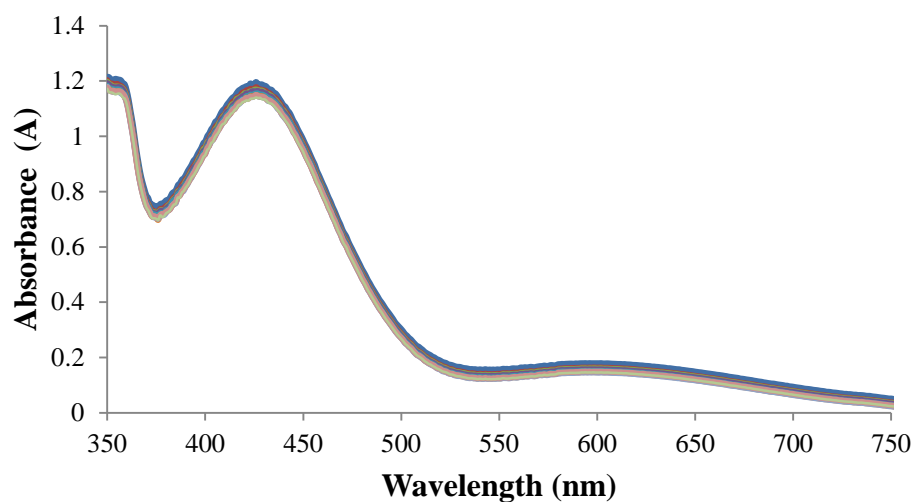
Plot of stability test of **11** (0.3 mM) with BSA (199mg, 1 ml) in Tris-buffer (5 mM, pH 7.4). No change is observed in the spectra for compound **11** suggesting the copper is stable in the macrocycle.

Stability test of compound **13** with BSA:
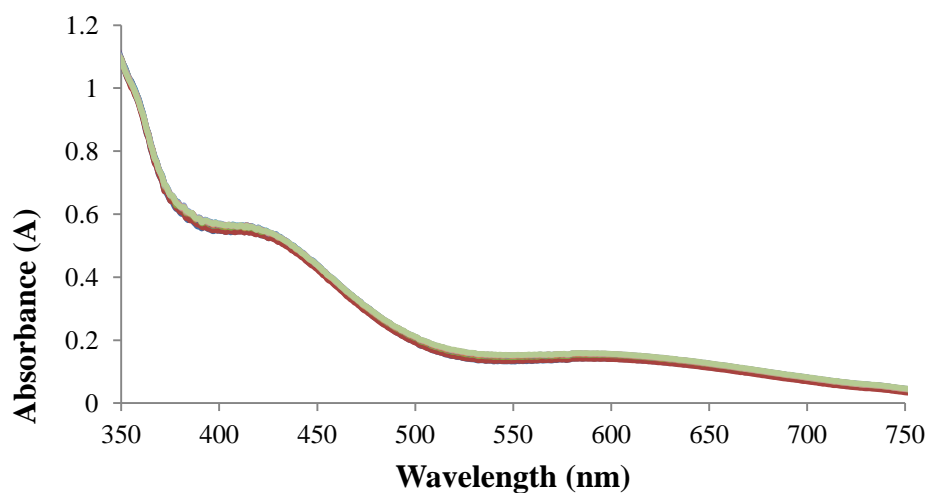
Plot of stability test of **13** (0.3 mM) with BSA (199mg, 1 ml) in Tris-buffer (5 mM, pH 7.4). No change is observed in the spectra for compound **13** suggesting the copper is stable in the macrocycle.

Appendix 3

Ascorbate reduction and hypochlorite oxidation data for N-substituted data

<u>Reduction/re-oxidation data for 12</u>
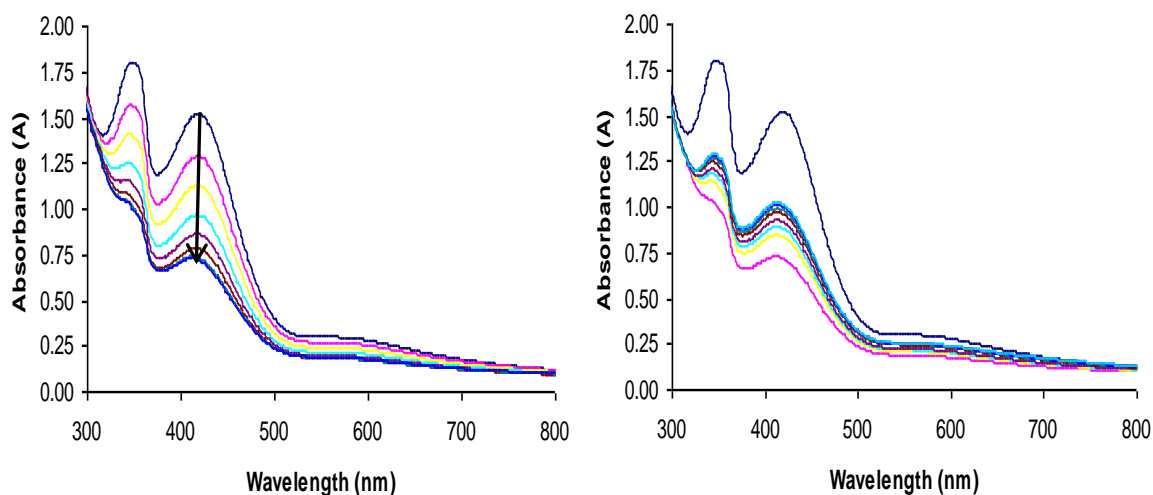
The left plot shows the spectrophotometric reduction of **12** (0.3mM) with ascorbic acid (10 mM) in Tris-buffer (5mM, pH 7.4) a 5 µl aliquot is added. The reduction is characterised by the absorption band at 420 nm. The top spectrum shows the original position of the complex prior to reduction and the bottom spectrum shows the complex after reduction, the direction is indicated by the arrow (left). The right plot shows the spectrophotometric analysis of HOCl oxidation of **12**, the 100mM solution hypochlorite in Tris-buffer (5mM, pH 7.4) was added in 5µl aliquots. The species being studied was generated *in-situ* using ascorbic acid as the reductant (left). The top spectrum shows the original position of the complex prior to reduction and the bottom spectrum shows the complex after reduction. The spectra in the middle show the oxidation with hypochlorite after no further changes were observed.

Reduction/reoxidation data for **11**
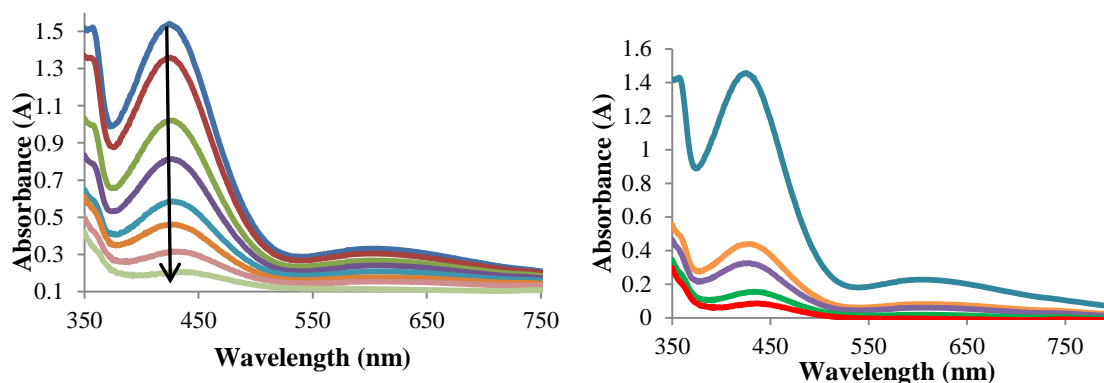
The left plot shows the spectrophotometric reduction of **11** (0.3mM) with ascorbic acid (10 mM) in Tris-buffer (5mM, pH 7.4) a 5 µl aliquot is added. The reduction is characterised by the absorption band at 420 nm. The top spectrum shows the original position of the complex prior to reduction and the bottom spectrum shows the complex after reduction, the direction is indicated by the arrow (left). The right plot shows the spectrophotometric analysis of HOCl oxidation of **11**, the 100mM solution hypochlorite in Tris-buffer (5mM, pH 7.4) was added in 5µl aliquots. The species being studied was generated *in-situ* using ascorbic acid as the reductant (left). The top spectrum shows the original position of the complex prior to reduction and the bottom spectrum shows the complex after reduction. The spectra in the middle show the oxidation with hypochlorite after no further changes were observed.

Appendix 4

Cyclic Voltammetry

Cyclic voltammetry is an effective and versatile electroanalytical technique that can be applied to the mechanistic study of redox systems. In basic terms, cyclic voltammetry produces a graph that can be interpreted to discover whether the processes of reduction and oxidation have occurred for an analyte.

An electrical potential is scanned linearly forward and then back, producing a triangular cycle of potential against time. The applied potential over a set time can be altered and this is known as the experimental scan rate.

Triangular Cycle
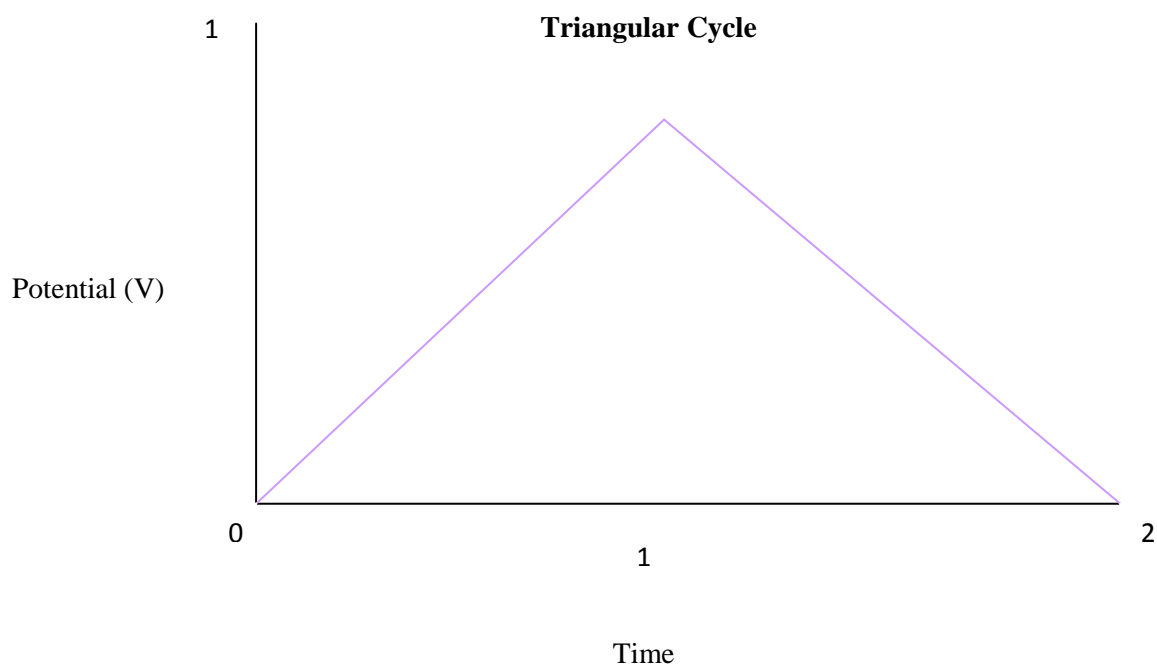
The potential is measured between a reference electrode and a working electrode, with current being measured between the same working electrode and an auxiliary electrode. A graph is then obtained showing current against potential.
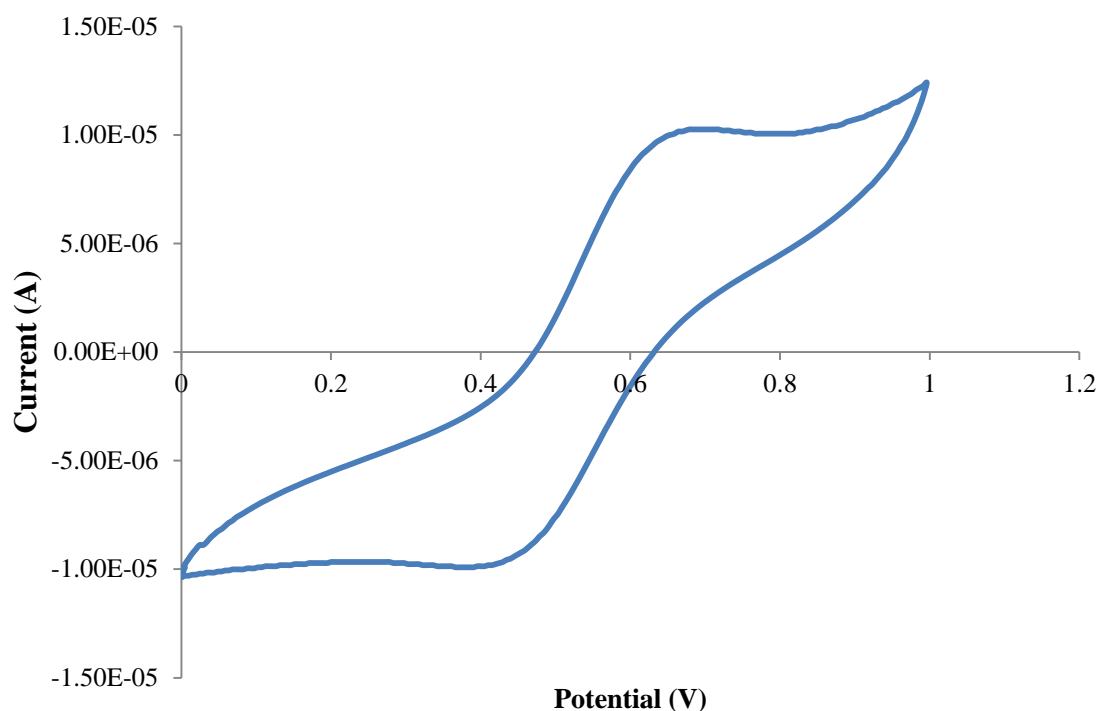
A typical reversible cyclic voltammetry redox curve

The graph can then be interpreted to determine the redox reversibility of a system.

- **True reversible:** Forward and backwards peak currents are equal in magnitude.
- **Quasi reversible:** Reductive peak appears at a more negative potential and the oxidative peak at a higher positive potential.
- **Irreversible:** Only one of either the reductive peak or the oxidative peak is observed.

Cyclic voltammetry has the ability to vary the scan rate over a wide range of values. This can prove beneficial as current intensity increases with increased scan rate.

Cyclic voltammetry data for N-substituted macrocycles

Cyclic voltammogram of compound 12 in the negative region
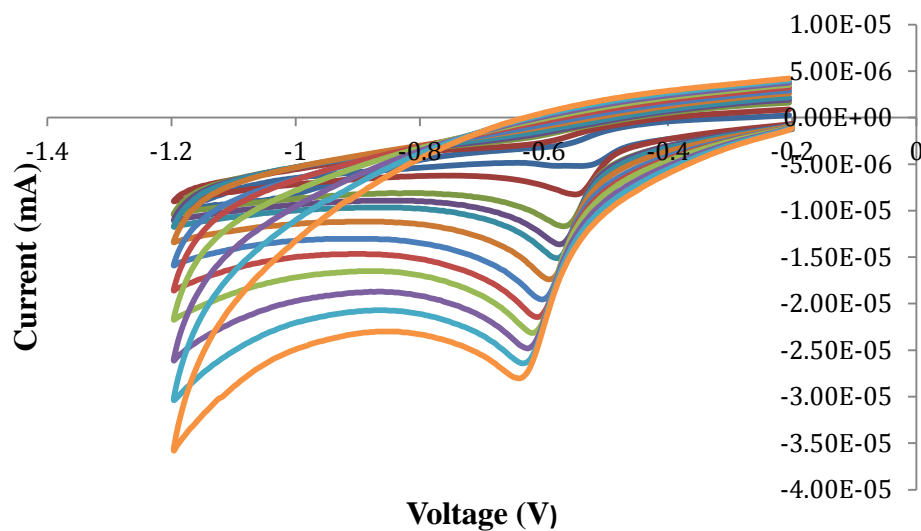
Cyclic voltammogram in the positive region of compound **12** in acetonitrile (0.1M ${}^{t}Bu_4NBF_4$: Potential reported vs. ferrocene) recorded over a scan rate range from 10mV-200mVs^{-1}.

Cyclic voltammogram of compound 11 in the negative region
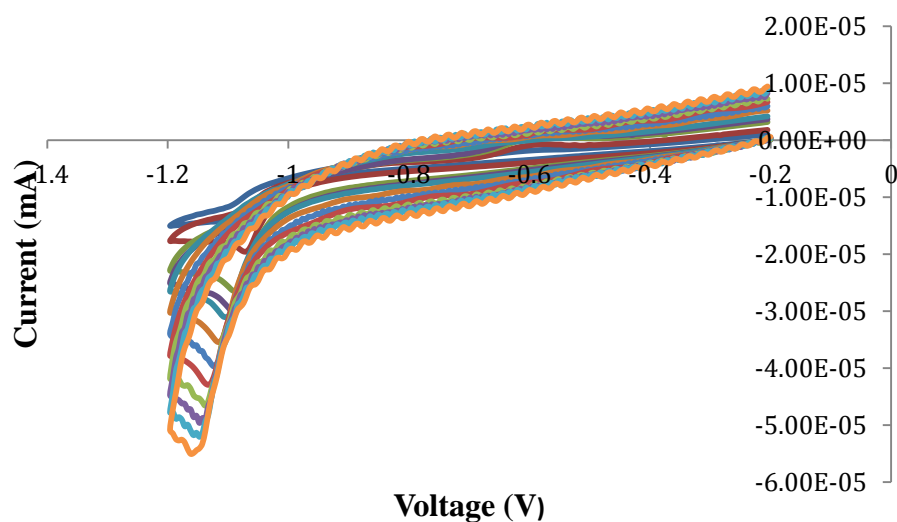
Cyclic voltammogram in the positive region of compound **11** in acetonitrile (0.1M ${}^{t}Bu_4NBF_4$: Potential reported vs. ferrocene) recorded over a scan rate range from 10mV-200mVs^{-1}.

Cyclic voltammogram of compound 13 in the negative region
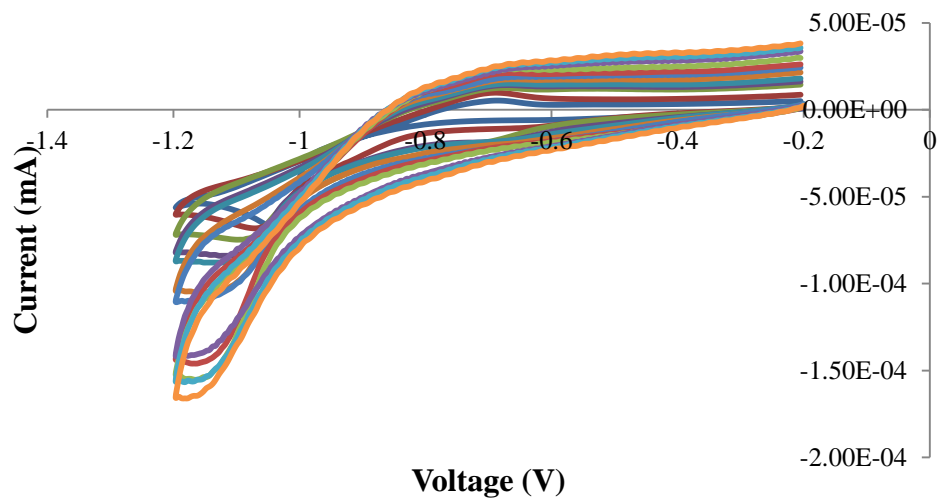
Cyclic voltammogram in the positive region of compound **13** in acetonitrile (0.1M ^{t}Bu$_4$NBF$_4$: Potential reported vs. ferrocene) recorded over a scan rate range from 10mV-200mV s^{-1}.

Cyclic voltammogram of compound 33 in the negative region
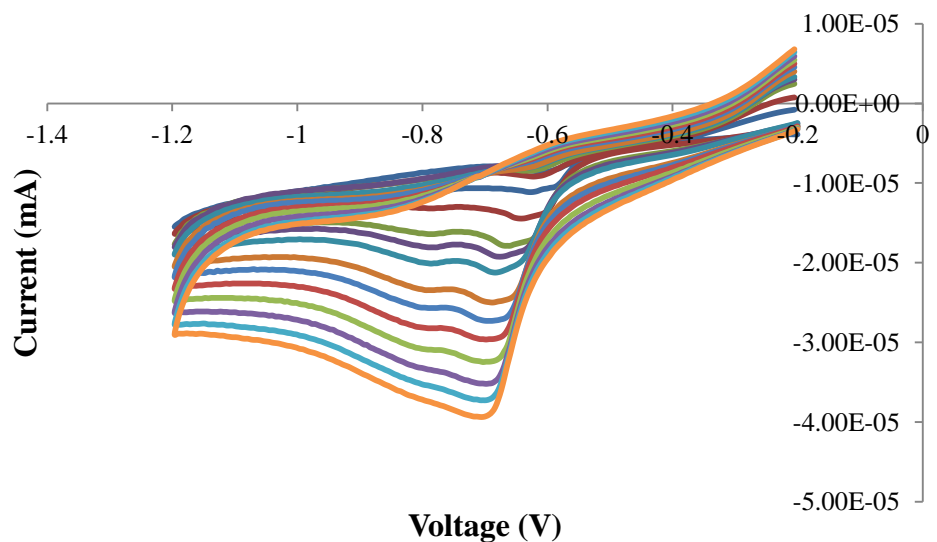
Cyclic voltammogram in the positive region of compound **33** in acetonitrile (0.1M ^{t}Bu$_4$NBF$_4$: Potential reported vs. ferrocene) recorded over a scan rate range from 10mV-200mV s^{-1}.

Cyclic voltammogram of compound 52 in the negative region
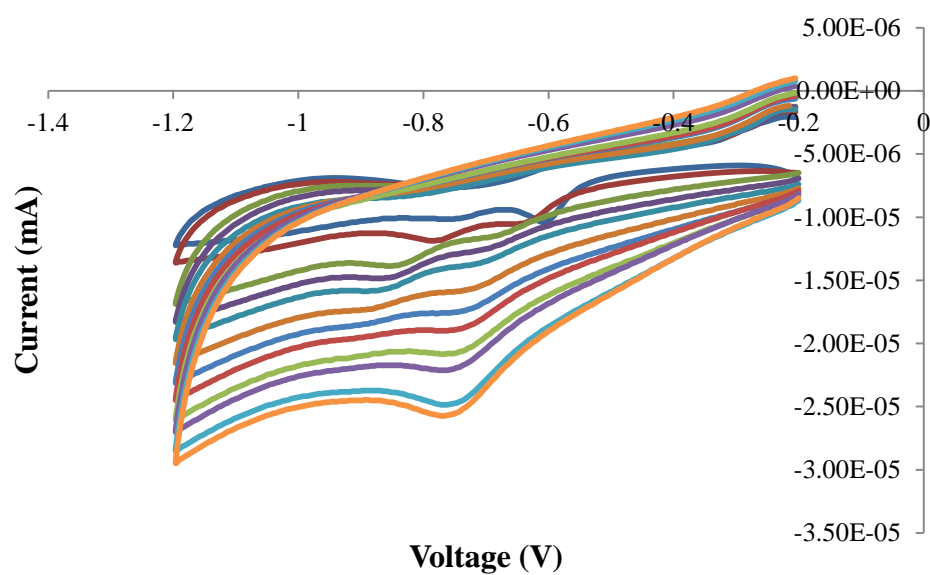
Cyclic voltammogram in the positive region of compound **52** in acetonitrile (0.1M $^tBu_4NBF_4$: Potential reported vs. ferrocene) recorded over a scan rate range from 10mV-200mV s^{-1}.

Appendix 5

T$_1$ Relaxation NMR data for N-substituted macrocycles

T$_1$ relaxation effect of 11:

T$_1$(1)s^{-1}	T$_1$(2)s^{-1}	T$_1$(3)s^{-1}	ln log(conc)	Average T$_1$ (s)	Standard deviation
0.576	0.469	0.531	-4.6052	0.525	0.053724606
2.252	2.164	2.019	-5.9915	2.145	0.117656279
5.513	4.696	5.639	-6.90776	5.283	0.511959308
6.952	7.276	7.257	-9.21034	7.162	0.181825007
9.563	8.56	8.982	-11.51293	9.035	0.503596068

Triplicate T$_1$ relaxation results of **11**.
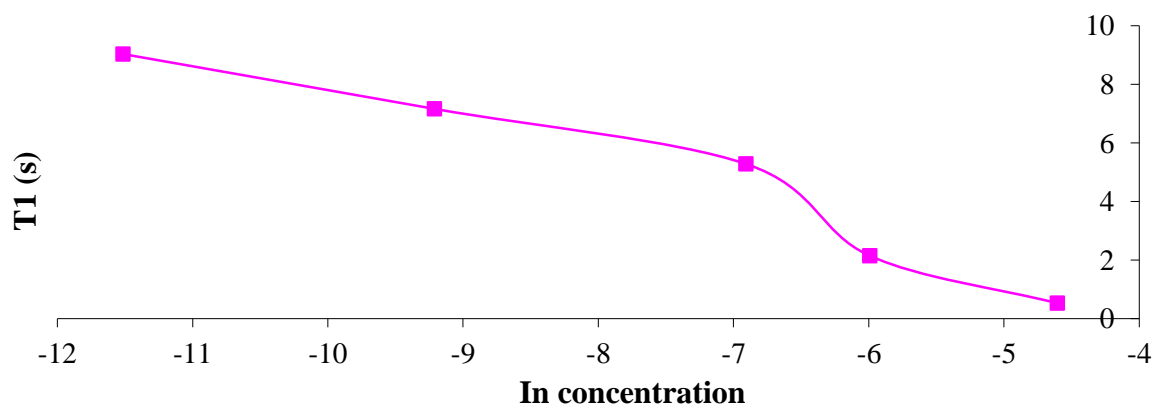
Figure 2.16: T$_1$ relaxation (s) vs. ln(concentration) of **11**.
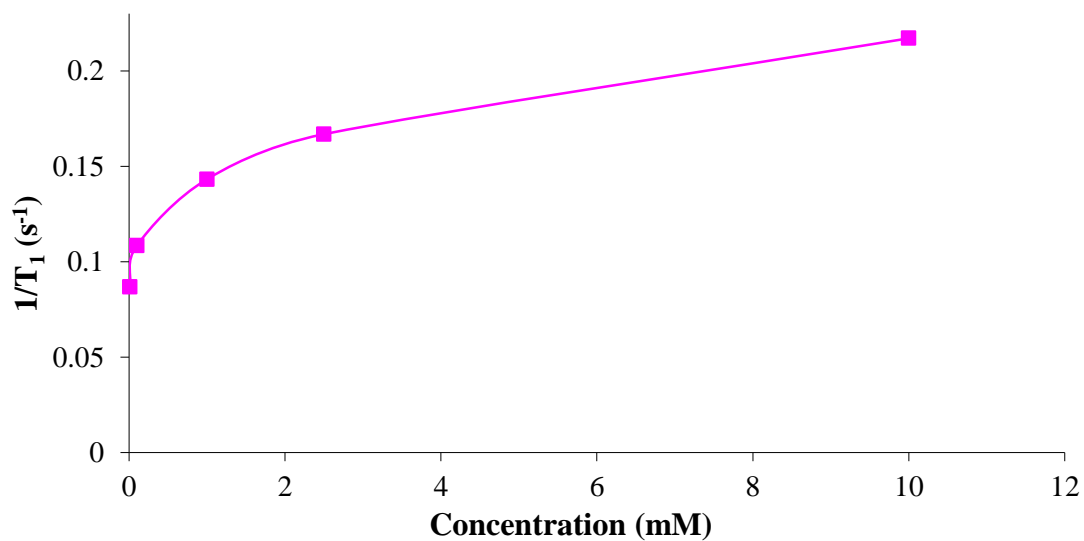
Gradient of relaxivity of **11**.

T$_1$ relaxation effect of 13:

T$_1$(1)s^{-1}	T$_1$(2)s^{-1}	T$_1$(3)s^{-1}	In log (conc)	Average T$_1$ (s)	Standard deviation
0.772	0.774	0.775	-4.6052	0.774	0.001527525
3.904	3.986	4.06	-5.9915	3.983	0.078034181
5.68	5.506	5.543	-6.90776	5.576	0.091664242
7.276	7.666	7.861	-9.21034	7.601	0.29786742
9.275	9.524	9.705	-11.51293	9.501	0.215894264

Triplicate T$_1$ relaxation results of **13**.
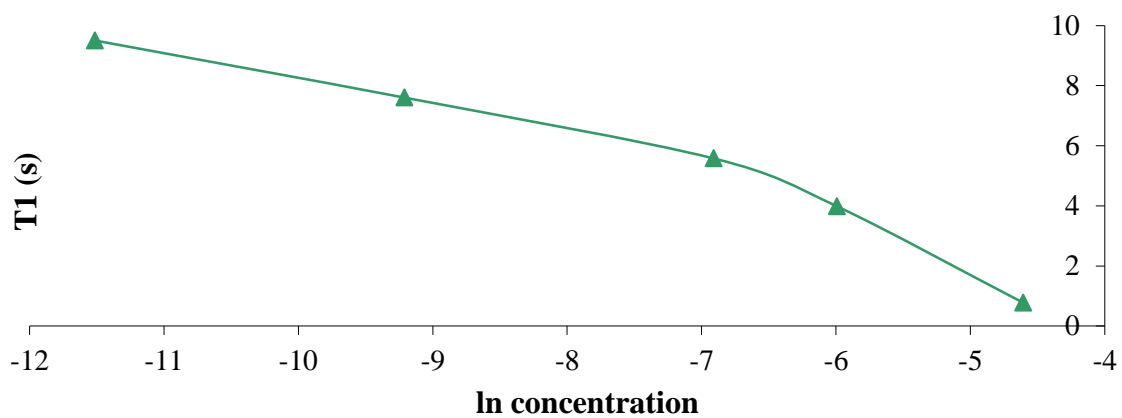
Figure 2.16: T_1 relaxation (s) vs. ln(concentration) of **13**.
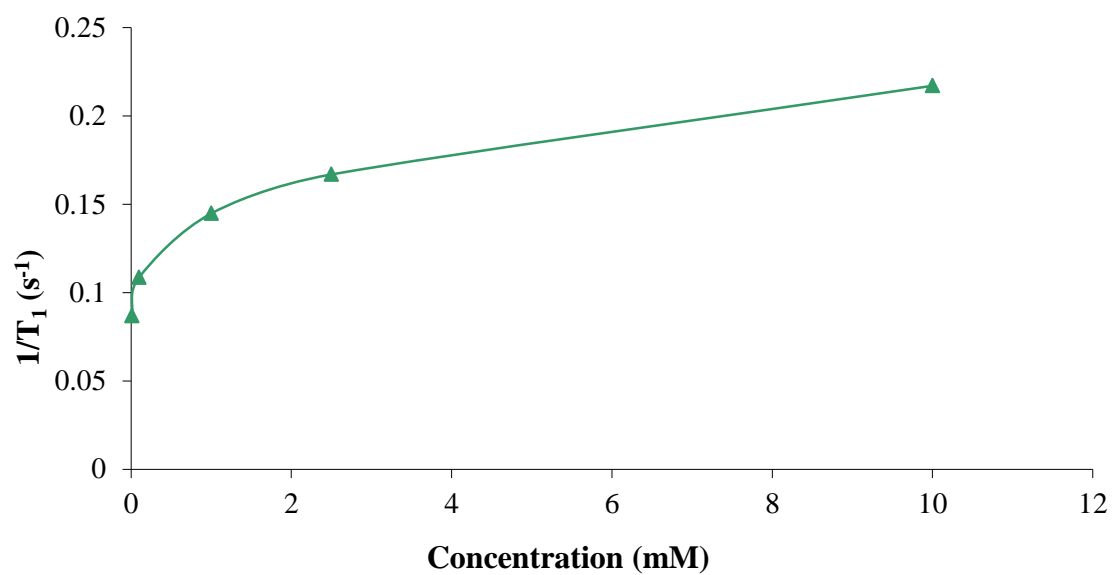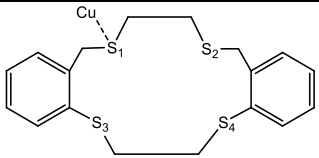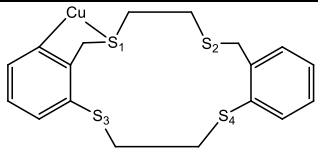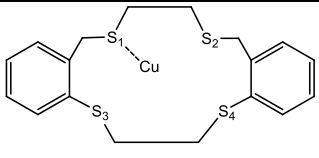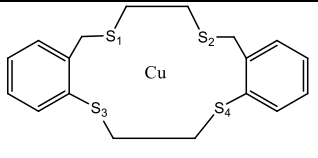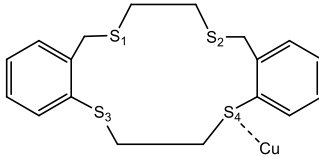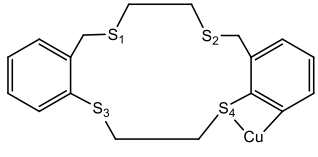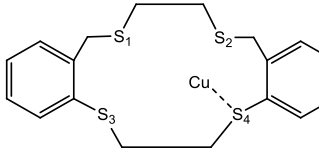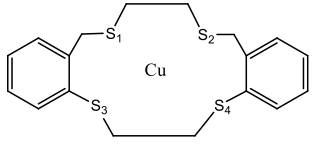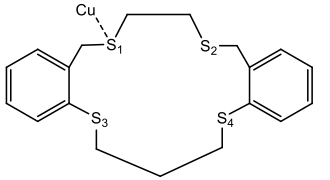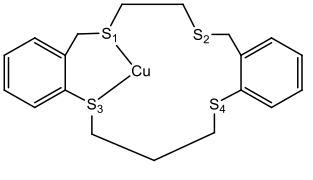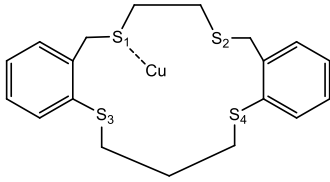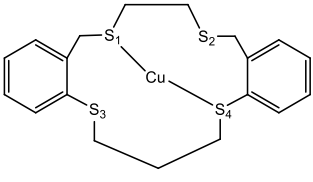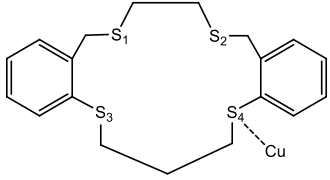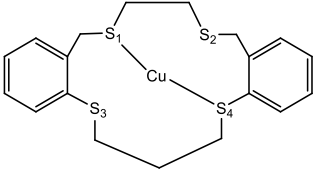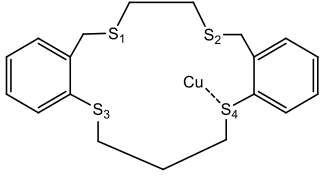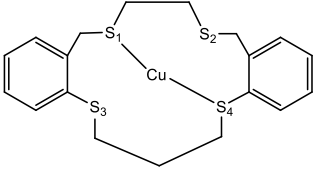
Figure 28: Gradient of relaxivity of **13**.

Appendix 6
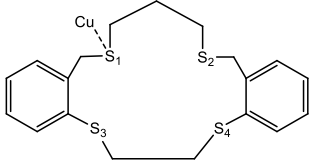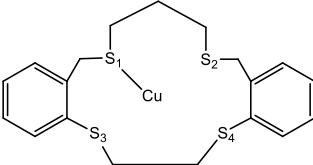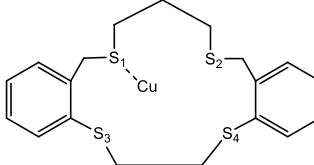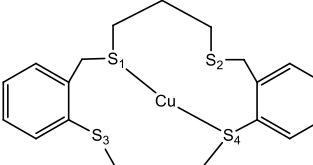
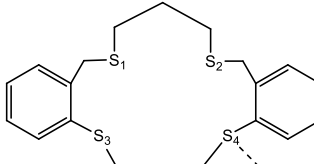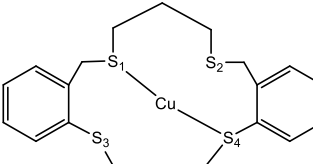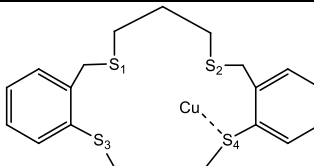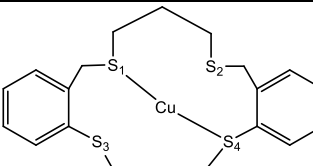# DFT calculations: Exo and endo positioning data

Initial Structure	Optimised Structure	Cu-S bond distance (Å)		Energy (A.U)
		S_1	2.297	-3931.22792925
		S_2	-	
		S_3	-	
		S_4	-	
		S_1	2.388	-3931.29940921
		S_2	2.385	
		S_3	2.402	
		S_4	2.400	
		S_1	-	-3931.20040953
		S_2	-	
		S_3	-	
		S_4	2.144	
		S_1	2.389	-3931.29940943
		S_2	2.383	
		S_3	2.403	
		S_4	2.399	
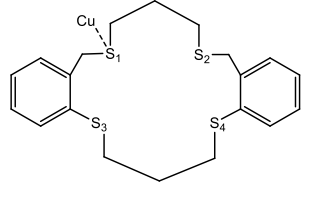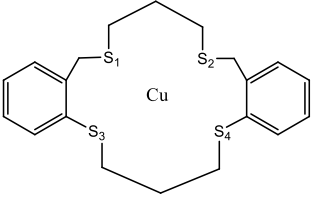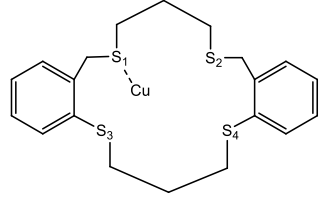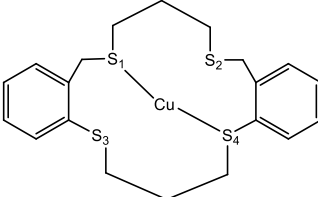
Results of DFT calculations of compound **39** where copper is introduced at exo and endo positions. Bonding has been predicted by Gaussview5 after compounds undergo optimisation and frequency analysis.

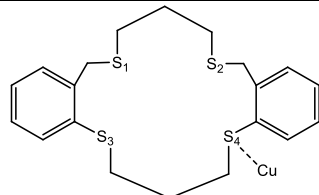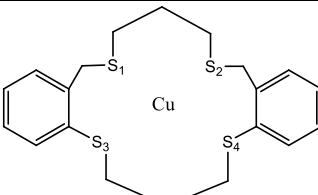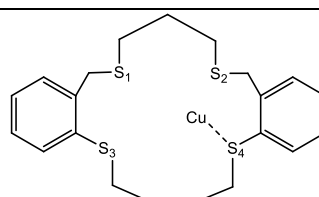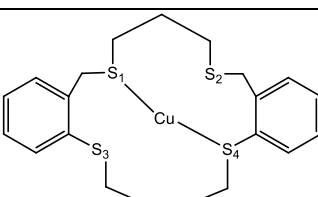| Initial Structure	Optimised Structure	Cu-S bond distance (Å)		Energy (A.U)
		S_1	2.164	-3970.56787011
		S_2	5.322	
		S_3	2.193	
		S_4	3.773	
		S_1	2.261	-3970.61782916
		S_2	2.889	
		S_3	2.573	
		S_4	2.286	
		S_1	2.243	-3970.62027671
		S_2	2.649	
		S_3	2.867	
		S_4	2.238	
		S_1	2.243	-3970.62027677
		S_2	2.649	
		S_3	2.867	
		S_4	2.238	

Results of DFT calculations of compound **41** where copper is introduced at exo and endo positions. Bonding has been predicted by Gaussview5 after compounds undergo optimisation and frequency analysis.

Initial Structure	Optimised Structure	Cu-S bond distance (Å)		Energy (A.U)
		S_1	2.262	-3970.61870643
		S_2	2.435	
		S_3	2.849	
		S_4	2.335	
		S_1	2.216	-3970.62118892
		S_2	2.405	
		S_3	3.566	
		S_4	2.225	
		S_1	2.220	-3970.62302395
		S_2	2.370	
		S_3	3.309	
		S_4	2.249	
		S_1	2.216	-3970.62118881
		S_2	2.406	
		S_3	3.565	
		S_4	2.225	

Results of DFT calculations of compound **43** where copper is introduced at exo and endo positions. Bonding has been predicted by Gaussview5 after compounds undergo optimisation and frequency analysis.

Initial Structure	Optimised Structure	Cu-S bond distance (Å)		Energy (A.U)
		S_1	2.634	-4009.94167338
		S_2	2.312	
		S_3	3.115	
		S_4	2.383	
		S_1	2.224	-4009.94747708
		S_2	3.314	
		S_3	3.754	
		S_4	2.243	
		S_1	2.312	-4009.94167338
		S_2	2.634	
		S_3	3.115	
		S_4	2.383	
		S_1	2.223	-4009.94747719
		S_2	2.428	
		S_3	3.755	
		S_4	2.244	

Results of DFT calculations of compound **45** where copper is introduced at exo and endo positions. Bonding has been predicted by Gaussview5 after compounds undergo optimisation and frequency analysis.